

IMPERIAL COLLEGE OF SCIENCE, TECHNOLOGY  
AND MEDICINE  
(University of London)

**STRUCTURAL DYNAMIC  
MODEL UPDATING  
USING  
EIGENSENSITIVITY ANALYSIS**

by

**Haeil Jung**

A thesis submitted to the University of London for the degree of  
Doctor of Philosophy.

Department of Mechanical Engineering  
Imperial College, London SW7, U.K.

January 1992

## ABSTRACT

Despite the highly sophisticated development of finite element methods, a finite element model for structural dynamic analysis can be inaccurate or even incorrect due to the difficulties of correct modelling, uncertainties on the finite element input data and geometrical oversimplification, **while** the modal data extracted from measurement are supposed to be correct, even though incomplete. Therefore, model updating schemes are developed which aim to improve or to correct the initial finite element model using modal test results.

In this thesis, the advantages and disadvantages (or limitations) of various model updating methods are discussed. One of the advantages of model updating using eigensensitivity analysis is that mode expansion is not required. However, this method requires large computational effort because of the repeated solution of the eigendynamic problem and repeated calculation of the sensitivity matrix. A sensitivity method is developed using arbitrarily chosen macro elements in this thesis at the error location stage in **order** to reduce the computational time and to reduce the number of experimental modes required. By this approach, the model updating problem which is generally **under-**determined can be transformed into an over-determined one and the updated analytical model can be a physically meaningful model.

The assumption that the test results represent the true dynamic behaviour of the structure, however, may not be correct because of various measurement errors. The errors involved in modal parameter estimation are investigated and their effects on estimated frequency response **functions(FRFs)** and on the modal parameters extracted from the **FRFs** are also investigated. The resultant 'experimental' modal data which contain possible **experimental** errors are used to update &corresponding analytical model to check the validity of the

updating method developed. Also, the sensitivity of the updating method to noise on the experimental data is investigated.

## ACKNOWLEDGMENTS

The author is most grateful to his supervisor, Prof. D.J. Ewins, for his sustained stimulus and guidance throughout the duration of this research and for his sustained advice in the preparation of the manuscript.

Many members of the Dynamic Section have helped with practical advice and discussion of experimental and computing problems. Special thanks are due in this regard to Mr. D.A. Robb and Dr. M. Imregun.

For their friendly cooperation and useful discussions throughout the duration of this work, the author also wishes to express his gratitude to **many** former and present colleagues in the Dynamic Section, especially to R. Lin, A. Nobari and Y. Ren.

Finally, the author is indebted to **Kia** Motors Corporation for providing the financial support throughout the whole period of this work.

## NOMENCLATURE

As this thesis embraces several different branches of dynamics, **there** is a certain amount of overlap between the symbols normally employed in the different branches. Therefore, most symbols are defined where they occur in the text, and only the most important of these are listed below.

$A$	cross-sectional area
$a_i$	mass correction coefficient of the <i>ith</i> element
$a_m$	measured acceleration
$A_r$	modal constant of the <i>rth mode</i>
$a_t$	<b>true</b> acceleration
$b_i$	stiffness correction coefficient of the <i>ith</i> element
$b_i^*$	complex stiffness correction coefficient of the <i>ith</i> element
$c$	viscous damping coefficient
$c_i$	damping correction coefficient of the <i>ith</i> element
$d$	structural damping diameter of a push rod (Appendix D)
$[D]_i$	structural damping matrix of the <i>ith</i> element
$[D_U]$	updated structural damping matrix
$e$	superscript for element matrix
$E$	Young's modulus
$e_j$	sensitivity coefficient
$f(t)$	actual force applied to the structure
$f_a$	natural frequency of the first axial mode
$f_A$	analytical natural frequency

$f_b$	<b>natural frequency</b> of the <b>first</b> bending mode
$f_m$	upper limit of measured frequency range
$f_x$	experimental <b>natural</b> frequency
$G_{(o)}$	<b>auto-spectrum</b> of measured acceleration $a(t)$
$G_{FA}(\omega)$	cross-spectrum between measured force $f(t)$ and measured acceleration $a(t)$
$G_{FF}(\omega)$	<b>auto-spectrum</b> of measured force $f(t)$
$H(\omega)$	frequency response function
$H_1, H_2$	FRF estimates
$i$	imaginary unit ( $= \sqrt{-1}$ )
$I$	area moment of inertia
$[I]$	identity matrix
$k$	stiffness
$k_a$	axial stiffness of a push rod
$k_b$	bending stiffness of a push rod
$[K]$	stiffness matrix
$[K_A]$	analytical stiffness matrix
$[K_a]_i$	axial stiffness matrix of the <b><i>ith</i></b> element
$[K_b]_i$	bending stiffness matrix of the <b><i>ith</i></b> element
$[K^e]_i$	stiffness matrix of the <b><i>ith</i></b> element
$[K]_i$	stiffness matrix of the <b><i>ith macro</i></b> element
$[K_U]$	updated analytical stiffness matrix
$[K^*]$	complex stiffness matrix
$[AK]$	stiffness error matrix
$l$	number of selected elements
$L$	number of macro elements length (Appendix B and Appendix D)
$m$	effective mass of that part of the structure to which the accelerometer is mounted
$m$	number of measured modes
$m_a$	<b>accelerometer mass</b>

$m_s$	shaker mass
$m'$	minimum number of measured modes
$[M]$	mass matrix
$[M_A]$	analytical mass matrix
$[M^e]_i$	mass matrix of the <i>ith</i> element
$[M]_i$	mass matrix of the <i>ith macro</i> element
$[M_u]$	<b>updated analytical mass matrix</b>
$[\Delta M]$	<b>mass error matrix</b>
$n$	number of measured coordinates
$n_i$	number of elements in the <i>ith macro</i> element
$N$	number of <b>DoFs</b> of a analytical <b>model</b>
$n_d$	number of averages
$n_1$	number of <b>modes used</b> for calculation of eigenvector sensitivity
$[O]$	null matrix
$p$	output force <b>from</b> the shaker
$\{p\}$	correction coefficient vector
$\{\Delta p\}$	difference vector of <b>correction</b> coefficients (whole elements)
$\{\Delta p'\}$	difference vector of correction coefficients (selected elements)
$[S]$	balanced sensitivity matrix (whole elements)
$[S^o]$	unbalanced sensitivity matrix (whole elements)
$[S']$	balanced sensitivity matrix (selected elements)
$t$	time
$T$	<b>record</b> length
$u$	subscript for updated data
$u(t)$	rectangular window
$u_i(t)$	displacements in x direction
$[U]$	left singular vector matrix
$v_i(t)$	displacements in y direction
$M$	right <b>singular</b> vector matrix

$w(t)$	<b>Hanning</b> window
$W(\omega)$	window spectrum
$x$	horizontal axis
$X$	subscript for experimental data
$y$	<b>vertical</b> axis
$\alpha(\omega)$	<b>receptance</b>
$\gamma^2(\omega)$	coherence function
$\{\Delta\}$	difference vector between experimental and analytical modal parameters
$\phi(\omega)$	phase angle
$\{\phi\}_r$	mass <b>normalised</b> eigenvector of the <b><i>rth mode</i></b>
$\{\phi_x\}_r$	<b>mass</b> normalised eigenvector of the <b><i>rth</i></b> experimental mode
$\{\Delta\phi\}_r$	difference between experimental and analytical eigenvectors of the <b><i>rth mode</i></b>
$[\Phi_x]$	<b>mass normalised</b> mode shape matrix
$\lambda_c$	arbitrary value between zero and the first non-zero eigenvalue
$\lambda_{ij}$	Lagrange multiplier
$\lambda_r$	eigenvalue for the <b><i>rth mode</i></b>
$\lambda_{xr}$	eigenvalue for the <b><i>rth mode</i></b>
$\Delta\lambda_r$	difference between <b>experimental</b> and analytical eigenvalues of the <b><i>rth mode</i></b>
$[\Lambda]$	eigenvalue matrix
$[\Lambda_x]$	experimental eigenvalue matrix
$\Psi_i(x)$	shape functions
$\sigma[\ ]$	<b>random</b> error of [ ]
$\sigma_i$	singular value of sensitivity matrix
$[\Sigma]$	singular value matrix
$\epsilon$	function to be <b>minimised</b>
$\epsilon_r[\ ]$	<b>normalised</b> random error of [ ]
$\rho$	density
$\eta_r$	modal damping of the <b><i>rth mode</i></b>
$\omega_m$	<b>measured</b> resonance frequency

$\omega_M$	<b>maximum</b> frequency
$\omega_r^2$	eigenvalue of the <b><i>r</i>th mode</b>
$\omega_t$	<b>true resonance</b> frequency
$[\omega_x^2]$	eigenvalue of <b>the <i>r</i>th mode</b>

## Operators and Symbols

$\text{Im}()$	imaginary part of a complex value
$\mathcal{O}()$	order of a value
$\text{Re}()$	real part of a complex value
$[ ]^H$	Hermitian (complex conjugate + <b>transpose</b> ) of a complex matrix
$[ ]^T$	transpose of a matrix
$[ ]^{-1}$	inverse of a matrix
$[ ]^+$	Moore-Penrose <b>generalised</b> inverse of a rectangular matrix
$   $	modulus
$\  \ $	Euclidian norm of a matrix
*	complex conjugate
*	<b>convolution</b> (Chapter 5)
$\wedge$	estimated value
$\cdot$	derivative with respect to time
$'$	derivative with respect to displacement

## Abbreviations

<b>DFT</b>	discrete Fourier transform
<b>DoF</b>	degree-of-freedom
<b>EMM</b>	error matrix method
<b>FE</b>	finite <b>element</b>

<b>FFT</b>	<b>fast Fourier transform</b>
<b>FRF</b>	<b>frequency response function</b>
<b>IEM</b>	<b>inverse eigensensitivity method</b>
<b>M A C</b>	<b>modal assurance criterion</b>
<b>SDOF</b>	<b>single degree-of-freedom</b>
<b>SVD</b>	<b>singular value decomposition</b>

# CONTENTS

	<b>Page</b>
<i>ABSTRACT</i>	i
<i>ACKNOWLEDGMENT</i>	iii
<i>NOMENCLATURE</i>	iv
<b><i>CHAPTER 1 INTRODUCTION</i></b>	<b>1</b>
1.1 <b>Structural</b> Dynamics Analysis	2
1.2 Analytical Modelling - FE Analysis	3
1.3 Experimental Modelling - Modal Testing	4
1.4 Linking FE Analysis and Modal Testing	6
1.5 Discussion on Related Research	7
1.6 Preview of the Thesis	10
<b><i>CHAPTER 2 MODEL UPDATING METHODS - A REVIEW</i></b>	<b>13</b>
2.1 Introduction	14
2.2 Model Updating Methods	15
2.2.1 Direct Methods	15
2.2.1.1 Berman's Method	16
2.2.1.2 Eigendynamic Constraint Method	18
2.2.2 Compatibility between Measured Modes and Analytical Model	21
2.2.3 Iteration Method - Inverse Eigensensitivity Method ( <b>IEM</b> )	23

2.3 Error Location Methods	27
<b>2.3.1 Error Matrix Method (EMM)</b>	27
2.3.2 <b>Modified</b> EMM	29
2.3.3 <b>IEM</b>	30
2.4 Concluding Remarks	42

## **CHAPTER 3 MODEL UPDATING USING IEM** 44

3.1 <b>Preliminaries</b>	45
3.2 Error Location Procedure	46
<b>3.2.1 Selection of Submatrices</b>	46
3.2.2 Eigensensitivity	47
3.2.3 Compatibility between Measured Modes and Analytical Model	52
3.2.4 Balancing the Sensitivity Matrix	53
3.3 Numerical Examples	57
3.3.1 Influence of Choice of Macro Elements on Error Location	59
3.3.2 Balancing Effect	63
3.4 Model Updating Procedure	66
3.5 Application to Bay Structure	71
3.6 Application to the GARTEUR Structure	74
3.6.1 The GARTEUR Structure	74
3.6.2 Eigensensitivity	77
3.6.3 Error Location Procedure	78
3.6.4 Model Updating Procedure	79
3.7 Concluding Remarks	90

<b>CHAPTER 4</b>	<b>ERROR SENSITIVITY OF THE <b>IEM</b></b>	91
4.1	Preliminaries	92
4.2	Sensitivity of <b>IEM</b> to Noise on Modal Parameters	93
4.2.1	Error Location Procedure	93
4.2.1.1	Sensitivity to Measurement Noise	93
4.2.1.2	Influence of Choice of Macro Elements on Error Location	95
4.2.2	Updating Procedure	95
4.3	Conclusions	100

## **CHAPTER 5** **ERRORS INVOLVED IN MODAL PARAMETER**

5.1	Preliminaries	102
5.2	Modal Testing of SAMM Structures	103
5.2.1	Description of Test Structures	103
5.2.2	Measurement	104
5.3	Errors in Modal Parameter Estimation	111
5.4	Measurement Errors	111
5.4.1	Nonlinearity of Structure	111
5.4.2	Nonstationarity of Structure	112
5.4.3	Mass Loading Effect of Transducers	112
5.4.4	Errors by Transducer Characteristics	113
5.4.4.1	Useful Frequency Range	113
5.4.4.2	Transverse Sensitivity	113
5.4.4.3	Mounting Effect	114
5.4.5	Shaker/Structure Interaction	114
5.4.6	Measurement Noise	117

5.5 Signal Processing Errors	118
5.5.1 Leakage	118
5.5.2 Effect of Window Functions	120
5.5.3 Effect of Averaging	123
<b>5.5.3.1</b> FRF Estimates	123
5.5.3.2 Coherence Function Estimates	124
5.6 Modal Analysis Errors	124
<b>5.6.1</b> Circle-Fit <i>Modal</i> Analysis	125
5.6.2 Line-Fit Modal Analysis	127
5.7 Numerical Case Studies	128
5.7.1 Mass Loading Effect	130
5.7.2 Shaker/Structure Interaction	131
5.7.3 Random Noise Effect	134
5.7.4 Averaging Effect	135
5.7.5 Leakage Error	137
5.8 Model Updating of Beam Structure	141
5.9 Conclusions	148
<i>CHAPTER 6 UPDATING OF DAMPED STRUCTURES</i>	149
6.1 <b>Preliminaries</b>	150
6.2 Complex Eigensensitivity	151
6.3 Application to the Bay Structure	157
6.3.1 Case 1 - Lightly Damped System	158
6.3.2 Case 2 - More Heavily Damped System	167
6.4 Conclusions	176

<i>CHAPTER 7 CONCLUSIONS</i>	177
7.1 General Conclusions	178
7.2 Contributions <b>of the</b> Present Research	183
7.3 Suggestions for Further Work	185
 <i>APPENDICES</i>	 186
APPENDIX <input type="checkbox"/> DERIVATION OF EIGENVALUE AND EIGENVECTOR DERIVATIVES	187
APPENDIX <input type="checkbox"/> <b>ELEMENT AND MACRO MATRICES</b>	190
APPENDIX <input type="checkbox"/> THE SINGULAR VALUE DECOMPOSITION	197
APPENDIX <input type="checkbox"/> DYNAMIC CHARACTERISTICS OF PUSH ROD	203
APPENDIX <input type="checkbox"/> GENFRF USER'S GUIDE	207
APPENDIX <input type="checkbox"/> BENDENTMJXHOD	236
 <i>REFERENCES</i>	 241

# CHAPTER 1

# **CHAPTER 1**

## **INTRODUCTION**

### **1.1 STRUCTURAL DYNAMICS ANALYSIS**

Due to increasing demands for better performance and the use of lighter structures in modern machinery, vibration engineers must have better testing and analysis tools than in the past. In the automotive industry, for example, weight reduction of a vehicle has been pursued for better fuel economy and vehicle speeds have become higher as engine performance has been improved, both of which result in various vibration and noise problems at high speed conditions. Yet, at the same time, requirements for reduction of vibration and noise are also increasing.

To solve vibration and noise problems in a structure, the dynamic behaviour of the structure needs to be understood and, subsequently, an accurate dynamic model needs to be developed. Analyses (or predictions) of the dynamic behaviour of the structure with such a model can reduce development cost and test effort. For example, the natural frequencies, at which the structure can be excited into resonance motion and may cause vibration and noise problems, calculated using the model can be used to modify the structural design in order to reduce vibration and noise by removing the natural frequencies outside the operating range. There are two ways of achieving a suitable

dynamic model of a structure: by theoretical prediction and by experimental measurement, respectively.

## 1.2 ANALYTICAL MODELLING - FE ANALYSIS

If the structure has a simple geometric shape and its physical properties are more or less uniform throughout, then a partial differential equation of motion of the form known as the 'wave equation' can be used to describe its dynamics. There are well-known solutions to the wave equation for simple structures such as beams, shafts, shells and plates. For complicated structures such as a vehicle body, however, these analytical approaches are often impractical because the approximations required are too restrictive to adequately describe their dynamics.

The requirement for a more generalised method of **modelling** the dynamics of large, complicated structures with nonhomogeneous physical properties has brought about the development of the finite element (FE) analysis. Due to advances in numerical methods and the availability of powerful computing facilities, FE analysis has become the most popular technique in structural dynamic analysis.

The fundamental principle of the FE method is to divide a complicated structure into many small elements such as plates, beams, shells, etc. The mass and stiffness matrices of an individual element, which is a simple, homogeneous element, can be obtained easily. The global mass and stiffness matrices of the structure can be assembled using these element matrices by considering connectivity and all the boundary conditions. Once the mathematical model has been built (or the mass and stiffness matrices have been constructed), the equations of motion can be solved by using various algorithms to obtain a description of the dynamic behaviour of the structure.

An FE model can be used to perform several types of analysis such as response prediction, structural coupling, stress analysis, life time prediction, structural dynamic modification, etc. Long before the construction of a real structure, it is possible to investigate its dynamic behaviour using the FE model so that any deficiencies in the design can be spotted early in the design stage where changes may cost much less than in the later stages.

FE models, however, can be inaccurate or even incorrect due to insufficient or inadequate modelling detail, geometrical over-simplification and uncertainties on the finite element input data. A survey which was carried out to assess the reliability of structural dynamic analysis capabilities [1] showed that numerical predictions (or FE analysis) of structural dynamic properties are not always as reliable as they are generally believed to be. This points to a need for vibration tests on the structure in order to confirm the validity of the FE model before it is used for detailed design analysis.

### **1.3 EXPERIMENTAL MODELLING - MODAL TESTING**

Apart from the aforementioned analytical approach to develop a dynamic model for a mechanical structure, another approach is to establish an experimental model for the structure by performing vibration tests and subsequent analysis on the measured data. This process is known as 'Modal Testing'. During the last two decades or so, modal testing has developed both in theory and in practice. Many techniques have been developed in order to extract more reliable modal parameters of structures from the test data. These techniques have been fruitful due largely to the introduction of the fast Fourier transform (FFT) algorithm and also to the development in recent years of powerful multi-channel FFT analysers and to fast data acquisition equipment. The availability of computer-controlled measurement equipment and special-purpose analysis

software has reduced the measurement time and human effort, and improved the reliability and accuracy of measured data and the modal properties extracted from them.

The principle of modal testing is to vibrate a structure with a known excitation so that natural frequencies, damping and mode shapes can be identified. There are two main excitation methods. These are referred to as single-point excitation and multi-point excitation (or normal mode method). The original multi-point excitation, which is the more traditional of the two and has been used in the aerospace industry to test large structures, attempts to excite the undamped (or normal) modes of a structure, one at a time, while the single-point excitation approach excites the structure to vibrate in several (all) of its modes simultaneously. There are many problems which make the multi-point excitation method difficult, time consuming and expensive to implement. The single-point excitation has gained much popularity in recent years because it is faster and easier to perform and is much cheaper to implement than multi-point excitation and is being used by many manufacturing industries, including the automotive industry. The single-point excitation method excites a structure at one coordinate and measures the consequent responses at all the coordinates of interest. A set of frequency response functions (**FRFs**) are obtained by dividing the Fourier transforms of the response signals by the transform of the input force. Modal parameters can be identified by performing further analysis (or curve-fitting) on this set of **FRFs**.

Not only is modal testing necessary to validate an FE model, it can be applied to various aspects. Modal testing can be used for troubleshooting vibration and noise problems in existing mechanical structures, which might be caused either by error in the design or construction of the structure or by wear, failure or malfunction in some of its components. Modal testing can also be used to construct dynamic models for components of a structure which are too difficult to model analytically.

## 1.4 LINKING FE ANALYSIS AND MODAL TESTING

At the design stage, an analytical model - especially an FE model - can be used to predict the vibration behaviour of a future structure and to modify the design of that structure if any deficiencies in the design are found before the structure is constructed. At later stage, when the structure has been constructed, modal testing can be performed to validate the FE model. Once the model is shown to predict measured behaviour with an acceptable accuracy, then it can be used for further analysis such as response prediction, structural coupling, stress analysis, life time prediction, etc.. However, test results are seldom in perfect agreement with the predictions of the FE model. Therefore the analyst and the experimentalist are faced with the problem of reconciling two modal databases for the same structure. Neither of these can be assumed to be perfect, but both have features which can be combined to give a more accurate description of the dynamics of the structure.

Because of the different limitations and assumptions implicit in the two approaches, the FE model and experimental modal model have different characteristics and different advantages and drawbacks. The FE model generally has a large number of coordinates so that the vibration characteristics can be described in detail and can cover a comparatively wide frequency range. However, due to **insufficient** or incorrect modelling, geometrical over-simplification and uncertainties on the element properties (especially the properties of joints which have not been fully explored), the FE model may well be inaccurate or even incorrect. In contrast, the experimental data or experimentally-derived modal properties are generally considered to be 'correct' or at least close to the true representation of the structure, because modal testing deals with the actual structure rather than an idealisation. However, due to the limited number of coordinates and modes which can be included (because of various restrictions in measurement), the information thus

obtained is available primarily as selected modal parameters, rather than the full spatial properties as provided by the FE model.

The principle of correlating the models derived from these two different approaches is to make use of the advantages of both and to overcome their disadvantages. Basically, it is believed that more confidence can be placed in the experimental modal data than in the FE model. Therefore, model updating schemes have been developed which aim to improve or to correct the initial FE model using **modal** test results.

## 1.5 DISCUSSION OF RELATED RESEARCH

Historically, model updating has been accomplished by a “trial-and-error” approach which was mainly dependent on the individual’s experience and intuition. With increasing complexity of the structures involved, model updating by this means becomes more difficult and systematic approaches are necessary. In recent years, a significant number of methods for updating an analytical model have been developed which use test data to identify or to improve an analytical model of a structure. One of the earliest publications is by **Rodden**[2] who used test data to identify directly structural influence coefficients. **Berman et. al.** [3] introduced a systematic approach in model updating: they improved an analytical mass matrix by finding the smallest changes which make a set of measured modes orthogonal and identified an ‘incomplete’ stiffness matrix by summing the contributions of the measured modes and with the use of the improved mass matrix. The stiffness matrix, however, does not resemble a true stiffness matrix. **Baruch et. al.** [4,5] formulated a procedure using Lagrange multipliers for minimising changes in matrices to satisfy specific constraints to update an analytical stiffness matrix under the assumption that the analytical mass matrix is correct. Later, having concluded that the assumption of a correct mass matrix is questionable, especially for a dynamic model which is often an approximate reduced version of a much larger model [6], **Berman et. al.** developed a

similar method for updating both the analytical mass and stiffness matrices [7] and applied the method to a practical structure [8]. Variations of these methods have been developed and investigated by **Wei**[9] and Caesar [10]. The aforementioned methods do not require iteration or eigenanalysis and the updated model possesses the ‘correct’ eigenvalues and eigenvectors. However, the modal parameters of the updated model outside the frequency range of the experimental data remain questionable and may become even worse than those of the original analytical model because the updated model does not seek to preserve the connectivity of the structure [11,12]. Another problem of those methods is that mode expansion is essential to overcome the inevitable incompatibility between the analytical model and the measured modes, and this may be an erroneous procedure, thus jeopardising model updating. Ibrahim [13] developed a method which used submatrices of system matrices as variables under the eigendynamic constraint. Thus, the physical connectivity of the analytical model can be preserved during the updating procedure. However, the updated model is not unique in the sense that it can be scaled by an arbitrary factor. Later, To [12] modified Ibrahim’s method by using the mass normalisation properties as another constraint to resolve the problem of uniqueness. These two methods, however, still require mode expansion to overcome the inevitable incompatibility between the analytical model and the measured modes.

Apart from these direct updating methods, Collins et. al. [14] introduced the concept of an inverse eigensensitivity method (**IEM**) in an iterative procedure to update an analytical model. Their method requires large computational effort because of the need for repeated solution of the eigendynamic problem and repeated calculation of the sensitivity matrix (or Jacobian matrix), especially for complicated structures with a large number of degrees of freedom. Later, Chen et. al. [15] introduced matrix perturbation theory to calculate the sensitivity matrix and to compute the new eigenvalues and eigenvectors. These iterative methods do not require mode expansion and the updated model preserves the physical connectivity. However, they do require large computational effort, and convergence is not guaranteed if the modelling errors are not small.

In addition to the methods summarised above, another approach to model updating has been developed under the assumption that the major errors in the analytical model are often isolated rather than distributed and thus that any attempt to update the whole analytical model is conceptually insufficient and practically unrealistic. Sidhu et. al. [16] developed the error matrix method (**EMM**) which aimed to locating major modelling errors in an analytical model rather than attempting to update the whole analytical model. Despite some advantages, this method does not succeed in locating **mismodelled** regions if the number of measured modes is insufficient. And when modelling errors are not small, this method cannot be applied because of the assumption that second- and **higher-order** terms in an expansion of  $[K]^{-1}$  and  $[M]^{-1}$  can be ignored. An alternative method was developed by He [17] to locate the modelling errors using a few measured modes available. Unlike the case of the EMM, there is no assumption that modelling errors are small, and error location is possible even with a very limited number of measured modes. Similar efforts for error location are also reported in Ref. [18] where the method is called 'force balance method'. The aforementioned error location methods require complete measured coordinates, which is not practical, or mode expansion to overcome the incompatibility between measured modes and analytical model, which, as mentioned before, may be an erroneous procedure thus jeopardising a successful location of the errors.

Zhang et. al. [19] employed the **IEM** to **localise** dominant error regions in an analytical model using real eigensolutions and then updated the model by correcting the selected parameters in an iterative calculation. As mentioned before, the **IEM** does not require mode expansion and its computational time will be reduced by locating error regions first and updating the analytical model using only the elements which are selected in error location procedure. However, the methods suggested by Zhang have been found to be unreliable.

## 1.6 PREVIEW OF THE THESIS

The objectives of this research are to develop a reliable, sensitive and systematic method for locating modelling errors in an analytical model using modal testing results and to develop an updating method which can produce an improved analytical model which can not only provide exact modal parameters measured in test but also predict correctly those modes outside frequency range of the experimental data and at the same time can reduce the number of experimental modes required as well as the computational time for updating.

Various methods to correct an analytical model using modal testing results are reviewed and their advantages and disadvantages (or limitations) are discussed in Chapter 2. All direct methods need a mode expansion procedure to overcome **the** incompatibility in the dimensions of the measured modes and the analytical model. The **IEM**, which is one of iterative methods, has an advantage over direct updating methods in the sense that it does not require a mode expansion procedure to be applied. However, convergence is not guaranteed if the modelling errors are not small. The convergence might be improved by locating error regions first and by correcting only **the** selected parameters by an iterative calculation. In Chapter 3, a version of the **IEM** using arbitrarily chosen macro elements is proposed at the error location stage in order to reduce the computational time and to reduce the number of experimental modes required. By this approach, the model updating problem which is generally underdetermined can be transformed into an over-determined one. The proposed method is applied to the GARTEUR structure which is used to represent a practical structure and to constitute a realistic problem in respect of the incompleteness of both measured modes and coordinates.

Even though many methods have been developed in recent years for updating analytical models for the dynamic analysis of a structure, and some of them have been proven to be quite successful, the methods are generally based on the assumption that the test data are

perfect or noise-free. For any updating method to be useful for application to practical structures, the sensitivity of the method to noise on the test data needs to be established. In Chapter 4, typical measurement errors are introduced by contaminating the modal parameters of the correct or modified structure with random noise of different levels and the method proposed in Chapter 3 is applied to a bay structure for which “experimental” data are noisy and incomplete.

The characteristics of real measurement errors might not result in random variations in the **modal** parameters. For the updating method to be useful in practical application, various error sources in testing should be considered in detail and more realistic **errors** rather than random noise should be introduced into the “experimental” data. In Chapter 5, various errors involved in modal parameter estimation are examined, and their effects on estimated **FRFs** and on the modal parameters extracted from the **FRFs** are also investigated. The resultant “experimental” modal data which contain representative experimental errors are used to update the corresponding analytical beam model to check the validity of the **IEM**.

Measured modal data are often complex because of inherent damping in real structures which can not be **modelled** by proportional damping, whereas the modal parameters of the corresponding analytical model are real. Updating methods developed so far generally assume that the experimental modal data are **real**, or postulate that the measured complex **data** have successfully been converted to real data. However, the deduced real modes may be erroneous because the experimentally-identified complex modes are : incomplete and the deduction itself relies on the analytical model which is erroneous. In Chapter 6, a modified version of **the** method suggested in Chapter 3 is developed to locate and to update damping elements together with mass and stiffness elements in analytical model using measured complex modal data. The proposed method is applied to the free-free bay structure which may constitute a realistic problem in respect of the incompleteness of both **measured** modes and coordinates

Finally, all the new developments in this thesis are reviewed in Chapter 7 together with suggestions for further research.

# CHAPTER 2

# CHAPTER 2

## MODEL UPDATING METHODS - A REVIEW

### 2.1 INTRODUCTION

One of the most important applications of modal testing is the validation of the mathematical model for the dynamic analysis of a structure - especially a finite element model - by comparing experimentally determined modal parameters with those obtained from the analytical model. Once the analytical model is shown to predict the measured behaviour, then it can be used with confidence for further analysis such as response prediction, structural coupling, stress analysis, life time prediction, etc. However, due to the difficulties of correct modelling, geometrical oversimplification and uncertainties on the finite element input data, the analytical model could be inaccurate or even incorrect. In contrast, modal testing is supposed to be capable of identifying the true modal parameters because it deals with real structures. Therefore, model updating schemes are developed which aim to improve or to correct the initial finite element model using modal test results.

Historically, model updating has been accomplished by a “trial-and-error” approach which was mainly dependent on the individual’s experience and intuition. With increasing

**complexity of the structures involved, model** updating becomes more difficult and systematic approaches are necessary.

## 2.2 MODEL UPDATING METHODS

In recent years, a significant number of methods for updating an analytical model have been developed, and these can be divided into direct methods and iterative methods. Direct methods usually require low computational effort, but the updated models do not always constitute physically meaningful models [ 11]. They tend to transform the physically meaningful models into-representative models. On the other hand, **iterative** methods require larger computational effort because of repeated solution of the eigendynamic problem and the pseudo-inversion of large matrices, though only some of these will always constitute physically meaningful models if they converge [20].

In the following **sections**, the advantages and disadvantages (or limitations) of various updating **methods** will be **reviewed/summarised**.

### 2.2.1 DIRECT METHODS

**Direct** updating methods seek to update a given mass matrix  $[M_A]$  and/or stiffness matrix  $[K_A]$  using measured eigenvalues  $[\Lambda_X]$  and eigenvectors  $[\Phi_X]$  under the equality constraints such as eigendynamic and orthogonality properties. These methods can themselves be **categorised** into two groups by the types of variables to be updated. The first group is to use individual elements of the system matrices as variables. Another group uses correction coefficients of element matrices as variables.

### 2.2.1.1 Berman's Method

A method for updating an analytical stiffness matrix was developed by Baruch under the assumption that the analytical mass matrix is correct [5]. Later, Berman et. al. developed a similar method for updating both the analytical mass and stiffness matrices [8]. Variations of these methods are given in Ref.[ 10]. The basic idea of the direct methods is to minimise the weighted Euclidian norm between the original incorrect matrices and the updated ones under the **equality** constraints.

In Berman's method [8], an **analytical** mass matrix is updated first and then, based on this updated mass matrix, the analytical stiffness matrix is updated. In his method, the objective function to be **minimised** for updating the mass matrix is

$$\epsilon = \| [M_A]^{-1/2} ([M_U] - [M_A]) [M_A]^{-1/2} \| \quad (2.1)$$

under the constraints

$$[M_U] = [M_U]^T \quad [\Phi_x]^T [M_U] [\Phi_x] = [I] \quad (2.2)$$

This minimisation problem can be easily solved using the method of Lagrange multipliers. Using Lagrange multipliers, a function to be minimised may be written

$$\Psi = \epsilon + \sum_{i=1}^m \sum_{j=1}^m \lambda_{ij} ([\Phi_x]^T [M_U] [\Phi_x] - [I]) \quad (2.3)$$

Equation (2.3) is differentiated with respect to each element of  $[M_U]$  and set to zero. Then using equation (2.2) to evaluate  $\lambda_{ij}$  yields the updated mass matrix which minimises  $\epsilon$  and satisfies equation (2.2):

$$[M_U] = [M_A] + [M_A] [\Phi_x] [m_a]^{-1} ([I] - [m_a]) [m_a]^{-1} [\Phi_x]^T [M_A] \quad (2.4)$$

where  $[m_a] = [\Phi_x]^T [M_A] [\Phi_x]$

Similarly, for updating a **stiffness** matrix, the objective function to be **minimised** can be **defined** as

$$\varepsilon = \| [M_U]^{-1/2} ( [K_U] - [K_A] ) [M_U]^{-1/2} \| \quad (2.5)$$

under the constraints

$$\begin{aligned} [K_U] [\Phi_x] &= [M_U] [\Phi_x] [\omega_x^2 \mathbf{1}], \\ [\Phi_x]^T [K_U] [\Phi_x] &= [\omega_x^2 \mathbf{I}] \\ [K_U] &= [K_U]^T \end{aligned} \quad (2.6)$$

Then the updated stiffness matrix becomes:

$$[K_U] = [K_A] + ( [\Delta] + [\Delta]^T ) \quad (2.7)$$

where  $[A] = \frac{1}{2} [M_U] [\Phi_x] ( [\Phi_x]^T [K_A] [\Phi_x] + [\omega_x^2 \mathbf{I}] ) [\Phi_x]^T [M_U] - [K_A] [\Phi_x] [\Phi_x]^T [M_U]$

This method does not require iteration or eigenanalysis and the updated model possesses the 'correct' eigenvectors and eigenvalues. However, the updated mass matrix using Berman's method cannot preserve the **connectivity** of the structure as shown in Refs [ 11, 12] because a connectivity constraint is not imposed. The updated stiffness matrix using the updated mass matrix, which is not correct, also cannot be correct. As a result, the updated model is not physically meaningful but is a representative model. Thus, the modal parameters of the updated model outside the range of the experimental data remain questionable and may become even worse than those of the original model. In general, an updated model should be able to be used for further analyses. A designer is not only interested in the correct representation of the dynamic characteristics of a structure but often he wants to use this model for stress analysis, life time prediction, etc. Another

problem of this method is **that** mode expansion is essential to overcome the inevitable incompatibility between the analytical model and the **measured** modes. Various expansion methods were investigated in Refs [21-23] but, so far, there is no expansion method which is satisfactory for **all** cases.

### 2.2.1.2 Eigendynamic Constraint Method

**As** mentioned before, the physical connectivity of the analytical models should be preserved during the updating process, and so the updated model should have the same connectivity as that of the original model. By using correction coefficients of submatrices of system matrices as variables instead of individual elements of system matrices, the connectivity constraint can be easily imposed. Ibrahim [13] developed a method which used submatrices of a system matrices as variables under the eigendynamic constraint. However, the updated model is not unique in the sense that it can be scaled by an arbitrary factor. The eigendynamic constraint method **described** below is similar to Ibrahim's method. However, the problem of uniqueness of the updated model was resolved by using the mass normalisation properties of measured modes as another constraint.

The method is formulated based on the eigendynamic equation and the mass normalisation relationship. For the **r<sup>th</sup>** mode

$$-\lambda_{xr} [M_U] \{\phi_x\}_r + [K_U] \{\phi_x\}_r = \{0\} \quad (2.8)$$

$$\{\phi_x\}_r^T [M_U] \{\phi_x\}_r = 1 \quad (2.9)$$

The updated mass and stiffness matrices can be written as

$$[M_U] = \sum_{j=1}^{L_1} a_j [M]_j \quad [K_U] = \sum_{j=1}^{L_2} b_j [K]_j \quad (2.10)$$

where  $a_j$  and  $b_j$  are correction factors to be determined and  $[M]_j$  and  $[K]_j$  are submatrices of system matrices such as

- 1) sub element matrices
- 2) finite element matrices
- 3) macro element matrices.

Substituting equation (2.10) into (2.8) results in a set of N linear algebraic equations:

$$[-\lambda_{xr}[M]_1 \{\phi_x\}_r \cdots -\lambda_{xr}[M]_{L_1} \{\phi_x\}_r \quad [K]_1 \{\phi_x\}_r \cdots [K]_{L_2} \{\phi_x\}_r] \begin{Bmatrix} a_1 \\ \cdot \\ a_{L_1} \\ b_1 \\ \cdot \\ b_{L_2} \end{Bmatrix} = \begin{Bmatrix} 0 \\ \cdot \\ \cdot \\ \cdot \\ 0 \end{Bmatrix} \quad (2.11)$$

Similarly, equation (2.9) becomes

$$[\{\phi_x\}_r^T [M]_1 \{\phi_x\}_r \cdots \{\phi_x\}_r^T [M]_{L_1} \{\phi_x\}_r \quad 0 \cdots 0] \begin{Bmatrix} a_1 \\ \cdot \\ a_{L_1} \\ b_1 \\ \cdot \\ b_{L_2} \end{Bmatrix} = 1 \quad (2.12)$$

Combining equation (2.11) and (2.12) yields:

$$\begin{bmatrix} -\lambda_{xr}[M]_1\{\phi_x\}_r & \dots & -\lambda_{xr}[M]_{L_1}\{\phi_x\}_r & [K]_1\{\phi_x\}_r & \dots & [K]_{L_2}\{\phi_x\}_r \\ \{\phi_x\}_r^T [M]_1\{\phi_x\}_r & \dots & \{\phi_x\}_r^T [M]_{L_1}\{\phi_x\}_r & 0 & \dots & 0 \end{bmatrix} \begin{Bmatrix} a_1 \\ \cdot \\ a_{L_1} \\ b_1 \\ \cdot \\ b_{L_2} \end{Bmatrix} = \begin{Bmatrix} 0 \\ \cdot \\ \cdot \\ 0 \\ \cdot \\ 1 \end{Bmatrix}$$

i.e.,

$$[A_T]_{(N+1) \times (L_1+L_2)} \{P\}_{(L_1+L_2) \times 1} = \{C_T\}_{(N+1) \times 1} \quad (2.13)$$

When there are  $m$  modes available, we can have  $m(N+1)$  linear algebraic equations:

$$\begin{bmatrix} [A_1] \\ [A_2] \\ \cdot \\ \cdot \\ \cdot \\ [A_m] \end{bmatrix} \{P\} = \begin{Bmatrix} \{C_1\} \\ \{C_2\} \\ \cdot \\ \cdot \\ \cdot \\ \{C_m\} \end{Bmatrix} \quad (2.14)$$

If  $m(N+1)$  is greater than number of unknowns,  $L_1+L_2$ , the problem becomes overdetermined and the SVD technique can be used to solve for the unknown vector (P) whose elements are the correction coefficients of system matrices.

This method does not require iteration or eigenanalysis and the updated model preserves the **connectivity** of the structure. However, like other direct methods, mode expansion is essential because of the large difference in the dimension between the measured modes and the analytical model. The number of coordinates measured is usually one or two orders of magnitude smaller than that in an analytical model. As can be seen in Refs [21-23], there is no effective expansion method so far.

### 2.2.2 COMPATIBILITY BETWEEN MEASURED MODES AND ANALYTICAL MODEL

One of the main problems of model updating is that experimental modal parameters are not directly compatible with those **from** the analytical model because:

- 1) the number of modes available **from** measurement ( $m$ ) is usually very limited ( $m \ll N$ ) and
- 2) the number of measured coordinates ( $n$ ) is less than the number of coordinates (or the number of **degrees** of freedom) of the analytical model ( $n < N$ ).

It is practically impossible to measure all the modes because of the limitation due to the characteristics of the experimental instruments such as accelerometers, force transducers, signal **analyser**, exciter, etc. The second restriction results from the fact that vibration measurements are too expensive to measure many coordinates and, some coordinates may be either technically difficult to measure, such as rotations, or physically inaccessible, such as the coordinates inside the structure.

The first restriction - incompleteness in the number of measured modes - can be resolved by using the corresponding modes from the analytical model and omitting the unmeasured modes which are usually the higher modes in practical situations. Therefore, there remains the problem of the large difference in the number of coordinates **between** the analytical model and measured modes. There are two possible solutions to this restriction:

- 1) expand the measured modes to include the unmeasured **coordinates** using an expansion method, or
- 2) use corresponding coordinates **from** the analytical model and omitting the unmeasured coordinates in model updating.

Until recently, model reduction techniques such as that suggested by **Guyan [24]** or the dynamic reduction technique **[25]** have been used to overcome the incompatibility. However, because the eigenproperties are not exactly **preserved** in a reduced model and the **connectivity** of the reduced model does not reflect the physical properties of the complete analytical model, **modelling** errors spread into neighbouring regions **[21]**, which makes model updating very difficult.

The alternative to reducing the analytical model is to expand the measured mode shapes. If mode expansion can be achieved successfully, the updating result can indicate mismodelled elements more precisely than the approximate error regions found when model reduction is used. Various mode expansion methods have been developed, and comparisons between various expansion methods can be found in **Refs.[22, 23]**. But until now, no expansion technique can interpolate the unmeasured coordinates satisfactorily.

The alternative approach to coping with the large difference in the number of coordinates between the analytical model and the measured modes is to use only the corresponding coordinates from the analytical model, omitting the unmeasured coordinates in model updating. As can be found in updating equations (equations **(2.4), (2.7), (2.13)**), this approach can not be applied to the direct methods because these methods require compatibility of all degrees of freedom between analysis and test. One of the most important advantages of an inverse eigensensitivity method (**IEM**), which will be explained later, is that it does not require mode expansion or model reduction because it is possible to use corresponding coordinates only.

### 2.2.3 ITERATION METHOD • INVERSE EIGENSENSITIVITY METHOD (IEM)

When the measured coordinates are incomplete, measured modes must be expanded for any direct method to be applied, which may be an erroneous procedure which jeopardises updating. The use of mode expansion can be avoided by using an **IEM** (or similar method) where only the coordinates which have been measured in the test are used for updating.

Collins et. al. [14] first introduced the **IEM** for model updating. Later, Chen et. al. [15] modified Collins' method by proposing a matrix perturbation method to calculate the sensitivity matrix and to compute the new modal parameters for the parameter estimation procedure.

The **IEM** uses modal parameters of an analytical model as initial values and the parameters are updated iteratively based on the differences between the analytical and measured values. Consider mathematically well-behaved functions  $f_i$  ( $i=1,2,\dots,m$ ) of  $L$  variables  $p_j$ ,  $j=1,2,\dots,L$ . If we denote  $\mathbf{p}$  as the entire vector of values  $p_j$ , then in the neighbourhood of  $\mathbf{p}_0$ , the functions can be expanded in a Taylor series:

$$f_i(\mathbf{p}) = f_i(\mathbf{p}_0) + \sum_{j=1}^L \frac{\partial f_i}{\partial p_j} \Delta p_j + \sum_{j=1}^L \sum_{k=1}^L \frac{\partial^2 f_i}{\partial p_j \partial p_k} \Delta p_j \Delta p_k + \dots \quad (2.15)$$

By neglecting terms of order  $\Delta \mathbf{p}^2$  and higher, equation (2.15) can be approximated as:

$$f_i(\mathbf{p}) - f_i(\mathbf{p}_0) = \sum_{j=1}^L \frac{\partial f_i}{\partial p_j} \Delta p_j \quad (2.16)$$

Inmanixform

$$\begin{Bmatrix} f_1(\mathbf{p}) - f_1(\mathbf{p}_0) \\ \vdots \\ f_m(\mathbf{p}) - f_m(\mathbf{p}_0) \end{Bmatrix} = \begin{bmatrix} \frac{\partial f_1}{\partial p_1} & \frac{\partial f_1}{\partial p_2} & \dots & \frac{\partial f_1}{\partial p_L} \\ \vdots & \vdots & \ddots & \vdots \\ \frac{\partial f_m}{\partial p_1} & \frac{\partial f_m}{\partial p_2} & \dots & \frac{\partial f_m}{\partial p_L} \end{bmatrix} \begin{Bmatrix} \Delta p_1 \\ \Delta p_2 \\ \vdots \\ \Delta p_L \end{Bmatrix} \quad (2.17)$$

For a structure under study, the parameters  $\mathbf{p}$  are to be identified and  $\mathbf{p}_0$  are the corresponding values used in the initial analysis. If the updated mass and stiffness matrices are written as in equation (2.10), the number of unknowns becomes  $L_1+L_2$ . Functions  $f_i(\mathbf{p})$  represent the measured modal parameters and  $f_i(\mathbf{p}_0)$  are the corresponding modal parameters obtained from the initial model. Equation (2.17) can be written as:

$$\begin{Bmatrix} \Delta \lambda_1 \\ \{\Delta \phi\}_1 \\ \vdots \\ \Delta \lambda_m \\ \{\Delta \phi\}_m \end{Bmatrix} = \begin{bmatrix} \frac{\partial \lambda_{A1}}{\partial a_1} & \dots & \frac{\partial \lambda_{A1}}{\partial a_{L1}} & \frac{\partial \lambda_{A1}}{\partial b_1} & \dots & \frac{\partial \lambda_{A1}}{\partial b_{L2}} \\ \frac{\partial \{\phi_A\}_1}{\partial a_1} & \dots & \frac{\partial \{\phi_A\}_1}{\partial a_{L1}} & \frac{\partial \{\phi_A\}_1}{\partial b_1} & \dots & \frac{\partial \{\phi_A\}_1}{\partial b_{L2}} \\ \vdots & \vdots & \vdots & \vdots & \ddots & \vdots \\ \frac{\partial \lambda_{Am}}{\partial a_1} & \dots & \frac{\partial \lambda_{Am}}{\partial a_{L1}} & \frac{\partial \lambda_{Am}}{\partial b_1} & \dots & \frac{\partial \lambda_{Am}}{\partial b_{L2}} \\ \frac{\partial \{\phi_A\}_m}{\partial a_1} & \dots & \frac{\partial \{\phi_A\}_m}{\partial a_{L1}} & \frac{\partial \{\phi_A\}_m}{\partial b_1} & \dots & \frac{\partial \{\phi_A\}_m}{\partial b_{L2}} \end{bmatrix} \begin{Bmatrix} \Delta a_1 \\ \vdots \\ \Delta a_{L1} \\ \Delta b_1 \\ \vdots \\ \Delta b_{L2} \end{Bmatrix} \quad (2.18)$$

or

$$\{\Delta\}_{m(n+1) \times 1} = [S]_{m(n+1) \times (L_1+L_2)} \{\Delta p\}_{(L_1+L_2) \times 1} \quad (2.19)$$

The elements of the sensitivity matrix [S] can be expressed as [see Appendix A]

$$\frac{\partial \lambda_r}{\partial p_i} = \{\phi\}_r^T \frac{\partial [K]}{\partial p_i} \{\phi\}_r - \lambda_r \{\phi\}_r^T \frac{\partial [M]}{\partial p_i} \{\phi\}_r \quad (2.20)$$

$$\frac{\partial \{\phi\}_r}{\partial p_i} = \sum_{j=1}^N c_{ij}^i \{\phi\}_j \quad (2.21)$$

$$c_{ij}^i = \begin{cases} \frac{\{\phi\}_j^T \left( \frac{\partial [K]}{\partial p_i} - \lambda_r \frac{\partial [M]}{\partial p_i} \right) \{\phi\}_r}{\lambda_r - \lambda_j} & (r \neq j) \\ -\frac{1}{2} \{\phi\}_j^T \frac{\partial [M]}{\partial p_i} \{\phi\}_r & (r = j) \end{cases}$$

If the number of **measured** modes  $m$  is greater than  $\left(\frac{L_1+L_2}{n+1}\right)$ , equation (2.19) becomes overdetermined and the unknown vector  $\{\Delta p\}$  can be calculated by premultiplying equation (2.19) by  $[S]^+$

$$\{\Delta p\} = [S]^+ \{\Delta\} \quad (2.22)$$

where  $^+$  is the Moore-Penrose **generalised** inverse. The corrections are then added to the solution vector

$$\{p\}_{\text{new}} = \{p\}_{\text{old}} + \{\Delta p\} \quad (2.23)$$

and the process is repeated iteratively to convergence because equation (2.18) is formulated based on first-order approximation. The flowchart of the whole procedure can be seen in Fig.2.1.

As explained previously, this method does not require mode expansion. In formulating equation (2.18), it is possible to use corresponding coordinates from the analytical mode shapes and to omit the unmeasured coordinates. The updated model will be physically meaningful model if it converges because physical **connectivity** is preserved. However, this method requires large computational effort because of repeated solution of the

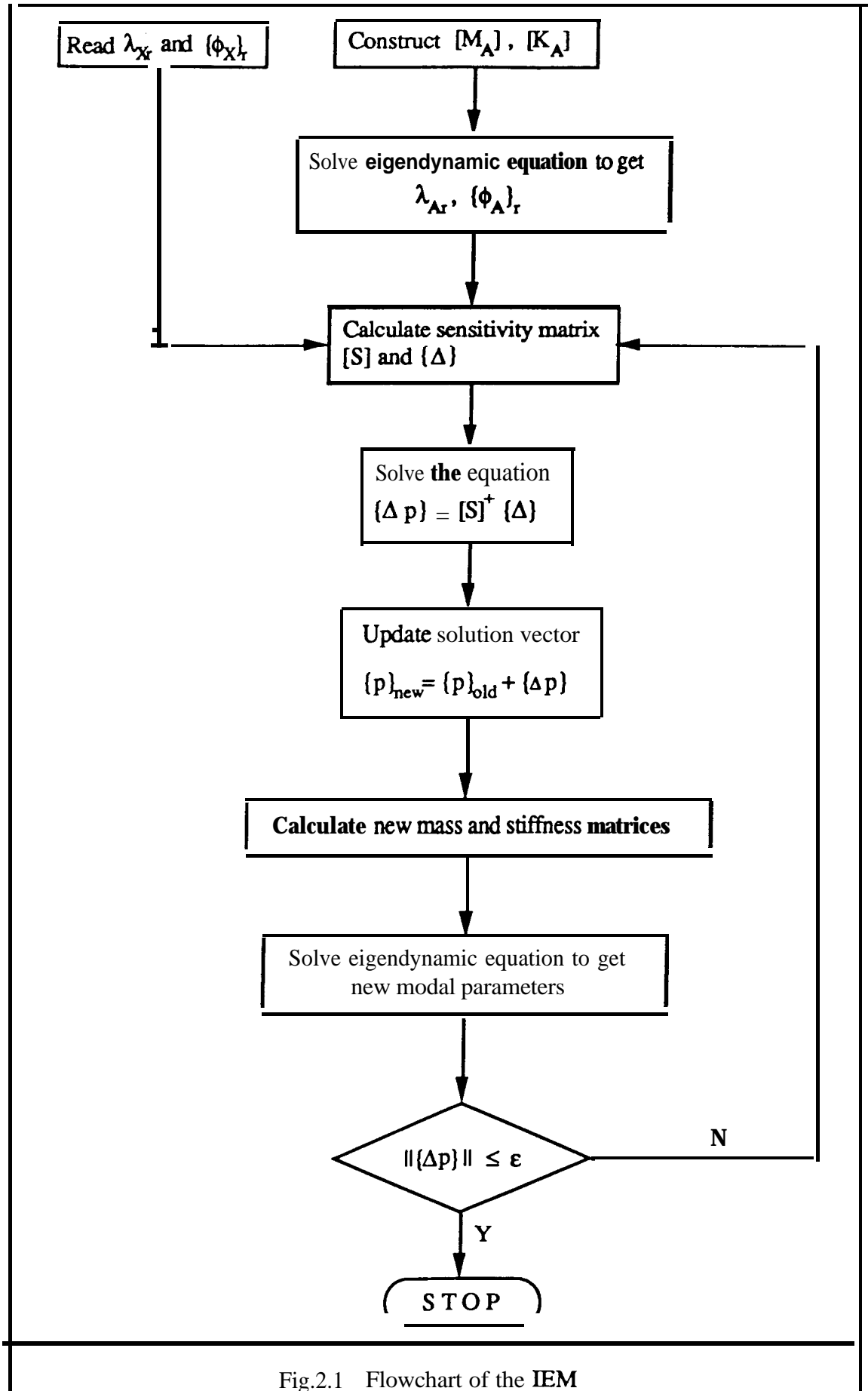


Fig.2.1 Flowchart of the IEM

cigendynamic problem and repeated calculation of the sensitivity matrix. Also, convergence is not guaranteed if modelling **errors** are not small.

## 2.3 ERROR LOCATION METHODS

In addition to the methods summarised above, another aspect of model updating is the location of mismodelled regions before an attempt is made to improve the analytical model. If this location is successful, then the model can be improved locally and this will be more efficient. Any attempt to update every element in the analytical model using only the limited information **from** the test results may not be physically realistic.

### 2.3.1 ERROR MATRIX METHOD (EMM)

The EMM [16] aims at locating major **modelling errors** in an analytical model rather than attempting to correct the whole analytical model. The difference between correct and an analytical stiffness matrices is **defined** as **stiffness** error matrix  $[\Delta K]$

$$[\Delta K] = [K_X] - [K_A] \quad (2.24)$$

If  $[\Delta K]$  is second-order in the sense of the Euclidean norm, **the error** matrix can be approximated as equation (2.25) by ignoring second and higher order terms in an expansion of  $[K_X]^{-1}$

$$[\Delta K] \cong [K_A] ([K_A]^{-1} - [K_X]^{-1}) [K_A] \quad (2.25)$$

$[K_X]^{-1}$  and  $[K_A]^{-1}$  can in turn be approximated using  $m$  measured and the corresponding analytical modes such that equation (2.25) becomes:

$$[\Delta K] \equiv [K_A] ( [\Phi_A] [\lambda_A]^{-1} [\Phi_A]^T - [\Phi_X] [\lambda_X]^{-1} [\Phi_X]^T ) [K_A] \quad (2.26)$$

where  $[\Phi_A]$  and  $[\Phi_X]$  are  $N \times m$  matrices and  $[\lambda_A]$  and  $[\lambda_X]$  are  $m \times m$  matrices.

Similarly, a mass error matrix can be expressed as:

$$[\Delta M] \equiv [M_A] ( [\Phi_A] [\Phi_A]^T - [\Phi_X] [\Phi_X]^T ) [M_A] \quad (2.27)$$

This method does not require the assumption that  $[M_A]$  is correct for locating stiffness modelling errors nor does it **require** the assumption that  $[K_A]$  is correct for locating mass modelling errors. Another advantage of the EMM is that it locates stiffness modelling errors using flexibility data where lower modes dominate. This accords with the fact that, in practical measurement, only the lower modes are readily available.

Despite these advantages, the **EMM** has some drawbacks. As shown in **Ref.[16]**, if the number of measured modes is insufficient, this method does not succeed in locating mismodelled regions. And when  $[AM]$  or  $[AK]$  is not small, this method cannot be applied because equation (2.25) and equation (2.27) are based on the assumption that second- and higher-order terms in an expansion of  $[K]^{-1}$  and  $[M]^{-1}$  can be ignored, respectively. Furthermore, this method requires mode expansion to overcome any incompatibility between the analytical model and measured modes.

## 23.2 MODIFIED EMM

In consideration of **the** limited number of measured modes available and inconclusive error location results, an alternative method [17] was developed to locate the **modelling** errors using a few measured modes available. This method uses the product of the error **matrix and a known matrix**:

$$\begin{aligned}
 [\Delta K] [\Phi_X] &= [K_X] [\Phi_X] - [K_A] [\Phi_X] \\
 &= [M_X] [\Phi_X] [\lambda_X] - [K_A] [\Phi_X] \\
 &= ([M_A] + [\Delta M]) [\Phi_X] [\lambda_X] - [K_A] [\Phi_X]
 \end{aligned} \tag{2.28}$$

Post-multiplying both sides of this equation by  $[\Phi_X]^T$  yields:

$$\begin{aligned}
 [\Delta K] ([\Phi_X] [\Phi_X]^T) - [\Delta M] ([\Phi_X] [\lambda_X] [\Phi_X]^T) \\
 = [M_A] ([\Phi_X] [\lambda_X] [\Phi_X]^T) - [K_A] ([\Phi_X] [\Phi_X]^T)
 \end{aligned} \tag{2.29}$$

Although error matrices cannot be obtained directly from this equation, the mismodelled regions can be revealed explicitly by estimating the right hand side of the equation which consists of known information. Similar efforts for error location are also reported in Ref. [18] where the method is called ‘force balance method’.

Unlike the case of the EMM, there is no assumption about  $[\Delta M]$  or  $[AK]$  and error location is possible even with a very limited number of measured modes. However, this method also requires complete measured coordinates, which is not practical, or mode expansion to overcome the incompatibility between measured modes and analytical model, which may be **erroneous** procedure thus jeopardising exact locating, as explained before.

### 2.3.3 IEM

Zhang et. al. [19] used the **IEM** to **localise** dominant error regions in an analytical **model** using real eigensolutions and then updated the model by correcting the selected parameters by an iterative calculation. To improve the condition of the sensitivity **matrix** in equation (2.18), the differences in eigenvalues and corresponding rows of the sensitivity matrix are divided by corresponding eigenvalues. Instead of solving equation (2.22) iteratively, they suggested two **error** location methods.

#### Method 1

A large element of the vector  $(Ap)$  represents either a dominant error region or a low sensitivity of the corresponding element. To distinguish the former **from** the latter, a sensitivity coefficient  $e_j$  is introduced to represent the sensitivity of the  $j$ th element:

$$e_j = \frac{\|\{\Delta_j\}\|}{\|\{\Delta\}\|} \quad (2.30)$$

where  $\{\Delta_j\} = \{S_j\} \Delta p_j$ ,  $\{S_j\}$  = the *j*th column of the sensitivity matrix. If both  $\Delta p_j$  and  $e_j$  are large, the corresponding element represents dominant errors, while the element which has large  $\Delta p_j$  but small  $e_j$  is not considered as a mismodelled **element**.

#### Method 2

A second method is to search for the best approximating **subspace** of a given dimension  $\delta$  which minimises the error

$$E = \Pi (A) - [S]^\delta \{\Delta p\}^\delta \quad (2.3.1)$$

where  $[S]^\delta$  is a submatrix of  $[S]$  and  $\{\Delta p\}^\delta$  is the corresponding subvector of  $(Ap)$ . An analysis of the errors obtained with subspaces of increasing dimension permits the selection of the most probable dominant errors.

As mentioned before, the **IEM** does not **require** mode expansion and computational time **will** be saved by locating **error** regions **first** and updating the analytical **model** using only those elements which are selected in error location procedure. However, the suggested methods have some problems. The sensitivity coefficient is independent of mismodelled regions. In other words, if an analytical model is **given, the** sensitivity coefficient of each element is constant irrespective of mismodelled regions. If **mismodelled** regions have low sensitivity, the first method cannot locate the error regions.

To illustrate this problem, the method has been applied to a bay structure shown in Fig.2.2, which is a part of the GARTEUR test case. The structure is **modelled** by 31 beam elements, and 3 **DoFs** are considered at each node, so that the total number of **DoFs** (**N**) is 90. Experimental data are obtained at 15 points as shown in Fig.2.2 in translational coordinates only (i.e.  $n = 30$ ). The first 10 experimental modes were used (i.e.  $m = 10$ ).

Two cases has been considered for comparison. In the first case, stiffness modelling errors are introduced by overestimating the stiffness matrices of the **12<sup>th</sup>**, 13<sup>th</sup> and 31<sup>st</sup> elements by 100 %, as shown in Fig.2.3. The first 10 ‘experimental’ and initial analytical natural frequencies are shown in Table 2.1.

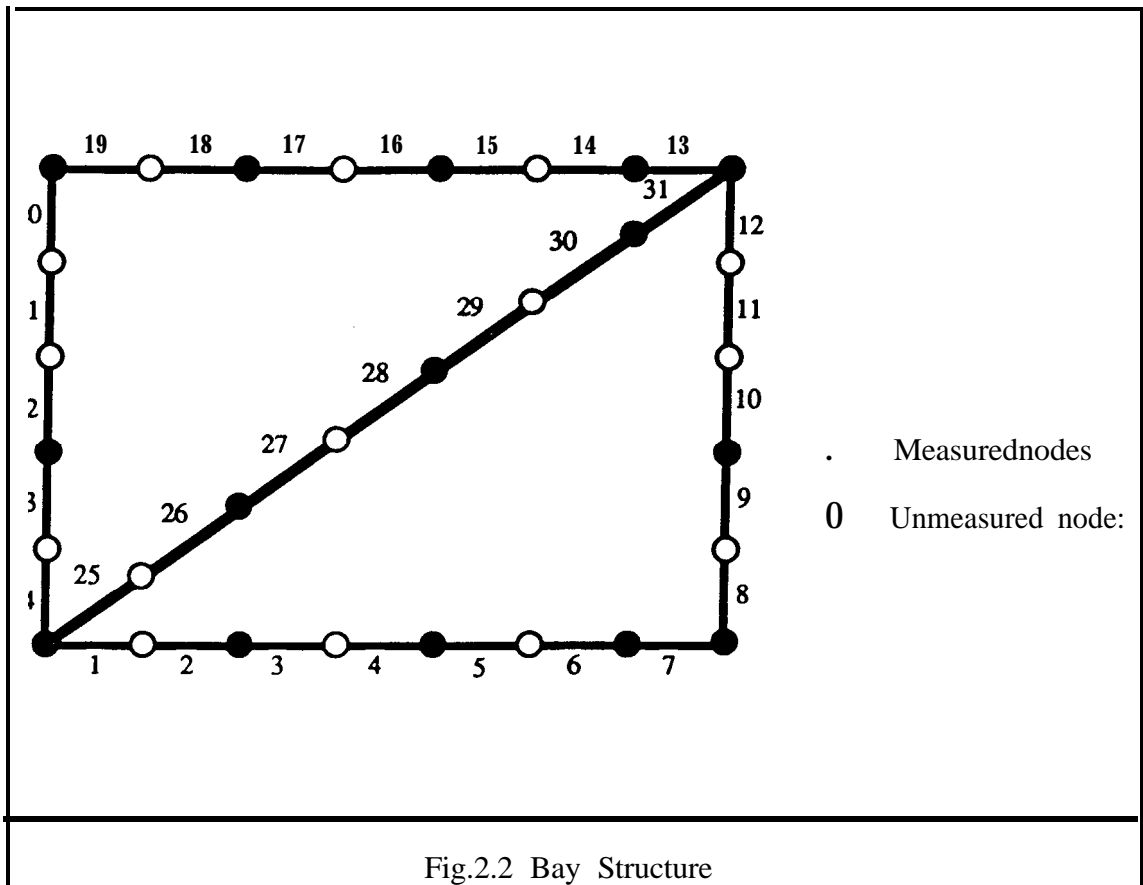
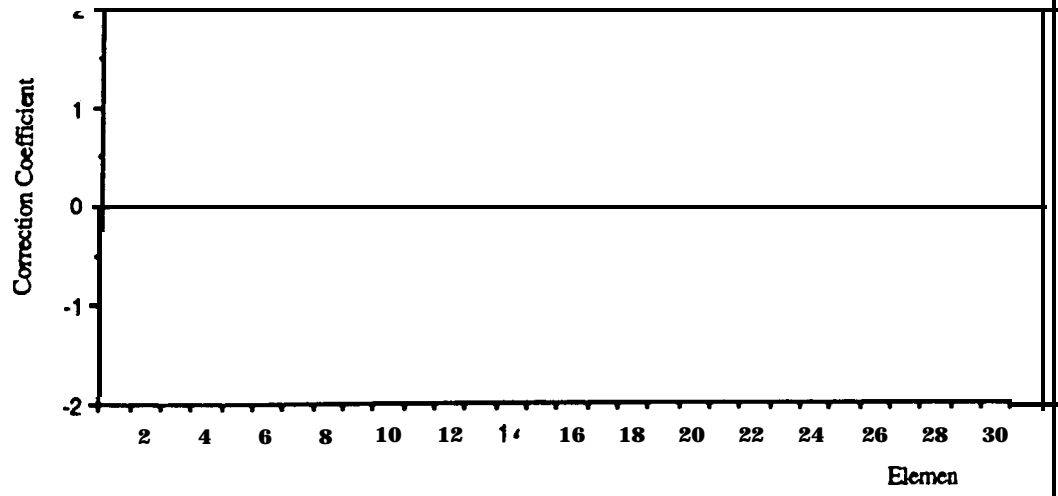


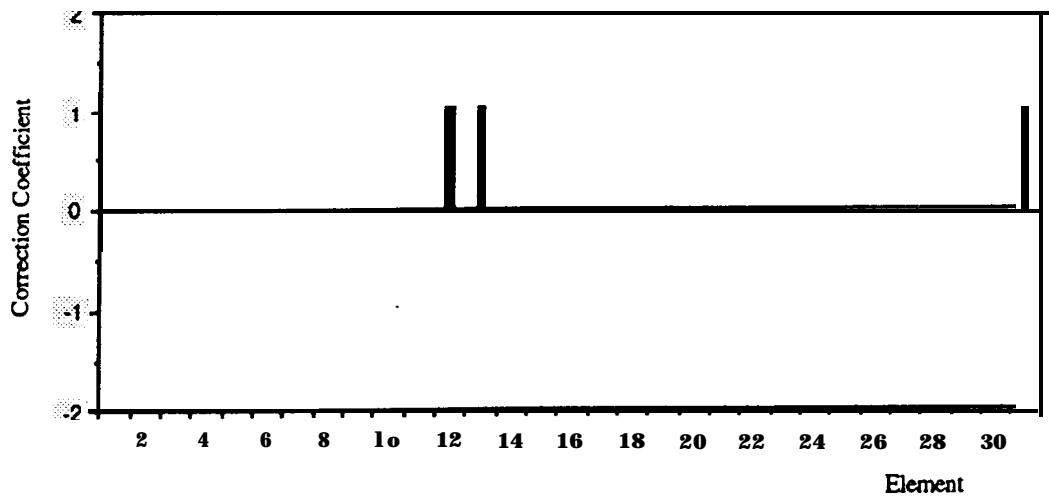
Table 2.1 Natural Frequencies of 'Experimental' and Initial Analytical Models (Case 1)

Mode	1	2	3	4	5	6	7	8	9	10
$f_x$ (Hz)	348.1	482.2	548.9	584.5	707.9	862.1	920.7	994.7	1101.1	1215.6
$f_A$ (Hz)	342.3	450.6	528.5	557.2	683.4	833.7	903.2	927.0	1066.6	1165.3
MAC	0.996	0.975	0.960	0.985	0.965	0.987	0.967	0.916	0.875	0.932

The sensitivity coefficients and  $(A_p)$  are shown in Fig.2.4 and Fig.2.5 with possible error regions. In this case, mismodelled regions which have relatively high eigensensitivity could be located with some extra elements.

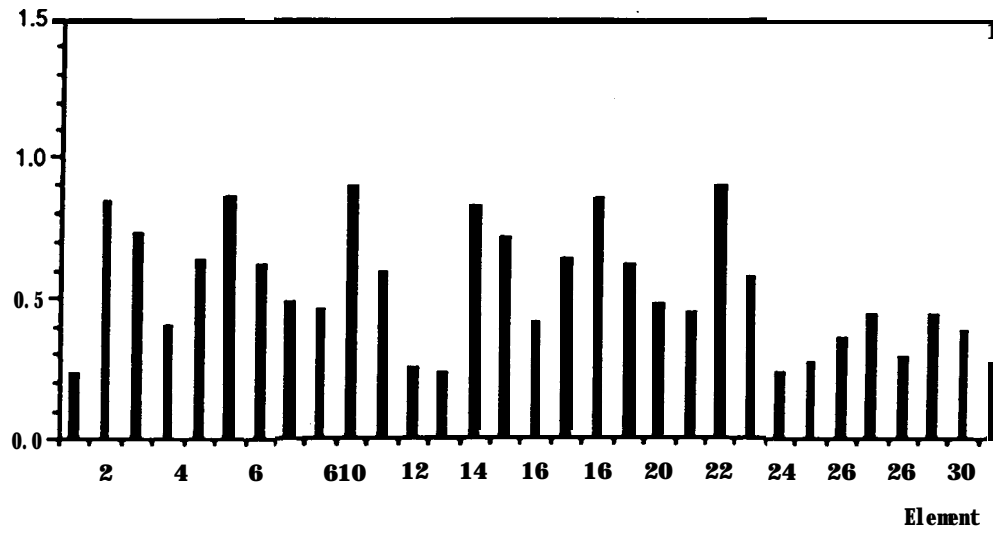


(a) MassErrors

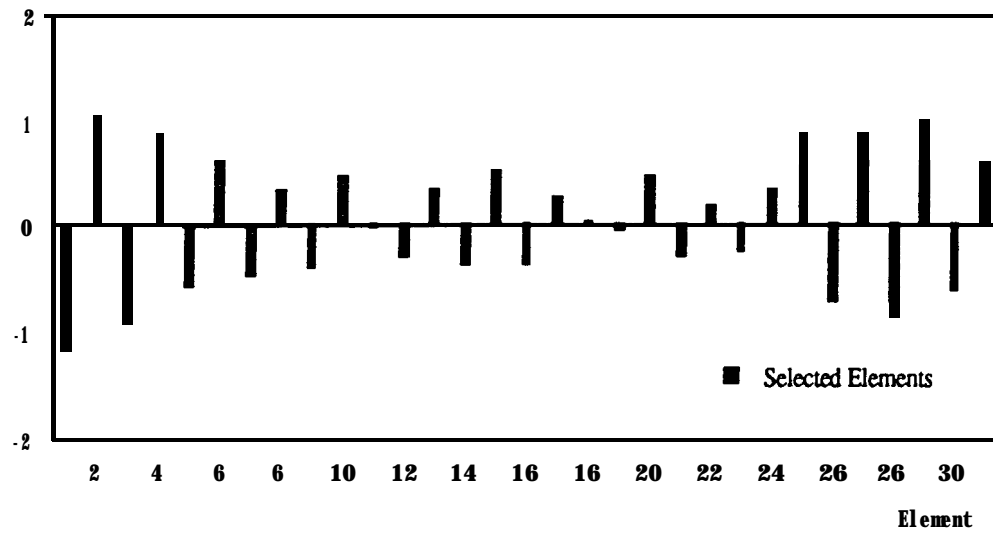


(b) Stiffness Errors

Fig.2.3 Modelling Errors

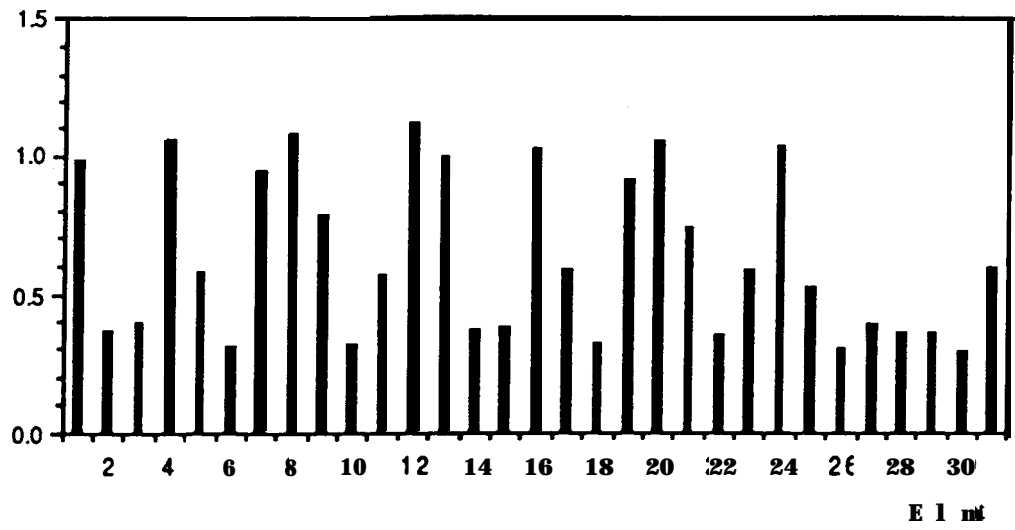


(a) Eigensensitivity of Mass Element

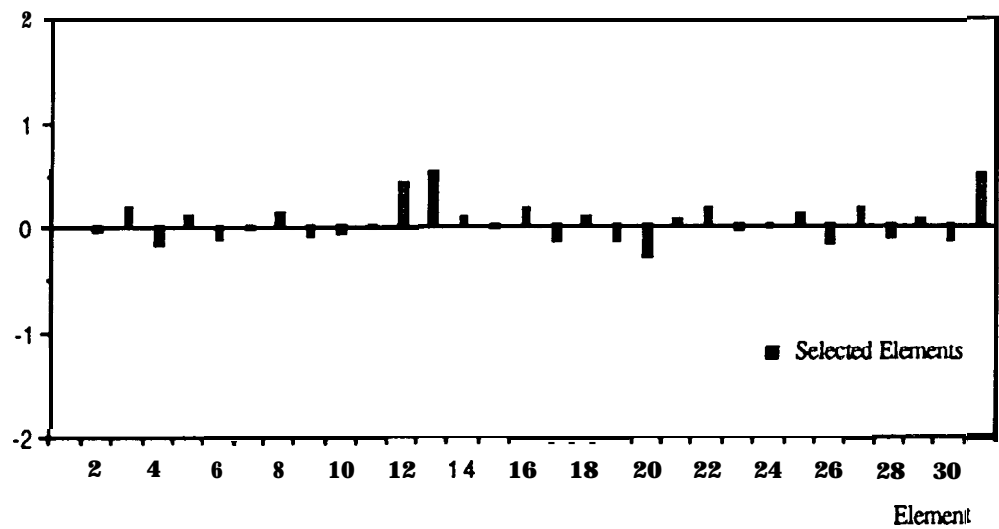


(b) Correction Coefficient

Fig.2.4 Error Location Results (Case 1 ; Mass Elements)



(a) Eigensensitivity of Stiffness Elements



(b) Correction Coefficient

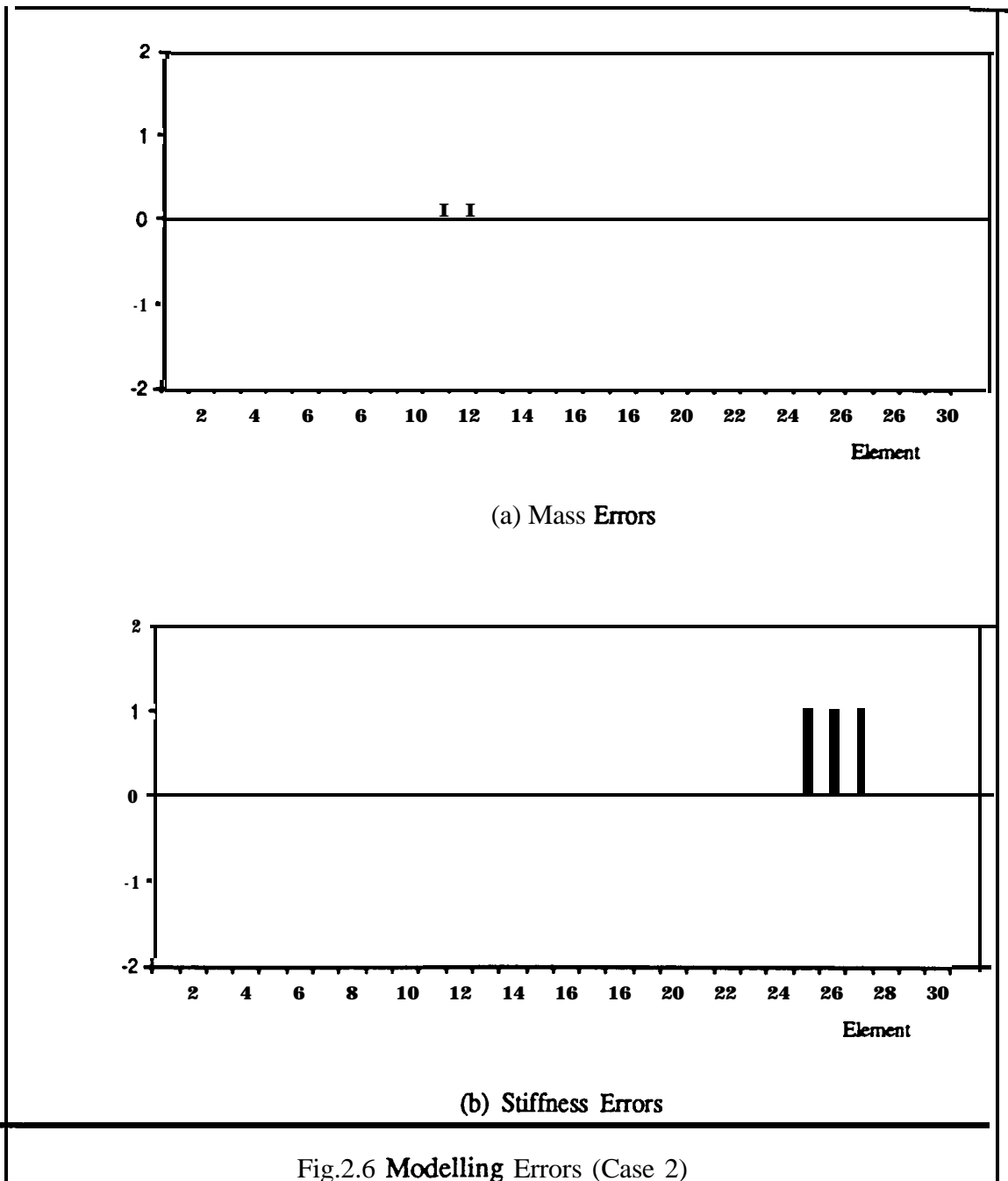
Fig.2.5 Error Location Results (Case1 ; Stiffness Elements)

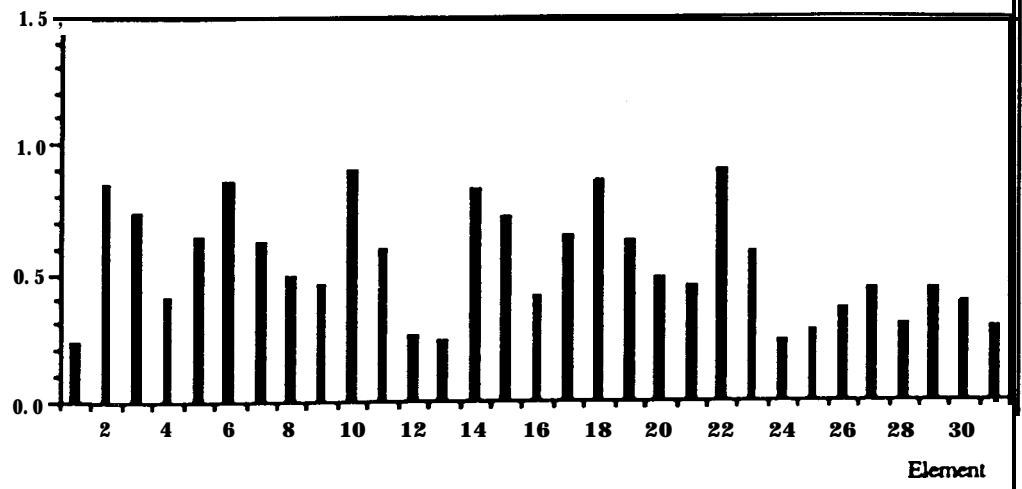
In the second case, mass and stiffness modelling errors are introduced by overestimating the mass matrices of the 1<sup>st</sup> and 12th elements by **50 %** and the stiffness matrices of the **25<sup>th</sup>**, 26th and 27th elements by **100 %**, as shown in Fig.2.6. The **first** 10 'experimental' and initial analytical natural frequencies are shown in Table 2.2.

**Table 2.2 Natural Frequencies of 'Experimental' and Initial Analytical Models (Case 2)**

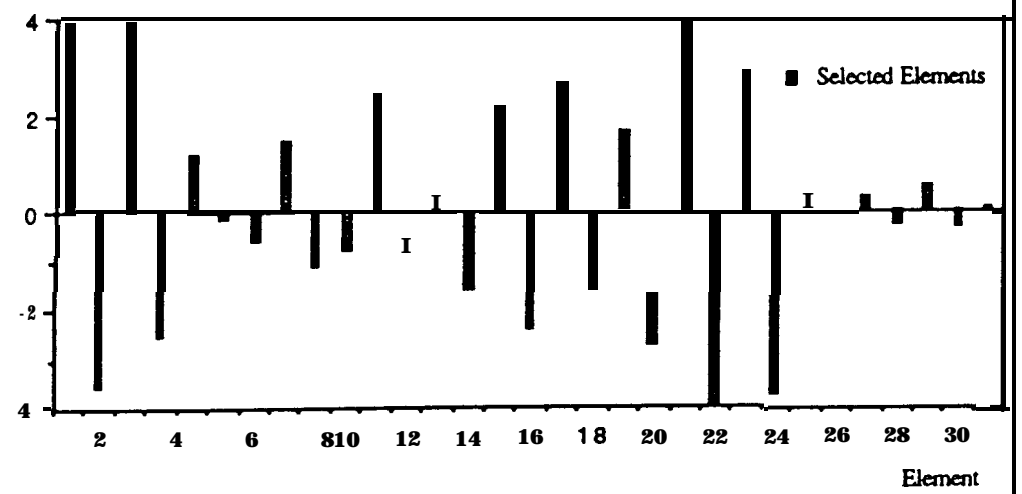
Mode	1	2	3	4	5	6	7	8	9	10
$f_x$ (Hz)	341.4	514.1	526.6	577.9	690.2	843.9	909.6	1014.1	1037.3	1153.5
$f_A$ (Hz)	342.3	450.6	528.5	557.2	683.4	833.7	903.2	927.0	1066.6	1165.3
MAC	0.973	0.931	0.964	0.987	0.953	0.947	0.986	0.898	0.925	0.813

The sensitivity coefficients and  $(A_p)$  are shown in Fig.2.7 and Fig.2.8 with possible **error** regions. In this case, error location failed because some mismodelled elements have relatively low eigensensitivity.



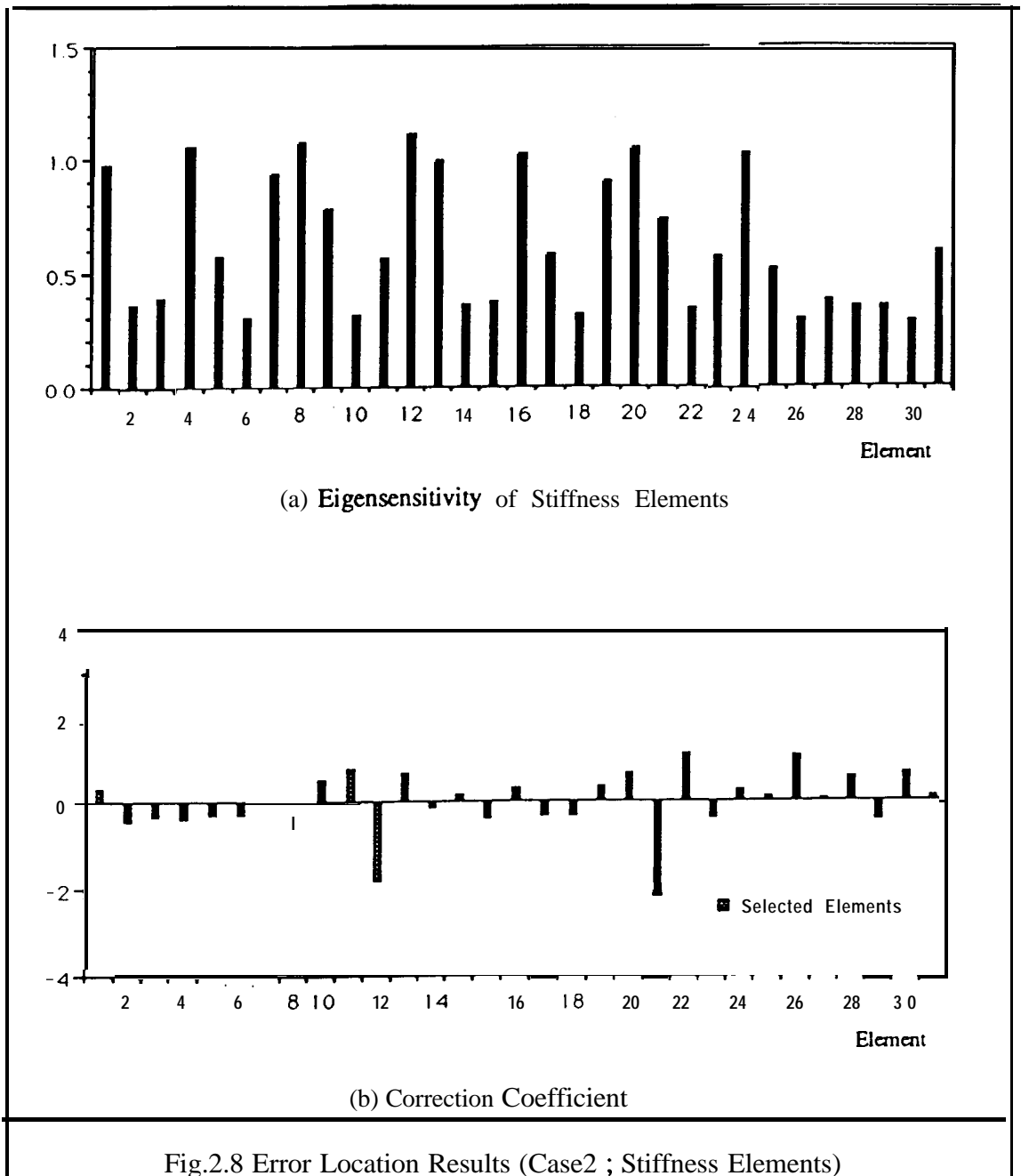


(a) Eigensensitivity of Mass Elements



(b) Correction Coefficient

Fig.2.7 Error Location Results (Case2 ; Mass Elements)



The second method has been applied to the same structure. In both cases error location failed as shown in Tables 2.3 and 2.4 - in the first case the 13<sup>th</sup> stiffness element was not located and in the second case the 27<sup>th</sup> stiffness element was not located.

**Table 2.3 Error Location Results (Case 1)**

$\delta$	Located Elements	$\{\Delta p\}$	$E_{min}$
1	K31	0.55	0.448
2	K31 K12	0.56 -0.06	0.504
3	K31 K12 M4	0.59 0.23 -0.01	0.514
4	K31 K12 M4 M26	0.56 0.24 0.43 -0.11	0.522
5	K31 K12 M4 M26 M1	0.48 0.23 0.45 0.26 -0.06	0.531
6	K31 K12 M4 M26 M1 M8	0.44 0.25 0.41 0.29 0.46 -0.14	0.534
7	K31 K12 M4 M26 M1 M8 M23	0.43 0.20 0.42 0.30 0.47 -0.45 -0.13	0.534
8	K31 K12 M4 M26 M1 M8 M23 M5	0.44 0.18 0.42 0.27 0.33 0.08 0.19 -0.13	0.512
9	K31 K12 M4 M26 M1 M8 M23 M5 M3	0.42 0.14 0.20 0.32 0.20 0.05 0.34 0.25 -0.12	0.528
10	K31 K12 M4 M26 M1 M8 M23 M5 M3	0.41 0.14 0.13 0.34 0.09 0.02 0.40 0.22 0.11 -0.12	0.539

(*cf.* actual mismodelled element s; K12, K13, K31)

Table 2.4 Error Location Results (Case 2)

$\delta$	Located Elements	$\{\Delta p\}$	$E_{\min}$
1	K25	0.17	0.455
2	K25 K26	0.97 0.20	0.567
3	K25 K26 M11	0.67 0.69 0.22	0.592
4	K25 K26 M11 K28	0.63 0.64 0.42 0.19	0.606
I	K25 K26 M11 K28 K9	0.26 1.05 0.40 0.46 0.18	0.627
6	K25 K26 M11 K28 K9 K30	0.34 0.94 0.24 0.38 -0.16 0.18	0.638
7	K25 K26 M11 K28 K9 K30 M12	0.27 1.02 0.26 0.41 -0.13 0.38 0.11	0.659
8	K25 K26 M11 K28 K9 K30 M12 K12	0.30 0.97 0.21 0.39 -0.15 0.36 0.14 0.11	0.638
9	K25 K26 M11 K28 K9 K30 M12 K12 M16	0.32 0.95 0.13 0.37 -0.09 0.35 0.28 -0.08 0.10	0.662
10	K25 K26 M11 K28 K9 K30 M12 K12 M16 K31	0.30 0.95 0.11 0.38 -0.10 0.35 0.27 -0.08 0.07 0.10	0.663

(cf. actual mismodelled elements; M1 1, M12, K25, K26, K27)

## 2.4 CONCLUDING REMARKS

An attempt has been made to review various updating methods which can be divided into two groups - direct methods and iterative methods. Direct methods are usually very fast and some methods produce exact modal parameters, but mode expansion is essential because of the large difference in the dimension between measured modes and the analytical model. The problem of mode expansion is that this procedure might be erroneous, thus jeopardising model updating procedure. On the other hand, iteration methods such as **IEM** do not **require** mode expansion procedure and the updated model can preserve physical **connectivity** and may become physically meaningful model - if it converges. However, this method requires large computational effort because of repeated solution of the eigendynamic problem and repeated calculation of the sensitivity matrix. Also, convergence is not guaranteed if **modelling errors** are not small.

Any attempt to update every element in the analytical model using only the limited information from typical test results may not be realistic. If mismodelled regions can be located in a **preliminary** step, model updating can be carried out more efficiently and more successfully. Therefore, error location is a fundamental **first** objective of the updating process.

Recent developments in the area of error location have been investigated. The **EMM** can locate mismodelled regions successfully even with a very limited number of measured modes if complete coordinates are measured, which is not practical assumption. Again, for the EMM to be successful, a reliable mode expansion method should be available.

The **IEM** does not require mode expansion and its computational time will be reduced by locating error regions **first** and updating the analytical model using only the elements which are selected in error location procedure. However, the methods suggested by



---

**Zhang** have been found to be unreliable. **Therefore**, more reliable error location method should be developed.

# CHAPTER 3

# CHAPTER 3

## MODEL UPDATING USING **IEM**

### 3.1 PRELIMINARIES

In the last Chapter, advantages and disadvantages (or limitations) of various model updating methods were discussed and it was noted that all direct methods needed mode expansion - and if this were erroneous, this might jeopardise the model updating procedure - to overcome the incompatibility in the dimensions of the measured modes ( $n$ ) and the analytical model ( $N$ ).

The **IEM**, which is one of iterative methods, has an advantage over direct updating methods in the respect that it does not require a mode expansion procedure. However, convergence is not guaranteed if modelling errors are not small. The convergence might be improved by locating error regions **first** and by correcting only the selected parameters by an iterative calculation. The methods suggested by Zhang [ 19] which are based on the **IEM** do not seem to be reliable as shown in the case studies in the previous Chapter.

In this Chapter, a version of the **IEM** using arbitrarily chosen macro elements, which is one of the iterative methods, is proposed at the error location stage in order to reduce the computational time and to reduce the number of experimental modes required. By this

approach, the model updating problem which is generally under-determined can be transformed into an over-determined one.

## 3.2 ERROR LOCATION PROCEDURE

### 3.2.1 SELECTION OF SUBMATRICES

The updated mass and stiffness matrices can be expressed as functions of the analytical ones, in the form:

$$[M_U] = \sum_{i=1}^L a_i [M]_i \quad (3.1)$$

$$[K_U] = \sum_{i=1}^L b_i [K]_i \quad (3.2)$$

where  $L$  is the number of elements and  $a_i$  and  $b_i$  are correction coefficients to be determined. If there is no error in the  $i^{\text{th}}$  element,  $a_i$  and  $b_i$  should be unity, whereas  $a_i$  or  $b_i \ll 1$  (or  $\gg 1$ ) indicates a mismodelled element.  $[M]_i$  and  $[K]_i$  are submatrices of system matrices and can be one of these forms:

- 1) subelement matrices
- 2) element matrices used for FE modelling
- 3) macro element matrices

The success of the IEM depends heavily on the choice of the submatrices  $[M]_i$  and  $[K]_i$ . If the structure under consideration is a complicated structure - most practical structures are usually very complicated, it might have many elements and data from experiment are usually very limited in the respect of the number of measured modes and the number of measured coordinates. In such a case, model updating using the IEM with element

matrices or subelement matrices requires quite a large computational effort and the result usually does not converge. The alternative is to use macro elements as submatrices.

The mass matrix of the  $i^{\text{th}}$  macro element  $[\mathbf{M}]_i$  is formed as a summation of individual element mass matrices

$$[\mathbf{M}]_i = \sum_{j=1}^{n_i} [\mathbf{M}^e]_j \quad (3.3)$$

where  $n_i$  is the number of mass elements in the  $i^{\text{th}}$  macro element and  $[\mathbf{M}^e]_j$  is the element mass matrix of the  $j^{\text{th}}$  element. The construction of the macro element is illustrated in Appendix B.

Similarly, for the stiffness matrix

$$[\mathbf{K}]_i = \sum_{j=1}^{n_i} [\mathbf{K}^e]_j \quad (3.4)$$

The influence of choice of macro elements on error location will be investigated later in this Chapter.

### 3.3.2 EIGENSENSITIVITY

If we denote  $(p)$  as the vector of correction coefficients  $(a_1, a_2, \dots, a_L, b_1, b_2, \dots, b_L)^T$ , then in the neighbourhood of  $(p_0) = \{1, 1, \dots, 1, 1, 1, \dots, 1\}^T$ , the  $r^{\text{th}}$  eigenvalue of the updated model can be expanded in a Taylor series:

$$\lambda_{Xr} = \lambda_{Ar} + \sum_{j=1}^{2L} \frac{\partial \lambda_{Ar}}{\partial p_j} \Delta p_j + \sum_{j=1}^{2L} \sum_{k=1}^{2L} \frac{\partial^2 \lambda_{Ar}}{\partial p_j \partial p_k} \Delta p_j \Delta p_k + \dots \quad (3.5)$$

By neglecting the second- and higher-order terms, equation (3.5) can be approximated as:

$$\lambda_{Xr} - \lambda_{Ar} = \Delta\lambda_r \approx \sum_{j=1}^{2L} \frac{\partial \lambda_{Ar}}{\partial p_j} \Delta p_j \quad (3.6)$$

Similarly, for the  $r^{\text{th}}$  eigenvector

$$\{\Delta\phi\}_r \approx \sum_{j=1}^{2L} \frac{\partial \{\phi_A\}_r}{\partial p_j} \Delta p_j \quad (3.7)$$

Inmatrixform

$$\begin{Bmatrix} \Delta\lambda_r \\ \{\Delta\phi\}_r \end{Bmatrix} = \begin{bmatrix} \frac{\partial \lambda_{Ar}}{\partial a_1} & \dots & \frac{\partial \lambda_{Ar}}{\partial a_L} & \frac{\partial \lambda_{Ar}}{\partial b_1} & \dots & \frac{\partial \lambda_{Ar}}{\partial b_L} \\ \frac{\partial \{\phi_A\}_r}{\partial a_1} & \dots & \frac{\partial \{\phi_A\}_r}{\partial a_L} & \frac{\partial \{\phi_A\}_r}{\partial b_1} & \dots & \frac{\partial \{\phi_A\}_r}{\partial b_L} \end{bmatrix} \begin{Bmatrix} \Delta a_1 \\ \vdots \\ \Delta a_L \\ \Delta b_1 \\ \vdots \\ \Delta b_L \end{Bmatrix} \quad (3.8)$$

or

$$\{\Delta_r\}_{(n+1) \times 1} = [S_r]_{(n+1) \times 2L} \{\Delta p\}_{2L \times 1} \quad (3.9)$$

The elements of the sensitivity matrix  $[S_r]$  can be obtained by taking derivatives of the following equations

$$([K] - \lambda_r [M]) \{\phi\}_r = \{0\}$$

$$\{\phi\}_r^T [M] \{\phi\}_r = 1$$

with respect to the correction coefficients as: [see Appendix A]

$$\frac{\partial \lambda_r}{\partial p_i} = \{\phi\}_r^T \frac{\partial [K]}{\partial p_i} \{\phi\}_r - \lambda_r \{\phi\}_r^T \frac{\partial [M]}{\partial p_i} \{\phi\}_r \quad (3.10)$$

$$\frac{\partial \{\phi\}_r}{\partial p_i} = \sum_{j=1}^N c_{rj}^i \{\phi\}_j \quad (3.11)$$

$$c_{rj}^i = \begin{cases} \frac{\{\phi\}_j^T \left( \frac{\partial [K]}{\partial p_i} - \lambda_r \frac{\partial [M]}{\partial p_i} \right) \{\phi\}_r}{\lambda_r - \lambda_j} & (r \neq j) \\ -\frac{1}{2} \{\phi\}_j^T \frac{\partial [M]}{\partial p_i} \{\phi\}_r & (r = j) \end{cases}$$

From equations (3.1) and (3.2), we can obtain

$$\begin{aligned} \frac{\partial [M]}{\partial a_i} &= [M]_i & \frac{\partial [M]}{\partial b_i} &= [0] \\ \frac{\partial [K]}{\partial a_i} &= [0] & \frac{\partial [K]}{\partial b_i} &= [K]_i \end{aligned} \quad (3.12)$$

Substituting equation (3.12) into equations (3.10) and (3.11) leads to

$$\frac{\partial \lambda_r}{\partial a_i} = -\lambda_r \{\phi\}_r^T [M]_i \{\phi\}_r \quad (3.13a)$$

$$\frac{\partial \lambda_r}{\partial b_i} = \{\phi\}_r^T [K]_i \{\phi\}_r \quad (3.13b)$$

$$\frac{\partial \{\phi\}_r}{\partial a_i} = \sum_{j=1}^N \alpha_{rj}^i \{\phi\}_j \quad (3.14a)$$

$$\alpha_{rj}^i = \begin{cases} -\frac{\lambda_r \{\phi\}_j^T [M]_i \{\phi\}_r}{\lambda_r - \lambda_j} & (r \neq j) \\ -\frac{1}{2} \{\phi\}_j^T [M]_i \{\phi\}_r & (r = j) \end{cases}$$

$$\frac{\partial \{\phi\}_r}{\partial b_i} = \sum_{j=1}^N \beta_{rj}^i \{\phi\}_j \quad (3.14b)$$

$$\beta_{rj}^i = \begin{cases} \frac{\{\phi\}_i^T [K]_i \{\phi\}_r}{\lambda_r - \lambda_j} & (r \neq j) \\ 0 & (r = j) \end{cases}$$

Equation (3.14) requires  $N$  eigenvectors for the calculation of the eigenvector derivatives. For a large system, only the lowest  $n_1$  modes ( $n_1 \ll N$ ) can be expected to be computed accurately. In addition, it may take long time to obtain  $N$  eigenvectors at each iteration

Lim et. al. [26] proposed a new method which could reduce the number of eigenvectors **required** for the calculation of the eigenvector derivatives. When  $r \ll n_1$ , the denominator of  $C_{rj}^i$  in equation (3.11) can be approximated as:

$$\lambda_r - \lambda_j \approx \lambda_c - \lambda_j \quad \text{for } j > n_1$$

where  $\lambda_c$  is a value between 0 and the first non-zero eigenvalue.

Thus,

$$\begin{aligned} \frac{\partial \{\phi\}_r}{\partial p_i} &\approx \sum_{j=1}^{n_1} c_{rj}^i \{\phi\}_j + \sum_{j=n_1+1}^N \frac{\{\phi\}_j^T \{g\}_r}{\lambda_c - \lambda_j} \{\phi\}_j \\ &\approx \sum_{j=1}^{n_1} c_{rj}^i \{\phi\}_j + \sum_{j=1}^N \frac{\{\phi\}_j^T \{g\}_r}{\lambda_c - \lambda_j} \{\phi\}_j - \sum_{j=1}^{n_1} \frac{\{\phi\}_j^T \{g\}_r}{\lambda_c - \lambda_j} \{\phi\}_j \end{aligned} \quad (3.15)$$

where

$$\{g\}_r = \left( \frac{\partial [K]}{\partial p_i} - \lambda_r \frac{\partial [M]}{\partial p_i} \right) \{\phi\}_r$$

From the orthogonality conditions

$$[\Phi]^T[K][\Phi] = [\Lambda]$$

$$[\Phi]^T[M][\Phi] = [I]$$

we get

$$[\Phi]^T[K - \lambda_c M][\Phi] = [\Lambda] - \lambda_c [I]$$

or

$$[\Phi]^{-1}[K - \lambda_c M]^{-1}[\Phi]^{-T} = ([\Lambda] - \lambda_c [I])^{-1}$$

Thus,

$$[K - \lambda_c M]^{-1} = [\Phi] ([\Lambda] - \lambda_c [I])^{-1} [\Phi]^T$$

$$= \sum_{j=1}^N \frac{\{\phi\}_i \{\phi\}_i}{\lambda_j - \lambda_c} \quad (3.16)$$

Substituting equation (3.16) into equation (3.15)

$$\frac{\partial \{\phi\}_r}{\partial p_i} \approx \sum_{j=1}^{n_1} c_{rj}^i \{\phi\}_j - [K - \lambda_c M]^{-1} \{g\}_r + \sum_{j=1}^{n_1} \frac{\{\phi\}_j^T \{g\}_r}{\lambda_j - \lambda_c} \{\phi\}_j \quad (3.17)$$

If we use equation (3.17) instead of equation (3.11), we need not calculate  $N$  eigenvectors at each iteration but only  $n_1$  eigenvectors ( $n_1 \ll N$ ) for the eigenvector derivatives. If there are no rigid body modes,  $\lambda_c$  can be set to be **zero**.

If  $m$  modes are measured, equation (3.9) becomes

$$\{\Delta\}_{m(n+1) \times 1} = [S^0]_{m(n+1) \times 2L} \{\Delta p\}_{2L \times 1} \quad (3.18)$$

### 3.2.3 COMPATIBILITY BETWEEN MEASURED MODES AND ANALYTICAL MODEL

As mentioned in Chapter 2, modal parameters obtained from a modal test are generally not compatible with those from the analytical model because

- 1) the number of modes available from measurement ( $m$ ) is usually very limited ( $m \ll N$ ) and
- 2) the number of measured coordinates ( $n$ ) is in general much less than the number of coordinates (or the number of degrees of freedom) of an analytical model ( $n < N$ ).

The mismatch in the number of measured modes ( $m$ ) and analytical modes ( $N$ ) can easily be overcome by using corresponding modes from the analytical model and omitting the unmeasured modes. In the formulation of the IEM, a mode-to-mode matching between the measured and analytical modes is essential. This matching can be performed by the use of MAC (Mode Assurance Criterion) [27] which is defined by

$$\text{MAC}(A_i, X_j) = \frac{|\{\phi_A\}_i^T \{\phi_X\}_j|^2}{|\{\phi_A\}_i^T \{\phi_A\}_i| |\{\phi_X\}_j^T \{\phi_X\}_j|} \quad (3.19)$$

It can be seen in the equation that the MAC values vary between zero and unity. If the experimental and analytical mode shapes used for the MAC are from the same mode, a value close to unity is expected, whereas if they relate to two different modes, a value close to zero should be obtained. Given a set of  $m_X$  experimental modes and a set of  $m_A$  analytical modes, we can calculate the  $m_X \times m_A$  MAC matrix, and use it to indicate which test mode relates to which analytical one. The analytical modes which correspond to the experimental modes are often not in the same sequence. The MAC matrix can sort out this reordering. This procedure should be performed at each iteration.

The coordinate mismatch can also be overcome by using corresponding coordinates from the analytical model and omitting the unmeasured coordinates in formulating equation (3.7).

### 3.2.4 BALANCING THE SENSITIVITY MATRIX

One problem in equation (3.18) is that the sensitivity matrix may be ill-conditioned because the magnitudes of the eigenvector derivatives are usually very small compared with the magnitudes of the eigenvalue derivatives. From equations (3.10) and (3.11)

$$\left| \frac{\partial \lambda_r}{\partial p_i} \right| = O \left( \lambda_r \{\phi\}_r^T \frac{\partial [M]}{\partial p_i} \{\phi\}_r \right) \quad (3.20)$$

$$\left\| \frac{\partial \{\phi\}_r}{\partial p_i} \right\| = O \left( \{\phi\}_r^T \frac{\partial [M]}{\partial p_i} \{\phi\}_r \right) \quad (3.21)$$

Therefore,

$$\left| \frac{\partial \lambda_r}{\partial p_i} \right| \approx \lambda_r \left\| \frac{\partial \{\phi\}_r}{\partial p_i} \right\| \quad (3.22)$$

So, instead of equation (3.18), we can write

$$\begin{pmatrix} \frac{\Delta\lambda_1}{\lambda_1} \\ \{\Delta\phi\}_1 \\ \vdots \\ \frac{\Delta\lambda_m}{\lambda_m} \\ \{\Delta\phi\}_m \end{pmatrix} = \begin{pmatrix} \frac{\partial\lambda_{\Lambda 1}}{\partial a_1}/\lambda_1 & \dots & \frac{\partial\lambda_{\Lambda 1}}{\partial a_L}/\lambda_1 & \frac{\partial\lambda_{\Lambda 1}}{\partial b_1}/\lambda_1 & \dots & \frac{\partial\lambda_{\Lambda 1}}{\partial b_L}/\lambda_1 \\ \frac{\partial\{\phi_{\Lambda}\}_1}{\partial a_1} & \dots & \frac{\partial\{\phi_{\Lambda}\}_1}{\partial a_L} & \frac{\partial\{\phi_{\Lambda}\}_1}{\partial b_1} & \dots & \frac{\partial\{\phi_{\Lambda}\}_1}{\partial b_L} \\ \vdots & & \vdots & & & \vdots \\ \frac{\partial\lambda_{\Lambda m}}{\partial a_1}/\lambda_m & \dots & \frac{\partial\lambda_{\Lambda m}}{\partial a_L}/\lambda_m & \frac{\partial\lambda_{\Lambda m}}{\partial b_1}/\lambda_m & \dots & \frac{\partial\lambda_{\Lambda m}}{\partial b_L}/\lambda_m \\ \frac{\partial\{\phi_{\Lambda}\}_m}{\partial a_1} & \dots & \frac{\partial\{\phi_{\Lambda}\}_m}{\partial a_L} & \frac{\partial\{\phi_{\Lambda}\}_m}{\partial b_1} & \dots & \frac{\partial\{\phi_{\Lambda}\}_m}{\partial b_L} \end{pmatrix} \begin{pmatrix} \Delta a_1 \\ \vdots \\ \Delta a_L \\ \Delta b_1 \\ \vdots \\ \Delta b_L \end{pmatrix}$$

or

$$\{\Delta\}_{m(n+1) \times 1} = [S]_{m(n+1) \times 2L} \{\Delta p\}_{2L \times 1} \quad (3.23)$$

A necessary condition for equation (3.23) to be over-determined is:

$$m(n+1) > 2L \quad \text{or} \quad m > \frac{2L}{n+1}$$

However, the eigenvector sensitivities are not always linearly independent. In practice, the number of measured modes should be more than twice of the minimum number in order to give a high probability of sufficient rank to matrix [S]. Using the SVD technique [49], the condition of the sensitivity matrix can be checked. The technique **also** can be used to solve  $\{\Delta p\}$ . If [S] is full rank, equation (3.23) can be rewritten as:

$$\{\Delta\}_{m(n+1) \times 1} = [U]_{m(n+1) \times m(n+1)} [\Sigma]_{m(n+1) \times 2L} [V]^T_{2L \times 2L} \{\Delta p\}_{2L \times 1} \quad (3.24)$$

where [U] and [V] are orthonormal matrices and  $[\Sigma]$  is a matrix with elements  $\sigma_{ij} = \sigma_i$  (singular values of [S]) for  $i = j$  and  $\sigma_{ij} = 0$  for  $i \neq j$ .

Because  $[U]$  and  $[V]$  are orthonormal and full rank matrices, the solution of equation (3.24) can be written as:

$$\{\Delta p\} = [V][\Sigma]^+ [U]^T \{\Delta\} \quad (3.25)$$

where  $^+$  is the Moore-Penrose generalised inverse and  $[\Sigma]^+$  consists of the inverse values of the non-zero Singular values  $\sigma_i$ .

The corrections are then added to the solution vector

$$\{p\}_{\text{new}} = \{p\}_{\text{old}} + \{\Delta p\} \quad (3.26)$$

and the process is iterated to convergence because equation (3.25) is not the correct answer since:

- i) equations (3.6) and (3.7) are only **first-order** approximations of eigenvalues and eigenvectors, respectively, and
- ii) subdomains do not necessarily **accord** exactly with modelled regions.

The flowchart of the whole procedure can be seen in Fig.3.1.

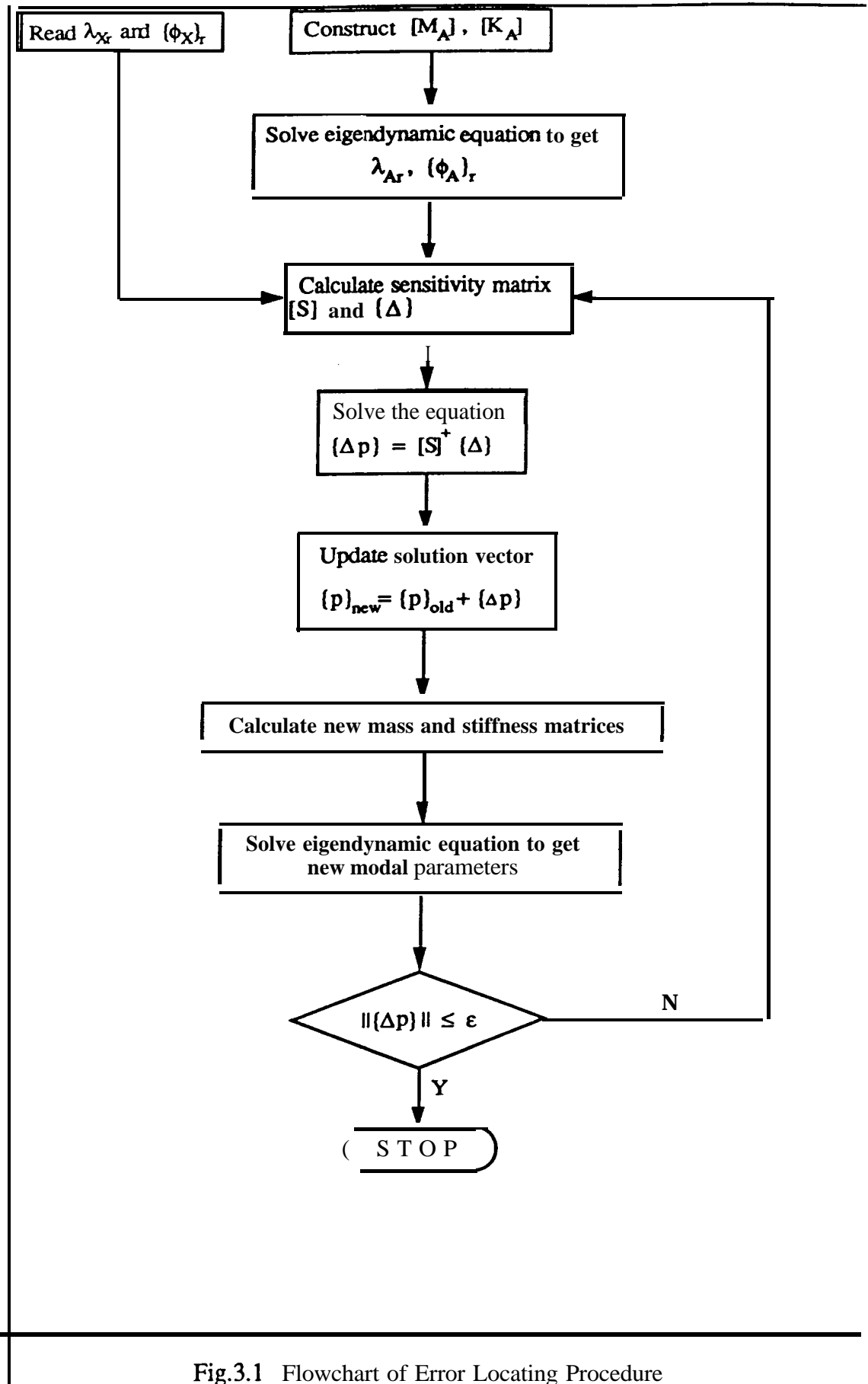


Fig.3.1 Flowchart of Error Locating Procedure

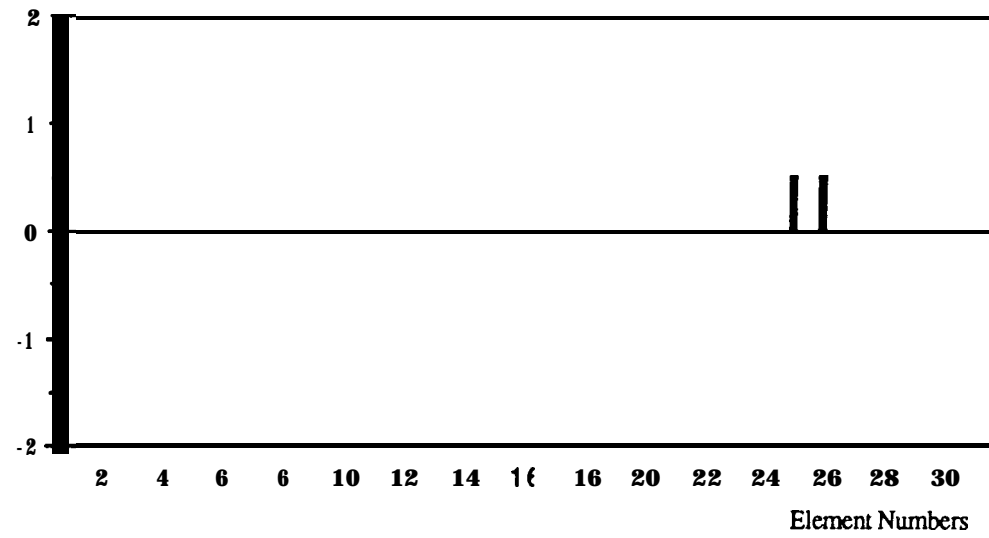
### 3.2 NUMERICAL EXAMPLES

The bay structure which had been used in Chapter 2 was **used** again to check the validity of the method suggested above. Mass and stiffness modelling errors were introduced by overestimating the mass matrices of the **25<sup>th</sup>** and **26<sup>th</sup>** elements by **50 %** and the stiffness matrices of the **12<sup>th</sup>**, **13<sup>th</sup>** and **31<sup>st</sup>** elements by **100 %**, as shown in Fig.3.2.

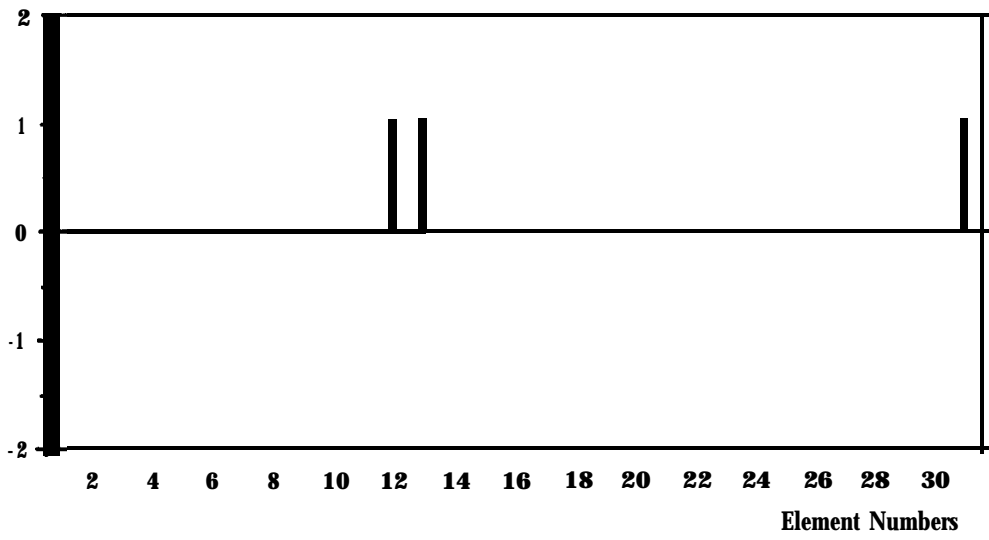
'Experimental' data were obtained for 15 points in translational coordinates only and the first 10 'experimental' modes were used, exactly as for the case studies in Chapter 2. The **first** 10 'experimental' and initial analytical models are shown in Table 3.1.

Table 3.1 Natural Frequencies of 'Experimental' and Initial Analytical Models

Mode	1	2	3	4	5	6	7	8	9	10
$f_x$ (Hz)	343.3	468.1	548.0	577.7	704.4	850.8	917.2	928.9	1099.3	1205.0
$f_A$ (Hz)	342.3	450.6	528.5	557.2	683.4	833.7	903.2	927.0	1066.6	1165.3
MAC	0.995	0.971	0.948	0.966	0.960	0.981	0.916	0.816	0.862	0.928



(a) Mass Errors

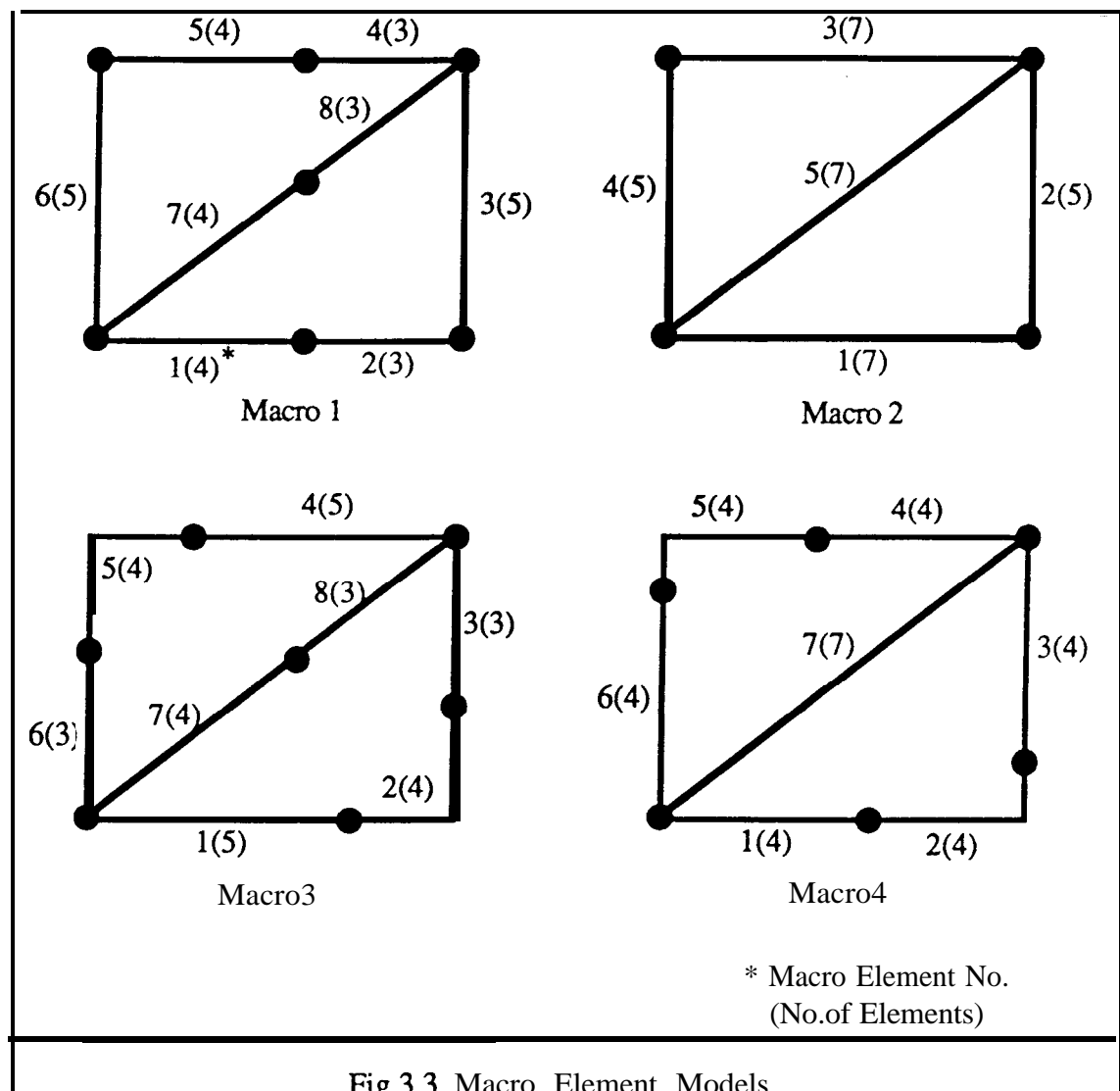


(b) Stiffness Errors

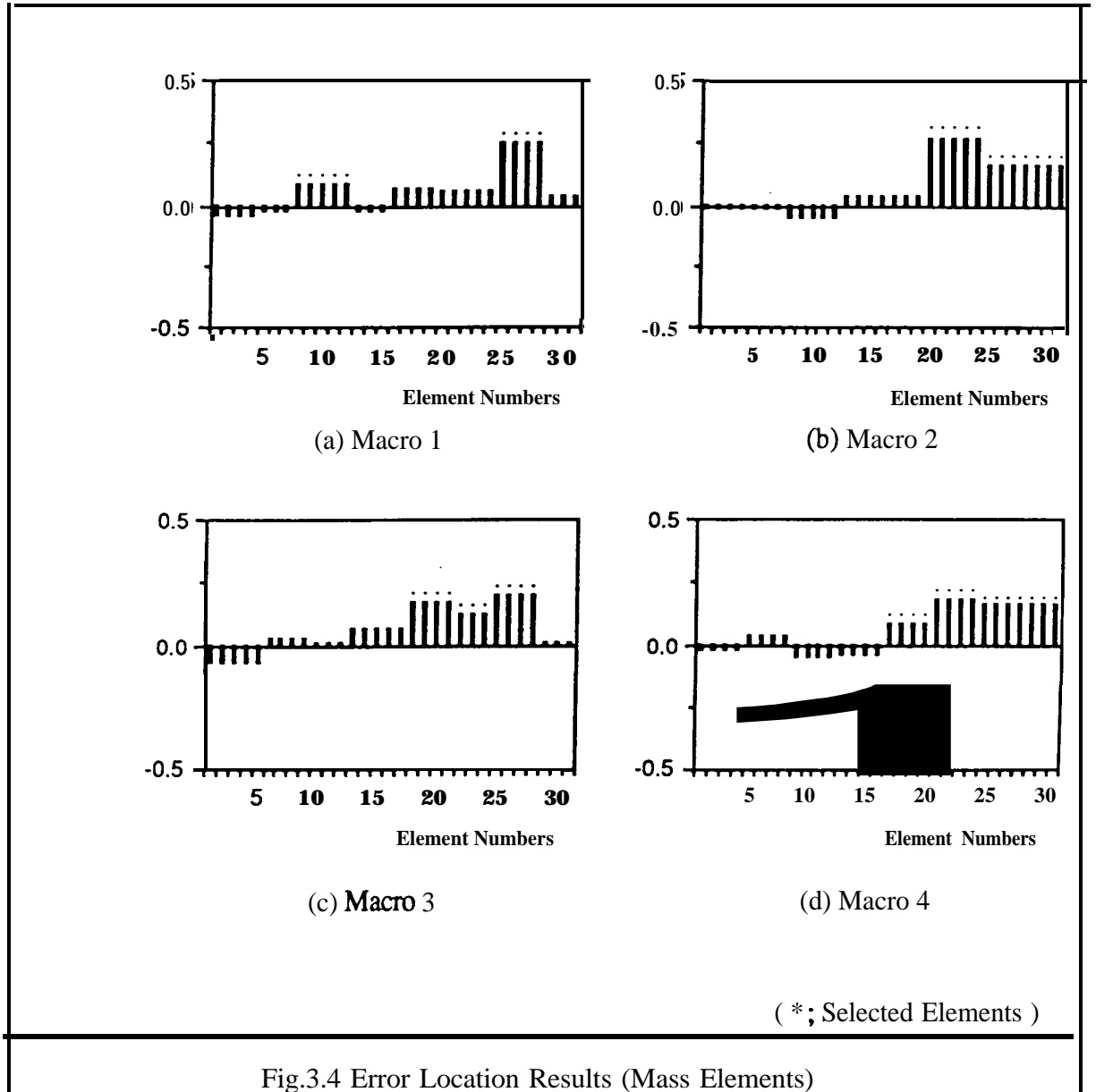
Fig.3.2 Modelling Errors

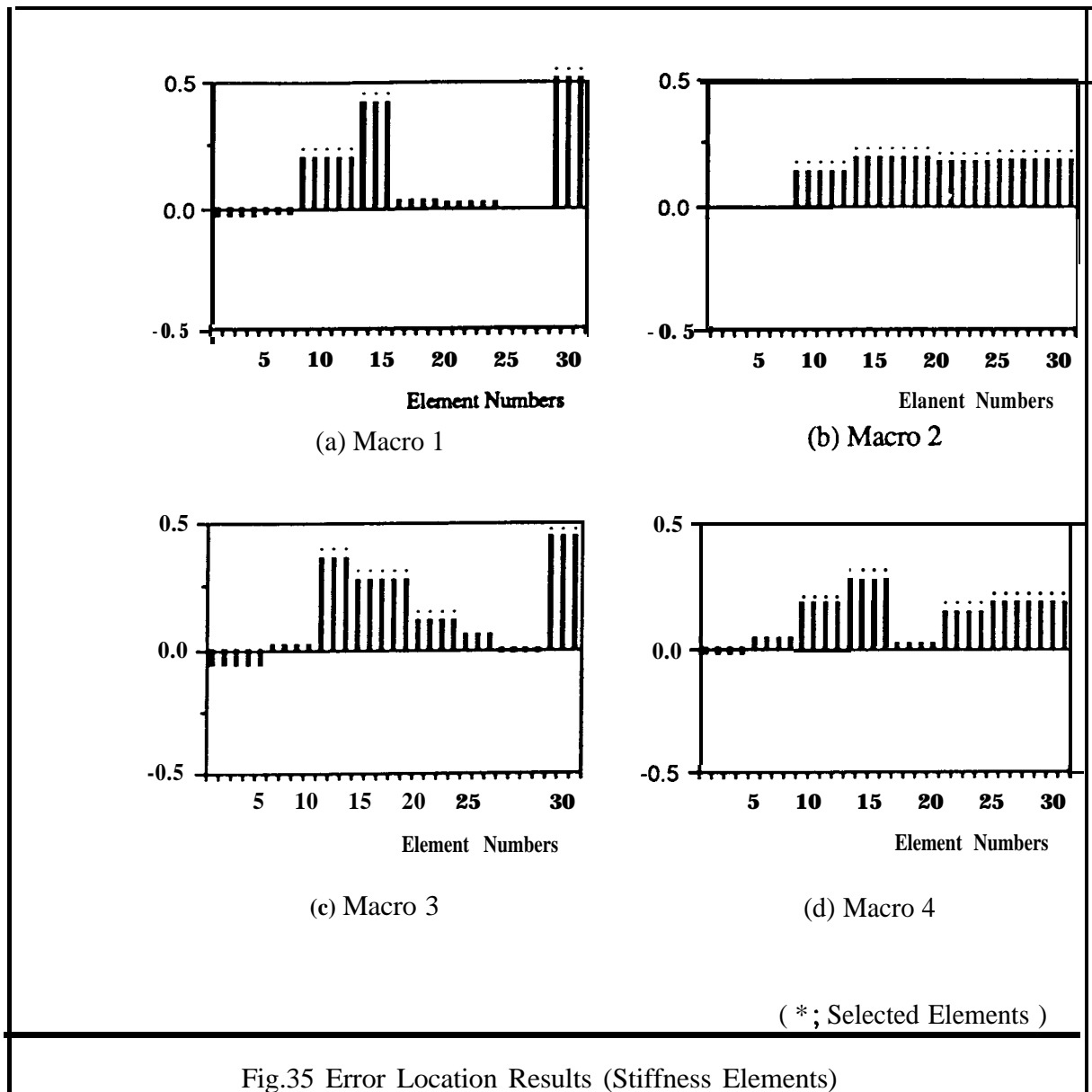
### 3.3.1 INFLUENCE OF CHOICE OF MACRO ELEMENTS ON ERROR LOCATION

In order to investigate the influence of the choice of macro elements on **error** location, 4 different macro element configurations - Macro 1, Macro 2, Macro 3 and Macro 4 (Fig.3.3) - were used. In each case, no macro element coincided exactly with one of the error regions.

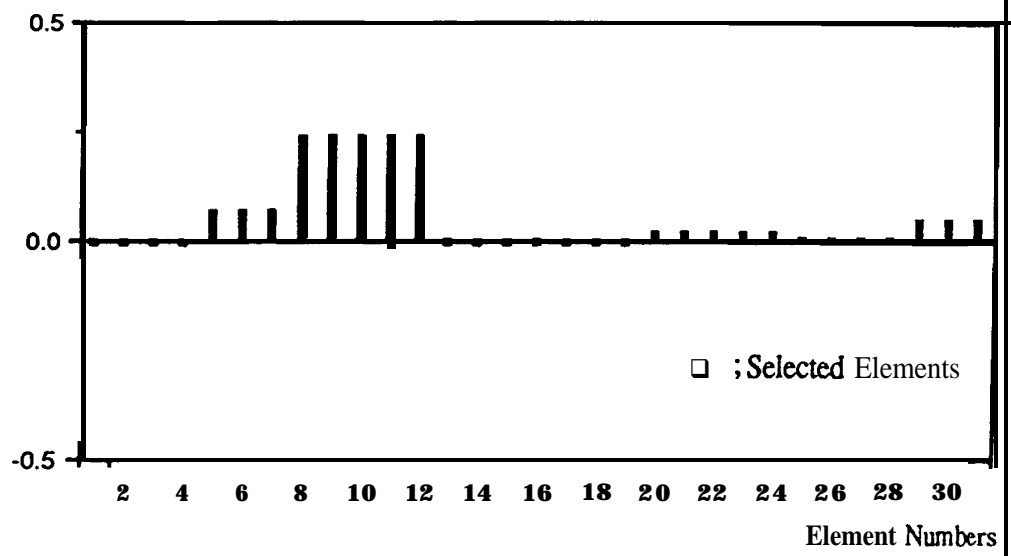


Using Macro 1, it took 4 iterations to converge and 20 elements - 9 mass elements and 11 stiffness elements - were identified as possibly harbouring modelling errors, as shown in Figs.3.4(a) and 3.5(a). Similar results were obtained using other macro models as shown in Figs.3.4 and 3.5. In each case, all mismodelled regions could be located in that they were included in the sites found by the method.

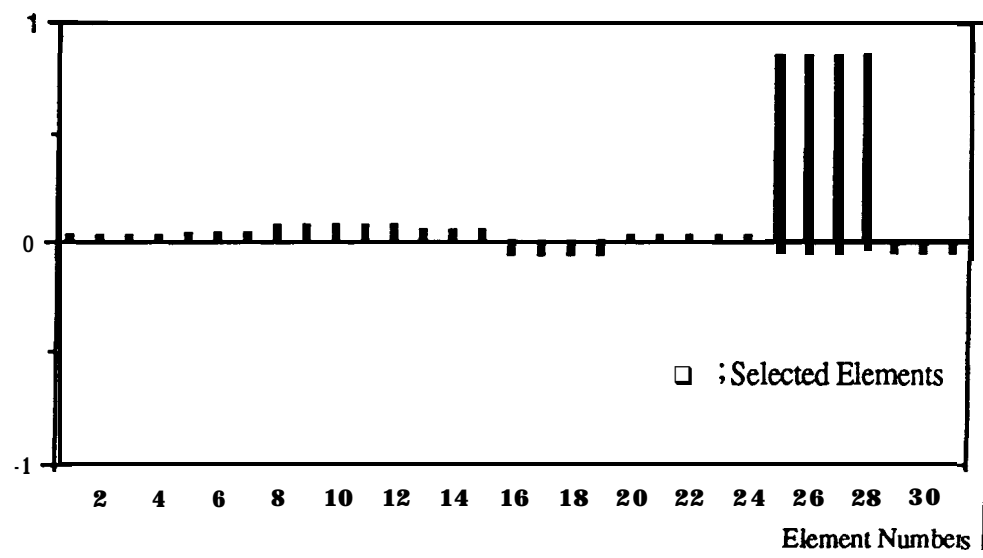




As a second case study, the same errors as the second case in Chapter 2 were used, for which case the two methods suggested by Zhang had failed to locate the error regions. Error location was carried out using Macro 1 model. The results are shown in Fig.3.6, from which it can be seen that the mismodelled elements (MI 1, MI 2, K25, K26 and K27) were all located.



(a) Mass Errors



(b) Stiffness Errors

Fig.3.6 Error Location Results (Case 2)

## 3.3.2 BALANCING EFFECT

As mentioned before, the sensitivity matrix  $[S^0]$  in equation (3.18) usually becomes ill-conditioned because the magnitudes of the eigenvector derivatives are very small compared with those of the eigenvalue derivatives, as shown in equation (3.22). To illustrate this problem, singular values of  $[S^0]$  were calculated using SVD and were compared with those of the balanced sensitivity matrix  $[S]$  in equation (3.23) in Table 3.2.

Table 3.2 Singular values of  $[S^0]$  and  $[S]$

i	$[S^0]$	$[S]$
1	$1.942 \times 10^7$	$5.724 \times 10^{-1}$
2	$1.938 \times 10^7$	$5.722 \times 10^{-1}$
3	$7.395 \times 10^6$	$5.722 \times 10^{-1}$
4	$2.052 \times 10^6$	$5.674 \times 10^{-1}$
5	$1.309 \times 10^6$	$5.623 \times 10^{-1}$
6	$6.203 \times 10^5$	$2.033 \times 10^{-1}$
7	$3.722 \times 10^2$	$1.801 \times 10^{-1}$
8	$1.800 \times 10^2$	$1.801 \times 10^{-1}$
9	$2.962 \times 10^{-1}$	$1.798 \times 10^{-1}$
10	$2.931 \times 10^{-1}$	$1.200 \times 10^{-1}$
11	$2.509 \times 10^{-1}$	$1.187 \times 10^{-1}$
12	$2.202 \times 10^{-1}$	$1.138 \times 10^{-1}$
13	$1.269 \times 10^{-1}$	$1.135 \times 10^{-1}$
14	$1.267 \times 10^{-1}$	$8.557 \times 10^{-2}$
15	$1.267 \times 10^{-1}$	$7.993 \times 10^{-2}$
16	$1.197 \times 10^{-1}$	$7.789 \times 10^{-2}$

The condition number - which is defined as the ratio of the largest of the  $\sigma_j$ 's to the smallest of  $\sigma_j$ 's - of  $[S^0]$  is  $1.63 \times 10^8$ , which is the indication of an ill-conditioned matrix, whereas the condition number of  $[S]$  is 7.34.

The rank of  $[S^0]$  can be calculated using SVD. If the rank of a matrix is  $r$ , then  $\sigma_{r+1}$  will be very small compared with the other singular values  $\sigma_i$  ( $i = 1, 2, \dots, r$ ). If we establish a criterion for the rejection or acceptance of small singular values, we shall have an answer concerning the value of the rank. This criterion may depend on the accuracy of the expected results and, in practice, may be difficult to establish. A reasonable solution is to calculate the consecutive ratios of the singular values  $\frac{\sigma_1}{\sigma_2}, \frac{\sigma_2}{\sigma_3}, \dots$ , then the ratio  $\frac{\sigma_r}{\sigma_{r+1}}$  will be very high compared with  $\frac{\sigma_{r-1}}{\sigma_r}$ . Therefore, the first peak  $\frac{\sigma_r}{\sigma_{r+1}}$  will indicate the value of

the rank. The consecutive ratios of the singular values of  $[S^0]$  are compared with those of  $[S]$  in Fig.3.7. It can be seen from the figure that  $[S^0]$  is rank deficient (the rank is 6) whereas  $[S]$  is rank full.

Values of  $\Delta p_i$  calculated based on the equation (3.18) are compared with those calculated based on the equation (3.23) in Table 3.3. It can be seen the former are meaningless because  $[S^0]$  is rank deficient.

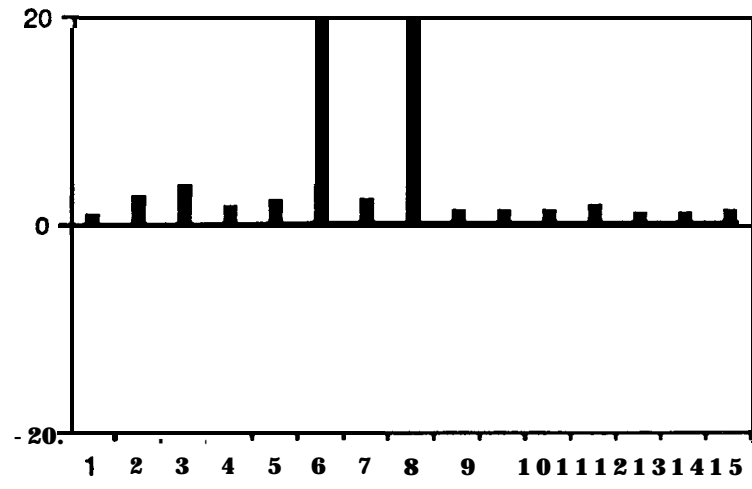
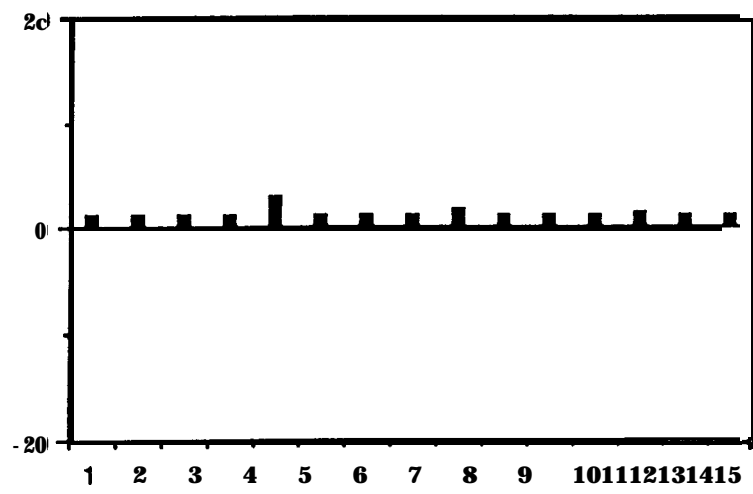
(a)  $[S']$ (b)  $[S]$ 

Fig.3.7 Rank of Sensitivity Matrix

Table 3.3 Comparison of Correction Coefficients (1 st Iteration Results)

Mass			Stiffness		
Macro Element	From Eq.(3.18)	From Eq.(3.23)	Macro Element	From Eq.(3.18)	From Eq.(3.23)
1	$-3.7 \times 10^3$	-0.06	1	$2.8 \times 10^3$	-0.04
2	$-2.8 \times 10^3$	0.05	2	$2.8 \times 10^3$	0.08
3	$1.8 \times 10^4$	0.35	3	$2.0 \times 10^4$	0.16
4	$-9.2 \times 10^3$	0.07	4	$-2.8 \times 10^3$	0.15
5	$-4.3 \times 10^3$	0.12	5	$-2.8 \times 10^3$	0.02
6	$-3.5 \times 10^4$	-0.02	6	$-2.0 \times 10^4$	0.01
7	$2.7 \times 10^4$	-0.05	7	$-2.2 \times 10^{-1}$	0.42
8	$1.4 \times 10^4$	0.29	8	$4.6 \times 10^{-1}$	0.35

### 3.4 MODEL UPDATING PROCEDURE

After locating regions where modelling errors might exist, the model improved by the error location procedure is refined by a **model** updating procedure. In the model updating process, the variables to be updated are not the correction coefficients of the macro elements but the correction coefficients of the individual elements from which the macro elements are assembled for the preceding error location procedure. The problem to be solved here is

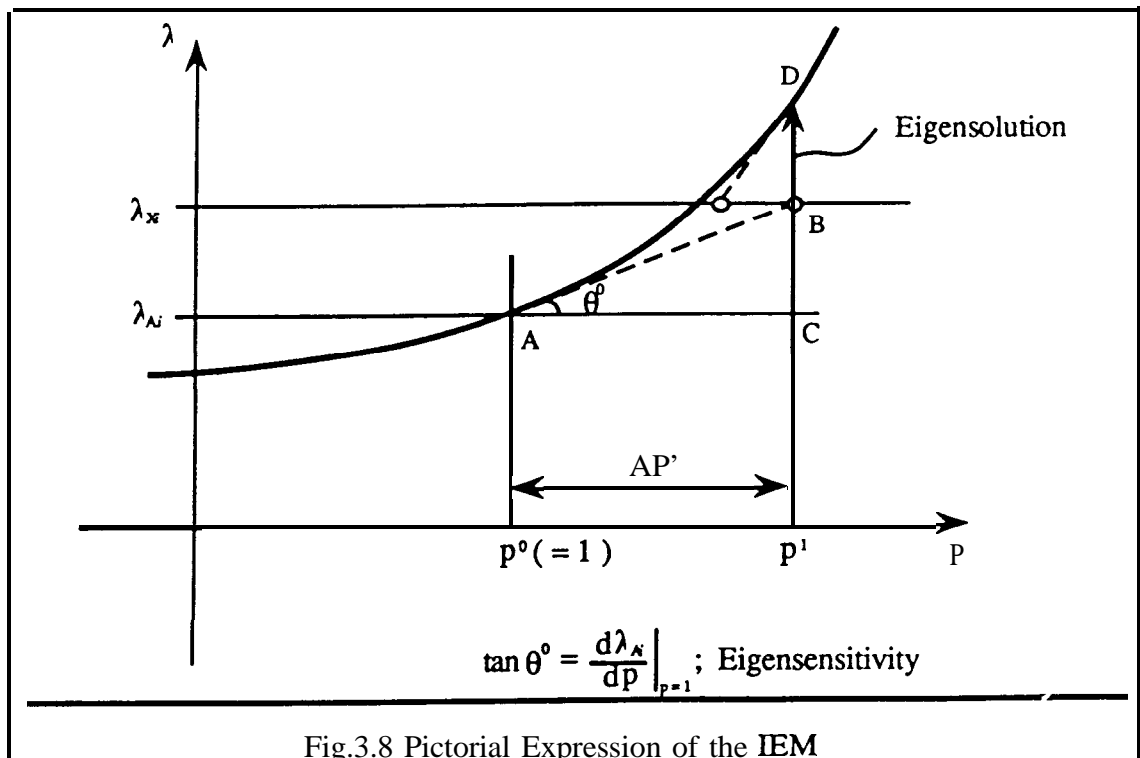
$$\{\Delta\}_{m(n+1) \times 1} = [S']_{m(n+1) \times l} \{\Delta p'\}_{l \times 1} \quad (3.27)$$

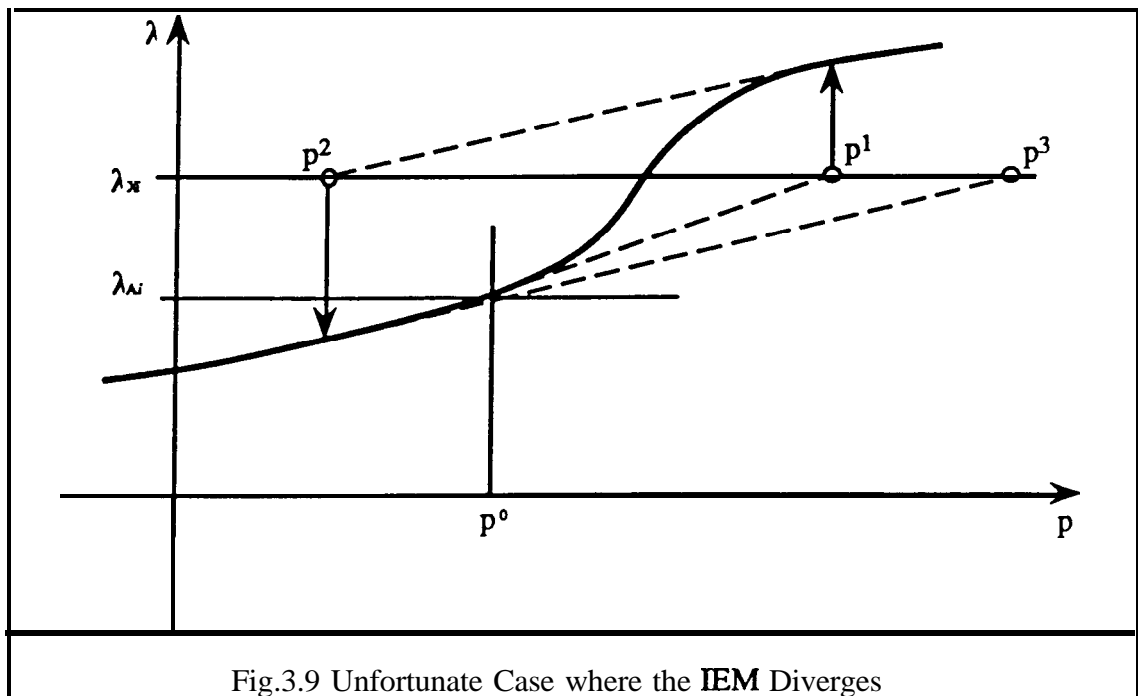
where  $l$  is the number of the selected elements from the error location procedure. Equation (3.27) is similar to equation (3.23). The differences are that  $\Delta p'$  represents the correction coefficients of the element matrix which might have modelling errors and  $[S']$

represents the sensitivity matrix of the elements selected in the error location procedure. Equation (3.27) should be solved iteratively because it is an approximate solution.

The IEM is, in fact, a multi-variable Newton-Raphson method. In Fig.3.8, the model updating process using IEM is illustrated graphically for the case of one variable. The slope of the curve  $\lambda = f(p)$  at the point  $A(p^0, \lambda_{A,i})$  corresponds to the eigenvalue sensitivity, and a segment AC corresponds to the solution of the equation (3.9). The process BD is equivalent to the calculation of the eigenvalue problem  $[K]\{\phi\} = \lambda[M]\{\phi\}$ .

When modelling errors are not small, in which case the higher-order terms in the Taylor series of eigenvalues and eigenvectors are important, the IEM can give grossly inaccurate, meaningless corrections as illustrated in Fig.3.9.



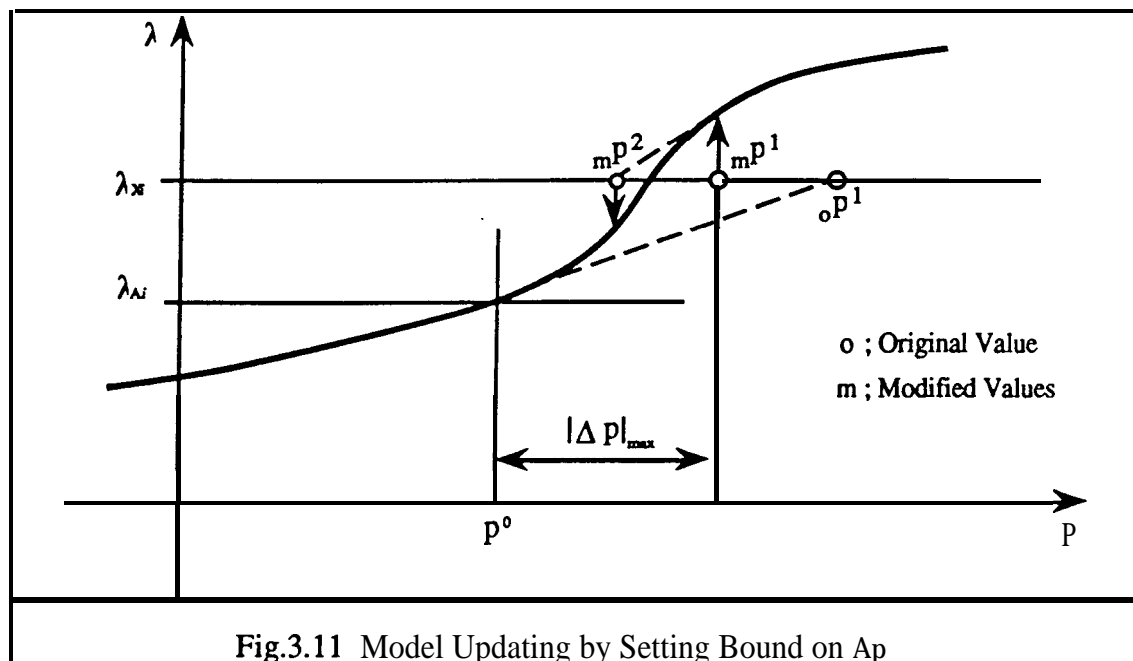
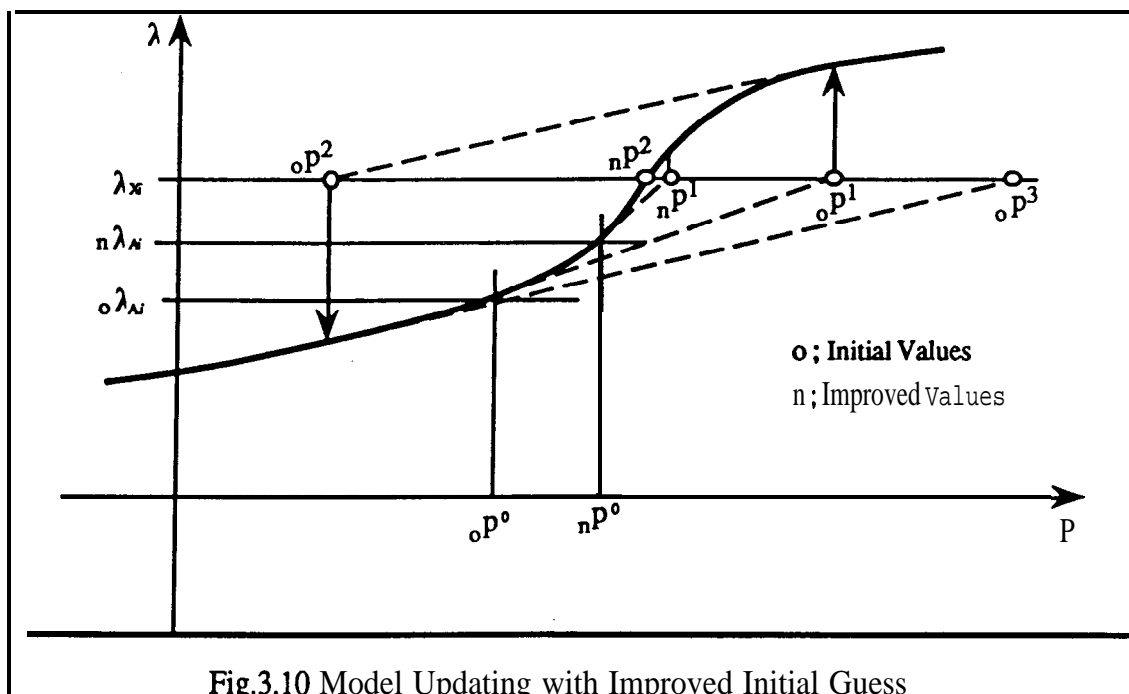


The convergence of the IEM can be improved by the following:

- 1) new initial guess and/or
- 2) setting bounds on  $\{\Delta p^i\}$ .

The resultant correction coefficients from the error location procedure can be considered as “improved” new initial guesses and these usually improve the convergence because the distance between the analytical and experimental models has been reduced by the error location procedure. This statement is illustrated in Fig.3.10. The second strategy to improve the convergence of the IEM is illustrated in Fig.3.11.

The flowchart of the whole procedure of the model updating can be seen in Fig.3.12.



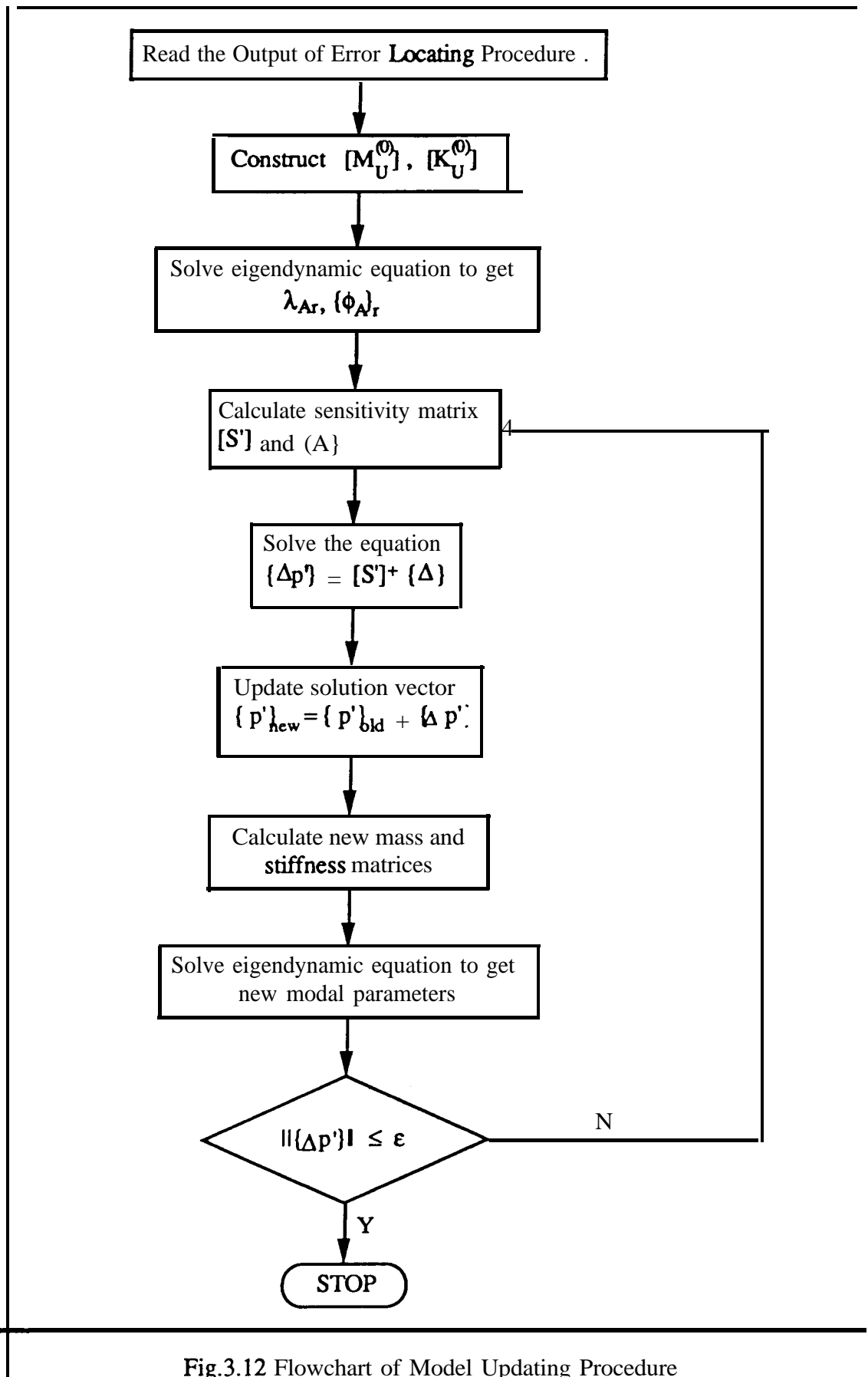
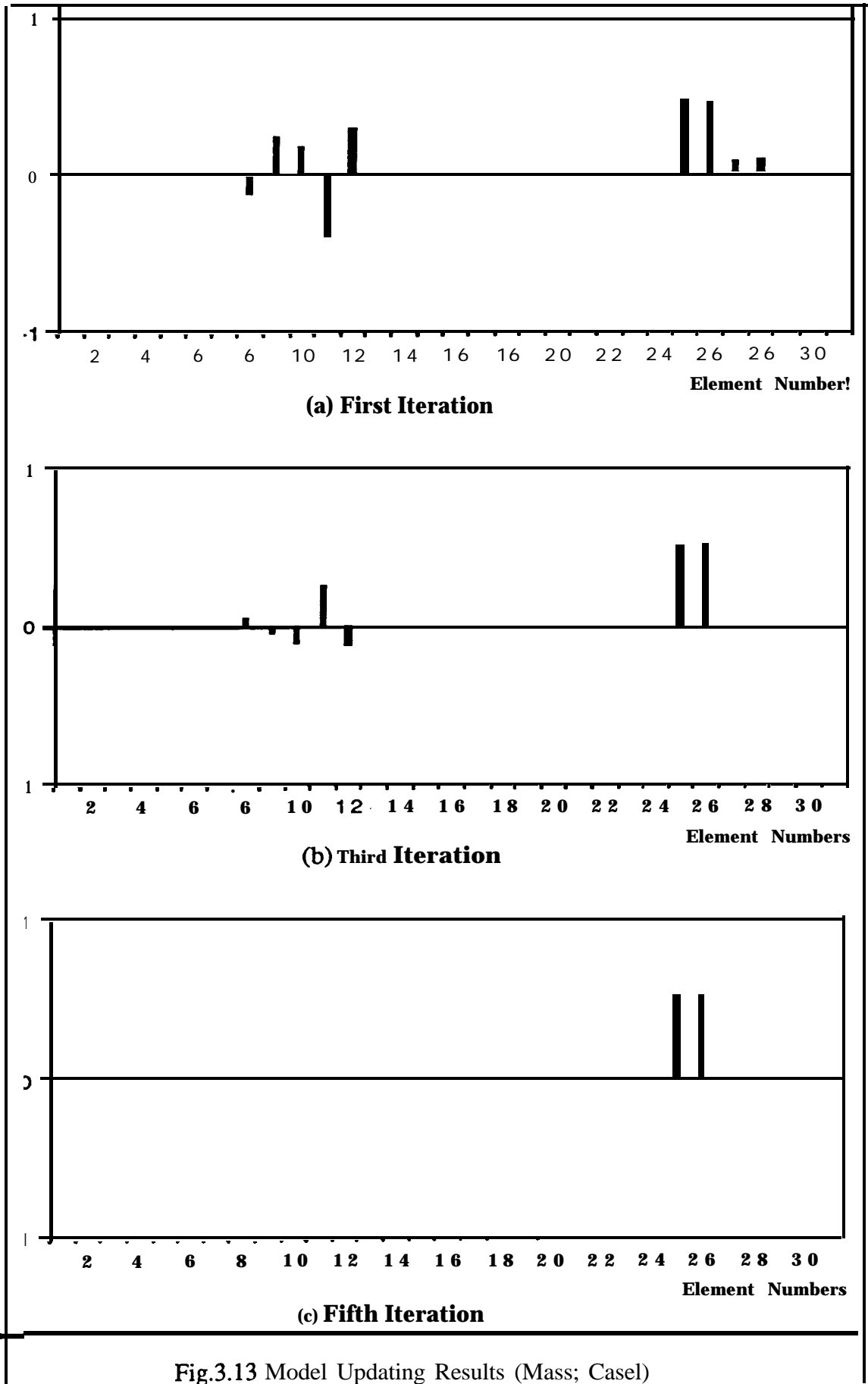
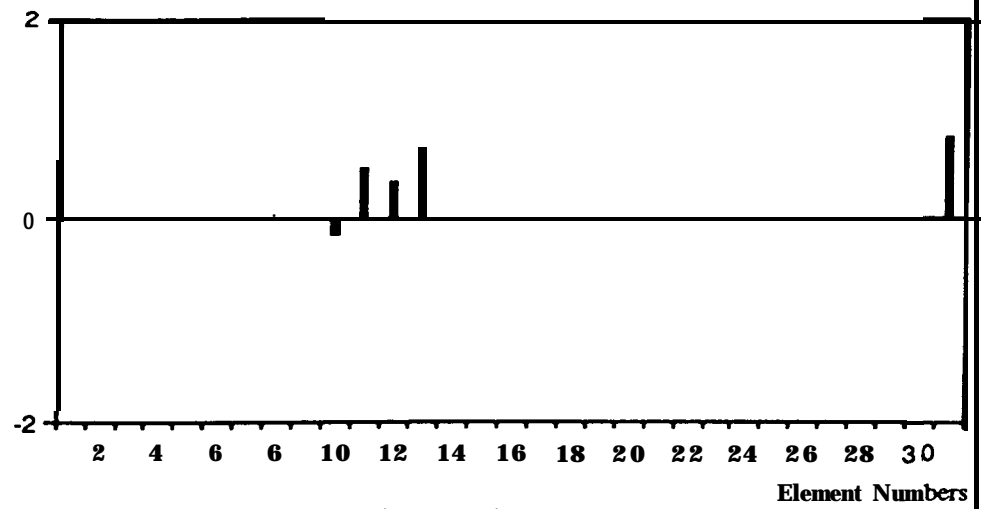


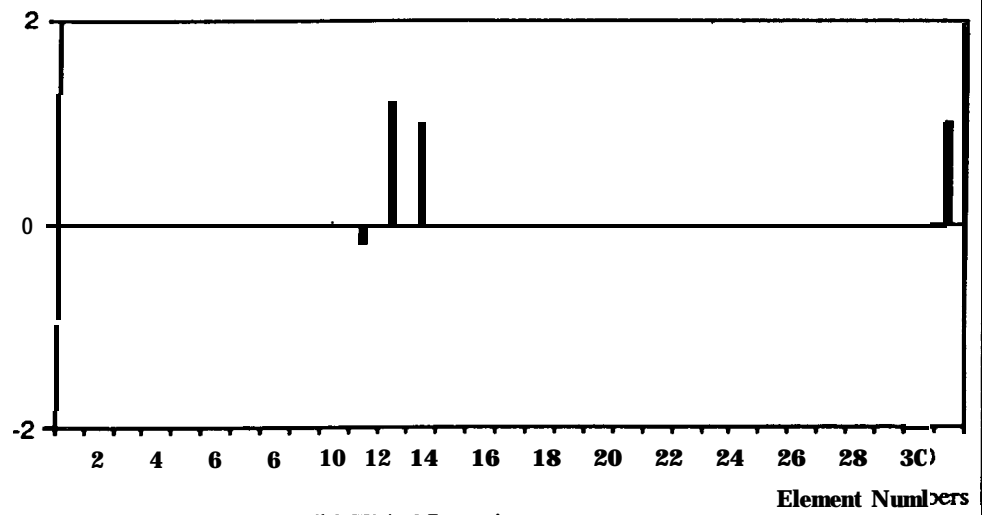
Fig.3.12 Flowchart of Model Updating Procedure



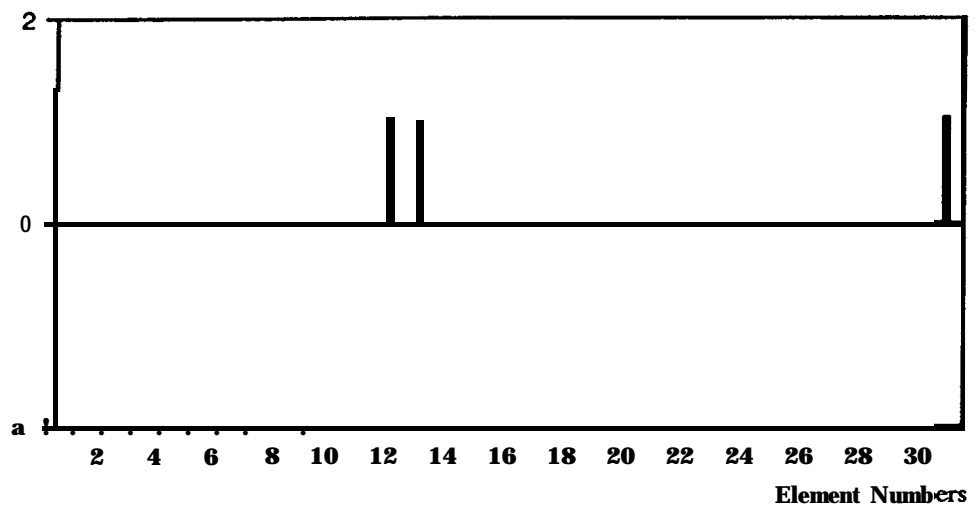




(a) First Iteration



(b) Third Iteration



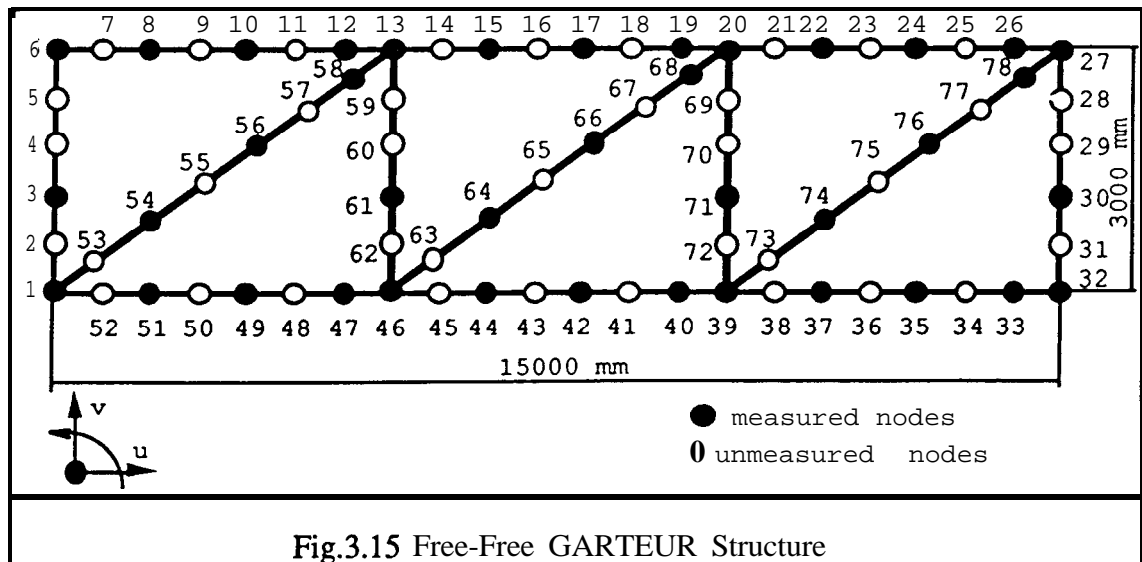
(c) Fifth Iteration

Fig.3.14 Model Updating Results (Stiffness ; Case1)

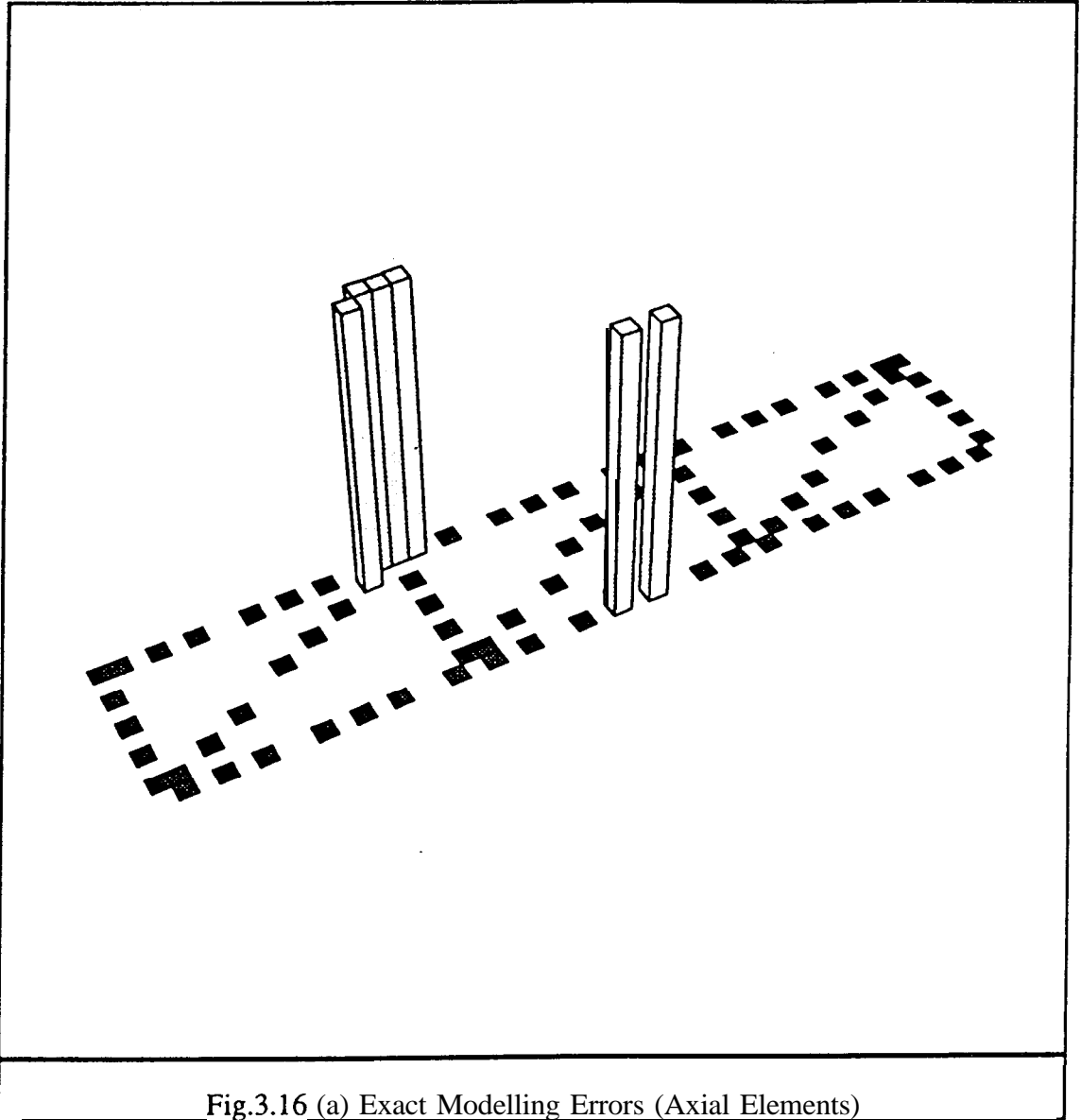
## 3.6 APPLICATION TO THE GARTEUR STRUCTURE

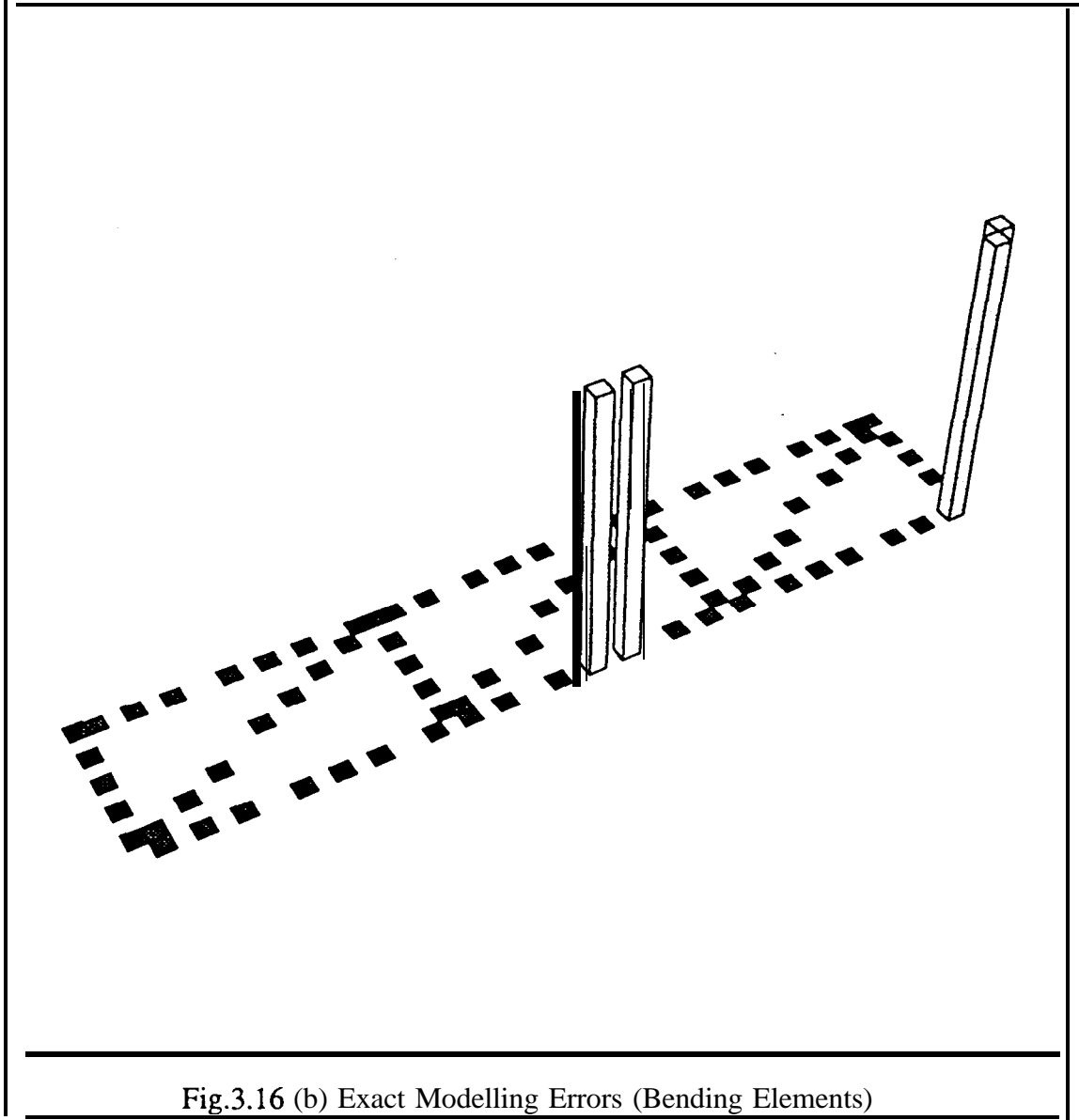
### 3.6.1 THE GARTEUR STRUCTURE

To check the validity of the aforementioned method to a practical structure, the method has been applied to a free-free structure known as the GARTEUR structure (Fig.3.15). The structure is modelled by 83 beam elements. It has 78 nodes and 3 DoFs are considered at each node, so that the number of total DoFs of the analytical model is 234. Each element is constructed by a superposition of an axial bar element and a bending beam element, and these pairs of elements are considered to be independent of each other. The element mass and stiffness matrices and necessary data are given in Appendix B.



Modelling errors are introduced in exactly the same way as those of GARTEUR 1 exercise - by overestimating the cross-section area of the 12<sup>th</sup>, 13<sup>th</sup>, 41<sup>st</sup>, 42<sup>nd</sup>, 59<sup>th</sup> and 60<sup>th</sup> elements by 100 %, and by underestimating the second moment of area of the 3<sup>1st</sup>, 32<sup>nd</sup>, 41<sup>st</sup> and 42<sup>nd</sup> elements by 50 %. The exact modelling errors are shown in Fig.3.16.





36 nodes are assumed to be 'measured in two translational directions (u and v directions) only as shown in Fig.3.15. The first 5 modes are assumed to be measured, and these and the corresponding analytical natural frequencies are shown in Table 3.5 together with their MAC values.

Table 3.5 Natural Frequencies of 'Experimental' and Initial Analytical Models

Mode	1	2	3	4	5
Experimental (Hz)	149.9	230.4	287.4	403.1	432.5
Analytical (Hz)	145.4	226.8	284.0	397.2	427.0
MAC	0.999	0.999	0.997	0.994	0.787

### 3.6.2 EIGENSENSITIVITY

In this exercise, it is not appropriate to express the updated stiffness matrix in the form of equation (3.2) and more independent physical design variables need to be considered. Because the cross-section area and area moment of inertia are considered to be independent variables, the updated stiffness matrix can be expressed as:

$$[K_U] = \sum_{j=1}^L c_j [K_a]_j + \sum_{j=1}^L d_j [K_b]_j$$

where  $[K_a]_j$  is the axial element stiffness matrix which is proportional to the cross-section area and  $[K_b]_j$  is the bending element stiffness matrix which is proportional to the second moment of area.

The eigensensitivities can be easily derived as:

$$\frac{\partial \lambda_r}{\partial c_i} = \{\phi\}_r^T [K_a]_i \{\phi\}_r$$

$$\frac{\partial \lambda_r}{\partial d_i} = \{\phi\}_r^T [K_b]_i \{\phi\}_r$$

$$\frac{\partial \{\phi\}_r}{\partial c_i} = \sum_{j=1}^N \gamma_{rj}^i \{\phi\}_j$$

$$\gamma_{rj}^i = \begin{cases} \frac{\{\phi\}_i^T [K_a]_i \{\phi\}_r}{\lambda_r - \lambda_j} & (r \neq j) \\ 0 & (r = j) \end{cases}$$

$$\frac{\partial \{\phi\}_r}{\partial d_i} = \sum_{j=1}^N \delta_{rj}^i \{\phi\}_j$$

$$\delta_{rj}^i = \begin{cases} \frac{\{\phi\}_j^T [K_b]_i \{\phi\}_r}{\lambda_r - \lambda_j} & (r \neq j) \\ 0 & (r = j) \end{cases}$$

### 3.6.3 ERROR LOCATION PROCEDURE

In the error location procedure, 26 macro elements were used as shown in Fig.3.17. No macro element coincides exactly with the error regions.

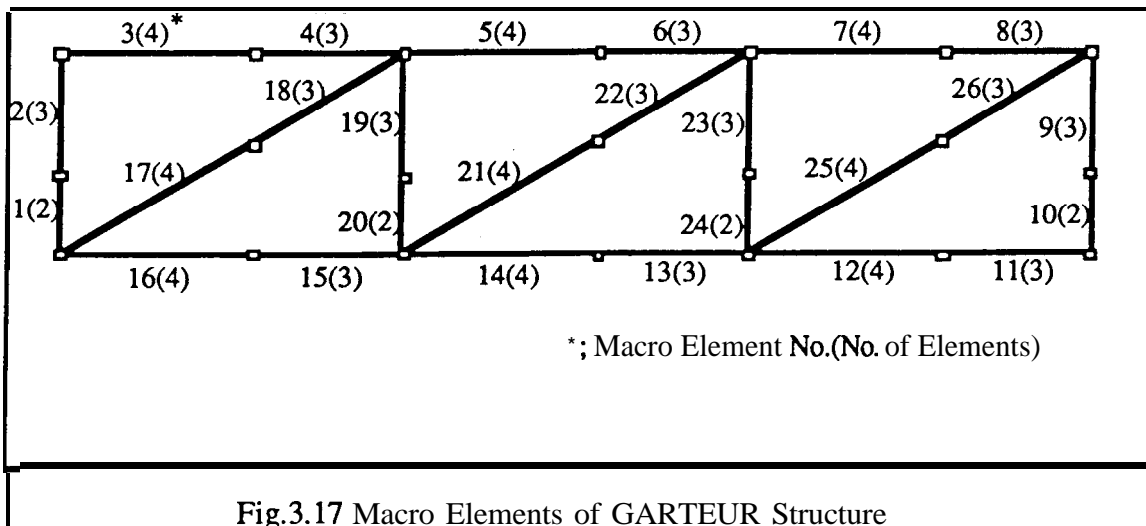


Fig.3.17 Macro Elements of GARTEUR Structure

The iteration results are shown in Fig.3.18 and Table 3.6. After 7 iterations, the analytical model converged to the experimental model and it became possible to locate possible error regions - 10 axial and 8 bending macro elements, or 32 axial and 34 bending elements.

Table 3.6 Natural Frequencies of 'Experimental' and Intermediate Analytical Models

Mode	1	2	3	4	5
Experimental (Hz)	149.9	230.4	287.4	403.1	432.5
Analytical (Hz)	149.8	230.3	287.4	403.1	432.5
M A C	1.000	1.000	0.999	0.999	0.999

### 3.6.4 MODEL UPDATING PROCEDURE

After locating possible error regions, the updating was carried out with the correction coefficients calculated as initial values. It can be seen in Figs.3.19 and 3.20 that estimates becomes very accurate after 8 iterations. The natural frequencies of the updated analytical model are compared with those of the experimental model in Table 3.7 together with MAC values.

Table 3.7 Natural Frequencies of 'Experimental' and Updated Analytical Models

	1	2	3	4	5
Experimental (Hz)	149.9	230.4	287.4	403.1	432.5
Analytical (Hz)	149.9	230.4	287.4	403.1	432.5
M A C	1.000	1.000	1.000	1.000	1.000

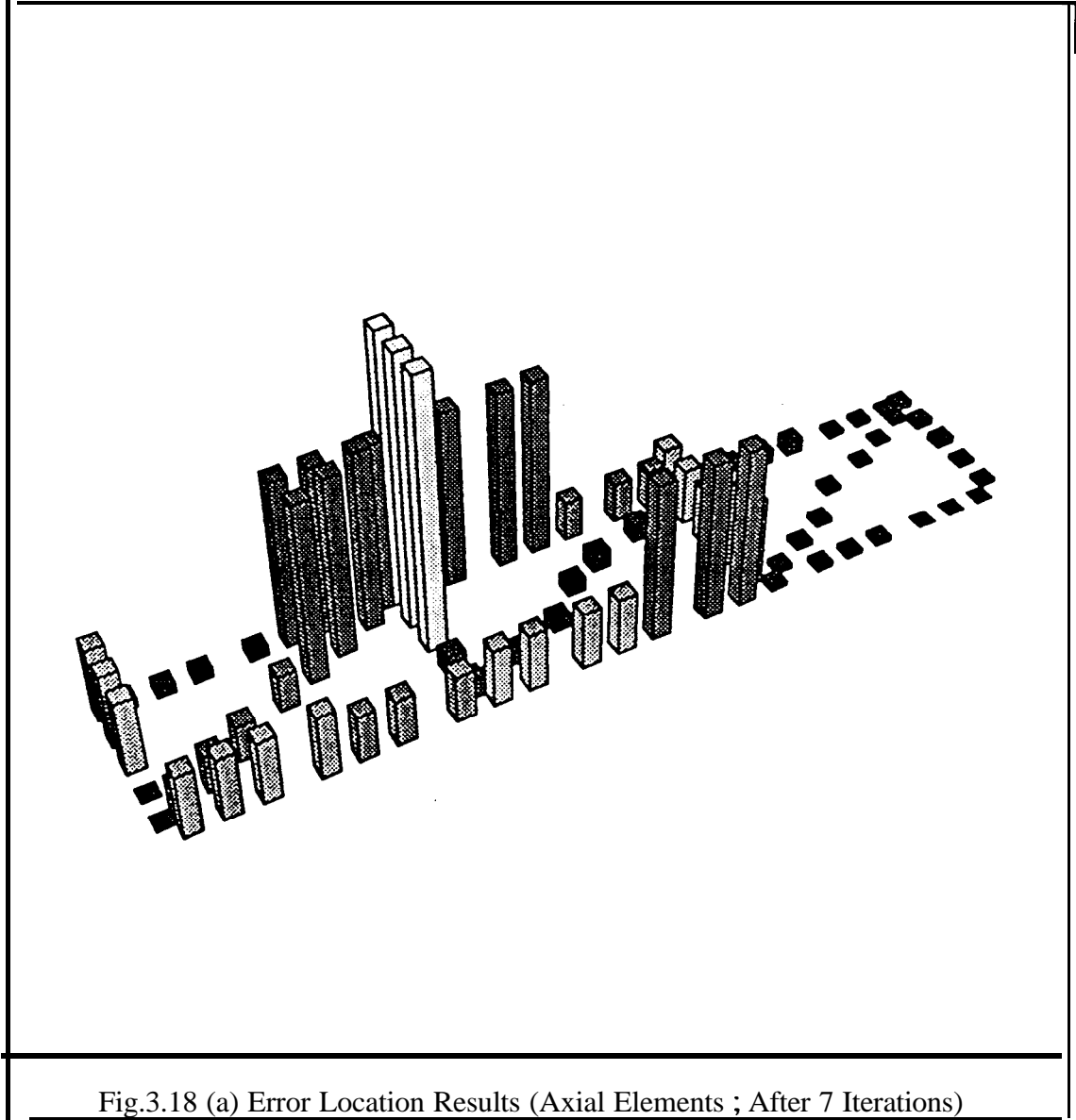
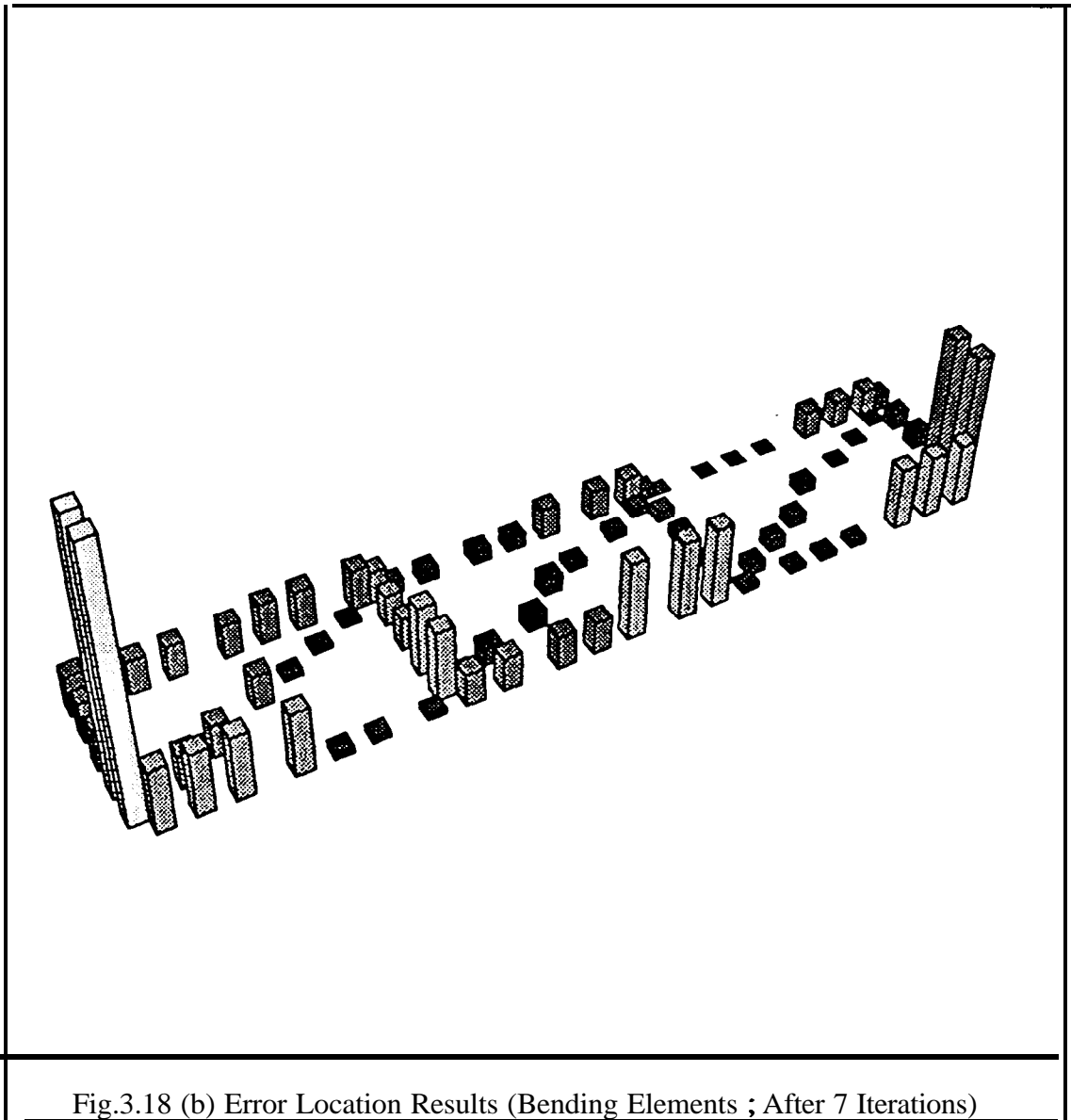


Fig.3.18 (a) Error Location Results (Axial Elements ; After 7 Iterations)



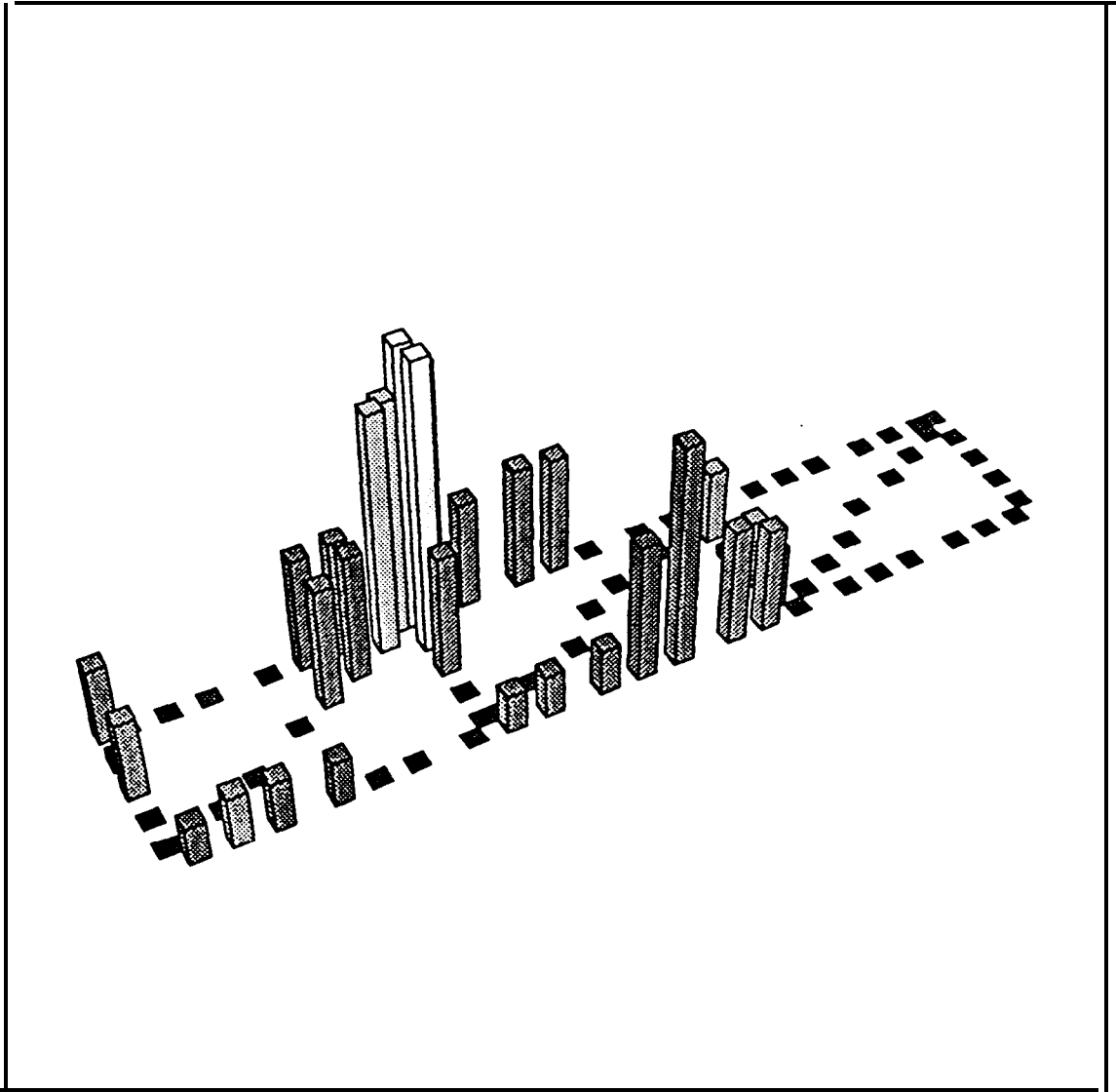
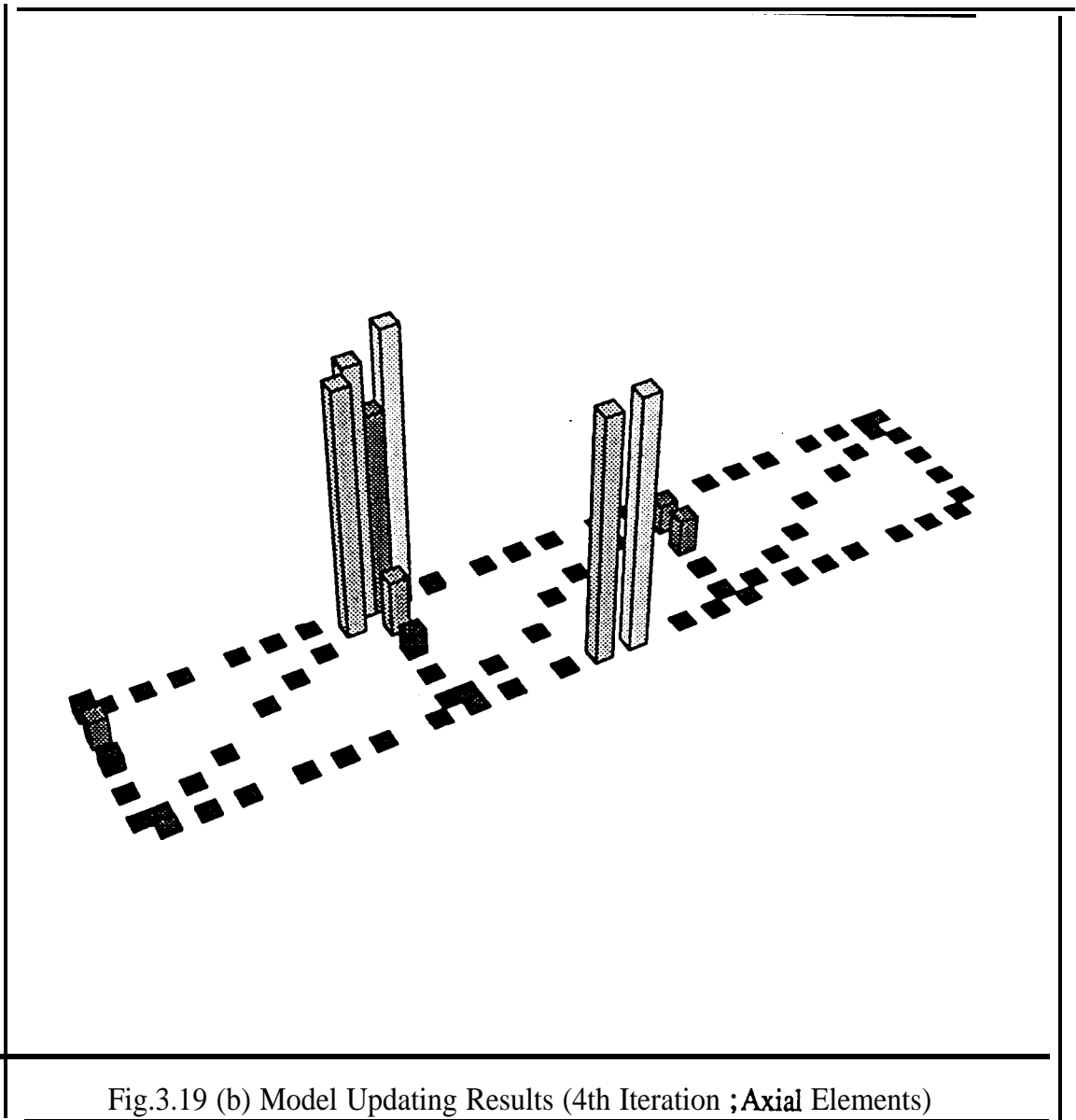
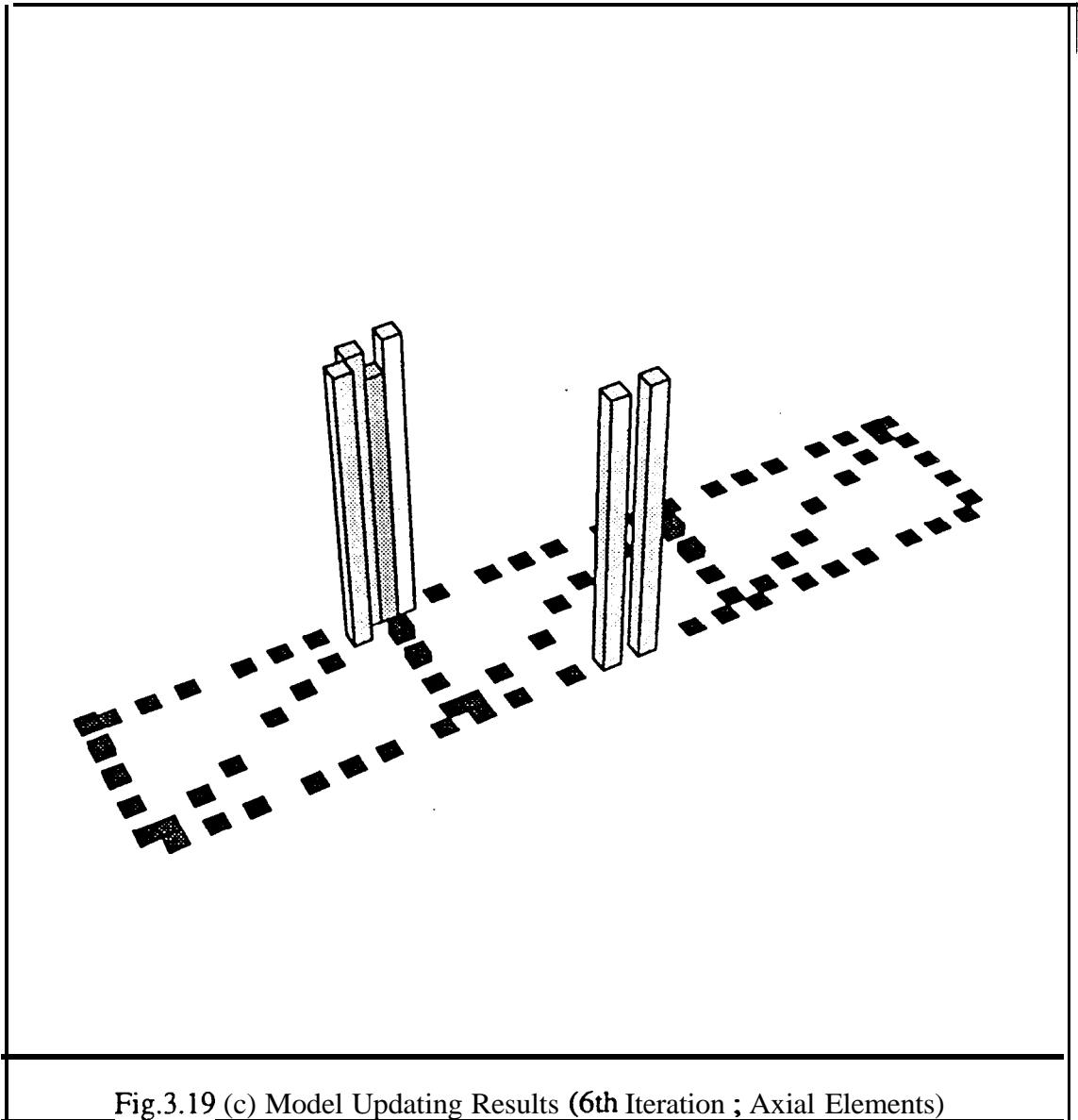
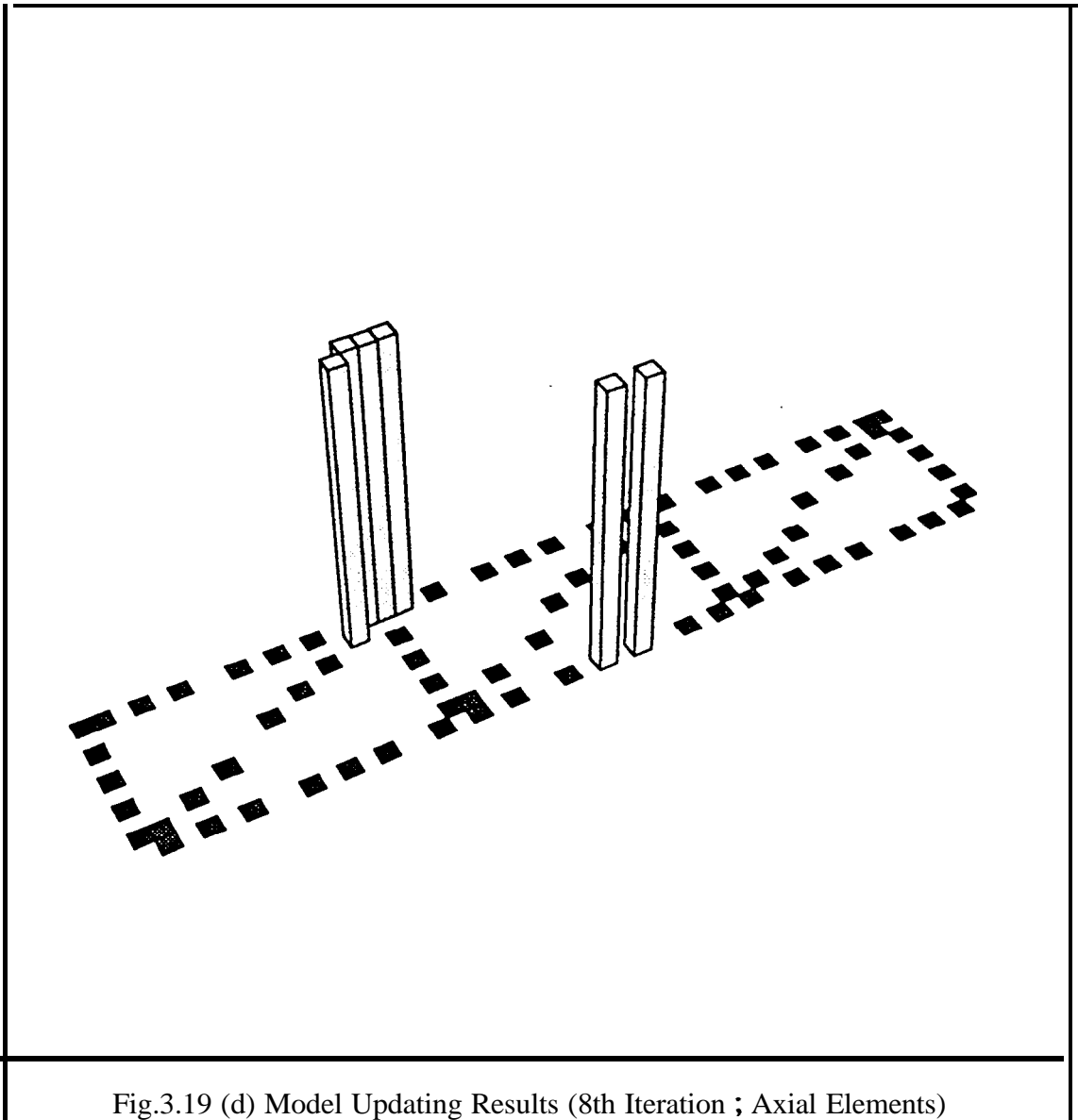
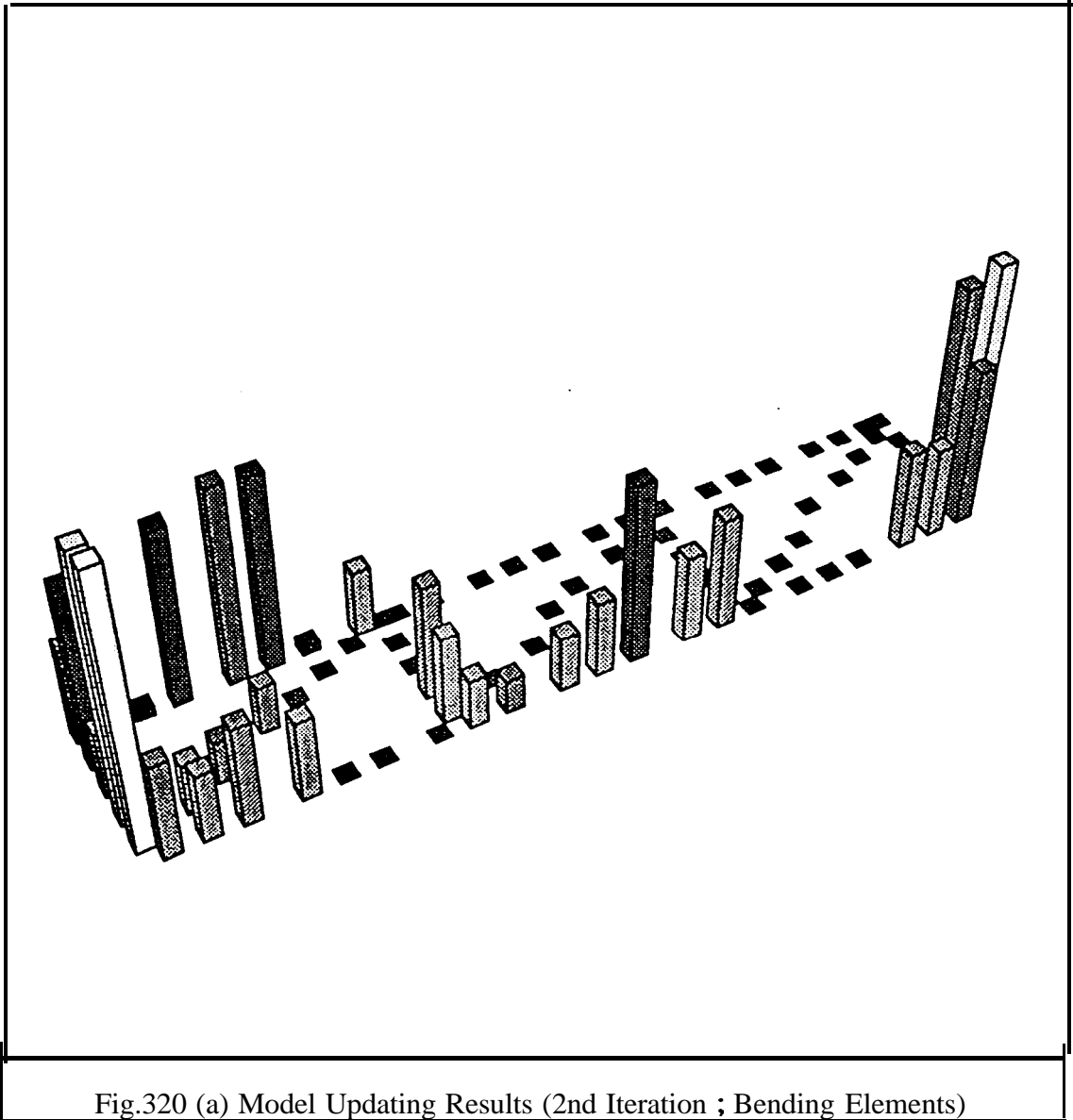


Fig.3.19 (a) Model Updating Results (2nd Iteration ; Axial Elements)









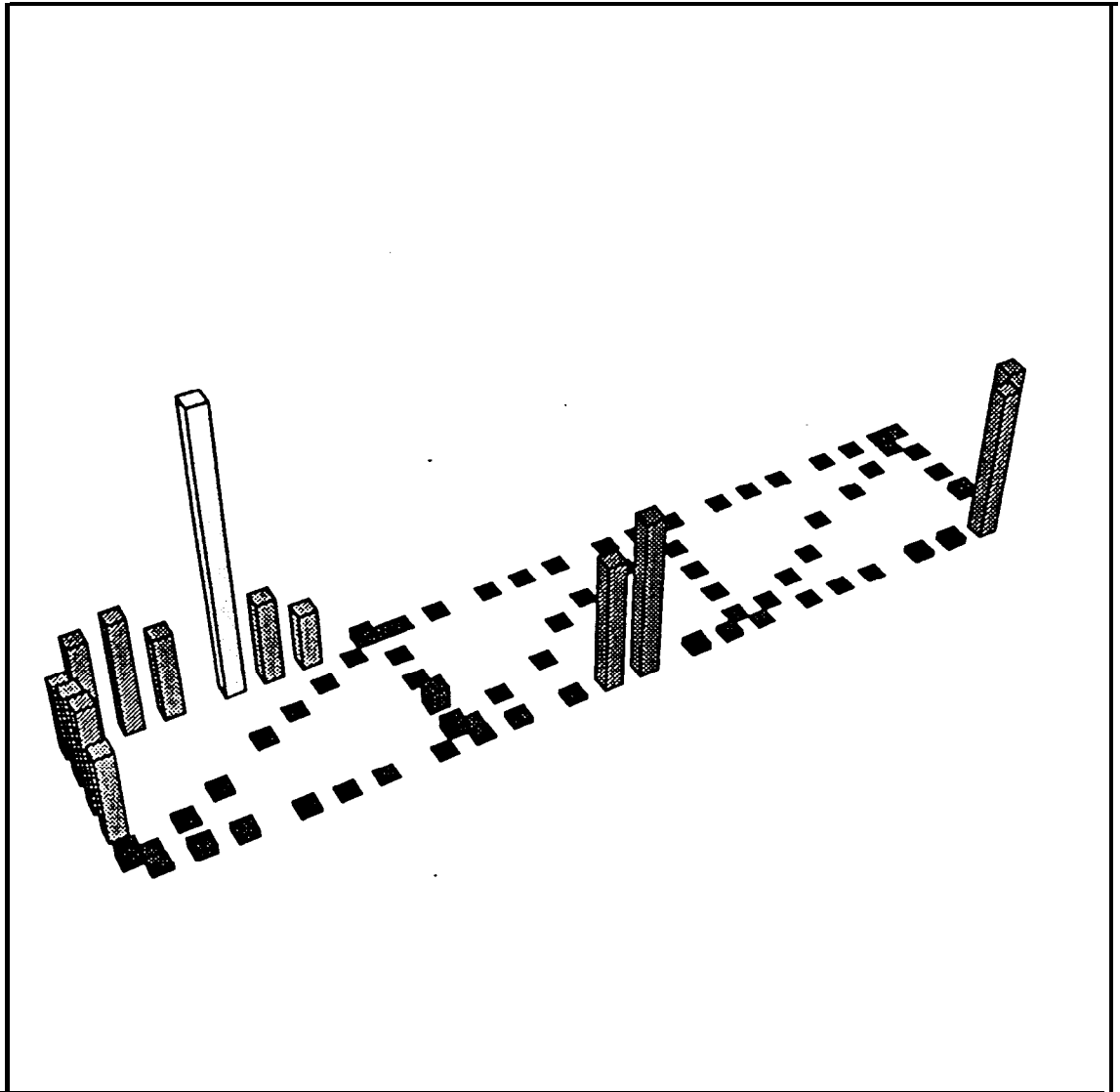
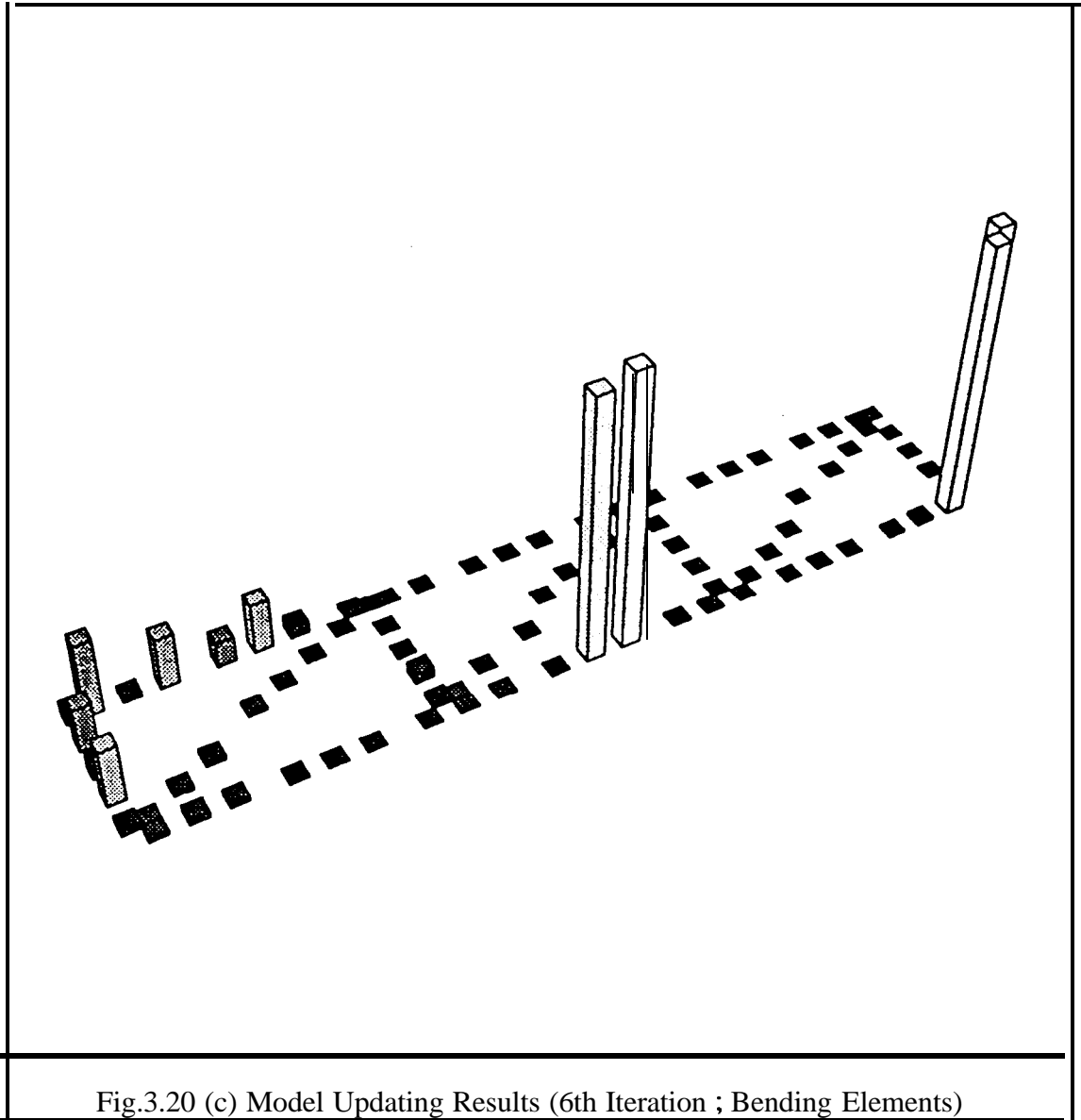
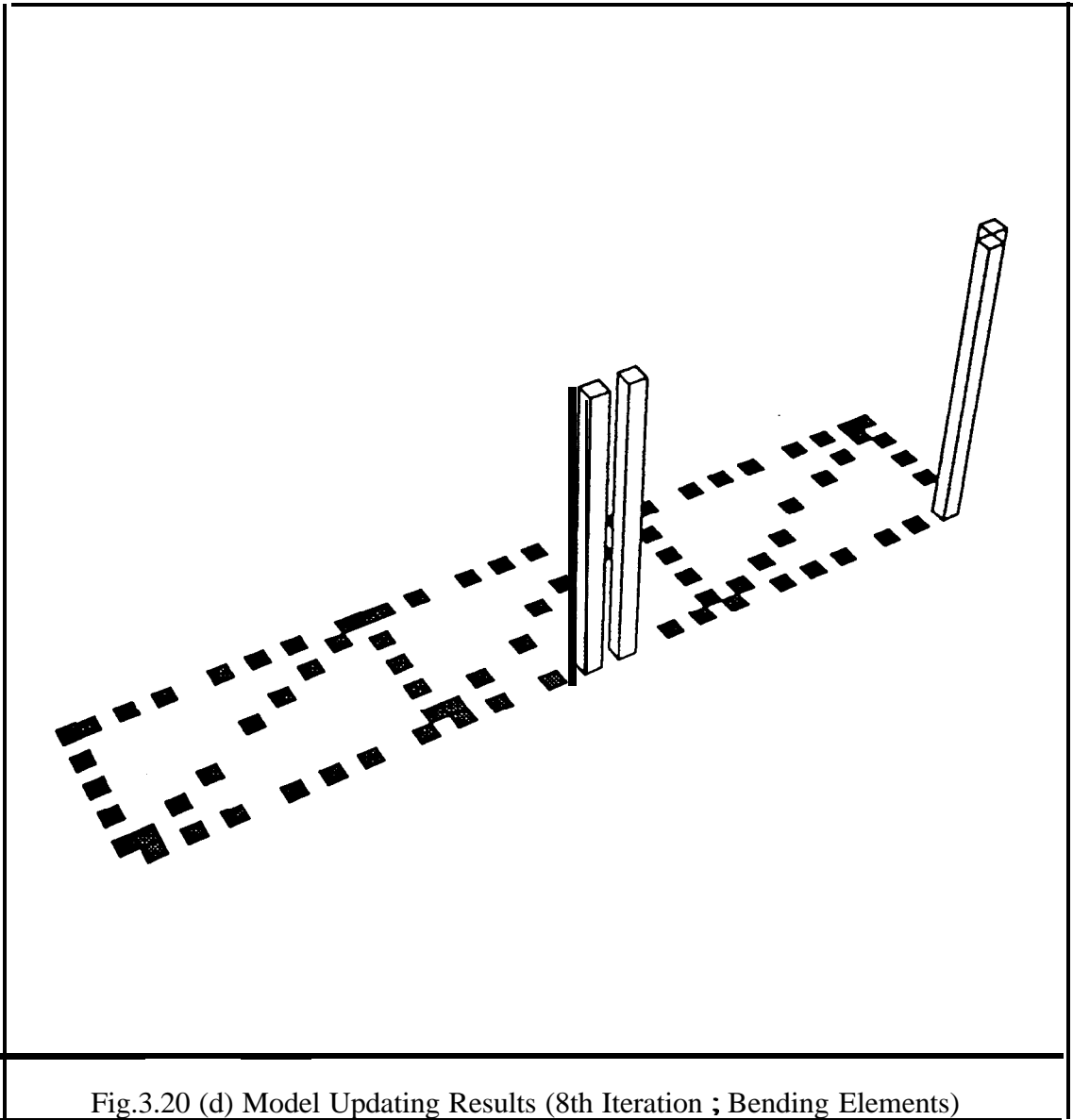


Fig.3.20 (b) Model Updating Results (4th Iteration ; Bending Elements)





ξ

### 3.7 CONCLUDING REMARKS

One of the advantages of model updating using eigensensitivity analysis is that **mode** expansion (or reduction) is not required. However, this method requires large computational effort because of the repeated solution of the eigendynamic problem and repeated calculation of the sensitivity matrix. In this Chapter, a sensitivity method using *arbitrarily chosen* macro elements has been proposed at the error location stage to reduce the computational time and to reduce **the** number of experimental modes required for subsequent updating. By this approach, the model updating problem, which is generally under-determined, can be transformed into an over-determined one and the updated analytical model is not influenced by the definition of macro elements.

It has been illustrated that the **IEM** is a multi-variable Newton-Raphson method and the convergence of the **IEM** can be improved by introducing error location procedure and by setting bounds on  $\{\Delta p\}$ .

The proposed method has been applied to the free-free GARTEUR structure which may represent a practical structure and constitute a realistic problem in respect of the incompleteness of both measured modes and coordinates. The updating results are quite accurate not only in modal parameters but also in correction coefficients of physical design variables.

The 'experimental' data of the case studies in this Chapter are noise-free data. However, because of various measurement errors, the assumption that the test results represent the true dynamic **behaviour** of the structure may not be correct - the experimental data can be affected by several types of measurement error. Thus, the sensitivity of the updating method itself to noise on the experimental data needs to be investigated.

# CHAPTER 4

# CHAPTER 4

## ERROR SENSITIVITY OF THE INVERSE EIGENSENSITIVITY METHOD

### 4.1 PRELIMINARIES

One of the most important objectives of modal testing is to validate the analytical model of a dynamic structure by comparing experimentally determined **modal** parameters - which are supposed to be correct - with those obtained from an analytical model. However, because of various measurement errors, the assumption that the test results represent the true modal **parameters** may not be correct.

To check the validity of a model updating method by numerical case studies, measurement errors must be considered. Even though many methods have been developed in recent years for updating analytical models for the dynamic analysis of a structure, and some of them have been proven to be quite successful, the methods are generally based on the assumption that the test data are perfect or noise-free. For any updating method to be useful for practical structures, the sensitivity of the method to noise on the test data needs to be established.

In this Chapter, typical measurement errors will be introduced by contaminating the modal parameters of the correct or modified structure with random noise of different noise levels to check the sensitivity of the **IEM** to noise on the test data.

## 4.2 SENSITIVITY OF IEM TO NOISE ON MODAL PARAMETERS

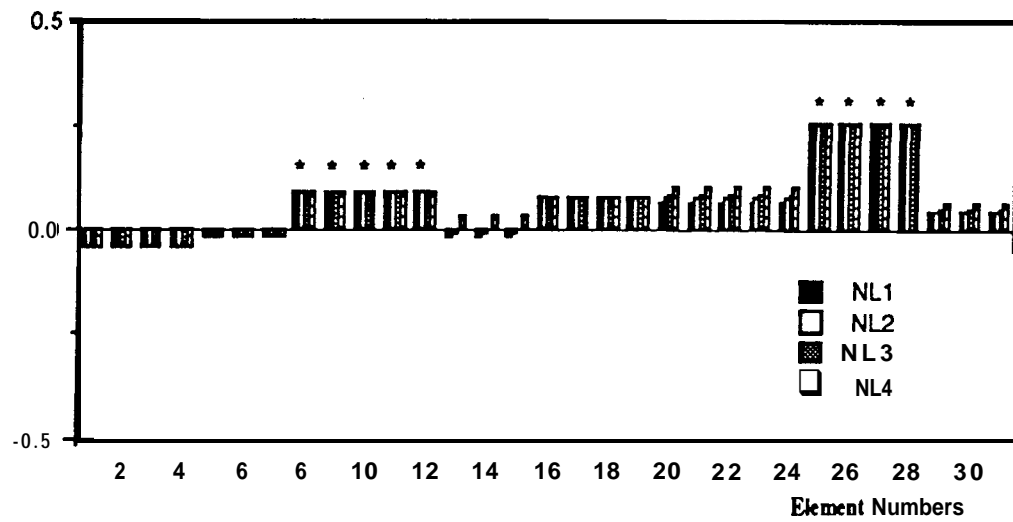
The **IEM** described in Chapter 3 has been applied to the bay structure which had been used in Chapter 2 and Chapter 3 to check the error sensitivity of the method. Mass and stiffness modelling errors were introduced by overestimating the mass matrices of the 25<sup>th</sup> and 26<sup>th</sup> elements by 50 % and the stiffness matrices of the 12<sup>th</sup>, 13<sup>th</sup> and 31<sup>st</sup> elements by 100 % as shown in Fig.3.2. Experimental data were obtained at 15 points in translational coordinates only and the first 10 “experimental” modes were used, as the case studies in Chapter 2 and Chapter 3.

### 4.2.1 ERROR LOCATION PROCEDURE

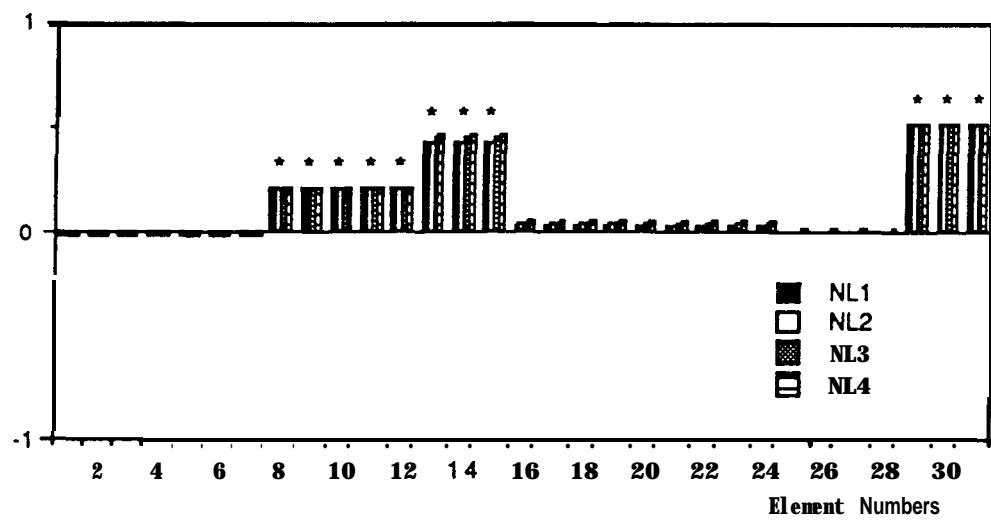
#### 4.2.1.1 Sensitivity to Measurement Noise

In order to investigate the sensitivity of the error location procedure to noise on the experimental data, the simulated experimental modal parameters were contaminated by 4 different random noise levels - **NL1** (no noise), **NL2** (0.2% in eigenvalues and 2% in eigenvectors), **NL3** (0.5% in eigenvalues and 5% in eigenvectors) and **NL4** (1% in eigenvalues and 10% in eigenvectors).

The error location procedure was carried out using the Macro 1 model shown in Fig.3.3, and the results are shown in Fig.4.1. In each case, all mismodelled regions can be located.



(a) Mass Modelling Errors (\*; Selected elements)



(b) Stiffness Modelling Errors (\*; Selected elements)

Fig.4.1 Error Location Results (Macro Model ;Macro1)

#### 4.2.1.2 Influence of Choice of Macro Elements on Error Location

In order to investigate the influence of choice of macro elements on error location, 4 different macro element configurations - Macro 1, Macro 2, Macro 3 and Macro 4 (Fig.3.3) - were used for error location. In each case, no macro element coincided exactly with the error regions. NL3 experimental data - 0.5% random noise in eigenvalues and 5% random noise in eigenvectors - were used. The error location results are shown in Fig.4.2, and again, **all mismodelled** regions have been located in each case.

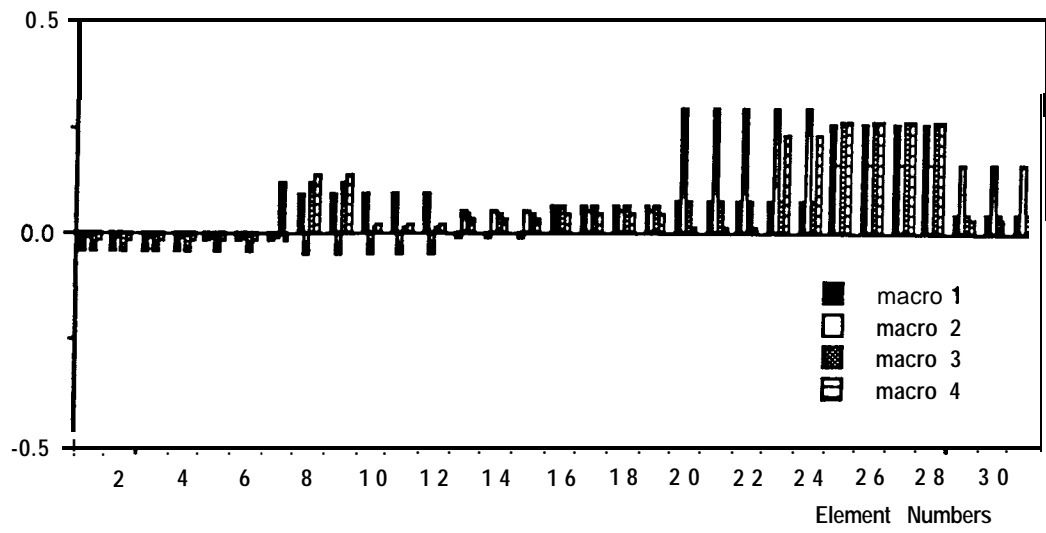
#### 4.2.2 UPDATING PROCEDURE

Using the results from the Macro 1 model and the NL3 experimental data - 0.5% random noise in eigenvalues and 5% random noise in eigenvectors - updating has been carried out. Natural frequencies of the "experimental" and initial analytical models are shown in Table 4.1 together with the mode shape correlations indicated by MAC values.

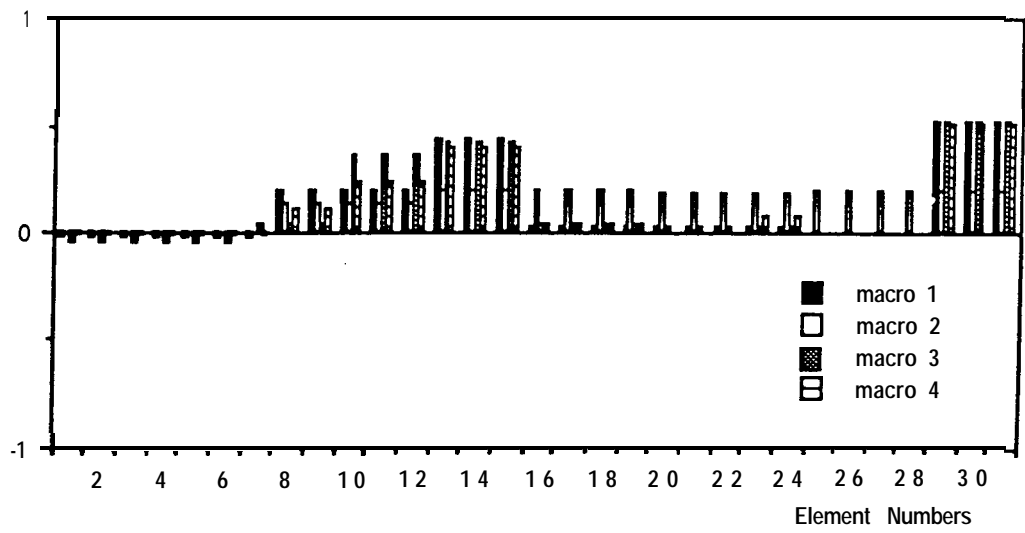
Table 4.1 Natural Frequencies of "Experimental" and Initial Analytical Models

Mode	1	2	3	4	5	6	7	8	9	10
$f_x$ (Hz)	342.8	467.7	548.1	578.3	705.7	848.9	915.9	928.5	1099.8	1206.6
$f_A$ (Hz)	342.3	450.6	528.5	557.2	683.4	833.7	903.2	927.0	1066.6	1165.3
MAC	0.995	0.970	0.944	0.966	0.960	0.982	0.914	0.821	0.868	0.927

20 elements were indicated as possibly having **modelling** errors - 9 mass elements and 11 stiffness elements - as shown in Fig.4.1. All the eigenvalue sensitivities were used because eigenvalues can be measured more accurately than eigenvectors. If the number of measured modes ( $m$ ) is greater than the number of unknowns ( $l$ ), only eigenvalue



(a) Mass Modelling Errors



(b) Stiffness Modelling Errors

Fig.4.2 Error Location Results (Noise Level; NL3)



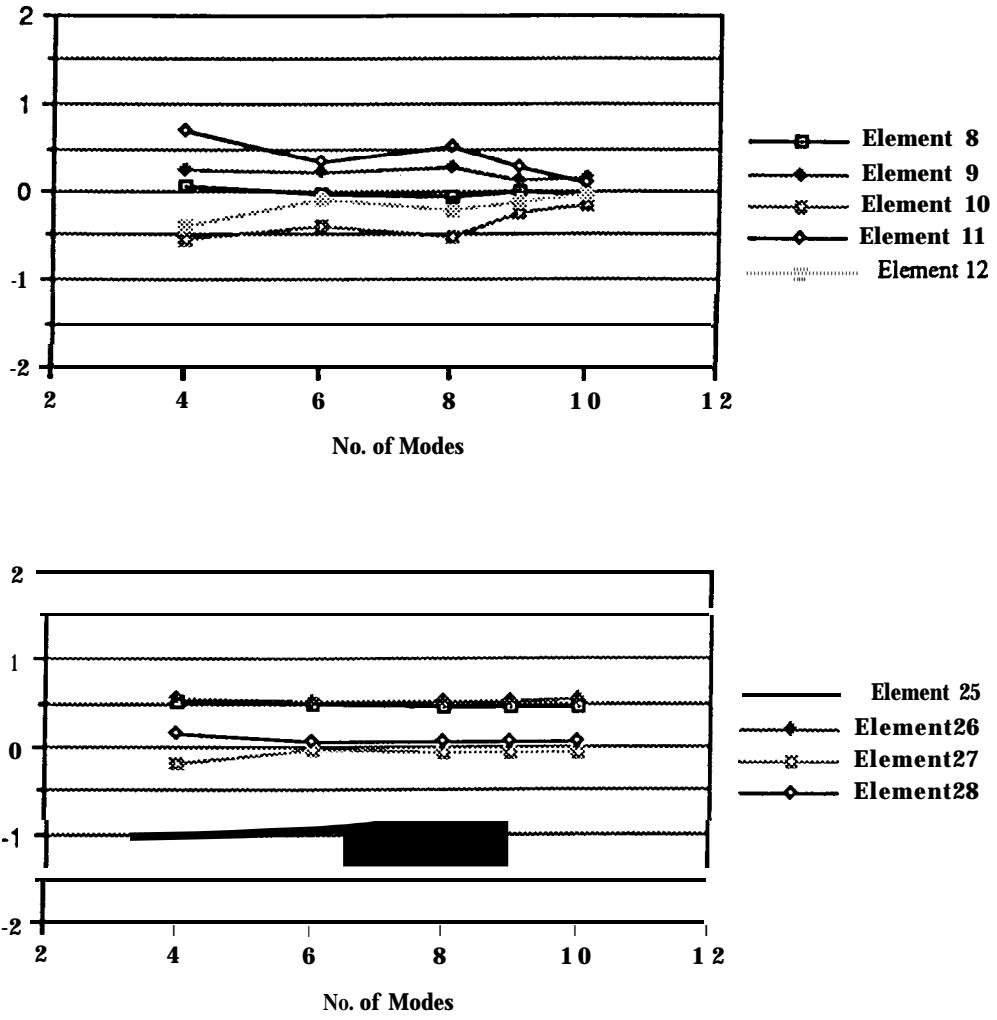


Fig.4.3 Model Updating Results - Mass Elements  
(Macro 1, NL3)

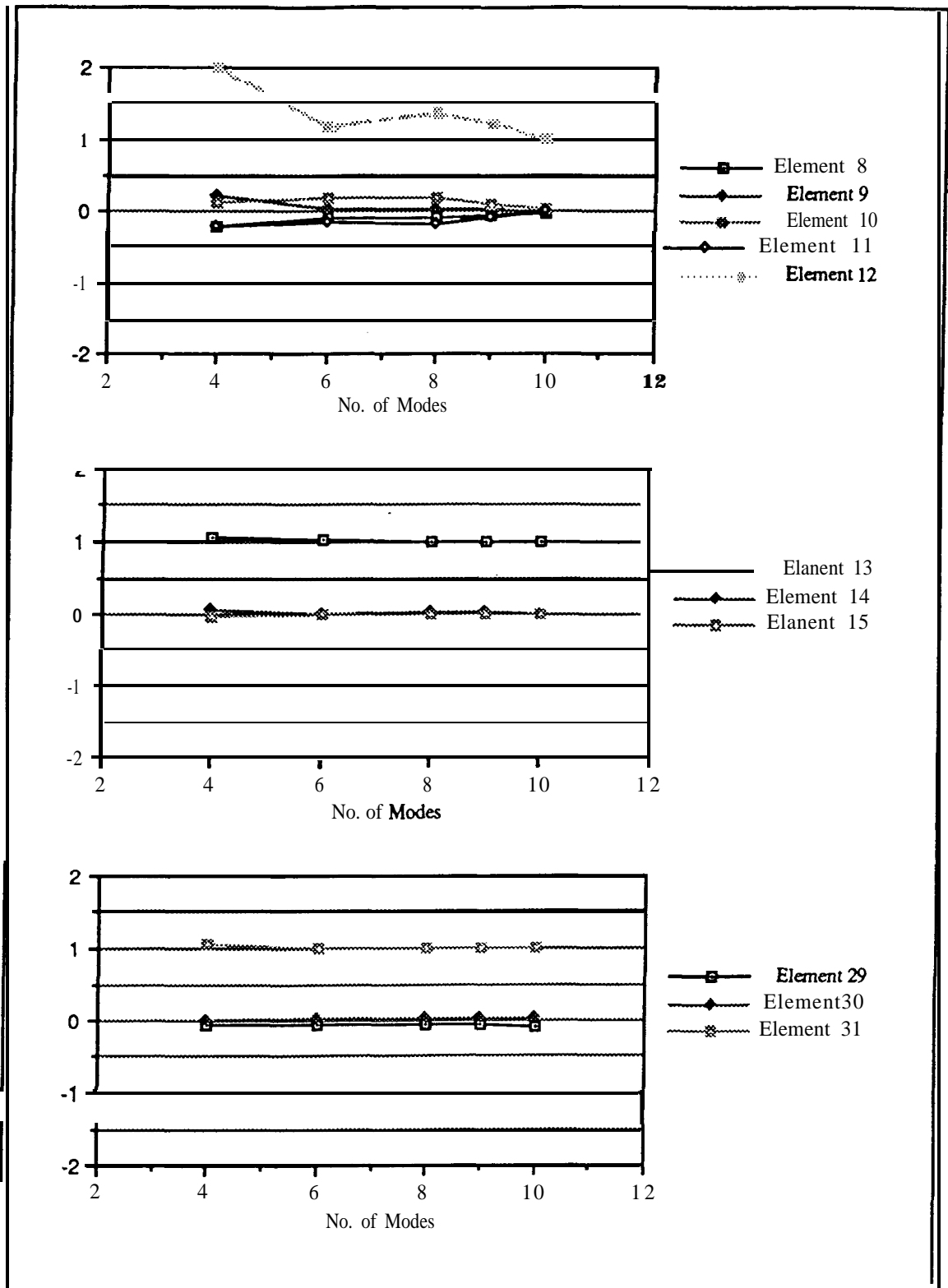


Fig.4.4 Model Updating Results - Stiffness Elements  
(Macro 1, NL3)

### 4.3 CONCLUSIONS

Model updating using arbitrarily chosen macro elements has been applied to a bay structure for which “experimental” data are noisy and incomplete. The error location procedure has been found to be very insensitive to the “measurement” errors - in the presence of measurement errors of up to 1 % in the eigenvalues and 10 % in the eigenvectors, it succeeds in locating the mismodelled regions. The updating results are quite accurate in terms of modal parameters **and**, moreover, in terms of correction factors, when sufficient eigensensitivity terms are used. In this case study, measurement errors were introduced by contaminating the modal parameters of the correct or modified structure with random noise.

However, in practice, the characteristics of the measurement errors might not result in random variations in the modal parameters. For the updating method to be useful in practical application, various error sources in testing - such as the mass loading effect of transducers, shaker/structure interaction, etc. - should be considered and more realistic errors rather than random noise should be included in the “experimental” data.

# CHAPTER 5

## CHAPTER 5

### ERRORS INVOLVED IN MODAL PARAMETER ESTIMATION FROM TEST DATA

#### 5.1 PRELIMINARIES

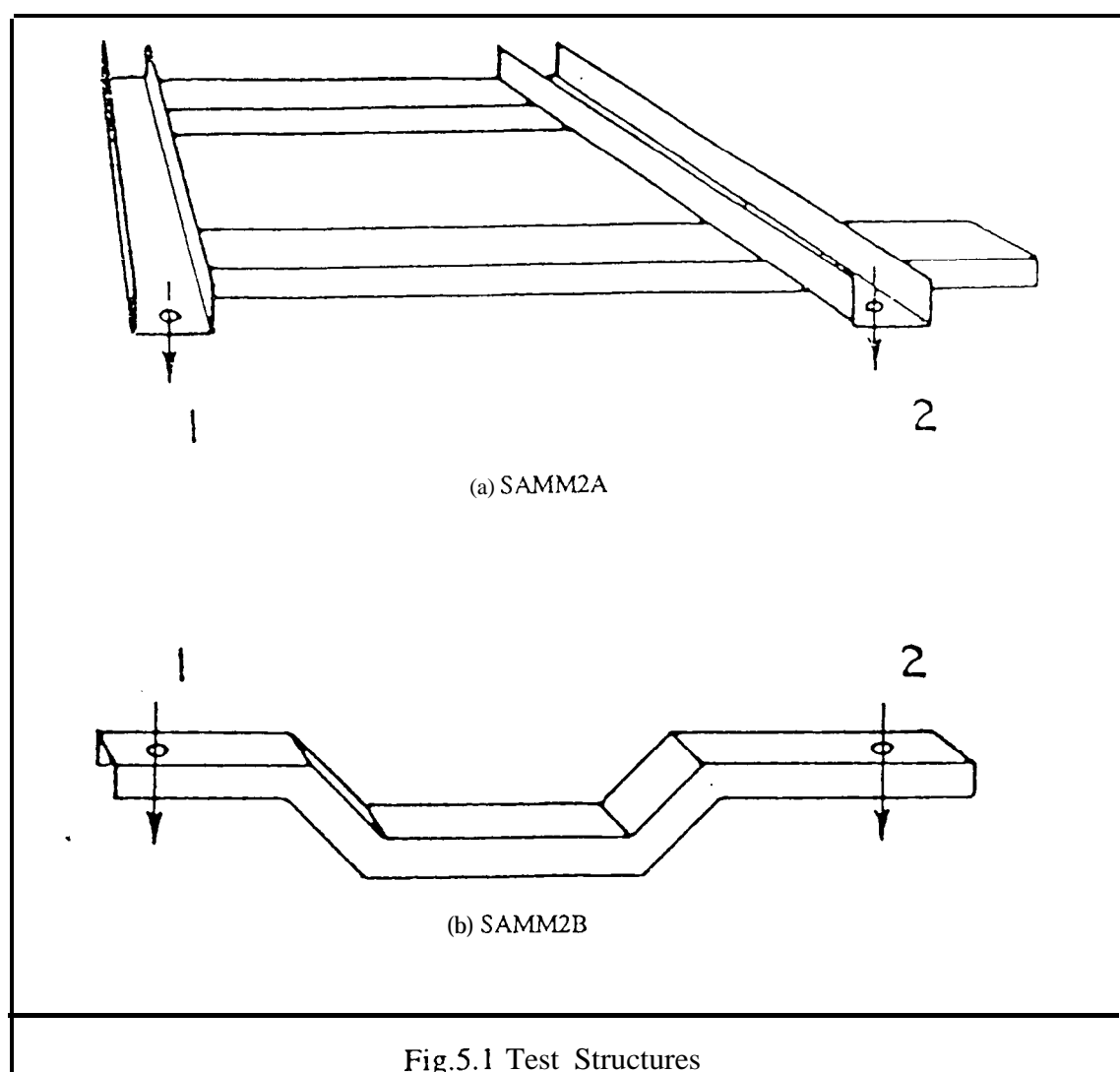
In Chapter 4, measurement errors were introduced by contaminating the modal parameters of the correct or modified structure with random noise of different levels to check the sensitivity of the **IEM** to noise on the test data. In practice, however, realistic measurement errors might not be represented by random errors on the modal parameters. For the updating method to be practical, various error sources in testing should be considered in detail and more realistic errors should be included in the “experimental” data. Therefore, the errors involved in modal parameter estimation from the test data will be discussed in detail, and the resultant “experimental” modal data which contain possible experimental errors will be used to update the corresponding analytical model to check the validity of the **IEM**.

## 5.2 MODAL TESTING OF SAMM STRUCTURES

### 5.2.1 DESCRIPTION OF TEST STRUCTURES

i

Vibration measurement was carried out with real structures called SAMM2A and 2B structures which had been used for the project to assess the State-of-the-Art of Mobility Measurements (SAMM) [28] to illustrate some measurement errors. The structures can be seen in the Fig.5.1. Two substructures 2A and 2B could be bolted together at two points by connecting adapters to form a complete structure 2C.



### 5.2.2 MEASUREMENT

In turn, each of the structures was suspended by light elastic bands to approximate a **free-free** condition. The highest rigid-body mode frequency was less than 10 % of that for the lowest elastic mode of the structures.

The frequency range of interest was 0 - 2.4 **kHz**, and this range was divided into 3 equal frequency ranges: 0 - 0.8 **kHz**, 0.8 - 1.6 **kHz** and 1.6 - 2.4 **kHz**. **SAMM2A** and **SAMM2B** - which are linear and lightly damped structures - were tested using three different excitation signals: pure random, pseudo-random and impact. When the excitation to the test structure is random or pseudo-random, it is necessary to use a push rod to connect the exciter to the test structure. Ideally, the push rod should be infinitely stiff for transmission of axial force, yet have zero bending stiffness to **allow** no moment or lateral force transfer [29]. A practical compromise to this ideal is needed to prevent the combination of the dynamics of the push rod - exciter system with those of the structure. Two push rods with different lengths were used to check the validity of the data obtained. The dimensions, properties and resonant frequencies of push rods can be seen in the Appendix D.

**FRFs** obtained using different excitation techniques are presented in Fig.5.2 to Fig.5.7.

As can be seen in the plots, all the techniques gave similar results. Discrepancies between various excitation techniques are found at the resonance frequencies of the test structures.

These discrepancies clearly indicate the leakage problem associated with light damping.

Because pseudo-random is essentially periodic, it does not suffer from leakage errors. On the other hand, the nonperiodic techniques (pure random and impact) suffer from leakage or window errors [29]. Another discrepancy - frequency shifts - can be found above 1.4 **kHz** (**SAMM2A**) and above 1.1 **kHz** (**SAMM2B**). These shifts result from the effects of the connection of the exciter to the test structure. On the other hand, in the case of impact testing there is no need for any connection, which means the resonance frequencies from

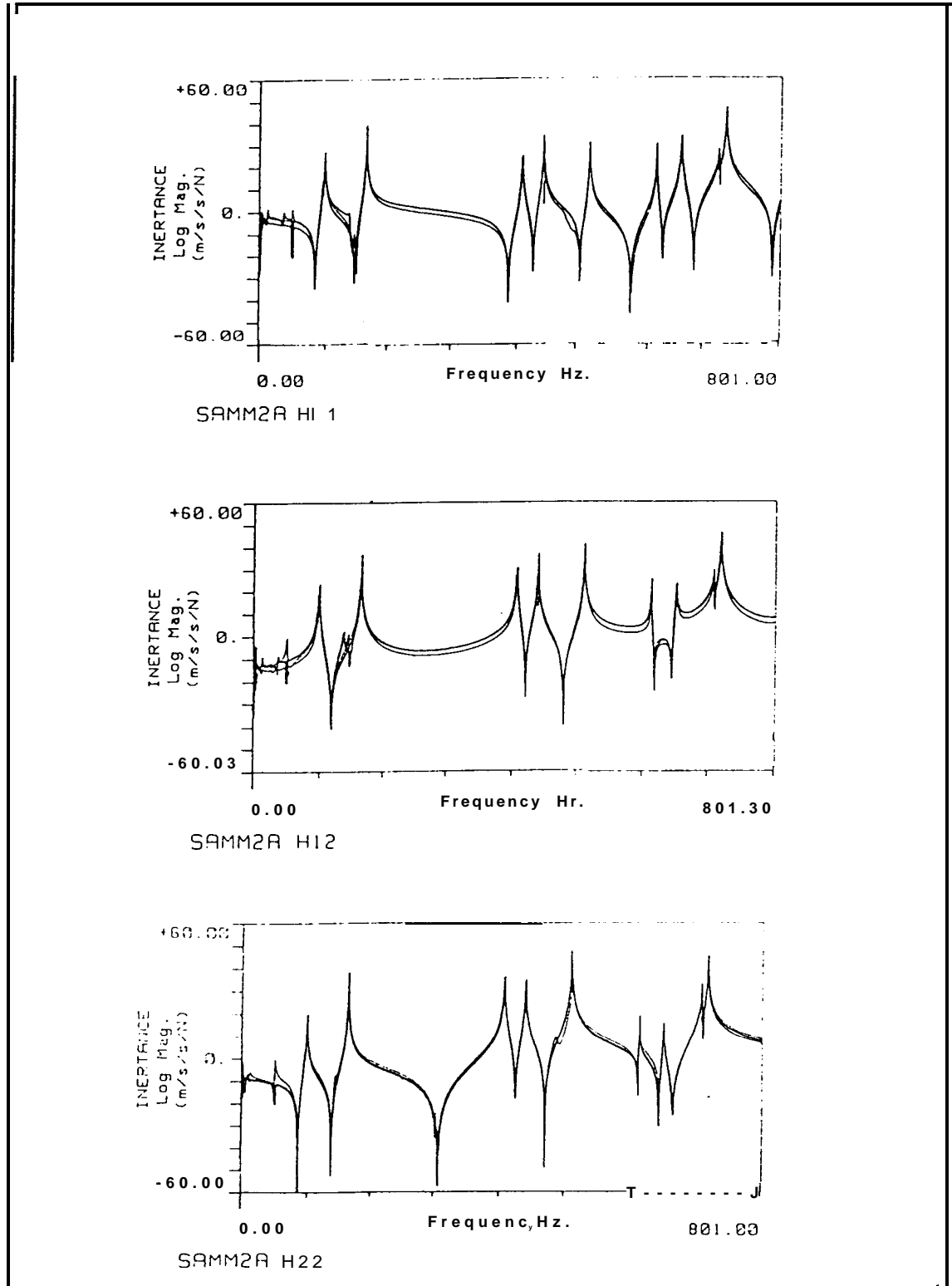
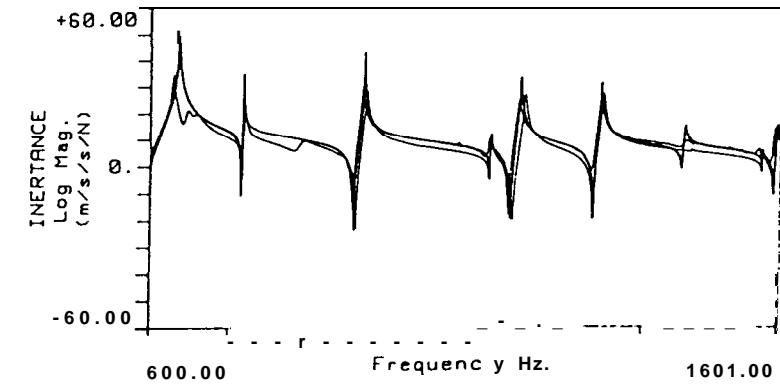
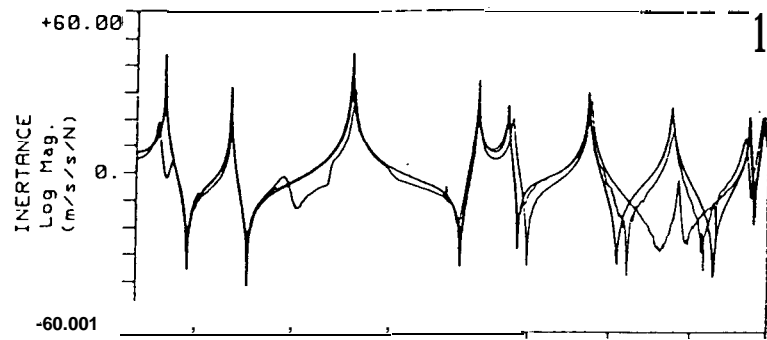


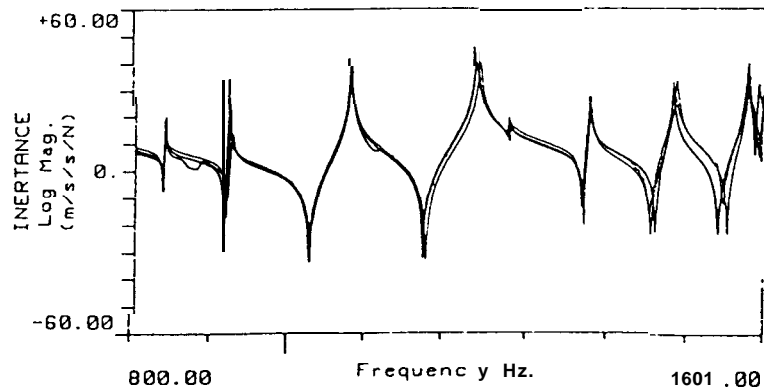
Fig.5.2 Comparison of FRFs from Different Excitation Techniques  
(SAMM2A ; 0 - 800 Hz)



SAMM2A H11



SAMM2A H12



SAMM2A H22

Fig.5.3 Comparison of FRFs from Different Excitation Techniques  
(SAMM2A; 800 - 1,600 Hz)

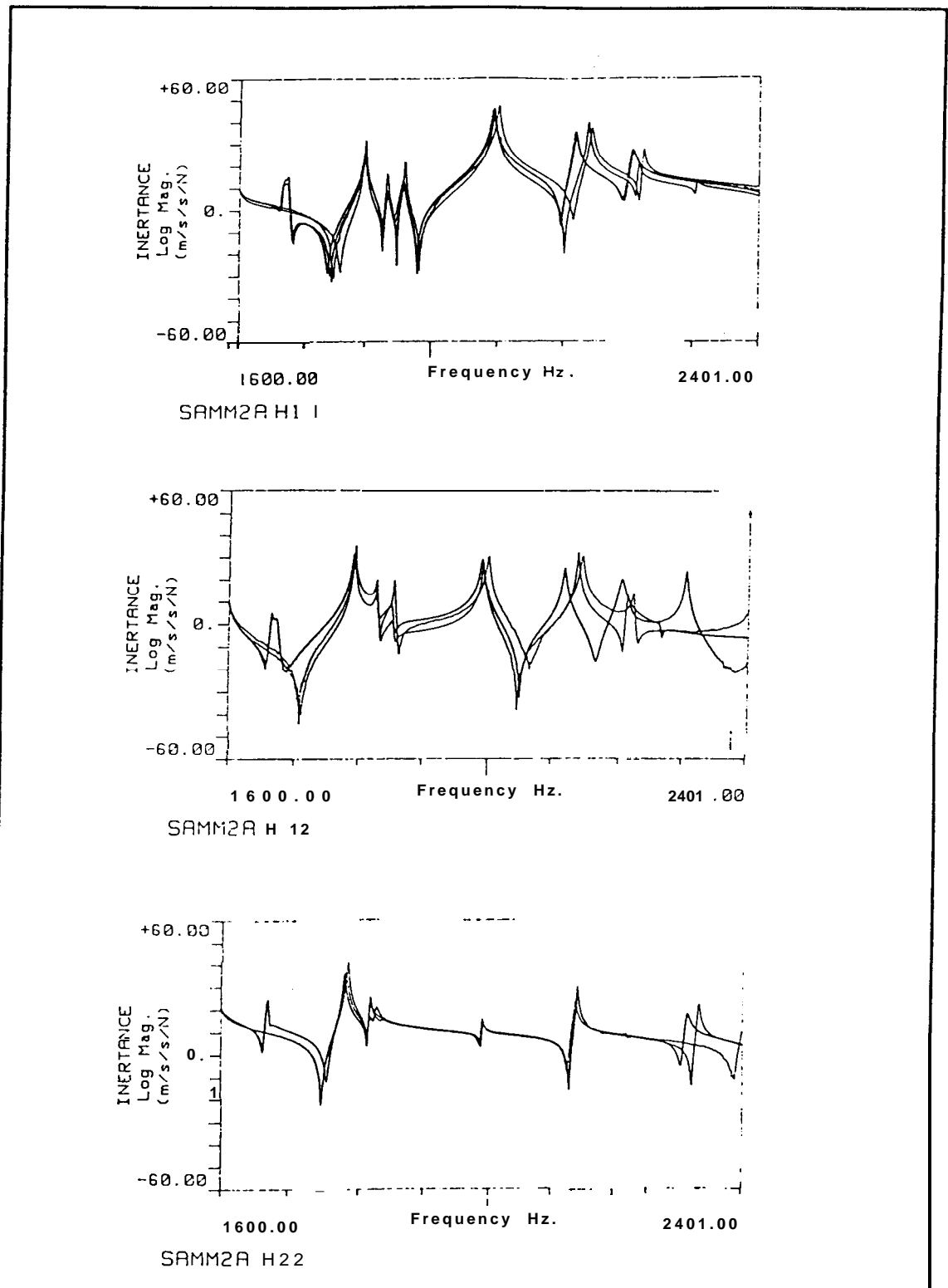
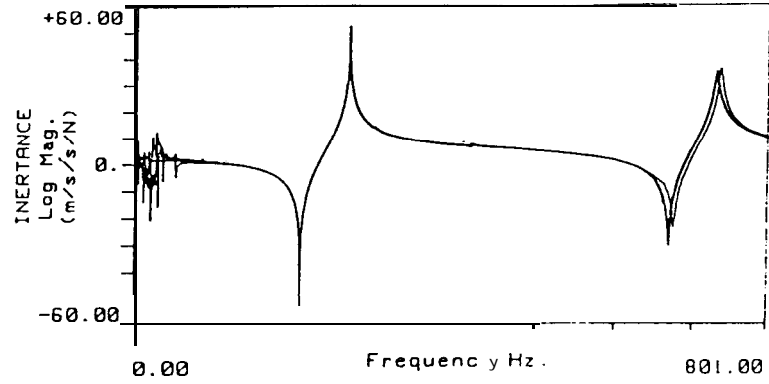
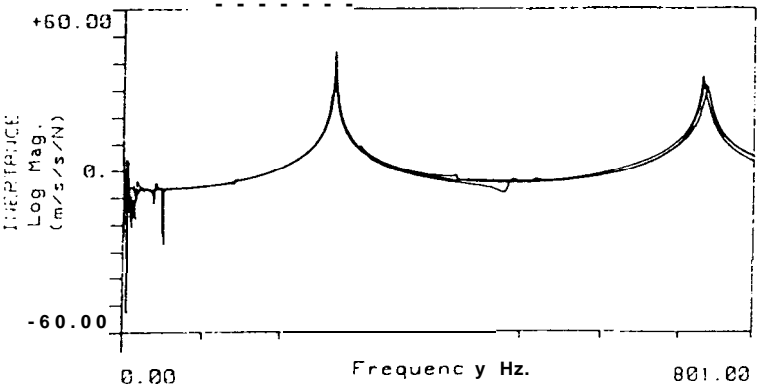


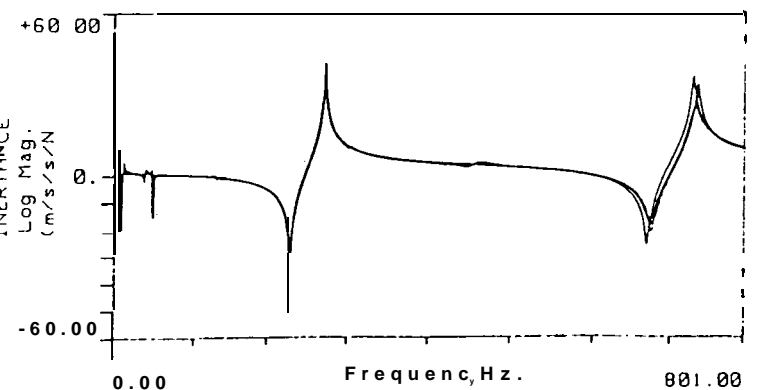
Fig.5.4 Comparison of FRFs from Different Excitation Techniques  
(SAMM2A; 1,600 - 2,400 Hz)



SAMM2BH1 1



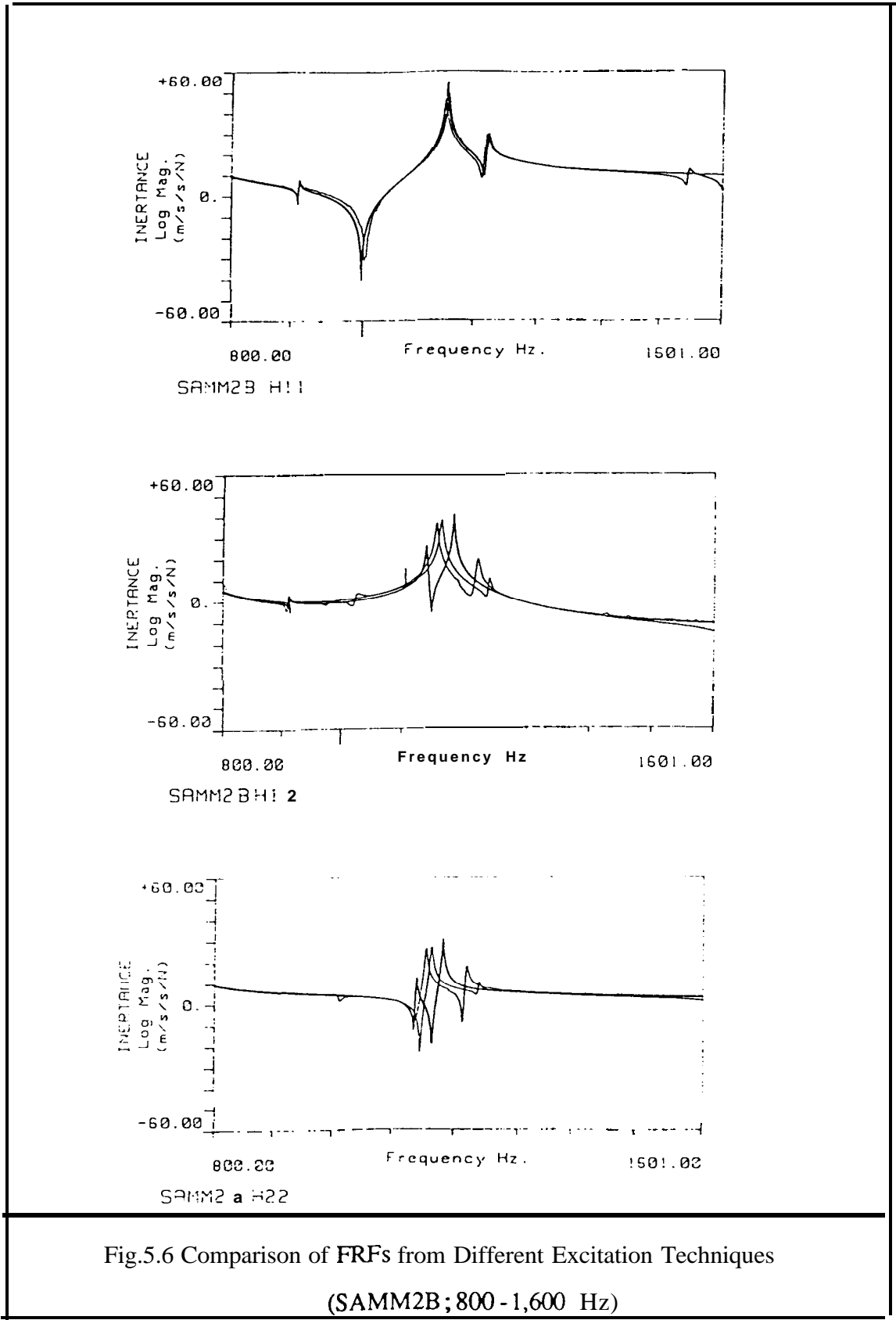
SAMM2B H12



SAMM2B H22

Fig.5.5 Comparison of FRFs from Different Excitation Techniques

(SAMM2B ; 0 - 800 Hz)



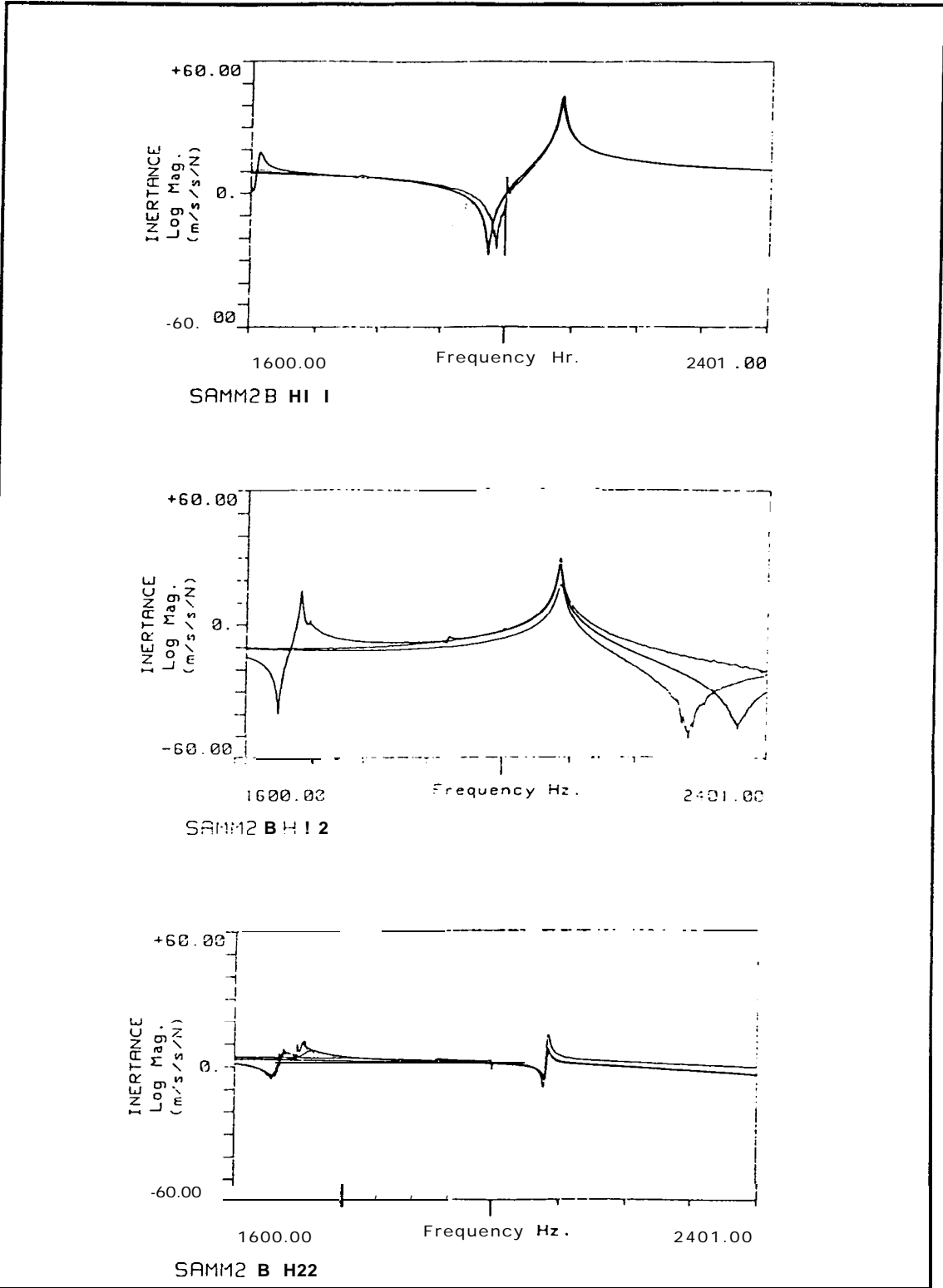


Fig.5.7 Comparison of FRFs from Different Excitation Techniques  
(SAMM2B; 1,600 - 2,400 Hz)

impact testing are correct. The gain in quality using an exciter was not considered large enough to justify the extra effort. In addition, the frequency shifts caused by the dynamics of an exciter-push rod system were too considerable to be ignored in the frequency range of interest.

### 5.3 ERRORS IN MODAL PARAMETER ESTIMATION

The characteristics of the real errors in experimentally-measured modal parameters might not be random, as supposed for the case in Chapter 4. For the updating method to be practical, various error sources in testing should be considered and more realistic errors should be included in the “experimental” data used for method validation.

The errors involved in modal parameter estimation can be **categorised** in three groups - measurement errors, signal processing errors and analysis errors, all of which will be discussed in detail in the following sections.

### 5.4 MEASUREMENT ERRORS

#### 5.4.1 NONLINEARITY OF STRUCTURE

One of the fundamental assumptions of modal analysis is that the structure is linear. This means that doubling the magnitude of the excitation force results in a doubling of the response, and that if two or more excitation patterns are applied simultaneously, the response of the structure is the sum of the individual responses to each of the forces acting alone. For many important kinds of structure, however, this assumption is not valid. There are many reasons for the system to be nonlinear:

- 1) violation of “small displacement” theory;

- 2) rattling of loosely fastened components;
- 3) nonlinear stiffness; or
- 4) nonlinear damping

Nonlinearity in the structure may shift energy from one frequency to many new frequencies thereby resulting in distortions in the measured FRF curves. One way to reduce the effect of nonlinearity is to randomise these contributions by using random excitation. Subsequent averaging will reduce these contributions in the same way as random noise is reduced.

#### 5.4.2 NONSTATIONARITY OF STRUCTURE

Another fundamental assumption of modal analysis is that the structure's properties are stationary. This means that the modal parameters of the structure are constant with time. Sometimes, the behaviour of a structure may change during the measurement period because of slipping joints or loosening bolts, etc. This kind of measurement error should be excluded on the test site by closely-controlled experimental procedure.

#### 5.4.3 MASS LOADING EFFECT OF TRANSDUCERS

When an accelerometer is mounted on a structure, the increase in overall mass combined with a change in the local stiffness will inevitably alter the dynamic properties of the structure. The acceleration of the part of the structure near the accelerometer and the resonance frequencies of the structure are modified according to the following relationship [30]:

$$a_m \approx a_t \frac{m}{m+m_a} \quad f_m = f_t \sqrt{\frac{m}{m+m_a}} \quad (5.1)$$

where  $a_m$ ; **measured** acceleration  
 $a_t$ ; true acceleration  
 $f_m$ ; **measured** resonance frequency  
 $f_t$ ; true resonance frequency  
 $m$ ; effective mass of that part of the **structure** to which the accelerometer is mounted  
 $m_a$ ; accelerometer mass

As a general rule, the accelerometer mass should be less than one tenth of the apparent mass of the modes of the structure. When the added mass is of the same order as the apparent mass of the modes of the structure, mass cancellation becomes essential.

## 5.4.4 ERRORS BY TRANSDUCER CHARACTERISTICS

### 5.4.4.1 Useful Frequency Range

The upper limit for measurements can be set to 30 % of the accelerometer's own natural frequency so that vibration components measured at this limit will be in error by less than + 10 % or to 20 % for errors of less than + 5 % if the accelerometer is properly fixed to the test structure. It should be noted that an accelerometer's useful frequency range is significantly higher, i.e. to  $\frac{1}{2}$  or  $\frac{2}{3}$  of its resonance, where 3 dB linearity is acceptable.

### 5.4.4.2 Transverse Sensitivity

† The transverse sensitivity of an accelerometer is its sensitivity to accelerations in a plane perpendicular to the main transducer axis. The transverse resonance frequency is just outside the upper frequency limit. At frequencies less than 16 % (10 %) of the main axis resonance frequency, transverse sensitivity can be kept below 10 % (3 %). The

transverse sensitivity can be reduced by aligning the minimum transverse sensitivity axis in the direction of maximum transverse acceleration.

#### 5.4.4.3 Mounting Effect

The method of attaching the accelerometer to the measurement point is one of the most critical factors in obtaining accurate results from measurements. Poor mounting results in a reduction in the mounted resonance frequency, which can severely limit the useful frequency range of the accelerometer. There are various methods of attaching the accelerometer to the test structure - such as stud mounting, cementing stud mounting, **wax** mounting, magnet mounting, etc. The advantages/disadvantages of various methods can be found in **Refs.[29,30]**.

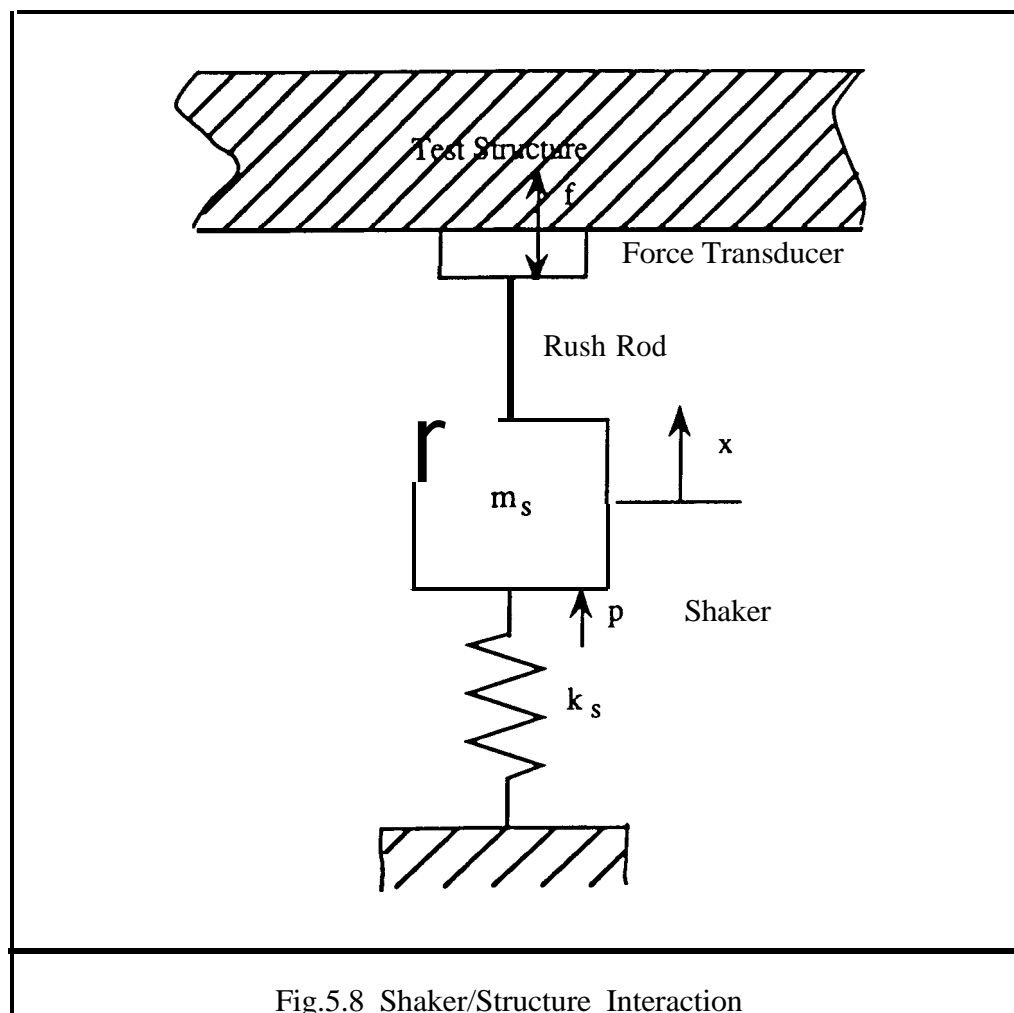
Local stiffness changes introduced by attaching the accelerometer to the structure should also be considered when it is attached to a flexible surface [29].

#### 5.4.5 SHAKER/STRUCTURE INTERACTION

When the excitation to the structure is a continuous signal, such as random or sinusoidal, a shaker must be attached to the structure, usually incorporating a force transducer. So long as the motion at the driving point of the shaker attachment remains **colinear** with the shaker axis, the dynamics of the excitation system can be removed by mass cancellation techniques. However, if the motion at the driving point includes rotation or transverse displacement, the resulting contamination of test data can no longer be removed. The solution is to attach the shaker to the **structure** through a push rod, which should have high axial stiffness for transmission of axial force but low lateral or bending stiffness to

allow little moment transfer. Guidance on how to design the push rod can be found in Refs.[31,32].

Apart from the effect of the push rod, shaker/structure interaction causes 'notches' in the input force spectrum at resonances of the structure [29,33]. Because little force is required to produce a large response near resonances, a large amount of the force generated in the shaker is used to excite the armature mass of the shaker. Fig.5.8 shows shaker/structure model.



The actual force applied to the structure can be calculated as follows:

$$p = f + m_s \ddot{x} \quad (5.2)$$

Fourier transform of equation (5.2) becomes

$$P(\omega) = F(\omega) + m_s H(\omega) F(\omega)$$

Thus

$$F(\omega) = H_i(\omega) P(\omega) \quad (5.3)$$

where  $H(\omega)$  is an inertance and

$$H_i(\omega) = \frac{1}{1 + m_s H(\omega)}$$

If  $P(\omega)$  is constant, the power spectra of input force and output response can be expressed as

$$\begin{aligned} G_{FF}(\omega) &= |H_i(\omega)|^2 G_{PP} \\ &= \frac{G_{PP}}{(1 + m_s H(\omega))(1 + m_s H^*(\omega))} \\ &= \frac{G_{PP}}{1 + m_s^2 [\{\operatorname{Re}(H(\omega))\}^2 + \{\operatorname{Im}(H(\omega))\}^2] + 2 m_s \operatorname{Re}(H(\omega))} \end{aligned} \quad (5.4)$$

$$\begin{aligned} G_{AA}(\omega) &= |H(\omega)|^2 G_{FF}(\omega) \\ &= |H_i(\omega)|^2 |H(\omega)|^2 G_{PP} \end{aligned} \quad (5.5)$$

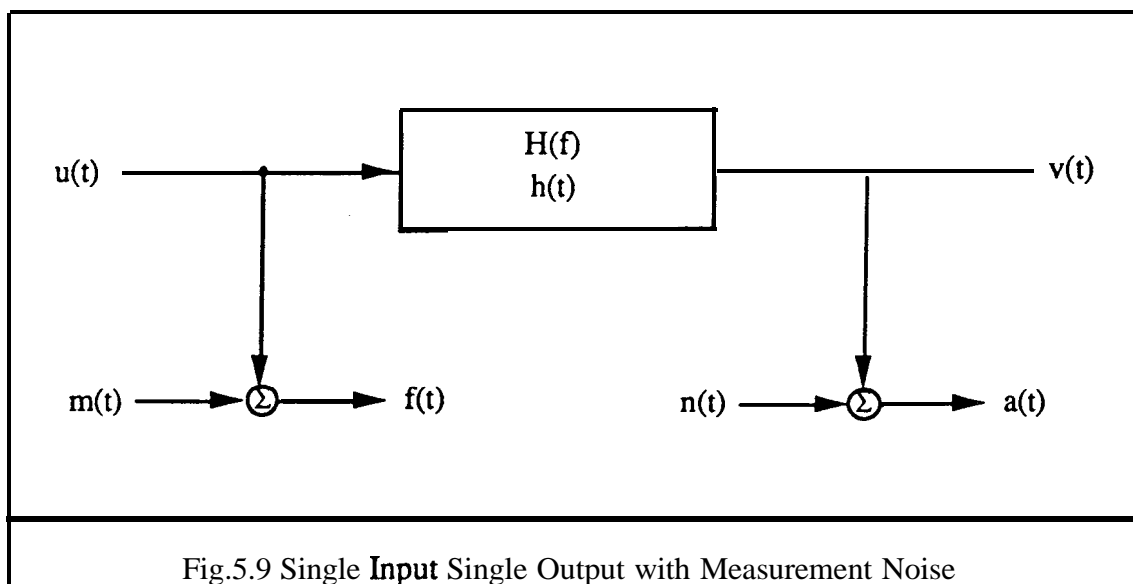
## 5.4.6 MEASUREMENT NOISE

If measured signals  $f(t)$  and  $a(t)$  are contaminated by measurement noise,  $m(t)$  and  $n(t)$  respectively, as in Fig.5.9, the FRF can be expressed as [34]

$$H_1(\omega) = \frac{G_{FA}(\omega)}{G_{FF}(\omega)} = \frac{H(\omega)}{1 + r_i} \quad (5.6)$$

$$H_2(\omega) = \frac{G_{AA}(\omega)}{G_{AF}(\omega)} = H(\omega) (1 + r_o) \quad (5.7)$$

where  $r_i$  is the input noise to signal ratio,  $\frac{G_{MM}}{G_{UU}}$ , and  $r_o$  is the output noise to signal ratio,  $\frac{G_{NN}}{G_{VV}}$ .



Near resonance, where  $r_o$  may become negligible,  $H_2(\omega)$  reduces bias error, while the reverse applies near antiresonance.

The coherence function can be expressed as

$$\gamma^2(\omega) = \frac{|G_{FA}(\omega)|^2}{G_{FF}(\omega) G_{AA}(\omega)} = \frac{H_1(\omega)}{H_2(\omega)} = \frac{1}{(1 + r_i)(1 + r_o)} \quad (5.8)$$

The presence of **uncorrelated** noise signals **will** be indicated in the coherence function.

## 5.5 SIGNAL PROCESSING ERRORS

### 5.5.1 LEAKAGE

Leakage is a phenomenon which may arise in the frequency domain description of a signal due to the time limitation of the **signal** before the **DFT** (Discrete Fourier Transform) calculation is performed. The **DFT** algorithm assumes that the signal to be transformed is periodic in the time window. If the periodicity assumption is not strictly valid, energy in one frequency region leaks into adjacent frequency regions causing the peak amplitudes to drop and the amplitudes in valleys to rise.

The finite Fourier transform of  $x(t)$  can be viewed as the transform of an unlimited time history  $v(t)$  multiplied by a rectangular window,  $u(t)$ , defined by

$$\begin{aligned} u(t) &= 1 && 0 \leq t \leq T \\ &= 0 && \text{otherwise} \end{aligned} \quad (5.9)$$

It follows that the Fourier transform of  $x(t)$  is the convolution of the Fourier transforms of  $u(t)$  and  $v(t)$ , namely,

$$X(\omega) = \int_{-\infty}^{+\infty} U(\Omega-\omega) V(Q) d\Omega \tag{5.10}$$

where  $U(\omega) = T \left\{ \frac{\sin(\omega T/2)}{\omega T/2} \right\} e^{-i \omega T/2}$

Similarly, the estimated spectrum  $\hat{G}(\omega)$  can be calculated by convolution of the window spectrum  $W(\omega)$  and the true spectrum  $G(\omega)$  [35]:

$$\begin{aligned} \hat{G}(\omega) &= W(\omega) * G(\omega) \\ &= \int_{-\infty}^{+\infty} W(\Omega-\omega) G(Q) d\Omega \end{aligned} \tag{5.11}$$

where  $W(\omega) = T \left\{ \frac{\sin(\omega T/2)}{\omega T/2} \right\}^2$

The shape of the window spectrum is shown in Fig.5.10.

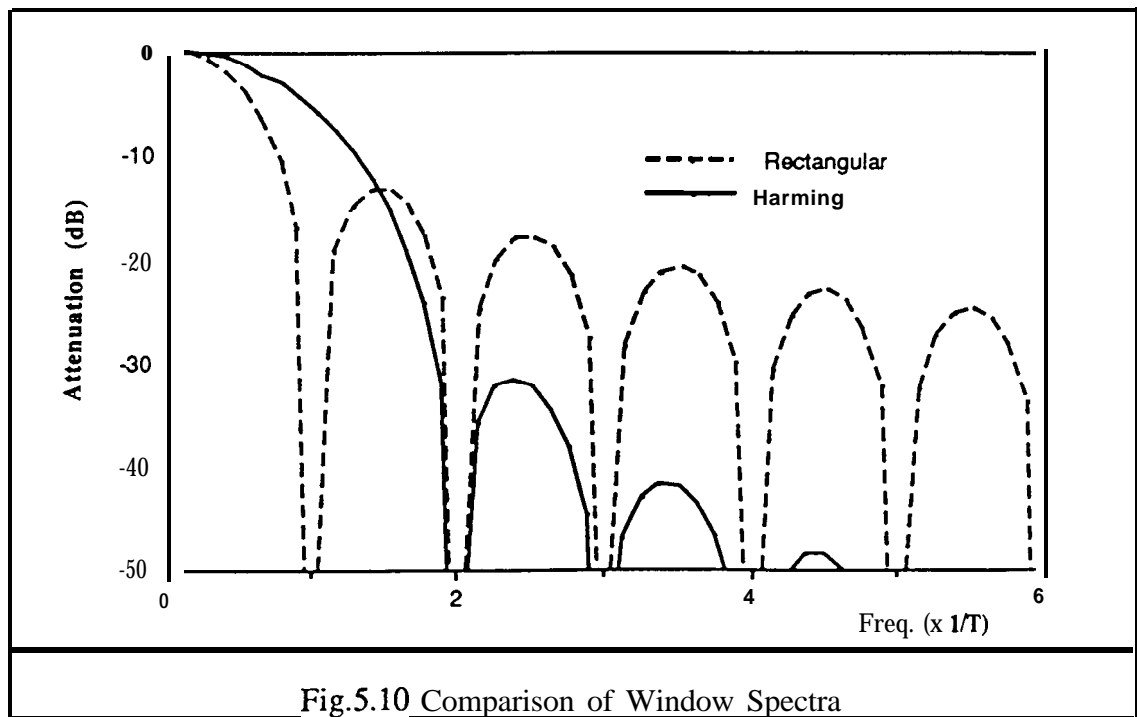


Fig.5.10 Comparison of Window Spectra

Leakage error is illustrated in Fig.5.11. Only in the case where the signal is periodic in the time window (a), is the output spectrum correct. If the periodicity assumption is not valid (b), the signal to be analysed has some very abrupt transitions at the ends of the time record, and, as a result, the **DFT** gives an erroneous result.

Leakage error can be reduced by

- 1) use of truly periodic excitation;
- 2) increasing the frequency resolution; or
- 3) windowing or weighting functions

### 5.5.2 EFFECT OF WINDOW FUNCTIONS

By introducing a time window that tapers the signal so as to present a more gradual entrance to and exit from the time history data to be analysed, the leakage problem can be reduced. Correct use of weighting functions is very important because the amount of leakage may depend on the type of weighting function used in the analysis. The Hanning window is normally used for continuous signals produced by random or sinusoidal excitations, while special force and exponential windows are used for impact tests.

The spectrum of a Hanning window, which is defined by

$$w(t) = \frac{1}{2} \left( 1 - \cos \frac{2\pi t}{T} \right) \quad 0 \leq t \leq T$$

$$= 0 \quad \text{otherwise}$$
(5.12)

can be expressed as [36],

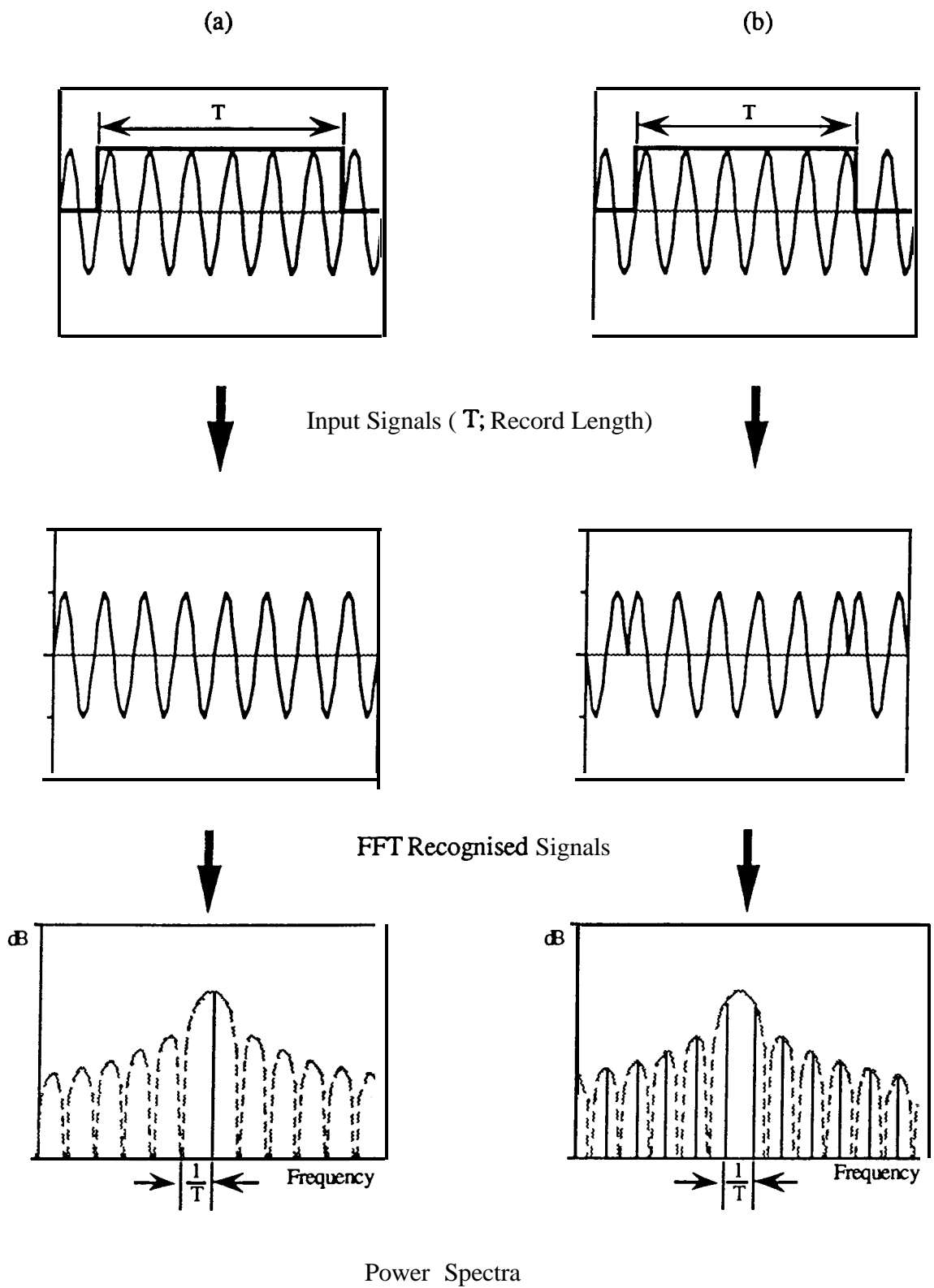


Fig.5.11 Sample Length and Leakage of Spectrum

$$W(\omega) = \left[ \frac{8}{3\omega^2 T} + \frac{2}{3T} \left\{ \frac{1}{(\omega + \frac{2\pi}{T})^2} + \frac{1}{(\omega - \frac{2\pi}{T})^2} \right\} + \frac{4}{T} \frac{1}{(\frac{2\pi}{T})^2 - \omega^2} \right] \sin^2(\omega T/2) \tag{5.13}$$

It can be seen in Fig.5.10 and Table 5.3 that the Hanning window gives better results than the rectangular window when applied to a signal which is not periodic in the time record.

Table 5.3 Comparison of Window Functions

Window	3 dB Bandwidth	Highest Sidelobe	Sidelobe fall-off rate
Rectangular	0.9 Δf	-13 dB	20 dB/decade
Hanning	1.4 Δf	-32 dB	60 dB/decade

The integration of equation (5.11) may readily be carried out numerically using Simpson’s rule

$$\int_{x_1}^{x_2} f(x) dx = h \left[ \frac{1}{3} f_1 + \frac{4}{3} f_2 + \frac{2}{3} f_3 + \frac{4}{3} f_4 + \dots + \frac{2}{3} f_{N-2} + \frac{4}{3} f_{N-1} + \frac{1}{3} f_N \right] + O(N^{-4}) \tag{5.14}$$

Therefore, if a Hanning window is used, the estimated spectrum can be calculated by

$$\hat{G}_i \approx \frac{1}{2T} \left\{ \frac{4}{3} W_{2.5} (G_{i+2.5} + G_{i-2.5}) + \frac{4}{3} W_{1.5} (G_{i+1.5} + G_{i-1.5}) + \frac{2}{3} W_1 (G_{i+1} + G_{i-1}) + \frac{4}{3} W_{0.5} (G_{i+0.5} + G_{i-0.5}) + \frac{2}{3} W_0 G_i \right\} \tag{5.15}$$

where  $W_i$  is a value of window spectrum at  $\frac{i}{T}$  Hz  
 $G_i$  is a value of hue spectrum at  $\frac{i}{T}$  Hz

### 5.5.3 EFFECT OF AVERAGING

Averaging errors can be divided into two types, bias errors and random errors. Bias errors are systematic errors introduced in the measurement or in the analysis, while random errors are the standard deviations of the estimates which are due to the fact that averaging is not performed over an infinitely long time.

#### 5.5.3.1 FRF Estimates

When a FRF is estimated using  $H_1(\omega)$  or  $H_2(\omega)$ , and the signals are random, there is a random error in both magnitude and phase. The normalised random error for the magnitude  $|\hat{H}(\omega)|$  and random error for the phase angle  $\hat{\phi}(\omega)$  are given by [34]

$$\epsilon_r[|\hat{H}(\omega)|] \approx \sqrt{\frac{1 - \gamma^2(\omega)}{\gamma^2(\omega) 2 n_d}} \quad (5.16)$$

$$\sigma[\hat{\phi}(\omega)] \approx \sin^{-1}\{\epsilon_r[|\hat{H}(\omega)|]\} \quad (5.17)$$

where  $\gamma^2(\omega)$  is coherence and  $n_d$  is the number of averages.

### 5.5.3.2 Coherence Function Estimates

The coherence function is estimated with **only** a limited accuracy **from** the auto and cross spectra estimates

$$\hat{\gamma}^2(\omega) = \frac{|\hat{G}_{FA}(\omega)|^2}{\hat{G}_{FF}(\omega) \hat{G}_{AA}(\omega)} \quad (5.18)$$

The normalised random error **is** given by [34]

$$\varepsilon_r[\hat{\gamma}^2(\omega)] \approx \frac{\sqrt{2} (1 - \gamma^2(\omega))}{\sqrt{\gamma^2(\omega) n_d}} \quad (5.19)$$

## 5.6 MODAL ANALYSIS ERRORS

Once **FRFs** are obtained, modal parameters can be extracted from the **FRFs** using one of various curve-fitting methods. This phase is often called ‘modal analysis’. Whatever methods are used, the task is the same: to find the coefficients in a theoretical expression for the **FRF** which most closely matches the measured data by using a least-squares method which can remove random errors in the **FRFs**.

There are many curve-fitting methods available [29] and they can be **categorised** into two groups - global or individual analysis. In global analysis, all the measured **FRFs** are analysed at the same time to extract the modal parameters for a given mode or modes. On the other hand, in individual analysis, one FRF is analysed at a time, therefore, to get modal parameters, all the **FRFs** should be analysed one by one.

Individual **FRFs** tend to exhibit slightly different modal parameters (natural frequencies and modal damping) because of:

- 1) mass loading effect of transducers;
- 2) shaker/structure interaction;
- 3) changes made to the structure during test;
- 4) nonstationarities of the structure and measurement system;

all of which will vary during the prosecution of the test. One of the main **difficulties** in individual analysis is the creation of a consistent data base from individually analysed **FRFs** because of these variation.

### 5.6.1 CIRCLE-FIT MODAL ANALYSIS

Near the resonance under study, the effect of all the other modes - which may be either constant or frequency-dependent - can be eliminated using an appropriate technique [29], thus, the behaviour of the structure can be dominated by a single mode. The Nyquist plot of **FRF** data for the mode can be treated as a circle [29].

The estimated FRF using a **DFT** analyser can be expressed as

$$\hat{H}_2(\omega) = \frac{\hat{G}_{XX}(\omega)}{\hat{G}_{XF}(\omega)} = \frac{\int_{-\infty}^{\infty} G_{XX}(\Omega) W(\Omega-\omega) d\Omega}{\int_{-\infty}^{\infty} G_{XF}(\Omega) W(\Omega-\omega) d\Omega}$$

$$= \frac{\int_{-\infty}^{\infty} |H(\Omega)|^2 |H_i(\Omega)|^2 G_{PP} W(\Omega-\omega) d\Omega}{\int_{-\infty}^{\infty} |H(\Omega)|^2 \frac{\omega_r^2 - \Omega^2 + i \eta_r \omega_r^2}{A_r} |H_i(\Omega)|^2 G_{PP} W(\Omega-\omega) d\Omega} \quad (5.20)$$

where  $H_i(\Omega) = \frac{1}{1 - m_s \Omega^2}$  (H(o) ; receptance)

If we define

$$C_1 = \int_{-\infty}^{\infty} |H(\Omega)|^2 |H_i(\Omega)|^2 W(\Omega-\omega) d\Omega$$

$$C_2 = \int_{-\infty}^{\infty} \Omega^2 |H(\Omega)|^2 |H_i(\Omega)|^2 W(\Omega-\omega) d\Omega$$

equation (5.20) becomes

$$\hat{H}_2(\omega) = \frac{A_r}{\omega_r^2 - \frac{C_2}{C_1} + i \eta_r \omega_r^2} \quad (5.21)$$

Similarly,

$$\hat{H}_1(\omega) = \frac{\hat{G}_{FX}(\omega)}{\hat{G}_{FF}(\omega)}$$

$$\frac{\int_{-\infty}^{\infty} |H(\Omega)|^2 \frac{\omega_r^2 - \Omega^2 - i \eta_r \omega_r^2}{A_r^*} |H_i(\Omega)|^2 G_{PP} W(\Omega-\omega) d\Omega}{\int_{-\infty}^{\infty} |H_i(\Omega)|^2 G_{PP} W(\Omega-\omega) d\Omega}$$

$$= \frac{1}{|A_r|^2} \frac{C_1}{C_3} \left\{ \left( \omega_r^2 - \frac{C_1}{C_3} \right)^2 + \eta_r^2 \omega_r^4 \right\} \hat{H}_2(\omega) \quad (5.22)$$

$$\text{where } C_3 = \int_{-\infty}^{\infty} |H_i(\Omega)|^2 G_{PP} W(\Omega - \omega) d\Omega$$

By comparing equation (5.21) with the true FRF, it can be shown that the  $\hat{H}_2(\omega)$  estimates lie on the true modal circle but in the wrong positions around the circle.  $\hat{H}_2(\omega)$  and  $H(o)$  values are identical if  $\frac{C_2}{C_1} = \omega^2$ , which is only satisfied at very fine frequency resolution. In contrast, it can be shown that  $\hat{H}_1(\omega)$  has the same phase angle as  $\hat{H}_2(\omega)$  but the magnitude is smaller and, as a result, always lies inside the true modal circle, by comparing equations (5.21) and (5.22). If the frequency resolution is increased, so reducing the leakage error,  $\hat{H}_1(\omega)$  tends to  $\hat{H}_2(\omega)$  which, in turn, tends to  $H(o)$ .

Curve-fitting concentrates on a few data points near resonance. If these data points are polluted by noise, or the frequency resolution is not sufficient to extract an accurate circle fit, this method may not be reliable. It also should be noted that these points (together with data points near antiresonances) are most liable to leakage and other errors.

### 5.6.2 LINE-FIT MODAL ANALYSIS

This method uses the fact that the reciprocal of receptance for a SDOF system has a very simple form when plotted as the real and imaginary part against frequency (or (frequency)<sup>2</sup>).

For a SDOF system,

$$a-l(o) = k - m \omega^2 + i d \text{ and/or } + i \omega c \quad (5.23)$$

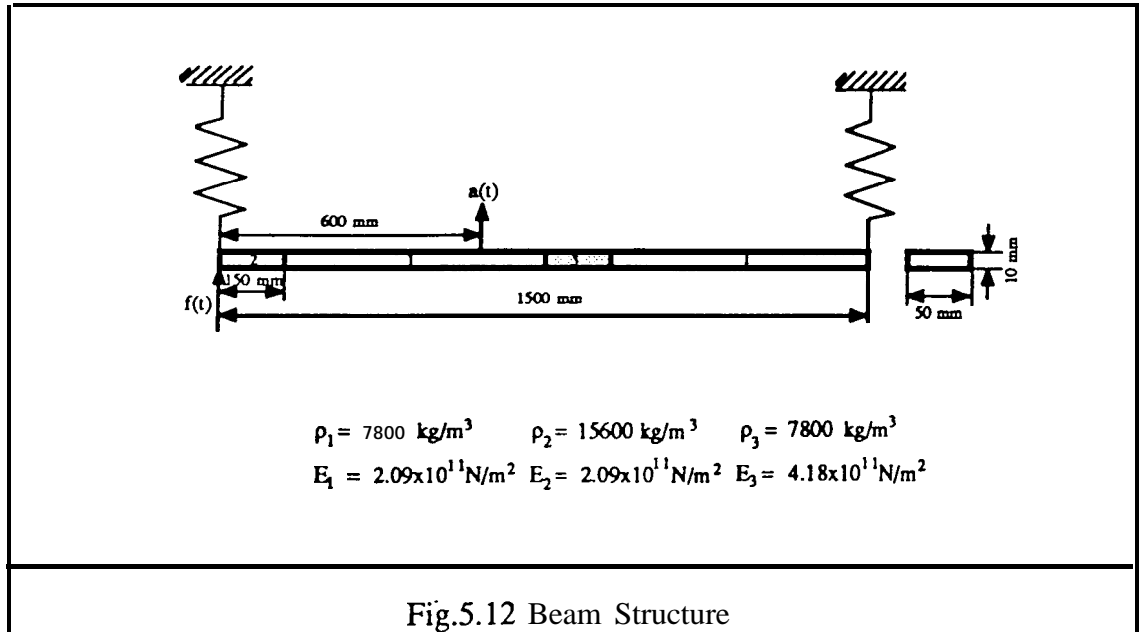
If  $\text{Re}(\alpha^{-1}(\omega))$  is plotted against  $\omega^2$ , then the result is a straight line whose intercept on the frequency axis gives the resonance frequency and whose slope gives the effective mass. If  $\text{Im}(\alpha^{-1}(\omega))$  is plotted against  $\omega$ , then the slope of the line indicates the magnitude of the viscous damping and the intercept on the magnitude axis gives the level of structural damping. This technique can be extended to MDOF systems by subtracting the effects of other modes before performing the analysis.

This method is useful for modes with insufficient data for circle-fitting, and is less sensitive to leakage errors than is circle-fitting because the data used are away from the immediate resonance region and the leakage error becomes maximum at the region and decreases very rapidly as the frequency moves away from resonance.

## 5.7 NUMERICAL CASE STUDIES

To investigate measurement errors - such as the mass loading effects of transducers, shaker/structure interaction, signal conditioning errors, signal processing errors etc. - on FRFs, a computer program has been written which can simulate the various measurement errors described above (Appendix E).

The test structure used in the following examples is a beam shown in Fig.5.12. The structure was considered to be “excited” at a free end of the beam by a shaker whose armature mass was 20 g. Periodic random excitation was “applied” throughout these case studies except in the case of leakage in which case pure random was also used for comparison. The response of the structure was “measured” using an accelerometer whose mass was 20 g. A force transducer of 10 g was assumed to “measure” input force. A two-channel FFT analyser which has 801 lines of frequency resolution was used to obtain frequency response functions. The frequency range of interest was 0 - 800 Hz.



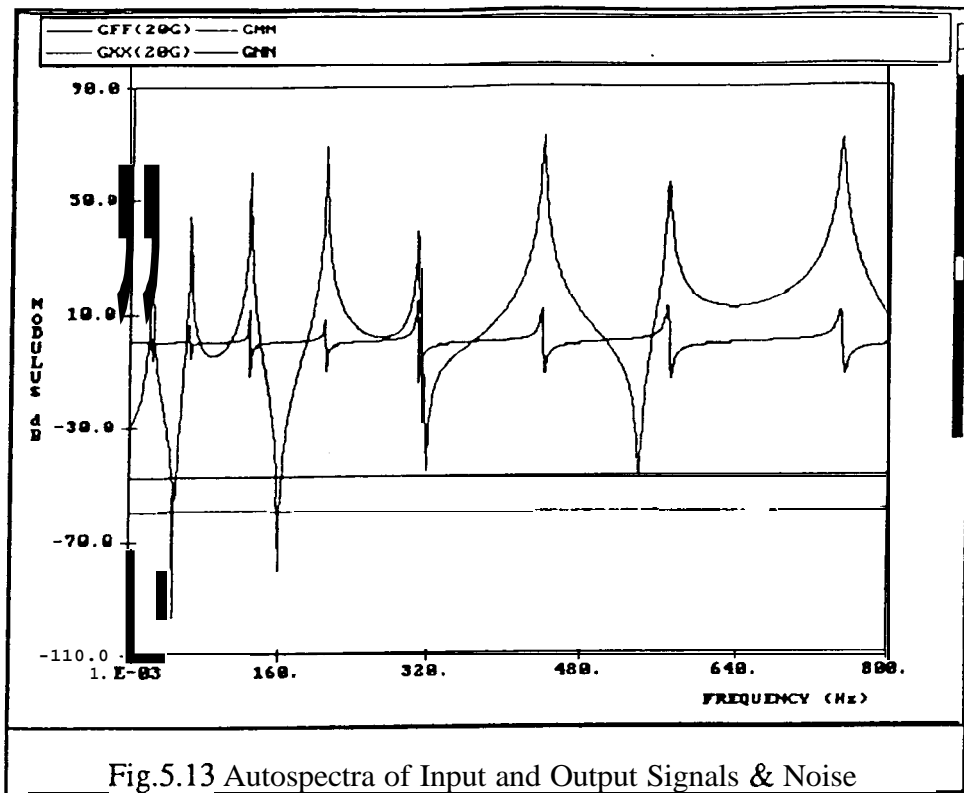
Input and output noise was assumed to be white noise. The ratio of the noise spectrum to the signal spectrum,  $\bar{r}$ , which is defined as

$$\bar{r} = G_N / \bar{G}_S$$

where  $G_S$  is a signal spectrum,  $G_N$  is a noise spectrum and  $\bar{G}_S$  which is defined by

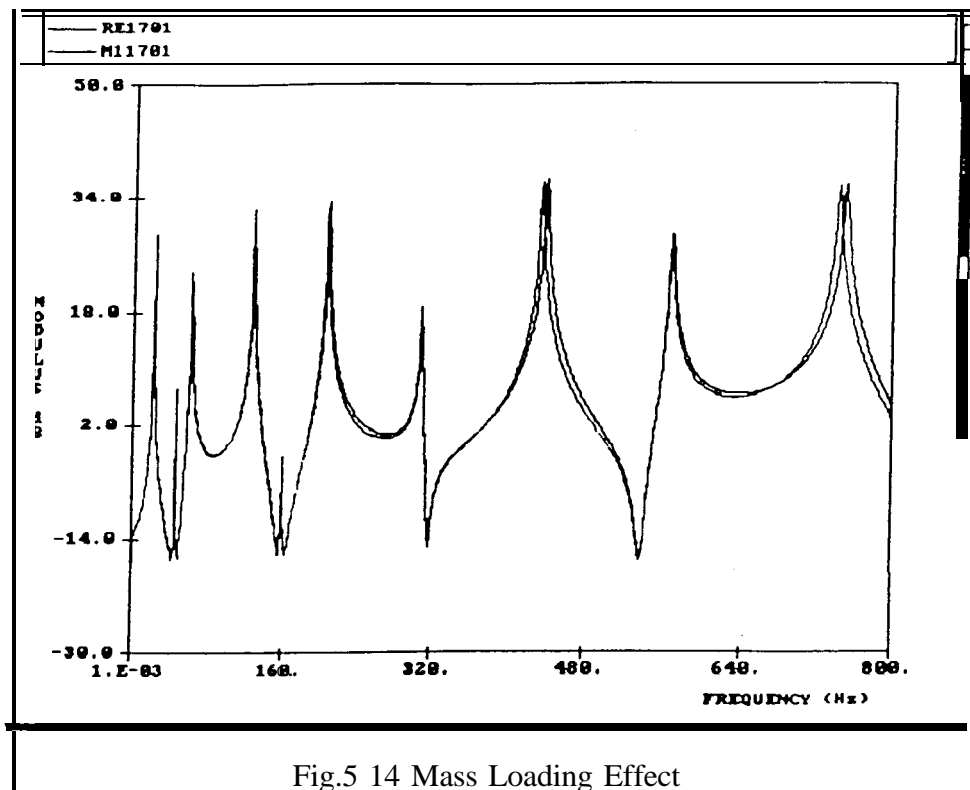
$$\bar{G}_S = \frac{\int_0^{\omega_M} G_S(\omega) d\omega}{\omega_M}$$

was assumed to be  $10^{-3}$  for the input(force) signal and  $10^{-4}$  for the output(response) signal. The autospectra of input and output signals - noise free - and random noise are shown in Fig.5.13.



### 5.7.1 MASS LOADING EFFECT

To investigate the mass loading effect of an accelerometer, the mass of the accelerometer was increased from 20 g to 100 g. The natural frequencies of all modes decreased (Fig.5.14). The natural frequency of the 6th mode decreased most because this mode has the smallest apparent mass, while that of the 5th mode hardly changed because that mode has the largest apparent mass.

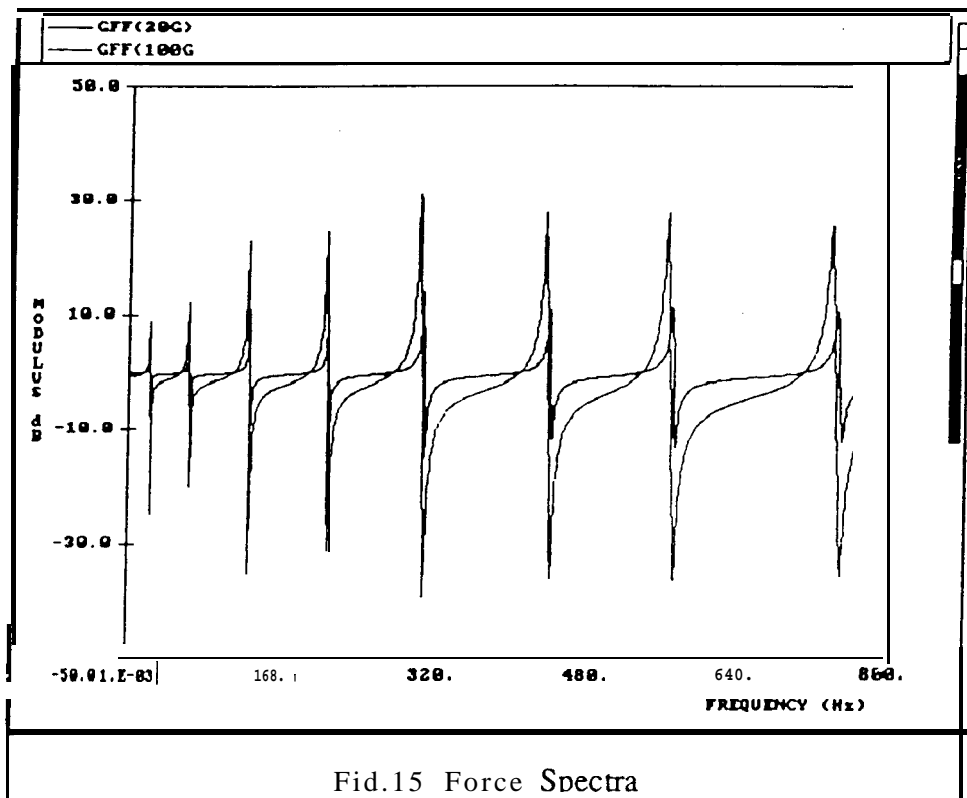


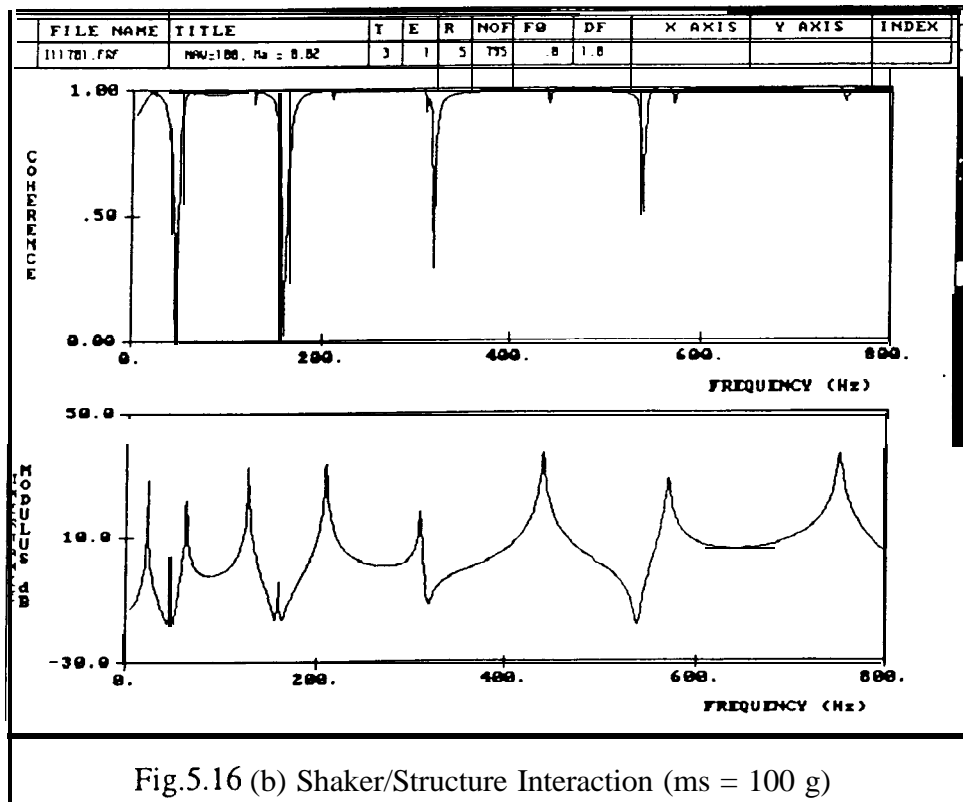
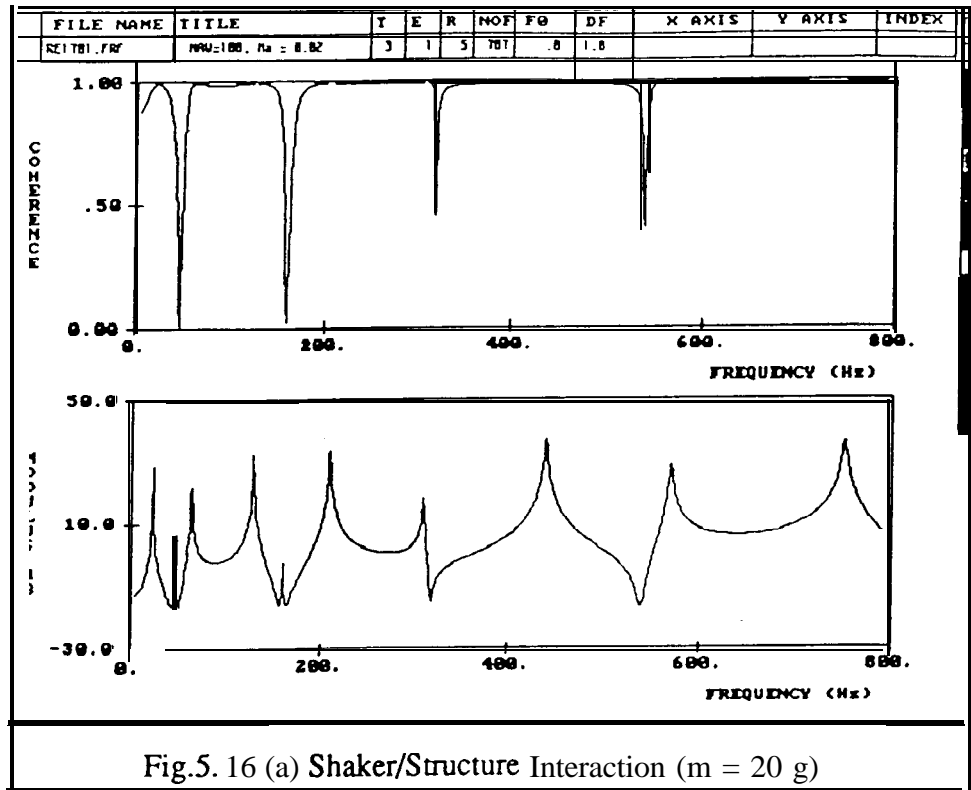
### 5.7.2 SHAKER/STRUCTURE INTERACTION

From equation (5.4), it can be shown that the force spectrum near a resonance is given by

$$G_{FF}(\omega) = \frac{G_{PP}}{1 + \frac{m_s^2 A_r^2}{\eta_r^2}}$$

if  $A_r$  is assumed to be real. The amplitude of the force spectrum at resonance decreases as the armature mass of the shaker increases - approximately proportional to the inverse square of  $m_s$  - as shown in Fig.5.15. The resulting FRFs are compared in Fig.5.16. The only differences are around resonances, where the heavier armature mass makes the coherence drop.





### 5.7.3 RANDOM NOISE EFFECT

Usually, in modal analysis, only those FRF data near resonances are used to extract the modal parameters. In these regions,  $H_2(\omega)$  reduces bias error from random noise because  $r_o$  may become negligible (equation (5.7)).

The output noise spectrum of  $\bar{r}_o = 10^{-4}$ , which may be achieved easily in random excitation, is shown in Fig.5.13 together with output signal spectrum. From Fig.5.17, it can be seen that near resonances, where curve fitting is usually performed, the effects of measurement random errors can be ignored. For example, near the 5th mode ( $f_r = 309.8$  Hz) which has maximum bias error, 304 Hz - 312 Hz, where curve fitting for the mode is usually performed, the normalised bias error is less than 4 % (0.06 - 3.2 %).

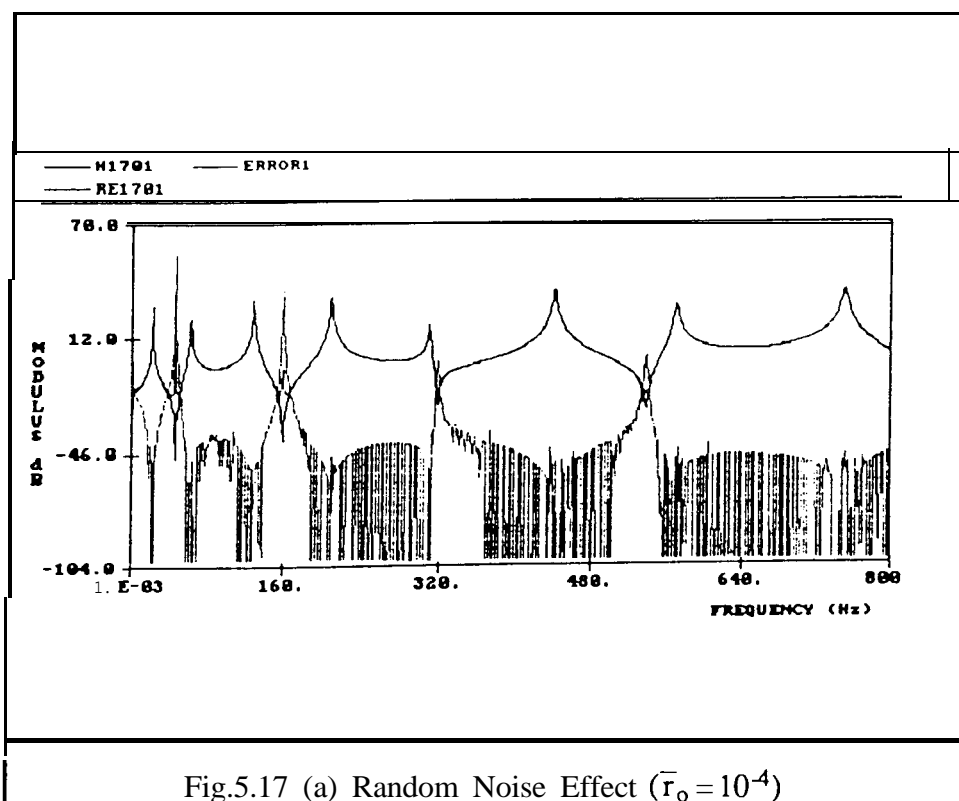
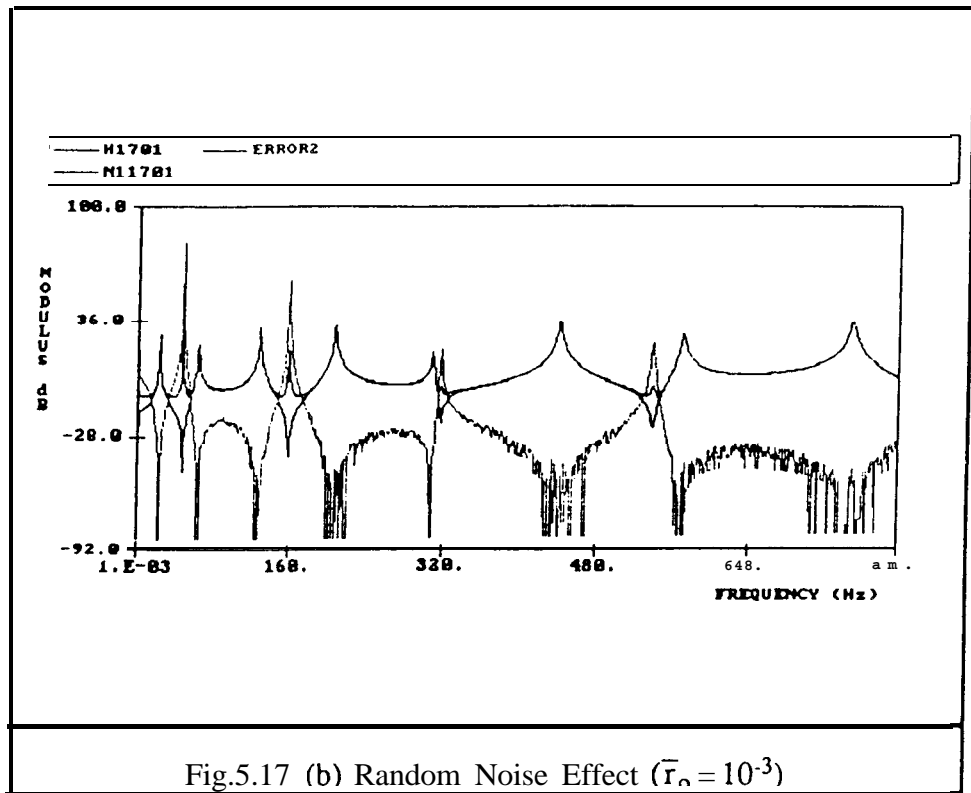


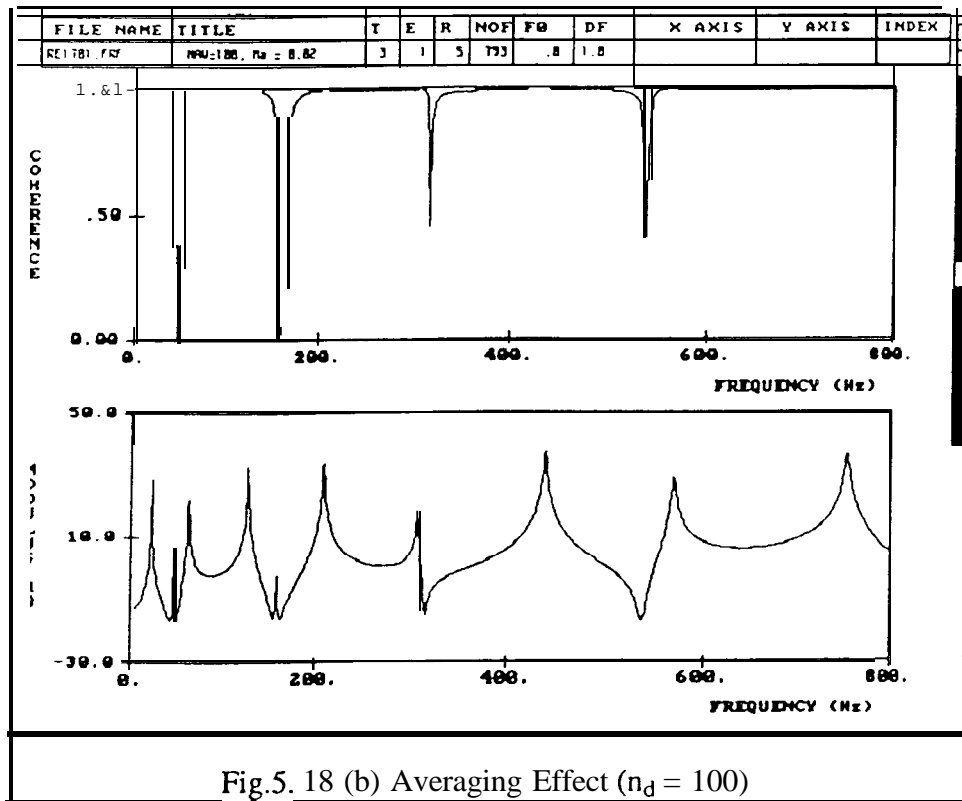
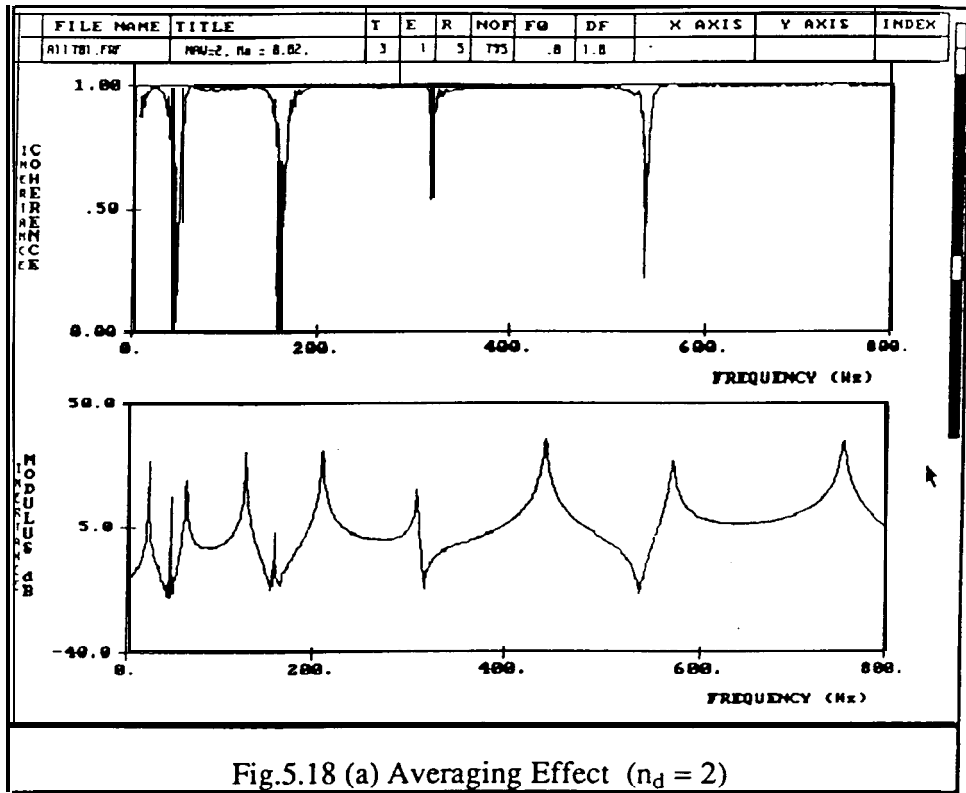
Fig.5.17 (a) Random Noise Effect ( $\bar{r}_o = 10^{-4}$ )



#### 5.7.4 AVERAGING EFFECT

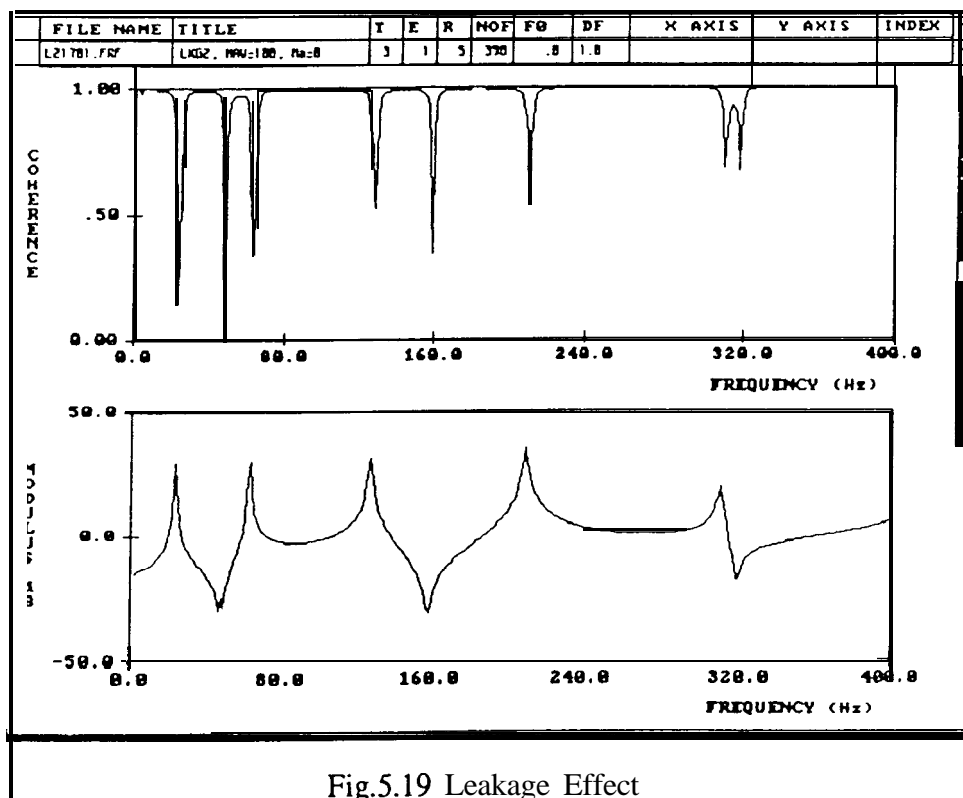
Averaging can reduce random errors in the FRFs and coherence estimates, but cannot reduce bias errors which may be caused by measurement noise, leakage, etc.

Random errors in FRFs and coherence estimates can be calculated using equations (5.16), (5.17) and (5.19). The lower the coherence is the more averages have to be performed to get a certain statistical accuracy because random errors are proportional to  $(n_d)^{-1/2}$ . Fig.5.18 shows the estimates of  $|H_2(\omega)|$  and  $\gamma^2(\omega)$  for different numbers of averages.



## 5.7.5 LEAKAGE ERROR

As discussed in sections 5.5.1 and 5.5.2, leakage causes deformation of the estimated spectra and therefore leads to bias errors in FRF estimates. If the resolution in the analysis is too coarse, compared with the bandwidth of the resonances, the coherence can detect this leakage by giving a value less than one around resonances and antiresonances, as in Fig.5.19. The coherence therefore gives a warning of potential bias errors in the FRF estimates. Fig.5.20 shows the relative error between true and estimated FRFs which is affected by leakage. It can be seen that the most contaminated regions are near resonances and antiresonances.



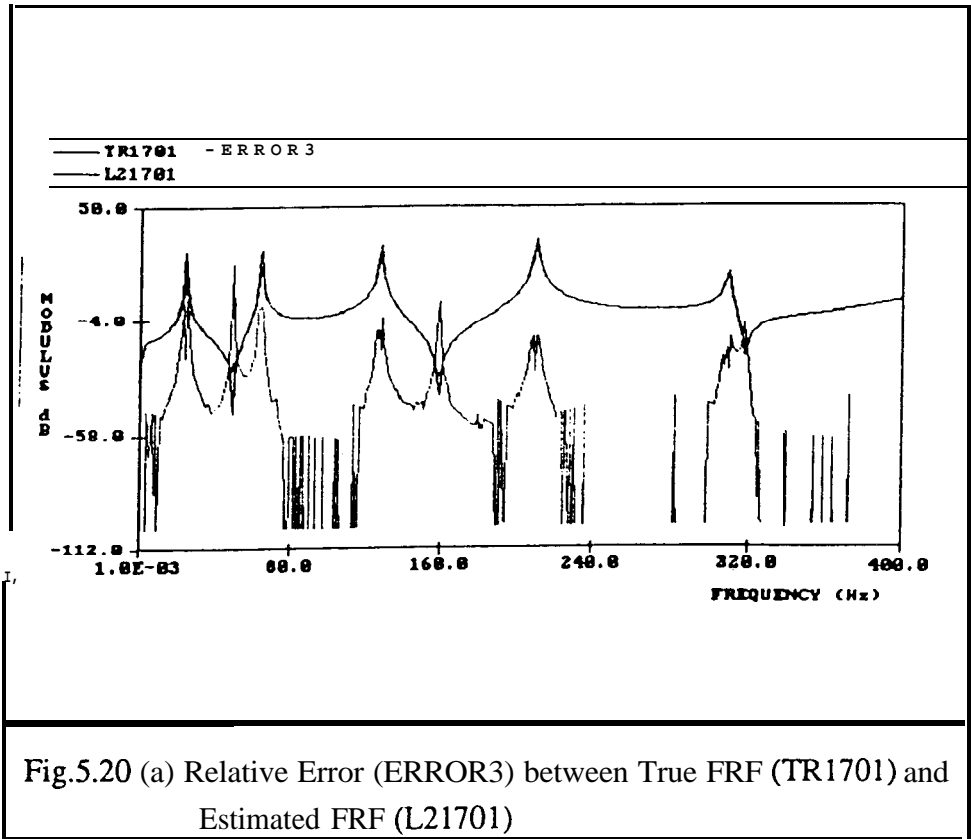


Fig.5.20 (a) Relative Error (ERROR3) between True FRF (TR1701) and Estimated FRF (L21701)

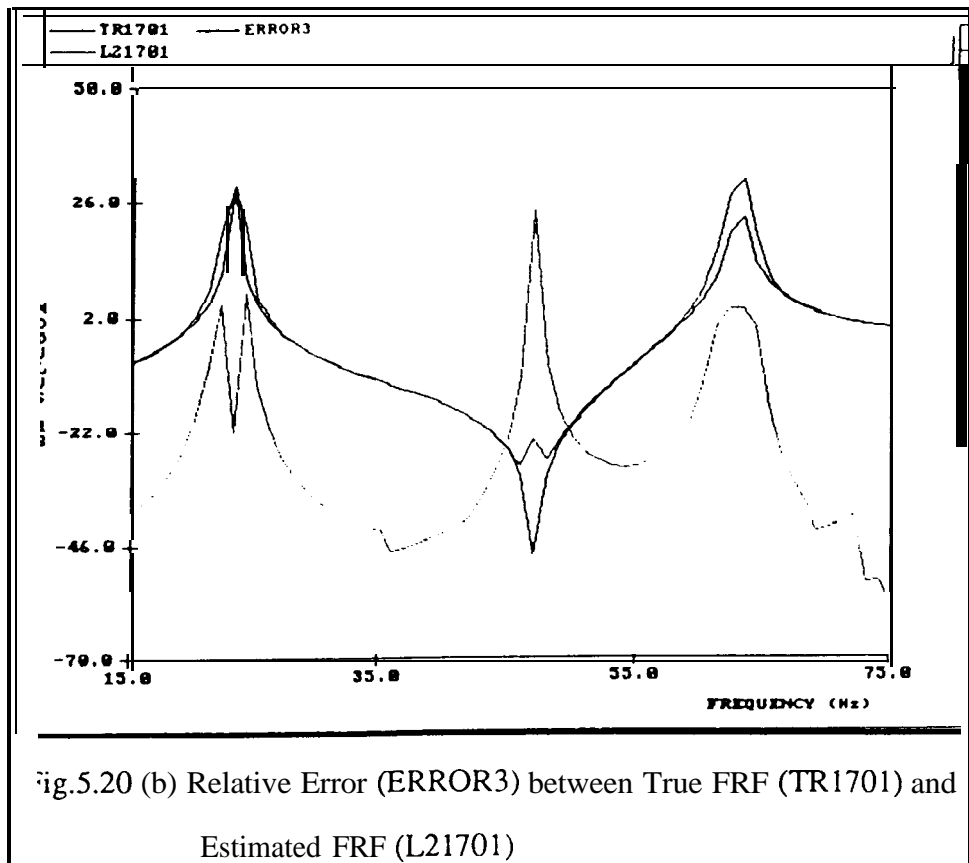


Fig.5.20 (b) Relative Error (ERROR3) between True FRF (TR1701) and Estimated FRF (L21701)

As discussed in section 5.6.1,  $\hat{H}_2(\omega)$  is less sensitive to the leakage errors than is  $\hat{H}_1(\omega)$  because  $\hat{H}_2(\omega)$  lies on the true modal circle (but in the wrong position). However, if the frequency resolution is insufficient for a mode to encompass some part of the modal circle, modal parameters extracted by circle-fitting may not be reliable, as shown in Fig.5.21.

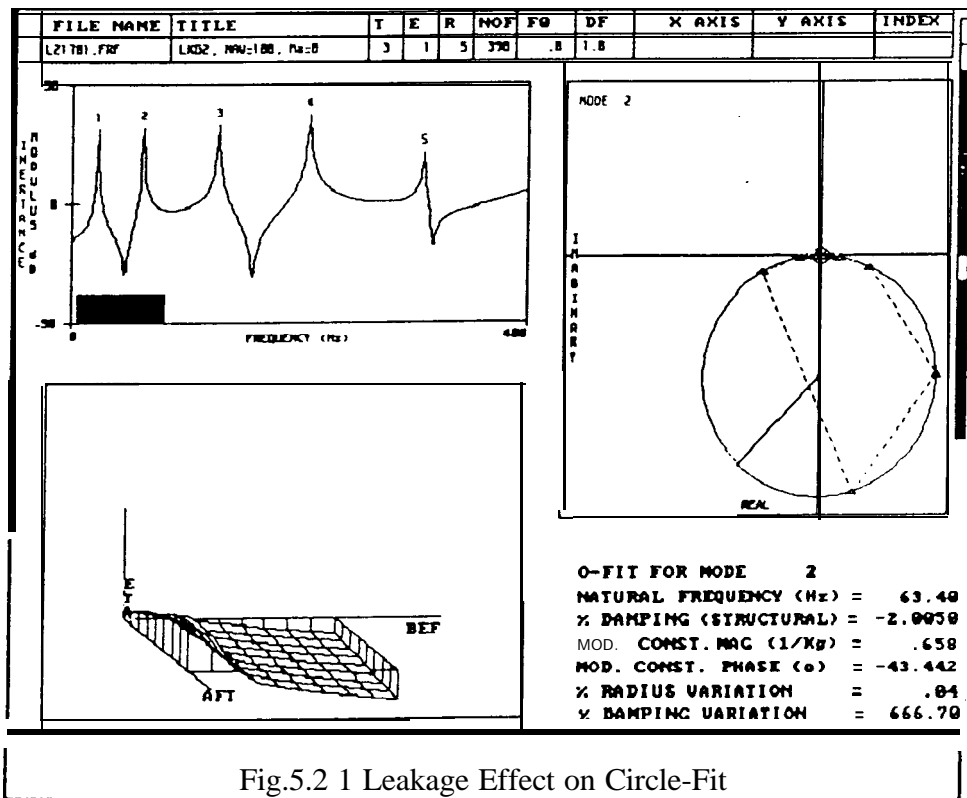
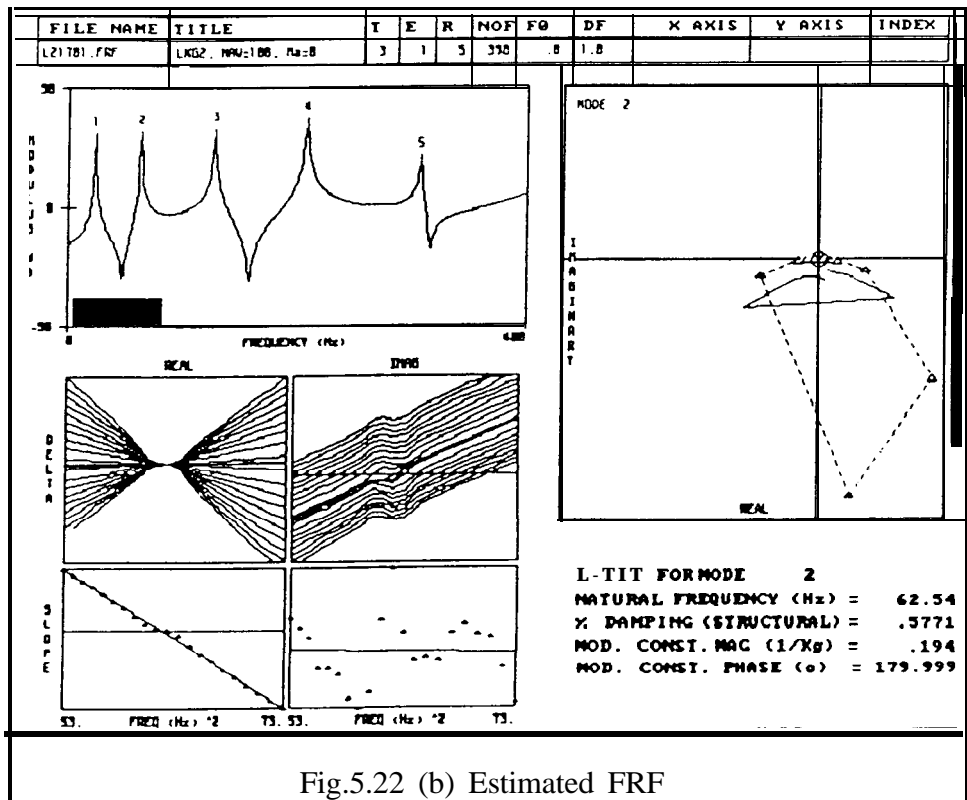
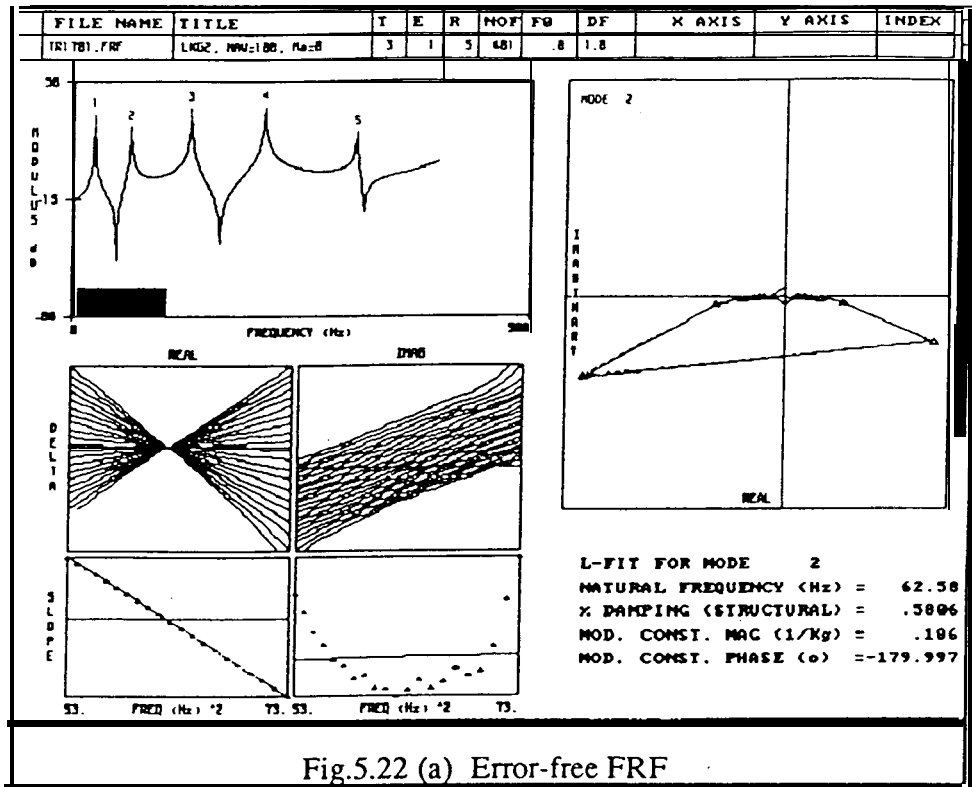


Fig.5.2 1 Leakage Effect on Circle-Fit

Fig.5.22 shows a Modified Line Fit analysis (or Bendent Method; see Appendix F) on the 2nd mode. It can be seen that the effect of leakage is dominant only near resonance and, therefore, has little effect on the extraction of modal parameters.



## 5.8 MODEL UPDATING OF BEAM STRUCTURE

The structure which featured in § 5.7 was also used to check the validity of the **IEM** on a practical structure which has realistic measurement errors. 20 beam elements were used to create an analytical model of the structure and 2 **DoFs** - one translational and one rotational **DoFs** - were considered at each node. Mass and stiffness **modelling** errors were introduced by overestimating the density of the 1st and 2nd elements by 100 % and the Young's Modulus of the 11th and 12th elements by 100 %, as shown in Fig.5.12.

A total of 11 points were “measured” in the vertical direction (Fig.5.23) using periodic random excitation in the **frequency** range of 0 - 800 Hz with excitation applied at a free end of the structure. The ratio of noise to signal spectra was assumed to be  $10^{-3}$  for force and  $10^{-4}$  for the response. An accelerometer of 20 g was moved from one location to the next location in order to measure all **FRFs**. As a result, each measured FRF was expected to have different mass loading effect.

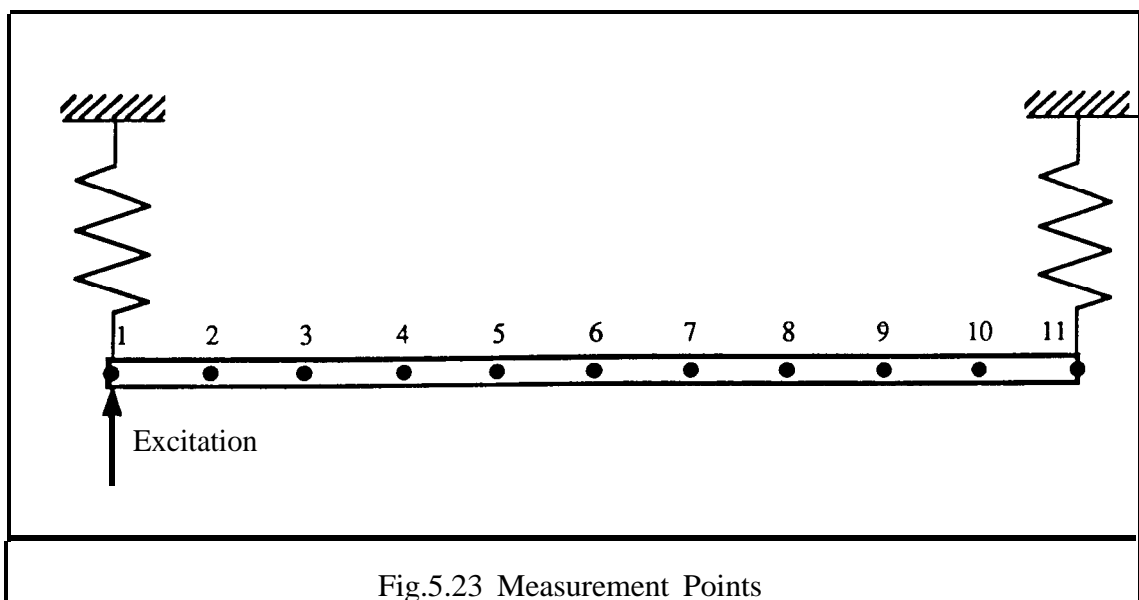


Fig.5.23 Measurement Points

Fig.5.24 shows one point and several transfer FRFs. In the measurement frequency range, 8 flexible modes are clearly seen.

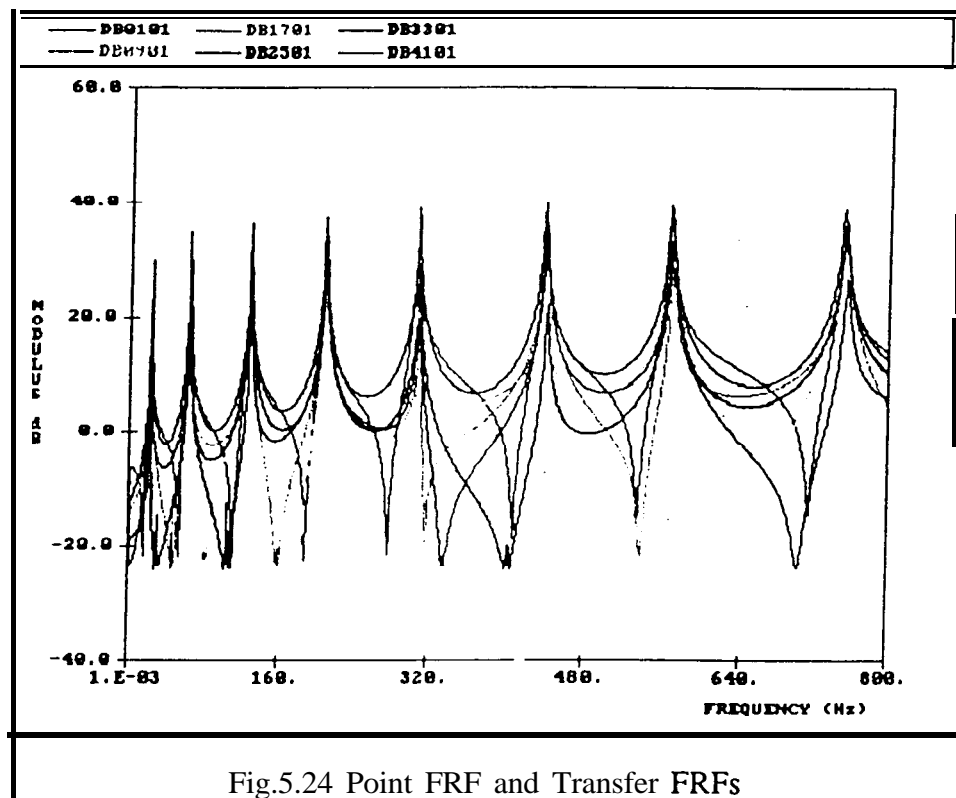


Fig.5.24 Point FRF and Transfer FRFs

The modal parameters of an individual FRF were extracted by modified Line Fit analysis using MODENT program [37]. All the identified modal parameters which exhibited slightly different values (natural frequencies and modal dampings) were then collated to obtain consistent modal parameters using MODESH [38]. The resultant parameters can be seen in Table 5.4. The first 8 “experimental” and initial analytical natural frequencies are compared in Table 5.5.

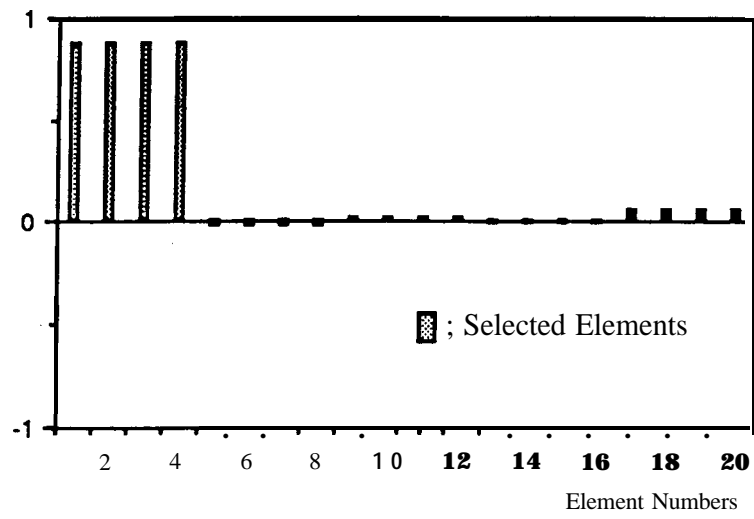
Table 5.4 Modal Parameters of "Experimental" Data

Mode	Natural Freq (Hz)				Modal Damping (%)			
	Min	Max	Mean	SD	Min	Max	Mean	SD
1	<b>22.9</b>	23.0	23.0	0.05	<b>0.98</b>	1.09	1.02	0.04
2	62.2	62.8	62.6	0.17	0.54	0.60	0.57	0.02
3	126.3	127.1	126.8	0.24	0.51	0.54	0.53	0.01
4	208.6	210.2	209.7	0.46	0.50	0.53	0.52	0.01
5	308.2	309.8	309.2	0.58	0.50	0.53	0.52	0.01
6	438.1	441.2	440.2	0.87	0.50	0.52	0.51	0.01
7	567.2	570.6	569.3	0.98	0.51	0.51	0.51	0.00
8	749.0	753.4	751.7	1.24	0.50	0.52	0.51	0.01

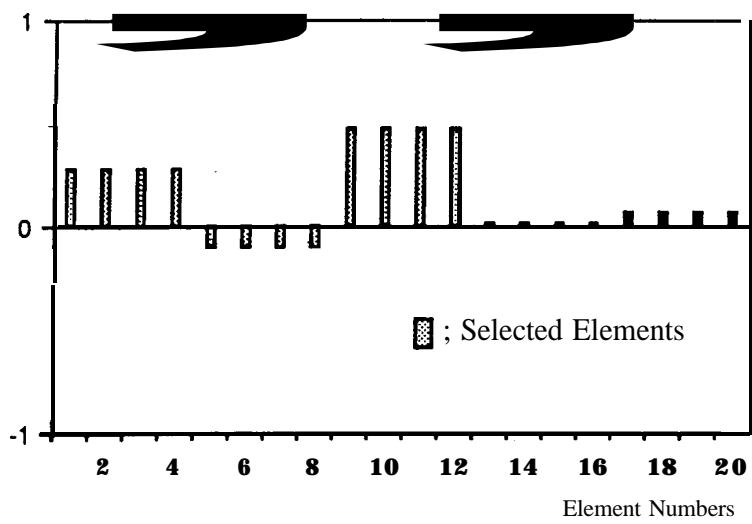
Table 5.5 Natural Frequencies of "Experimental" and Initial Analytical Models

Mode	1	2	3	4	5	6	7	8
$f_x$ (Hz)	23.0	62.5	126.8	209.7	309.2	440.2	569.3	751.7
$f_A$ (Hz)	23.6	65.2	127.8	211.3	315.7	441.1	587.5	755.2
MAC	0.959	0.952	0.962	0.956	0.962	0.928	0.931	0.904

In the error location procedure, 5 macro elements were used and each macro element had 4 individual elements. The error location results are shown in Fig.5.25 and Table 5.6. After 4 iterations, it became possible to locate possible error regions - 4 mass elements and 12 stiffness elements.



(a) Mass Error



(b) Stiffness Errors

Fig.5.25 Error Location Results

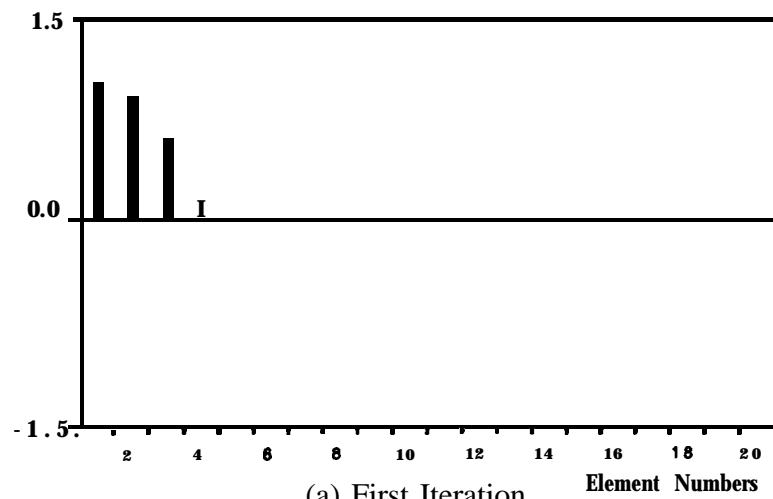
Table 5.6 Natural Frequencies of "Experimental" and Intermediate Analytical Models

Mode	1	2	3	4	5	6	7	8
$f_x$ (Hz)	23.0	62.5	126.8	209.7	309.2	440.2	569.3	751.7
$f_A$ (Hz)	23.1	61.7	126.7	205.8	313.9	440.0	578.1	748.6
MAC	1.000	0.995	0.987	0.988	0.980	0.993	0.994	0.988

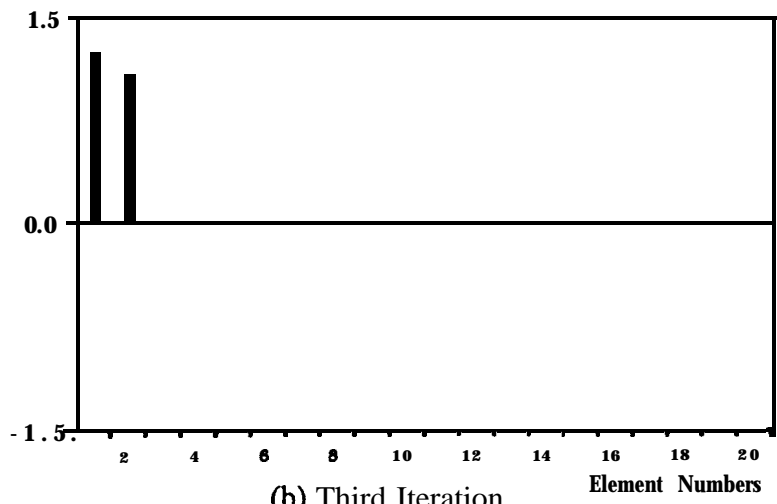
After locating possible error regions, the updating was carried out with the correction coefficients calculated as initial values. It can be seen in Figs 5.26 and 5.27 that the estimates became quite accurate after 5 iterations. The natural frequencies of the updated analytical model are compared with the experimental ones in Table 5.7.

Table 5.7 Natural Frequencies of "Experimental" and Updated Models

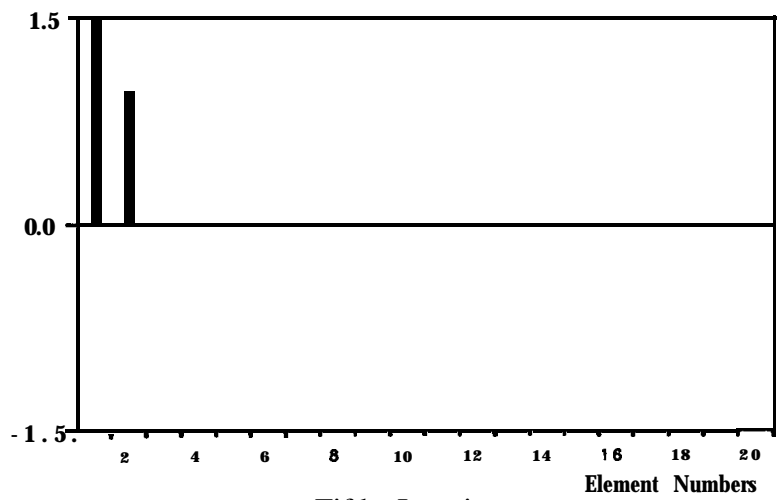
Mode	1	2	3	4	5	6	7	8
$f_x$ (Hz)	23.0	62.5	126.8	209.7	309.2	440.2	569.3	751.7
$f_A$ (Hz)	22.8	62.3	126.5	209.7	309.1	441.0	570.2	753.7
MAC	0.999	1.000	1.000	0.999	1.000	0.999	0.999	0.999



(a) First Iteration

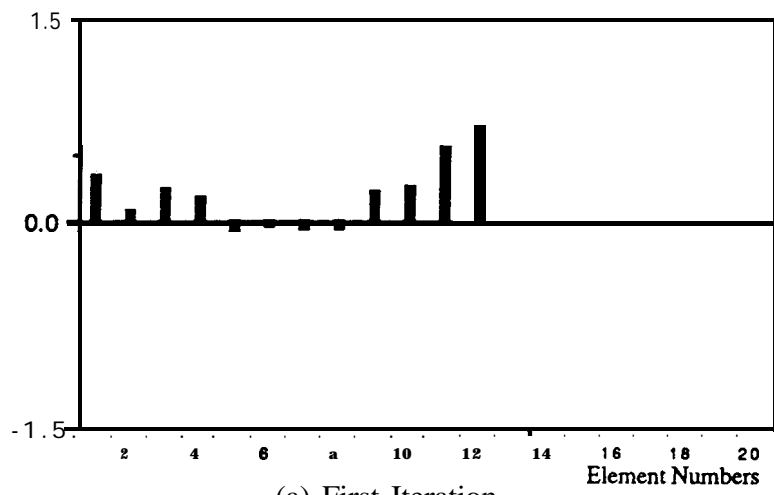


(b) Third Iteration

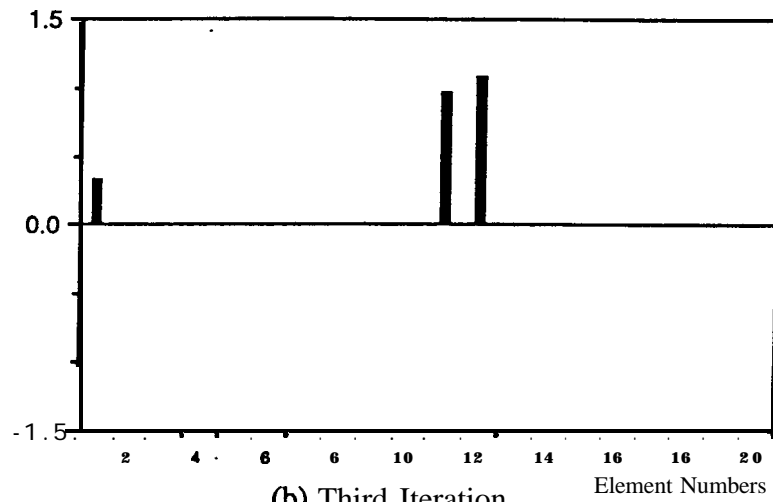


(c) Fifth Iteration

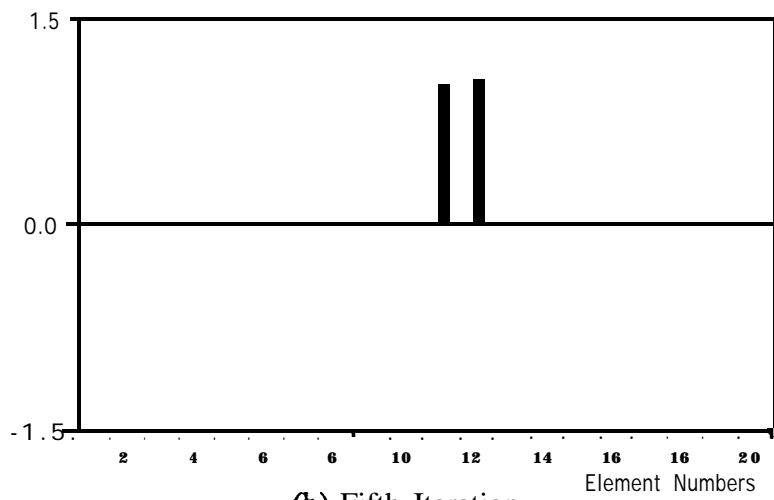
Fig.526 Model Updating Results (Mass)



(a) First Iteration



(b) Third Iteration



(b) Fifth Iteration

Fig.5.27 Model Updating Results (Stiffness)

## 5.9 CONCLUSIONS

The characteristics of typical measurement errors might not result in random variations in the modal parameters which are eventually derived from the measured data. For model updating methods to be useful in practical application, various error sources in testing - such as the mass loading effect of transducers, shaker/structure interaction, etc. - should be considered and more realistic errors rather than random noise should be included in the “experimental” data

The errors involved in modal parameter estimation - such as measurement errors, signal processing errors and errors in modal analysis - have been investigated, and their effects on estimated **FRFs** and on the modal parameters extracted from the **FRFs** have also been investigated. A computer program has been written to simulate various measurement and signal processing errors. The “experimental” **FRFs** calculated using this program can be used to test the performance of different modal parameter identification programs and, thus, of the various applications to which these modal data are put.

The resultant “experimental” modal data which contained representative experimental errors have been used to update the corresponding analytical beam model to check the validity of the **IEM**. The mismodelled regions were located successfully, and the updating results were found to be quite accurate, not only in modal parameters but also in correction coefficients or physical design variables.

# CHAPTER 6

## CHAPTER 6

### UPDATING OF DAMPED STRUCTURES

#### 6.1 PRELIMINARIES

In the previous Chapters, location of mismodelled regions in an analytical model and updating the model were carried out using corresponding experimental modal data which were all real (i.e. for undamped systems). However, in most cases, experimental modal data from a real structure are not real but complex, even if the structure is lightly damped. If a structure is lightly damped, the modal data from measurement are often treated as real modes, and the method suggested in Chapter 3 can be used to update the corresponding analytical model. However, some practical structures are more heavily damped and the measured modal data cannot be regarded as real, whereas the modal data from the corresponding (undamped) analytical model are real.

There are two possible approaches to resolve this incompatibility. One approach is to deduce the undamped modes - real modes - from the measured complex modes [19,39,40]. Then the method suggested in Chapter 3 can be used to update the analytical model using the deduced real modes. However, the deduced real modes are often only a rough approximation because the experimentally identified complex modes are incomplete and the deduction itself relies on the analytical model which is erroneous.

An alternative approach is to use the experimental complex modes directly to update the analytical model. A method has been developed by He [17] to locate the damping elements in an analytical model using measured complex modes. However, this method requires a complete set of measured coordinates, which is not practical, or the use of mode expansion, which may be an erroneous procedure thus **jeopardising** exact location, in order to overcome the incompatibility between the measured modes and the analytical model. In this Chapter, a complex inverse eigensensitivity method will be introduced to locate and to update the damping elements together with the mass and stiffness elements which have modelling errors, using measured complex modal parameters.

## 6.2 COMPLEX EIGENSENSITIVITY

The updated damping matrix can be expressed as equation (6.1) in the same way as the mass and stiffness matrices in equation (3.1) and (3.2)

$$[D_U] = \sum_{i=1}^L c_i [D]_i \quad (6.1)$$

where  $L$  is the number of elements,  $c_i$  are correction coefficients to be determined and  $[D]_i$  is a submatrix of the system damping matrix.

The governing equations of motion for a MDOF system with structural damping and no external forcing can be written in matrix form as:

$$[M]\{\ddot{x}\} + [K]\{x\} + i [D]\{x\} = \{0\} \quad (6.2)$$

By assuming a solution of the form:

$$\{\mathbf{x}\} = \{\mathbf{x}\} e^{i\mu t}$$

we can obtain a complex **eigenproblem**

$$([\mathbf{K}] + i[\mathbf{D}] - \lambda_r [\mathbf{M}]) \{\phi\}_r = \{0\} \quad (\mu_r^2 = \lambda_r) \quad (6.3)$$

where  $\{\phi\}_r$  is **normalised** such that

$$\{\phi\}_r^T [\mathbf{M}] \{\phi\}_r = 1 \quad (6.4)$$

The solution of this eigenproblem is in the form of two matrices containing complex eigenvalues and complex eigenvectors in contrast with the undamped case where eigenvalues and eigenvectors are all real.

Differentiating **equation** (6.3) with respect to updating variable  $p_i$  gives

$$\left( \frac{\partial[\mathbf{K}]}{\partial p_i} + i \frac{\partial[\mathbf{D}]}{\partial p_i} - \frac{\partial \lambda_r}{\partial p_i} [\mathbf{M}] - \lambda_r \frac{\partial[\mathbf{M}]}{\partial p_i} \right) \{\phi\}_r + ([\mathbf{K}] + i[\mathbf{D}] - \lambda_r [\mathbf{M}]) \frac{\partial \{\phi\}_r}{\partial p_i} = \{0\} \quad (6.5)$$

Pre-multiplying equation (6.5) by  $\{\phi\}_r^T$  leads to

$$\frac{\partial \lambda_r}{\partial p_i} = \{\phi\}_r^T \left( \frac{\partial[\mathbf{K}]}{\partial p_i} + i \frac{\partial[\mathbf{D}]}{\partial p_i} \right) \{\phi\}_r - \lambda_r \{\phi\}_r^T \frac{\partial[\mathbf{M}]}{\partial p_i} \{\phi\}_r \quad (6.6)$$

The eigenvector derivatives can be expressed as linear combinations of all eigenvectors of the system if the eigenvalues are assumed distinct, because  $N$  eigenvectors are linearly independent and they can be used as a set of bases vectors for spanning  $N$ -dimensional space. Thus,

$$\frac{\partial\{\phi\}_r}{\partial p_i} = \sum_{j=1}^N \alpha_{rj}^i \{\phi\}_j \quad (6.7)$$

Substituting equation (6.7) into equation (6.5) and pre-multiplying equation (6.5) by  $\{\phi\}_k^T$

$$\begin{aligned} & \{\phi\}_k^T \left( \frac{\partial[\mathbf{K}]}{\partial p_i} + i \frac{\partial[\mathbf{D}]}{\partial p_i} - \frac{\partial\lambda_r}{\partial p_i} [\mathbf{M}] - \lambda_r \frac{\partial[\mathbf{M}]}{\partial p_i} \right) \{\phi\}_r + \{\phi\}_k^T ([\mathbf{K}] + i[\mathbf{D}] - \lambda_r [\mathbf{M}]) \\ & \sum_{j=1}^N \alpha_{rj}^i \{\phi\}_j = 0 \end{aligned} \quad (6.8)$$

If  $k \neq r$ ,

$$\{\phi\}_k^T \left( \frac{\partial[\mathbf{K}]}{\partial p_i} + i \frac{\partial[\mathbf{D}]}{\partial p_i} - \lambda_r \frac{\partial[\mathbf{M}]}{\partial p_i} \right) \{\phi\}_r + \alpha_{rk}^i (\lambda_k - \lambda_r) = 0 \quad (6.9)$$

Thus,

$$\alpha_{rk}^i = \frac{\{\phi\}_k^T \left( \frac{\partial[\mathbf{K}]}{\partial p_i} + i \frac{\partial[\mathbf{D}]}{\partial p_i} - \lambda_r \frac{\partial[\mathbf{M}]}{\partial p_i} \right) \{\phi\}_r}{\lambda_r - \lambda_k} \quad (6.10)$$

$\alpha_{rr}^i$  can be obtained by differentiating equation (6.4) with respect to  $p_i$

$$2\{\phi\}_r^T [\mathbf{M}] \frac{\partial\{\phi\}_r}{\partial p_i} + \{\phi\}_r^T \frac{\partial[\mathbf{M}]}{\partial p_i} \{\phi\}_r = 0 \quad (6.11)$$

Substituting equation (6.7) into equation (6.11) leads to

$$\alpha_{rr}^i = -\frac{1}{2} \{\phi\}_r^T \frac{\partial[\mathbf{M}]}{\partial p_i} \{\phi\}_r \quad (6.12)$$

From equations (3.1), (3.2) and (6.1), we get

$$\begin{aligned}
 \frac{\partial[M]}{\partial a_i} &= [M]_i & \frac{\partial[M]}{\partial b_i} &= [0] & \frac{\partial[M]}{\partial c_i} &= [0] \\
 \frac{\partial[K]}{\partial a_i} &= [0] & \frac{\partial[K]}{\partial b_i} &= [K]_i & \frac{\partial[K]}{\partial c_i} &= [0] \\
 \frac{\partial[D]}{\partial a_i} &= [0] & \frac{\partial[D]}{\partial b_i} &= [0] & \frac{\partial[D]}{\partial c_i} &= [D]_i
 \end{aligned} \tag{6.13}$$

Substituting equation (6.13) into equation (6.6) leads to

$$\frac{\partial \lambda_r}{\partial a_i} = -\lambda_r \{\phi\}_r^T [M]_i \{\phi\}_r \tag{6.14a}$$

$$\frac{\partial \lambda_r}{\partial b_i} = \{\phi\}_r^T [K]_i \{\phi\}_r \tag{6.14b}$$

$$\frac{\partial \lambda_r}{\partial c_i} = i \{\phi\}_r^T [D]_i \{\phi\}_r \tag{6.14c}$$

and substituting equation (6.13) into equations (6.10) and (6.12) leads to

$$\frac{\partial \{\phi\}_r}{\partial a_i} = \sum_{j=1}^N \alpha_{rj}^i \{\phi\}_j \tag{6.15a}$$

$$\alpha_{rj}^i = \begin{cases} -\frac{\lambda_r \{\phi\}_i^T [M]_i \{\phi\}_r}{\lambda_r - \lambda_j} & (r \neq j) \\ -\frac{1}{2} \{\phi\}_j^T [M]_i \{\phi\}_r & (r = j) \end{cases}$$

$$\frac{\partial \{\phi\}_r}{\partial b_i} = \sum_{j=1}^N \beta_{rj}^i \{\phi\}_j \tag{6.15b}$$

$$\beta_{rj}^i = \begin{cases} \frac{\{\phi\}_i^T [K]_i \{\phi\}_r}{\lambda_r - \lambda_j} & (r \neq j) \\ 0 & (r = j) \end{cases}$$

$$\frac{\partial \{\phi\}_r}{\partial c_i} = \sum_{j=1}^N \gamma_{rj}^i \{\phi\}_j \quad (6.15c)$$

$$\gamma_{rj}^i = \begin{cases} \frac{i \{\phi\}_i^T [D]_i \{\phi\}_r}{\lambda_r - \lambda_j} & (r \neq j) \\ 0 & (r = j) \end{cases}$$

If we assume that the element damping matrix has the same distribution as the element stiffness matrix, i.e.,

$$[D]_i = \alpha [K]_i$$

(noting that this assumption is not the same as  $[D] = \alpha[K]$ , which is “proportional” damping, since the modal parameters generally remain complex under the assumption  $[D]_i = \alpha[K]_i$ ), then a complex stiffness matrix  $[K^*]$  which is defined as:

$$[K^*] \equiv [K] + i [D] = \sum_{i=1}^L b_i [K]_i + i \sum_{i=1}^L c_i [D]_i$$

can be expressed as:

$$\begin{aligned} [K^*] &= \sum_{i=1}^L (b_i + i \alpha c_i) [K]_i \\ &= \sum_{i=1}^L b_i^* [K]_i \end{aligned}$$

where  $b_i^* = b_i + i \alpha c_i$

Therefore,

$$\frac{\partial [K^*]}{\partial b_i^*} = [K]_i$$

Substituting equation (6.13) and (6.16) into equation (6.6), (6.10) and (6.12) leads to

$$\frac{\partial \lambda_r}{\partial b_i^*} = \{\phi\}_r^T [K]_i \{\phi\}_r \quad (6.16a)$$

$$\frac{\partial \{\phi\}_r}{\partial b_i^*} = \sum_{j=1}^N \beta_{rj}^i \{\phi\}_j \quad (6.16b)$$

$$p_{rj}^i = \begin{cases} \frac{\{\phi\}_i^T [K]_i \{\phi\}_r}{\lambda_r - \lambda_j} & (r \neq j) \\ 0 & (r = j) \end{cases}$$

The first-order Taylor expansions of the modal parameters can be written as:

$$\begin{Bmatrix} \frac{\Delta \lambda_1}{\lambda_1} \\ \{\Delta \phi\}_1 \\ \vdots \\ \frac{\Delta \lambda_m}{\lambda_m} \\ \{\Delta \phi\}_m \end{Bmatrix} = \begin{bmatrix} \frac{\partial \lambda_{A1}}{\partial a_1} / \lambda_1 & \dots & \frac{\partial \lambda_{A1}}{\partial a_L} / \lambda_1 & \frac{\partial \lambda_{A1}}{\partial b_1^*} / \lambda_1 & \dots & \frac{\partial \lambda_{A1}}{\partial b_L^*} / \lambda_1 \\ \frac{\partial \{\phi_A\}_1}{\partial a_1} & \dots & \frac{\partial \{\phi_A\}_1}{\partial a_L} & \frac{\partial \{\phi_A\}_1}{\partial b_1^*} & \dots & \frac{\partial \{\phi_A\}_1}{\partial b_L^*} \\ \vdots & \vdots & \vdots & \vdots & \vdots & \vdots \\ \frac{\partial \lambda_{Am}}{\partial a_1} / \lambda_m & \dots & \frac{\partial \lambda_{Am}}{\partial a_L} / \lambda_m & \frac{\partial \lambda_{Am}}{\partial b_1^*} / \lambda_m & \dots & \frac{\partial \lambda_{Am}}{\partial b_L^*} / \lambda_m \\ \frac{\partial \{\phi_A\}_m}{\partial a_1} & \dots & \frac{\partial \{\phi_A\}_m}{\partial a_L} & \frac{\partial \{\phi_A\}_m}{\partial b_1^*} & \dots & \frac{\partial \{\phi_A\}_m}{\partial b_L^*} \end{bmatrix} \begin{Bmatrix} \Delta a_1 \\ \vdots \\ \Delta a_L \\ \mathbf{Ab}; \\ \vdots \\ \Delta b_L^* \end{Bmatrix} \quad (6.17)$$

or

$$\{\Delta\}_{m(n+1) \times 1} = [S]_{m(n+1) \times 2L} \{\Delta p\}_{2L \times 1}$$

is

which is very similar to equation (3.23). However, in equation (6.17),  $\{A\}$ ,  $[S]$  and  $\{Ap\}$  are not real, as in equation (3.23), but complex. The real parts of  $a_i$  ( $i = 1, 2, \dots, L$ ) represent mass correction coefficients and the real parts of  $b_i^*$  ( $i = 1, 2, \dots, L$ ) represent

stiffness correction coefficients, while the imaginary parts of  $\mathbf{b}_i^*$  represent damping correction coefficients.

† The correction coefficients vector ( $\Delta p$ ) can be calculated as:

$$\{\Delta p\} = ([S]^T [S])^{-1} [S]^T \{\Delta\} \quad (6.18)$$

then,  $\{\Delta p\}$  is added to the solution vector to update the vector

$$\{p\}_{\text{new}} = \{p\}_{\text{old}} + \{\Delta p\} \quad (6.19)$$

and the process is iterated until convergence is achieved.

### 6.3 APPLICATION TO THE BAY STRUCTURE

The structure which had been used in previous Chapters (Fig.2.2) was used again to check the validity of the method proposed above. The structure is **modelled** by 31 beam elements, and 3 **DoFs** are considered at each node, so that the total number of **DoFs** ( $N$ ) is 90. Experimental data were obtained at 15 points as shown in Fig.2.2 in translational coordinates only (i.e.  $n = 30$ ). The first 10 experimental modes were used (i.e.  $m = 10$ ).

Mass and stiffness **modelling** errors were introduced by overestimating the mass matrices of the **25<sup>th</sup>** and **26<sup>th</sup>** elements by 50 % and the stiffness matrices of the **12<sup>th</sup>**, **13<sup>th</sup>** and **31<sup>st</sup>** elements by 100 %. In addition, the **1<sup>st</sup>** and **2<sup>nd</sup>** elements were supposed to have damping of  $[D]_i = 0.05 [K]_i$  (Case 1; lightly damped case) and of  $[D]_i = 0.3 [K]_i$  (Case 2; more heavily damped case).

### 6.3.1 CASE 1

It should be noted that the modal parameters of the 'analytical' model (undamped) are real while those of the 'experimental' version are complex because this system is damped. The modal parameters of the **first** 10 'experimental and analytical modes are compared in Table 6.1 together with MAC values. For complex modes, MAC can be expressed as:

$$\text{MAC}(A_i, X_j) = \frac{|\{\phi_A\}_i^T \{\phi_X\}_i^*|^2}{|\{\phi_A\}_i^T \{\phi_A\}_i^*| |\{\phi_X\}_j^T \{\phi_X\}_j^*|}$$

It should be noted that the MAC values are still **real** even if mode shapes are complex. **The** eigenvectors of the first two 'experimental' and analytical modes are compared in Tables 6.2 and 6.3.

Table 6.1 Natural Frequencies of 'Experimental' and Analytical Models (Case 1)

Mode No.	Experimental		Analytical Nat. Freqs.	MAC Values
	Nat. Freqs.	Loss Factors		
1	343.3	0.003	342.3	0.995
2	468.1	0.002	450.6	0.971
3	548.2	0.012	528.5	0.948
4	577.7	0.002	557.2	0.966
5	704.4	0.007	683.4	0.960
6	850.9	0.004	833.7	0.981
7	917.2	0.003	902.3	0.914
8	928.9	0.000	927.0	0.814
9	1099.4	0.002	1066.6	0.862
10	1205.0	0.006	1165.3	0.927

**Table 6.2 Eigenvectors of 'Experimental' and Analytical Models (Case 1: Mode1)**

Coords	Exp.(x10 <sup>-1</sup> )	Anal.(x10 <sup>-1</sup> )	Coords	Exp.(x10 <sup>-1</sup> )	Anal.(x10 <sup>-1</sup> )
1	0.723(0°)	0.748(0°)	41	0.253( 180°)	0.246( 180°)
2	0.260(0°)	0.236(0°)	46	0.202( 180°)	0.123(180°)
7	0.355(0°)	0.370(0°)	47	0.254(1 SO°)	0.244(180°)
8	0.260(0°)	0.248(0°)	52	0.316(0°)	0.380(0°)
13	0.134(175°)	0.134( 180°)	53	0.231(180°)	0.220( 180°)
14	0.234(0°)	0.233(0°)	58	0.726(0°)	0.754(0°)
19	0.578( 180°)	0.593( 180°)	59	0.205(180°)	0.192(180°)
20	0.193(0°)	0.205(0°)	67	0.715(0°)	0.740(0°)
22	0.733(180°)	0.754( 180°)	68	0.080(2°)	0.072(0°)
23	0.176(0°)	0.192(0°)	76	0.406(- 1°)	0.398(0°)
28	0.717(180°)	0.742(1 SO°)	77	0.154(0°)	0.121(0°)
29	0.016(-177°)	0.019( 180°)	82	0.159(-179°)	0.138(180°)
37	0.725(-179°)	0.748(180°)	83	0.415(-178°)	0.420(180°)
38	0.243(180°)	0.236(180°)	88	0.648( 180°)	0.610(180°)
40	0.651(180°)	0.585(180°)	89	0.222( 1 SO°)	0.188(180°)

Table 6.3 Eigenvectors of 'Experimental' and Analytical Models (Case 1: Mode 2)

Coords.	Exp.(x10 <sup>-1</sup> )	Anal.(x10 <sup>-1</sup> )	Coords.	Exp.(x10 <sup>-1</sup> )	Anal.(x10 <sup>-1</sup> )
1	0.058(-176°)	0.008(180°)	41	0.017(-160°)	0.020(180°)
2	0.046(173°)	0.024(180°)	46	0.389(-178°)	0.459(180°)
7	0.459(177°)	0.353(180°)	47	0.053(-175°)	0.060(180°)
8	0.047(175°)	0.033(180°)	52	0.476(-179°)	0.459(180°)
13	0.579(178°)	0.496(180°)	53	0.145(-179°)	0.143(180°)
14	0.102(179°)	0.097(180°)	58	0.269(180°)	0.196(180°)
19	0.342(179°)	0.354(180°)	59	0.265(180°)	0.250(180°)
20	0.188(180°)	0.195(180°)	67	0.117(-179°)	0.061(180°)
22	0.129(-177°)	0.196(180°)	68	0.207(179°)	0.172(180°)
23	0.238(180°)	0.250(180°)	76	1.289(0°)	1.220(0°)
28	0.043(-173°)	0.102(180°)	77	0.786(0°)	0.738(0°)
29	0.192(-179°)	0.223(180°)	82	1.410(0°)	1.520(0°)
37	0.034(-7°)	0.008(180°)	83	0.850(0°)	0.926(0°)
38	0.024(-164°)	0.024(180°)	88	0.387(0°)	0.669(0°)
40	0.064(-175°)	0.195(180°)	89	0.206(1°)	0.399(0°)

The Macro 1 model (Fig.3.3) which has 8 macro elements (i.e.  $L = 8$ ) was used in the error location procedure. This means that no macro element coincided exactly with any of the error regions. A necessary condition for the sensitivity  $[S]$ , which is  $m(n-l) \times 2L$ , to be rank full is:

$$m(n+1) > 2L \text{ or } m > \frac{2L}{n+1}$$

However, the eigenvector sensitivities are not always linearly independent. In practice, the number of measured modes should be more than twice of the minimum number in order to give a high probability of sufficient rank to matrix  $[S]$ . In this case study, 10 modes were used as mentioned above.

The location process took 5 iterations to convergence and 27 elements - 9 mass elements, 11 stiffness elements and 7 damping elements - were identified as possible error regions as shown in Fig.6.1.

The resultant natural frequencies of the ‘improved’ analytical model are compared with those of the ‘experimental’ modes in Table 6.4.

Table 6.4 Natural Frequencies of ‘Experimental’ and Intermediate Models (Case 1)

Mode	1	2	3	4	5	6	7	8	9	10
$f_x$ (Hz)	343.3	468.1	548.2	577.7	704.4	850.9	917.2	928.9	1099.4	1205.0
$f_A$ (Hz)	347.9	462.9	545.1	586.7	705.1	858.6	921.6	928.5	1082.9	1192.9
MAC	0.992	0.986	0.976	0.979	0.982	0.984	0.991	0.979	0.989	0.982

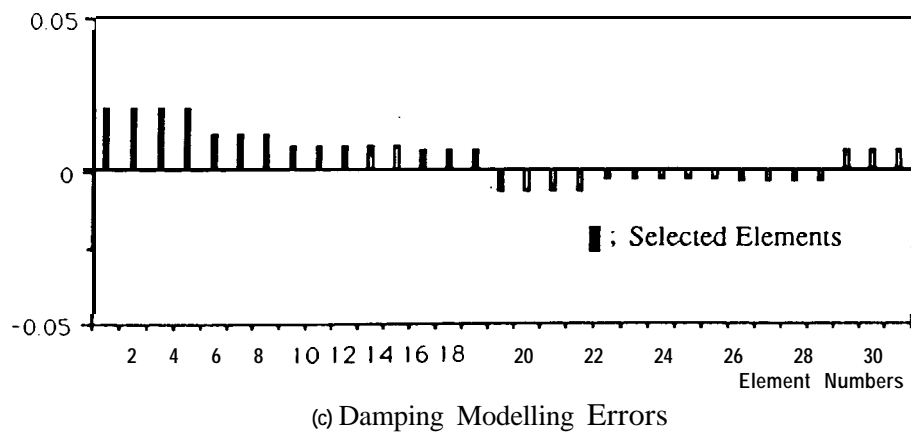
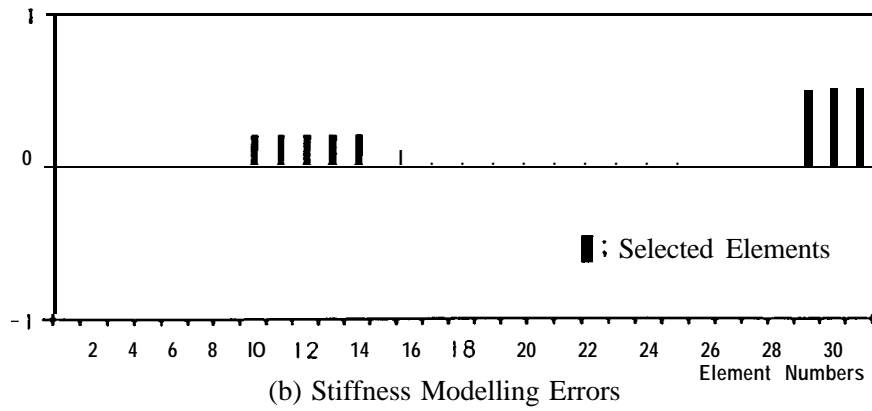
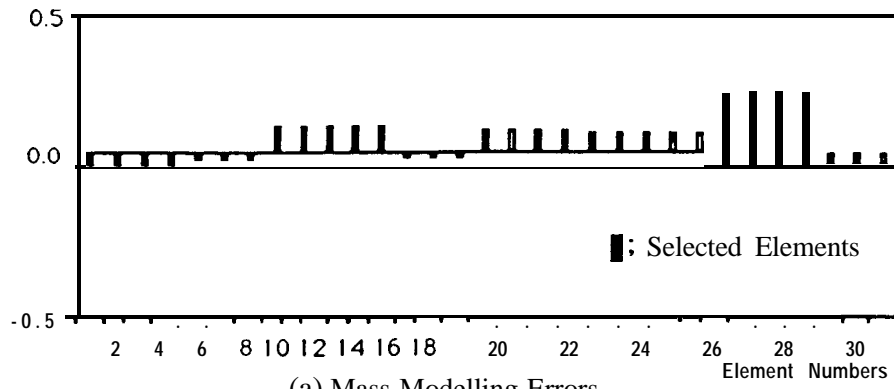


Fig.6.1 Error Location Results





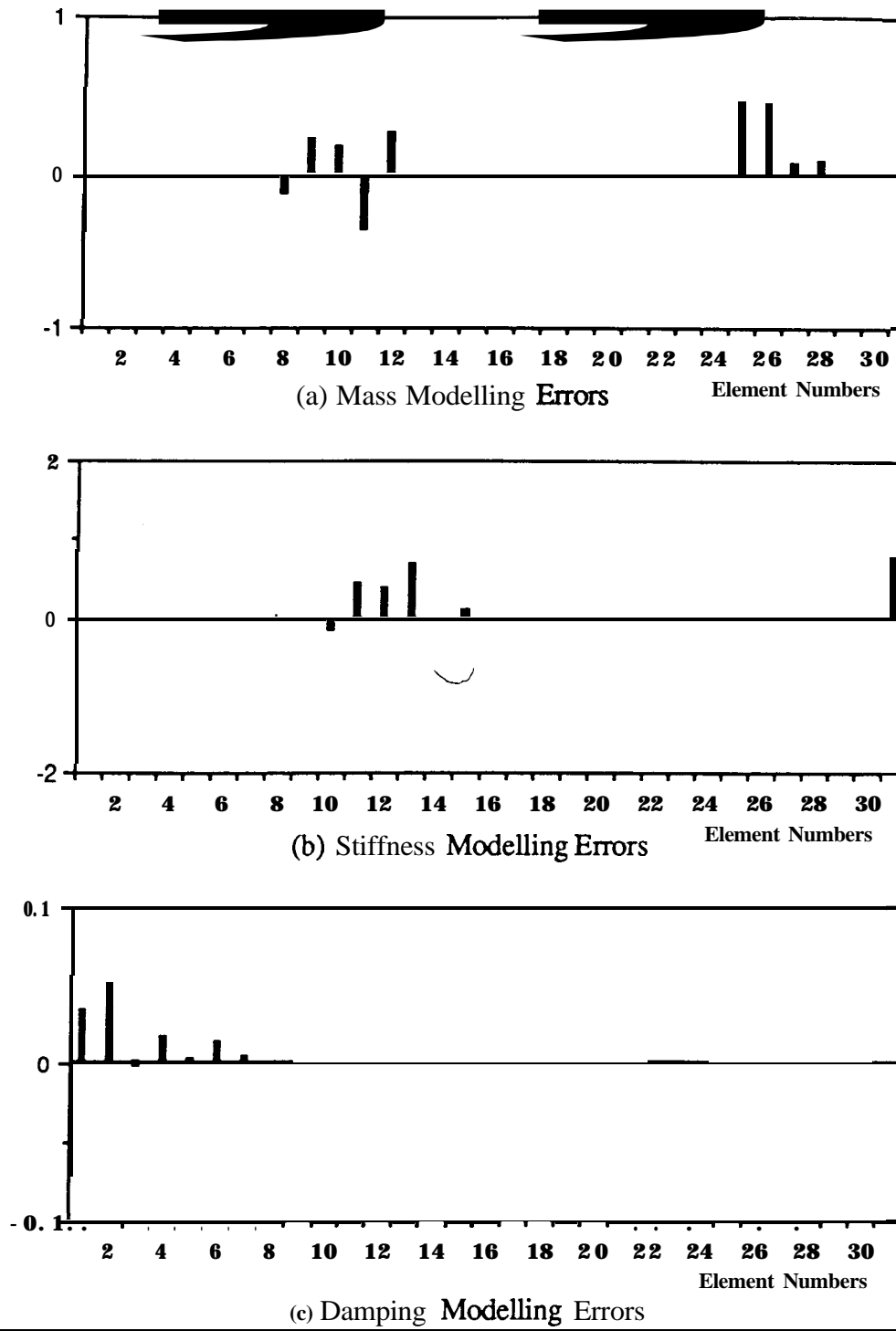
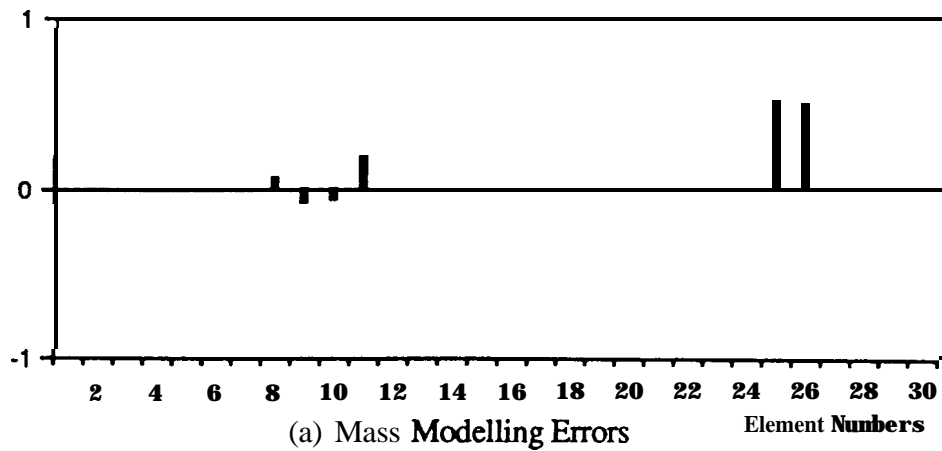
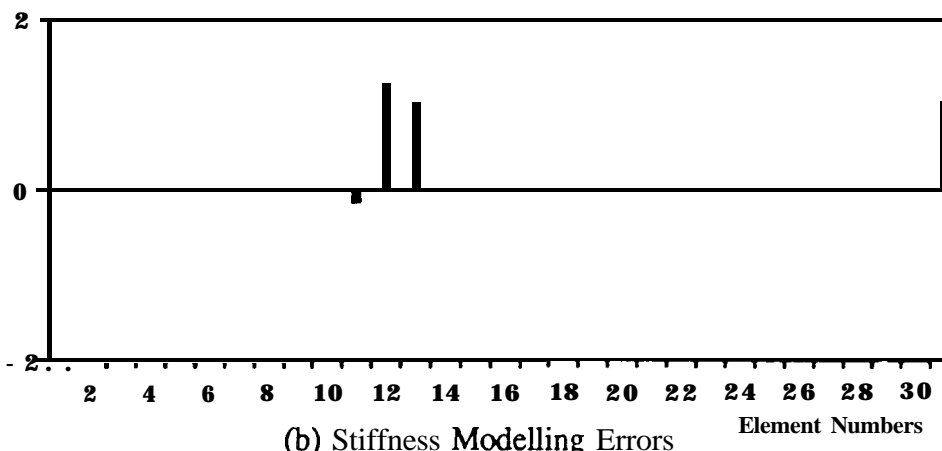


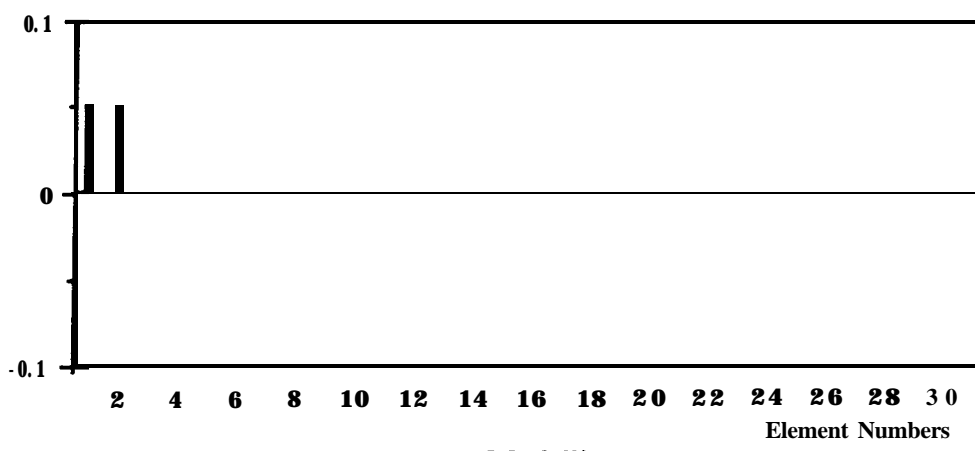
Fig.6.2 Model Updating Results (Case 1; First Iteration)



(a) Mass Modelling Errors



(b) Stiffness Modelling Errors



(c) Damping Modelling Errors

Fig.6.3 Model Updating Results (Case 1; Third Iteration)

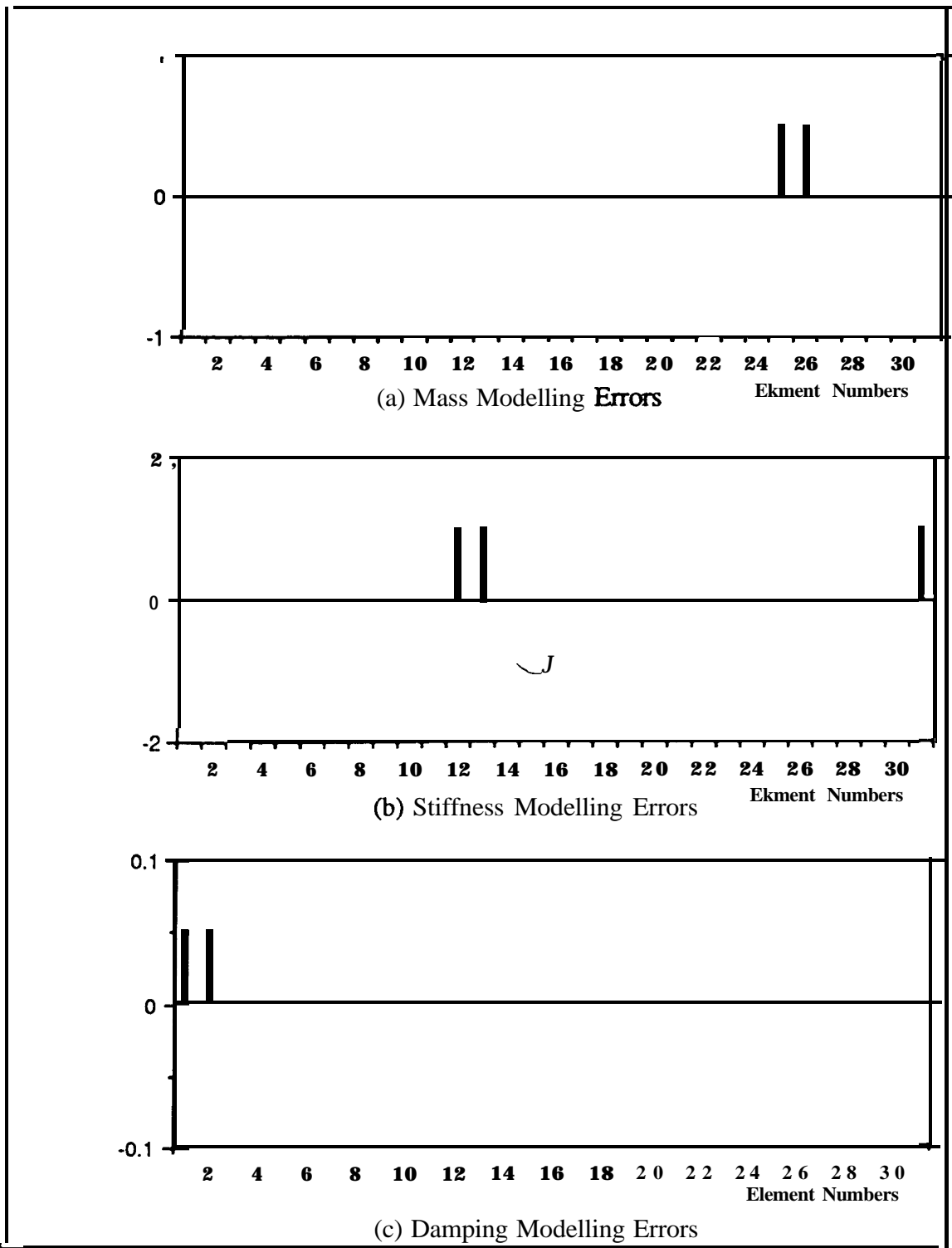


Fig.6.4 Model Updating Results (Case 1; Fifth Iteration)

### 6.3.2 CASE 2

For the more heavily damped case, the damping properties in the 1<sup>st</sup> and 2<sup>nd</sup> elements were increased to 0.3  $[K]_i$ . The modal parameters of the first 10 'experimental' and analytical modes are compared in Table 6.6 together with **MAC** values. The eigenvectors of the first two 'experimental' and analytical modes are compared in Tables 6.7 and 6.8.

**Table 6.6 Natural Frequencies of 'Experimental' and Analytical Models (Case 2)**

Mode No.	Experimental		Analytical Nat. Freqs.	MAC Values
	Nat. Freqs.	Loss Factors		
1	344.3	0.019	342.3	0.992
2	469.2	0.013	450.6	0.967
3	552.1	0.071	528.5	0.927
4	578.5	0.013	557.2	0.960
5	704.7	0.043	683.4	0.948
6	852.8	0.024	833.7	0.978
7	918.7	0.018	902.3	0.885
8	928.9	0.002	927.0	0.791
9	1100.5	0.010	1066.6	0.854
10	1206.2	0.038	1165.3	0.890

Table 6.7 Eigenvectors of 'Experimental' and Analytical Models (Case 2: Mode 1)

Coords.	Exp.(x10 <sup>-1</sup> )	Anal.(x10 <sup>-1</sup> )	Coords	Exp.(x10 <sup>-1</sup> )	Anal.(x10 <sup>-1</sup> )
1	0.717(-2°)	0.748(0°)	41	0.256(-178°)	0.246(180°)
2	0.259(2°)	0.236(0°)	46	0.204(-178°)	0.123(180°)
7	0.379(12°)	0.370(0°)	47	0.255(-179°)	0.244(180°)
8	0.262(1°)	0.248(0°)	52	0.315(-1°)	0.380(0°)
13	0.117(153°)	0.134(180°)	53	0.231(180°)	0.220(180°)
14	0.235(1°)	0.233(0°)	58	0.730(0°)	0.754(0°)
19	0.574(178°)	0.593(180°)	59	0.203(177°)	0.192(180°)
20	0.194(1°)	0.205(0°)	67	0.711(-1°)	0.740(0°)
22	0.735(180°)	0.754(180°)	68	0.084(8°)	0.072(0°)
23	0.177(1°)	0.192(0°)	76	0.399(-4°)	0.398(0°)
28	0.719(180°)	0.742(180°)	77	0.153(-2°)	0.121(0°)
29	0.017(-167°)	0.019(180°)	82	0.166(-172°)	0.138(180°)
37	0.727(180°)	0.748(180°)	83	0.452(-173°)	0.420(180°)
38	0.247(-177°)	0.236(180°)	88	0.652(-179°)	0.610(180°)
40	0.653(-179°)	0.585(180°)	89	0.227(-177°)	0.188(180°)

**Table 6.8 Eigenvectors of 'Experimental' and Analytical Models (Case 2: Mode 2)**

Coords.	Exp.(x10 <sup>-1</sup> )	Anal.(x10 <sup>-1</sup> )	Coords.	Exp.(x10 <sup>-1</sup> )	Anal.(x10 <sup>-1</sup> )
1	0.064(-162°)	0.008( 180°)	4 1	0.027(-129°)	0.020( 180°)
2	0.035( 140°)	0.024( 180°)	4 6	0.412(-173°)	0.459(180°)
7	0.411(163°)	0.353(180°)	4 7	0.060(-158°)	0.060( 180°)
8	0.041(154°)	0.033(180°)	5 2	0.493(-175°)	0.459( 180°)
13	0.542( 169°)	0.496( 180°)	53	0.149(-175°)	0.143(180°)
14	0.100(171°)	0.097(180°)	5 8	0.270(180°)	0.196(180°)
19	0.337(177°)	0.354(180°)	59	0.265(180°)	0.250(180°)
20	0.190(178°)	0.195(180°)	67	0.121(-175°)	0.061(180°)
22	0.142(-168°)	0.196(180°)	68	0.199(173°)	0.172(180°)
23	0.242(179°)	0.250(180°)	76	1.299(1°)	1.220(0°)
28	0.055(-154°)	0.102(180°)	77	0.800(2°)	0.738(0°)
29	0.205(-174°)	0.223(180°)	82	1.419(1°)	1.520(0°)
37	0.026(-38°)	0.008(180°)	83	0.856(0°)	0.926(0°)
38	0.036(-134°)	0.024(180°)	88	0.381(-2°)	0.669(0°)
40	0.076(-158°)	0.195(180°)	89	0.198(-8°)	0.399(0°)

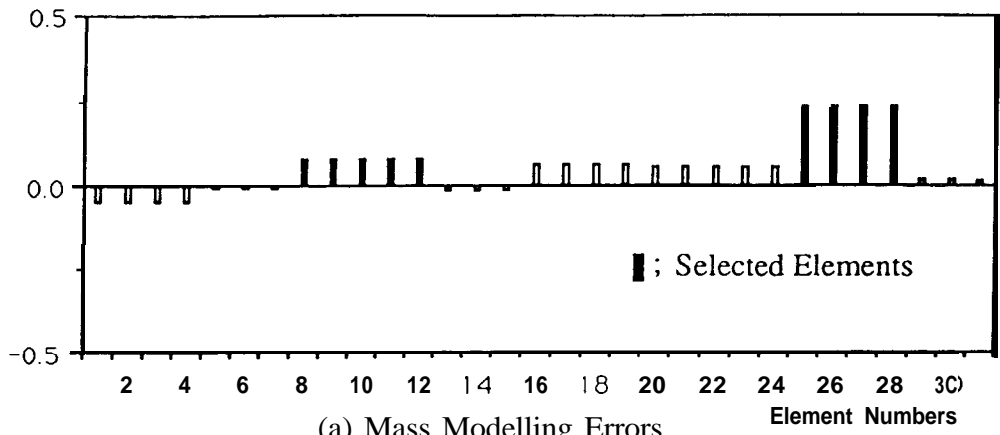


The same macro model as that of Case 1 was used for error location. It took 6 iterations to converge and 27 elements - 9 mass elements, 11 stiffness elements and 7 damping elements - were identified as possible error regions, as shown in Fig.65

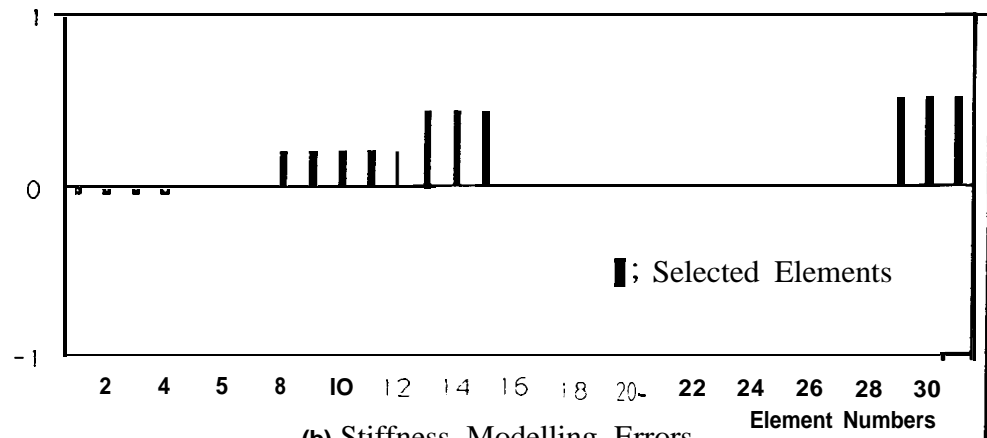
The resultant natural **frequencies** of the 'improved' analytical model are compared with **those** of the 'experimental' modes in Table 6.9.

Table 6.9 Natural Frequencies of 'Experimental' and Intermediate Models (Case 2)

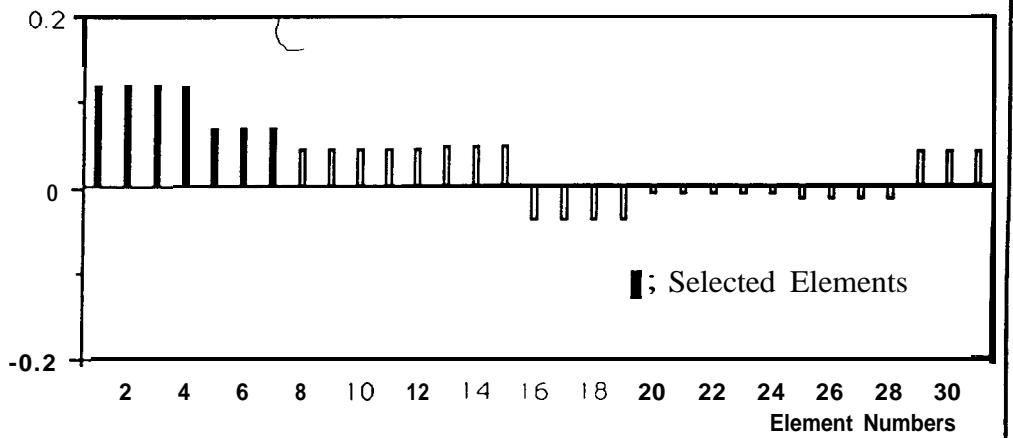
Mode	1	2	3	4	5	6	7	8	9	10
$f_x$ (Hz)	344.3	469.2	552.1	578.5	704.7	852.8	918.7	928.9	1100.5	1206.1
$f_A$ (Hz)	348.5	463.7	547.6	586.7	706.7	860.5	923.4	929.3	1084.9	1193.6
MAC	0.992	0.986	0.967	0.975	0.977	0.984	0.989	0.980	0.985	0.982



(a) Mass Modelling Errors



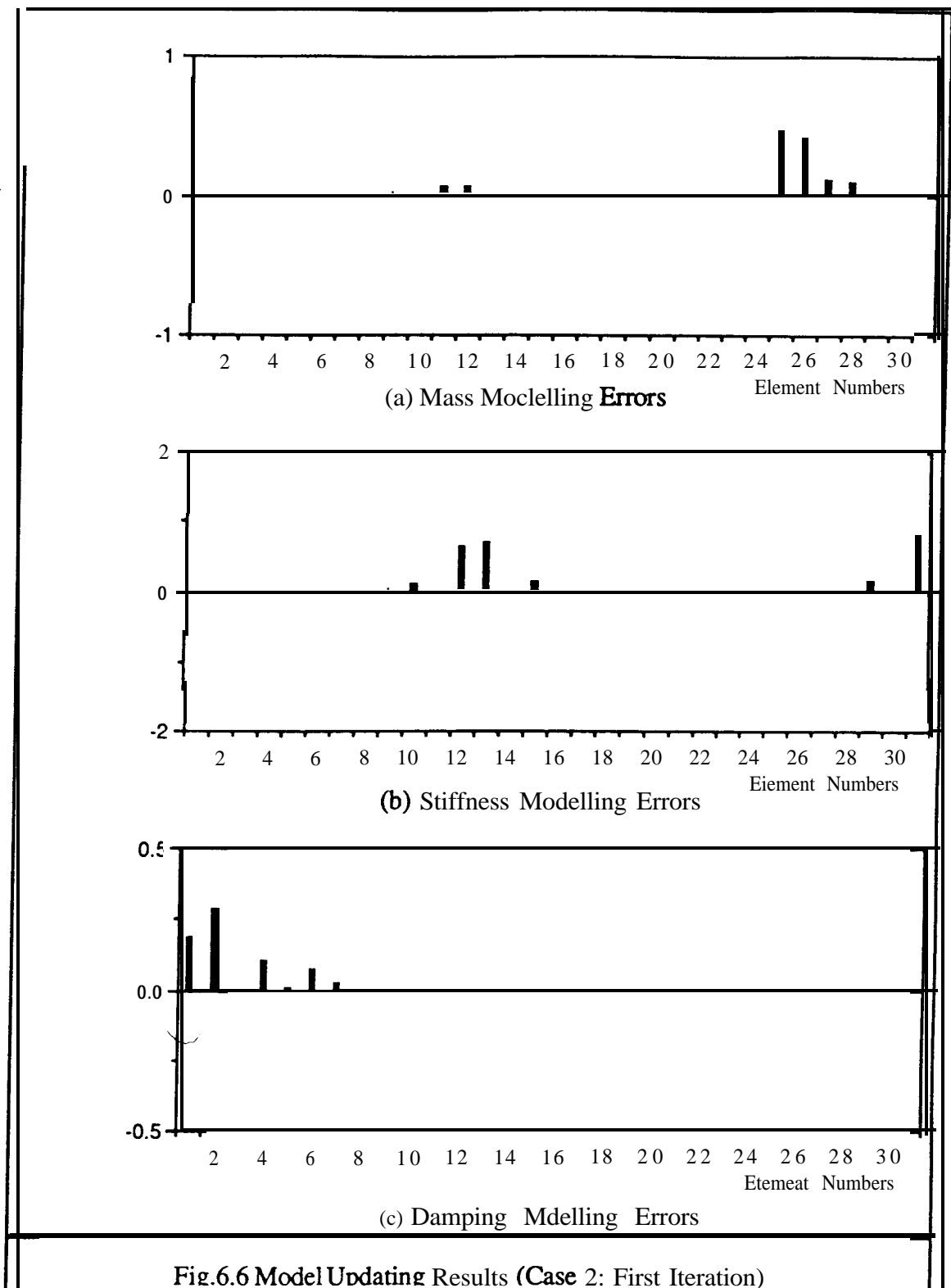
(b) Stiffness Modelling Errors

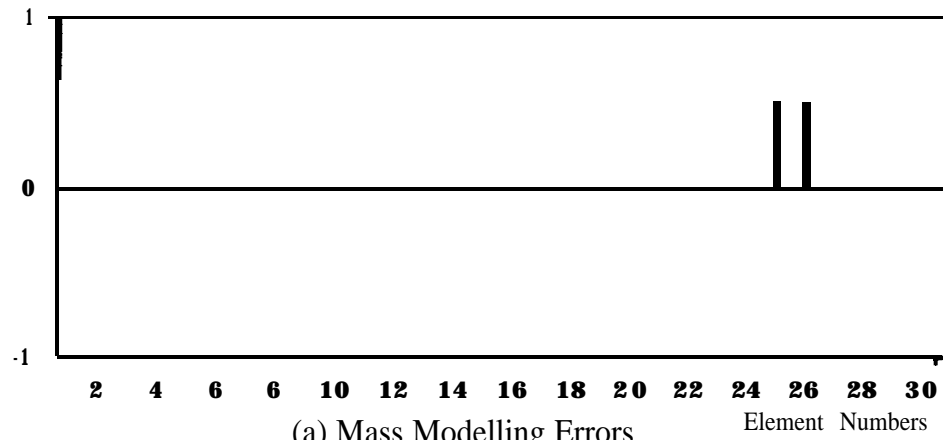


(c) Damping Modelling Errors

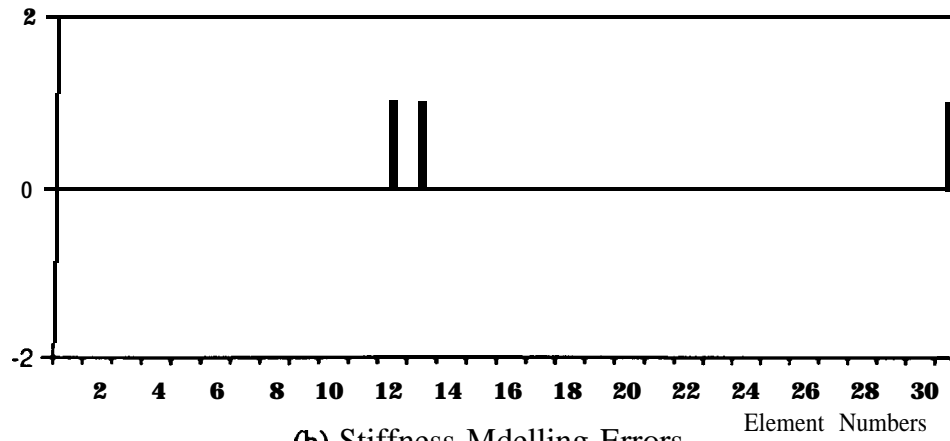
Fig.6.5 Error Location Results (Case 2)



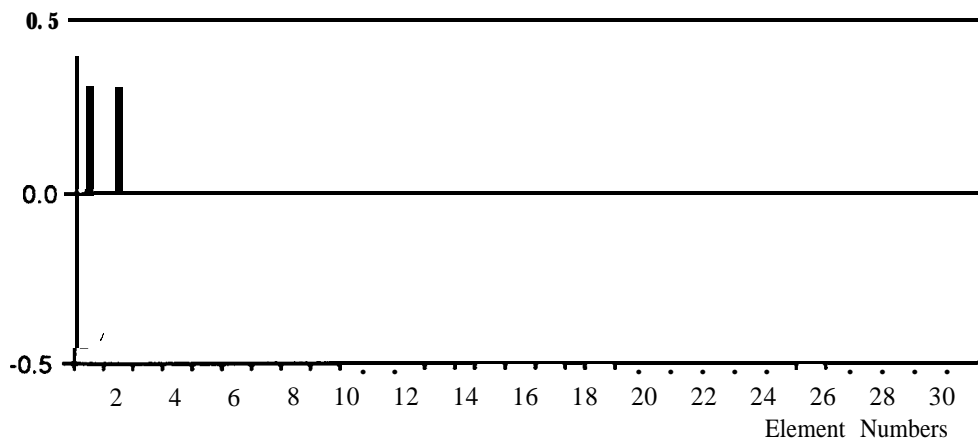




(a) Mass Modelling Errors

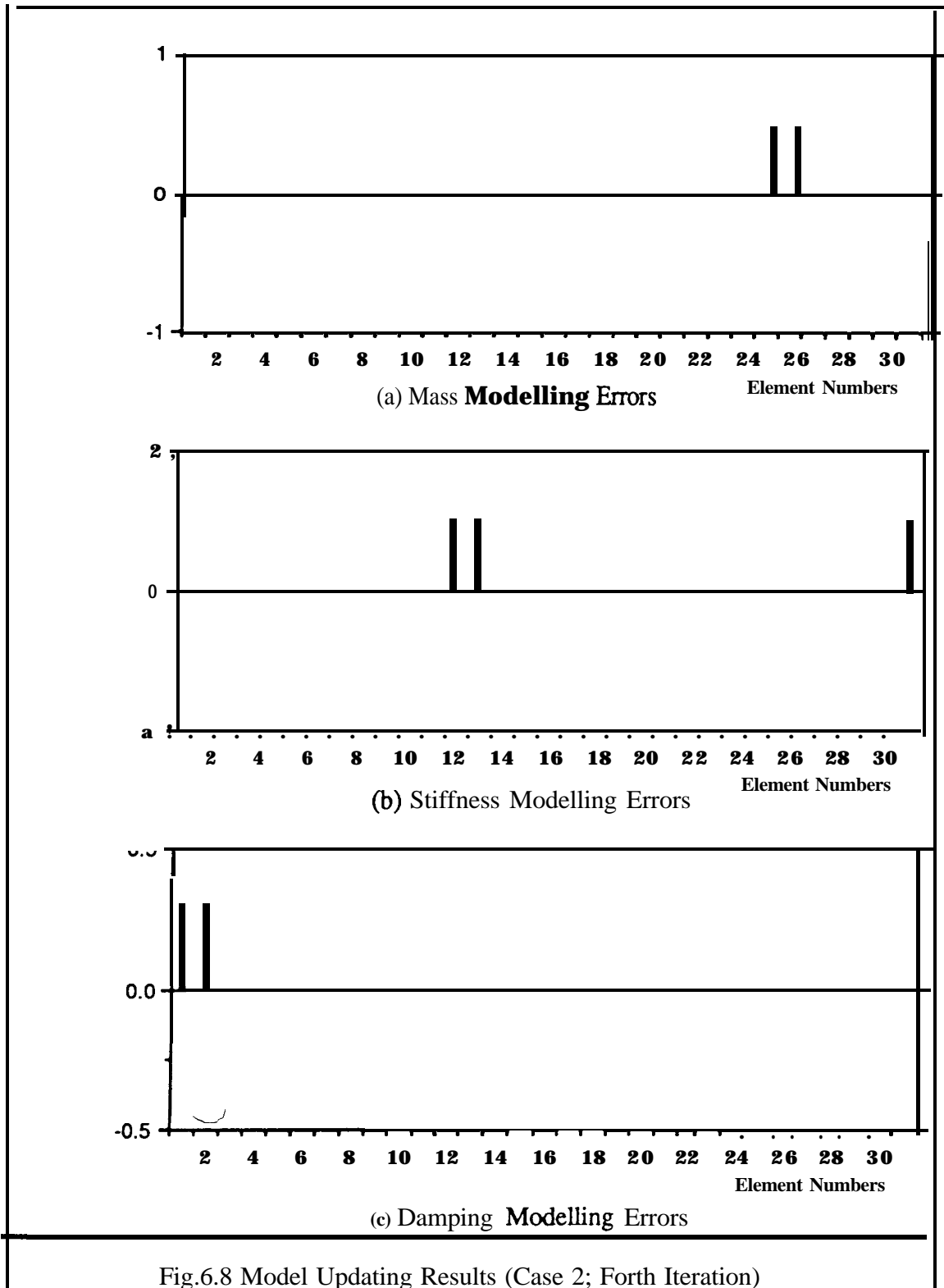


(b) Stiffness Modelling Errors



(c) Damping Modelling Errors

Fig.6.7 Model Updating Results (Case 2; Third Iteration)



## 6.4 CONCLUSIONS

The damping properties of most vibrating structures are not distributed in a similar way to the mass or stiffness. Rather, damping often results from the joints between various components of a structure. As a result, measured modal data are often complex, while the **modal** parameters of the corresponding analytical model are real.

Updating methods developed so far generally assume that the experimental modal data are **real, or** postulate that the measured complex data have successfully been converted to real data. However, the deduced real modes may be erroneous because the **experimentally-**identified complex modes are incomplete and the deduction itself relies on the analytical model which is erroneous.

A method has been developed to locate and to update damping elements together with mass and stiffness elements in analytical model using measured complex modal data. The proposed method has been applied to the free-free bay structure which may constitute a realistic problem in respect of the incompleteness of both measured modes and coordinates. The updating results are quite accurate not only in modal parameters but also in correction coefficients namely, physical design variables.

# CHAPTER 7

# CHAPTER 7

## CONCLUSIONS

### 7.1 GENERAL CONCLUSIONS

Due to advances in numerical methods and the availability of powerful computing facilities, FE modelling has become the most popular technique in structural dynamic analysis. However, the dynamic responses obtained from FE analysis are seldom in perfect agreement with modal testing results. Therefore a model updating procedure should be introduced in order to adjust the analytical model so that the analysis and test results agree, and so that a valid model is available for design calculations.

It should be noted that modal parameters obtained from a modal test are generally not fully compatible with those from the analytical model because

- 1) the number of modes available from measurement ( $m$ ) is usually very **limited** ( $m \ll N$ ),
- 2) the number of measured coordinates ( $n$ ) is in general much less than the number of coordinates (or the number of degrees of freedom) of an analytical model ( $n < N$ ) and
- 3) in most cases, experimental **modal** data from a real structure are not real but

complex, even if the structure is lightly damped, while the modal parameters of the corresponding analytical model are real.

Any incompatibilities between measured modes and the analytical model should be resolved before an updating procedure is applied, or alternatively, an updating method should be used which can handle the incompatibilities.

Various methods have been proposed to improve an analytical model of a mechanical structure using modal test results. Review and numerical studies have revealed some inherent problems of those methods. One of the main problems of direct updating methods, such as function minimisation methods and the error matrix method, is that the updated model is a numerically-optimised one rather than a physically-meaningful model. As a result, the modes outside frequency range of the experimental data remain questionable or may become even worse than those of the original analytical model. Another problem with these methods is that mode expansion is often required in order to overcome the inevitable incompatibility between the analytical model and the measured modes. This might itself be an erroneous procedure, thus jeopardising the subsequent model updating. On the other hand, iteration methods such as **IEM** which do not require such expansion usually do not converge if the modelling errors are not small.

Any attempt to update every element in the analytical model using only the limited information available from typical test results may not be realistic. If mismodelled regions can be located in a preliminary step, model updating can be carried out more efficiently and more successfully. Therefore, error location is a fundamental first objective of the updating process. Recent developments in the area of error location have been investigated. The EMM can locate mismodelled regions successfully even with a very limited number of measured modes if complete coordinates are measured, although this is not a very practical proposition. Again, for the EMM to be successful, a reliable mode expansion method should be available. The **IEM** does not require mode expansion and its computational time will be reduced by locating error regions first and updating the

analytical model using only the elements which are selected in an error location procedure. However, the **IEM** had been found to be unreliable from case studies in Chapter 2, from which it was concluded that more reliable error location methods needed to be developed.

The objectives of this research **were** decided based on these findings, and were:

- 1) to develop a reliable, sensitive and systematic method to locate modelling errors in an **analytical** model using modal testing results, and
- 2) to develop an updating method which can produce an improved analytical model that can not only reproduce the exact modal parameters measured in a test but also predict correctly those modes outside frequency range of the experimental data and at the same time can reduce the number of experimental modes and the computational time for updating.

An inverse eigensensitivity method using arbitrarily-chosen macro elements has been proposed at the error location stage to reduce the computational time and to reduce the number of experimental modes required for subsequent updating. By this approach, the model updating problem, which is generally under-determined, can be transformed into an over-determined one and an updated analytical model can be found which is not influenced by the definition of the macro elements. The proposed method has been applied to the free-free **GARTEUR** structure which represents a practical structure and constitutes a realistic problem in respect of the incompleteness of both measured modes and coordinates. The updating results were quite accurate, not only in modal parameters but also in correction coefficients for the physical design variables.

The assumption that the test results represent the true dynamic behaviour of a test structure, however, may not be correct. Experimental data can be affected by several types of measurement error in spite of the highly-developed instrumentation and modal parameter extraction techniques now available. Thus, the sensitivity of the updating

method itself to noise on the experimental data needs to be investigated. The proposed method has been applied to a Bay structure for which “experimental” data are noisy and incomplete. The error location procedure has been found to be very insensitive to the “measurement” errors - in the presence of measurement errors of up to 1 % in the eigenvalues and 10 % in the eigenvectors, it succeeded in locating the correct mismodelled regions. The updating results were quite accurate in terms of modal parameters and, moreover, in terms of correction factors, when sufficient eigensensitivity terms **are** used. In this case study, measurement errors were introduced by contaminating the modal parameters of the **correct** or modified structure with random noise.

In practice, the characteristics of measurement errors might not result in random variations in the modal parameters. For the updating method to be useful in practical application, various error sources in testing - such as the mass loading effect of transducers, shaker/structure interaction, etc. - should be considered and more realistic errors rather than random noise should be included in the “experimental” data. The errors involved in modal parameter estimation - such as measurement errors, signal processing errors and errors in modal analysis - have been considered in detail, and their effects on estimated **FRFs** and on the modal parameters extracted from the **FRFs** have also been investigated. A computer program has been written to simulate various measurement and signal processing errors. The “experimental” **FRFs** generated using this program can be used to test the performance of different modal parameter identification programs and, thus, of the various applications to which these modal data are put.

The resultant “experimental” modal data which contained representative experimental errors have been used to update the corresponding analytical beam **model** to check the validity of the **IEM**. The mismodelled regions were located successfully, and the updating results were found to be quite accurate, not only in the modal parameters themselves but also in correction coefficients for the physical design variables.

The damping properties of most vibrating structures are not distributed in a similar way to the mass or stiffness. Rather, damping often results from the joints between various components of a structure and, as a result, measured modal data often are complex, while the modal parameters of the corresponding analytical model are real. Updating methods developed so far assume that the experimental modal data are real, or postulate that the measured complex data have successfully been converted to real data. However, the deduced real modes may be erroneous because the experimentally identified complex modes are incompatible and the deduction itself relies on the analytical model which is erroneous.

A method has been developed to locate and to update damping elements together with the mass and stiffness elements in an analytical model using measured complex modal data. The proposed method has been applied to the free-free Bay structure, constituting a realistic problem in respect of the incompleteness of both measured modes and coordinates. The updating results were quite accurate, not only in modal parameters but also in correction coefficients namely, physical design variables, which means that this method can handle all the inherent incompatibilities between measured modes and an the analytical model.

## 7.2 CONTRIBUTIONS OF THE PRESENT RESEARCH

As a final review, the contributions of this research are listed chapter by chapter so that it becomes clear which parts of the work constitute new developments to the subject.

### Chapter 2 - Model Updating Methods - A Review

- review of various updating methods and critical discussion on their advantages and disadvantages/limitations.
- discussion on incompatibility between measured modes and an analytical model and, on the solutions to their problems
- review of various error location methods and critical discussion on their advantages and disadvantages/limitations, especially on the **IEM** based on some numerical case studies

### Chapter 3 - Model Updating Using **IEM**

- development of a **modified IEM** which can locate modelling errors successfully and can produce an updated analytical model which preserves physical **connectivity** and predicts unmeasured modes correctly.
- investigation of the effect of balancing of the sensitivity matrix for error location procedure using the SVD technique
- a detailed explanation of the **IEM** and suggestions for improving the convergence of the **IEM** and graphical explanation of the methods

#### **Chapter 4 - Error Sensitivity of the Inverse Eigensensitivity Method**

- investigation of the sensitivity of the method proposed in Chapter 3 to noise on the experimental data based on a bay structure

#### **Chapter 5 - Errors Involved in Modal Parameter Estimation from Test Data**

- investigation of errors involved in modal parameter estimation and their effect on estimated **FRFs** and on the modal parameters
- development of a computer program which can be used to simulate various measurement and signal processing errors
- exploitation of the capability of the **IEM** in model updating with consideration of the problems of modal and coordinate incompleteness, and of representative experimental errors

#### **Chapter 6 - Updating of Damped Structures**

- extension of the method proposed in Chapter 3 to damped systems, which means the proposed method can handle the last (or the most fundamental) incompatibility between measured modes and the analytical model - real analytical modes and complex experimental modes.

### 7.3 SUGGESTIONS FOR FURTHER WORK

The study undertaken in this thesis has revealed that some further investigations and developments may be necessary or interesting in future work.

In this study, the application is made only to a numerical study and a comparatively simple structure due to the limited period of time available. Even though updating results are shown to be quite accurate in the case studies undertaken, the proposed method should be applied to more complicated structures with more complicated elements such as shell and/or plate elements which might be more commonly used than beam elements in FE analysis of mechanical structures, in order to check the wider validity of the method.

In the investigation of the errors involved in **modal** parameter estimation from test results, various measurement and signal processing errors and errors in modal analysis have been included. However, the effect of a push rod (or a stinger), which is essential to connect an exciter to a test structure when random or sinusoidal excitation is used, on the test results has not been included. The push rod effect should be investigated and included in the computer program for simulating experimental data.

The proposed updating method requires mass and stiffness matrices of the each element of an analytical model of a structure to calculate a sensitivity matrix, and eigenproblem should be solved in every iteration. For the method to be more practical or more flexible, interfacing the updating program with existing FE package is necessary.

# APPENDICES

## APPENDIX A

### DERIVATION OF EIGENVALUE AND EIGENVECTOR DERIVATIVES

Sensitivity analysis has widely been used in many engineering fields such as system dynamics modification [41,42] and identification of dynamic systems or model updating [14,19,43-45]. In these applications, eigenvector and eigenvalue derivatives with respect to design parameters are required. Wittrick [46] obtained the first derivatives of eigenvalues for real symmetric systems, while Fox et. al. [47] extended these results to include the first derivatives of eigenvectors. The process in this Appendix follows closely the one given in Ref. [47].

The eigenvalue problem of a mechanical system can be expressed as:

$$([K] - \lambda_r [M]) \{\phi\}_r = \{0\} \quad (\text{A.1})$$

$$\{\phi\}_r^T [M] \{\phi\}_r = 1 \quad (\text{A.2})$$

∴

Differentiating (A.1) with respect to an updating variable  $p_r$  gives

$$\left( \frac{\partial [K]}{\partial p_i} - \frac{\partial \lambda_r}{\partial p_i} [M] - \lambda_r \frac{\partial [M]}{\partial p_i} \right) \{\phi\}_r + ([K] - \lambda_r [M]) \frac{\partial \{\phi\}_r}{\partial p_i} = \{0\} \quad (\text{A.3})$$

Pre-multiplying (A.3) by  $\{\phi\}_r^T$  leads to

$$\frac{\partial \lambda_r}{\partial p_i} = \{\phi\}_r^T \frac{\partial [\mathbf{K}]}{\partial p_i} \{\phi\}_r - \lambda_r \{\phi\}_r^T \frac{\partial [\mathbf{M}]}{\partial p_i} \{\phi\}_r \quad (\text{A-4})$$

Note that the equation (A.4) includes only the eigenvalue and eigenvector under consideration, therefore a complete solution of eigenproblem is not needed to obtain these derivatives.

The eigenvector derivatives can be expressed as linear combinations of all eigenvectors of the system if the eigenvalues are assumed distinct, because  $N$  eigenvectors are linearly independent and they can be used as a set of basis vectors for spanning  $N$ -dimensional space. Thus,

$$\frac{\partial \{\phi\}_r}{\partial p_i} = \sum_{j=1}^N c_{rj}^i \{\phi\}_j \quad (\text{A.5})$$

Substituting (AS) into (A.3) and pre-multiplying (A.3) by  $\{\phi\}_k^T$

$$\{\phi\}_k^T \left( \frac{\partial [\mathbf{K}]}{\partial p_i} - \frac{\partial \lambda_r}{\partial p_i} [\mathbf{M}] - \lambda_r \frac{\partial [\mathbf{M}]}{\partial p_i} \right) \{\phi\}_r + \{\phi\}_k^T ([\mathbf{K}] - \lambda_r [\mathbf{M}]) \sum_{j=1}^N c_{rj}^i \{\phi\}_j = 0 \quad (\text{A.6})$$

If  $k \neq r$ ,

$$\{\phi\}_k^T \left( \frac{\partial [\mathbf{K}]}{\partial p_i} - \lambda_r \frac{\partial [\mathbf{M}]}{\partial p_i} \right) \{\phi\}_r + c_{rk}^i (\lambda_k - \lambda_r) = 0 \quad (\text{A.7})$$

Thus,

$$c_{rk}^i = \frac{\{\phi\}_k^T \left( \frac{\partial[\mathbf{K}]}{\partial p_i} - \lambda_r \frac{\partial[\mathbf{M}]}{\partial p_i} \right) \{\phi\}_r}{\lambda_r - \lambda_k} \quad (\text{A.8})$$

$c_{rr}^i$  can be obtained by differentiating (A.2) with respect to  $p_i$

$$2\{\phi\}_r^T [\mathbf{M}] \frac{\partial\{\phi\}_r}{\partial p_i} + \{\phi\}_r^T \frac{\partial[\mathbf{M}]}{\partial p_i} \{\phi\}_r = 0 \quad (\text{A.9})$$

Substituting (A.5) into (A.9) leads to

$$c_{rr}^i = -\frac{1}{2} \{\phi\}_r^T \frac{\partial[\mathbf{M}]}{\partial p_i} \{\phi\}_r \quad (\text{A.10})$$

Thus,

$$\frac{\partial\{\phi\}_r}{\partial p_i} = \sum_{j=1}^N c_{rj}^i \{\phi\}_j \quad (\text{A.11})$$

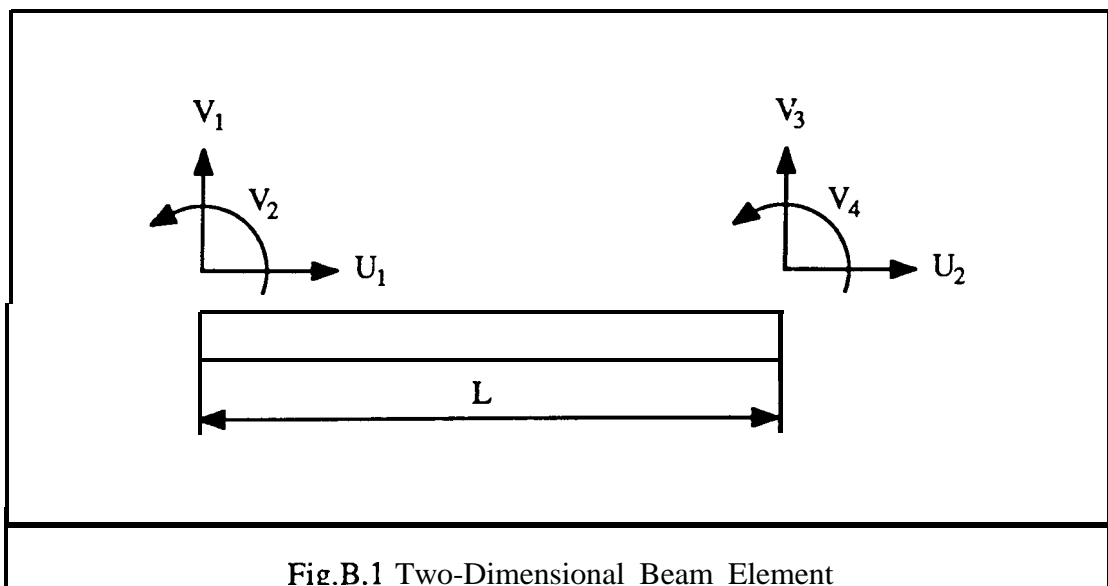
$$c_{rj}^i = \begin{cases} \frac{\{\phi\}_j^T \left( \frac{\partial[\mathbf{K}]}{\partial p_i} - \lambda_r \frac{\partial[\mathbf{M}]}{\partial p_i} \right) \{\phi\}_r}{\lambda_r - \lambda_j} & (r \neq j) \\ -\frac{1}{2} \{\phi\}_j^T \frac{\partial[\mathbf{M}]}{\partial p_i} \{\phi\}_r & (r = j) \end{cases}$$

## APPENDIX B

### ELEMENT AND MACRO-ELEMENT MATRICES

#### B.1 MASS AND STIFFNESS MATRICES OF FE MODEL

Each beam element used in this thesis is the superposition of an axial bar element and a Bernoulli-Euler beam. The coordinates of the beam element are shown in Fig.B. 1.



### Axial Motion

The simplest approximation of axial displacement within the element employs the displacement at the two ends and is given by

$$u(x,t) = \psi_1(x) u_1(t) + \psi_2(x) u_2(t)$$

The shape functions can be derived by considering axial deformation under static loads

$$\frac{\partial}{\partial x} \left( AE \frac{\partial u}{\partial x} \right) = 0$$

which satisfy boundary conditions

$$u(0,t) = u_1(t) \quad u(L,t) = u_2(t)$$

such as:

$$\psi_1(x) = 1 - \frac{x}{L} \quad \psi_2(x) = \frac{x}{L} \quad (\text{B.1})$$

Stiffness coefficients  $k_{ij}$  and mass coefficients  $m_{ij}$  are given by [48]

$$k_{ij} = \int_0^L EA \psi_i' \psi_j' dx \quad (\text{B.2a})$$

$$m_{ij} = \int_0^L \rho A \psi_i \psi_j dx$$

Substituting equation (B.1) into (B.2a) and (B.2b) gives the following stiffness and mass matrices for a uniform element

### Axial Motion

The simplest approximation of axial displacement within the element employs the displacement at the two ends and is given by

$$u(x,t) = \psi_1(x) u_1(t) + \psi_2(x) u_2(t)$$

The shape functions can be derived by considering axial deformation under static loads

$$\frac{\partial}{\partial x} \left( AE \frac{\partial u}{\partial x} \right) = 0$$

which satisfy boundary conditions

$$u(0,t) = u_1(t) \quad u(L,t) = u_2(t)$$

such as:

$$\psi_1(x) = 1 - \frac{x}{L} \quad \psi_2(x) = \frac{x}{L} \quad (\text{B.1})$$

Stiffness coefficients  $k_{ij}$  and mass coefficients  $m_{ij}$  are given by [48]

$$k_{ij} = \int_0^L EA \psi_i' \psi_j' dx \quad (\text{B.2a})$$

$$m_{ij} = \int_0^L \rho A \psi_i \psi_j dx$$

Substituting equation (B.1) into (B.2a) and (B.2b) gives the following stiffness and mass matrices for a uniform element

$$[K_a^e] = \frac{AE}{L} \begin{bmatrix} 1 & -1 \\ -1 & 1 \end{bmatrix} \quad (\text{B.3a})$$

$$[M_a^e] = \frac{\rho AL}{6} \begin{bmatrix} 2 & 1 \\ 1 & 2 \end{bmatrix} \quad (\text{B.3b})$$

### Transverse Motion

Let the displacement coordinates for transverse motion be the end displacements and slopes as

$$v(x,t) = \sum_{i=1}^4 \psi_i(x) v_i(t)$$

The shape functions can be derived by considering the equilibrium equation for a beam loaded only at its ends

$$\frac{\partial^2}{\partial x^2} \left( EI \frac{\partial^2 v}{\partial x^2} \right) = 0$$

which satisfy boundary conditions

$$v(0,t) = v_1(t)$$

$$v'(0,t) = v_2(t)$$

$$v(L,t) = v_3(t)$$

$$v'(L,t) = v_4(t)$$

such as:

$$[K_a^e] = \frac{AE}{L} \begin{bmatrix} 1 & -1 \\ -1 & 1 \end{bmatrix} \quad (\text{B.3a})$$

$$[M_a^e] = \frac{\rho AL}{6} \begin{bmatrix} 2 & 1 \\ 1 & 2 \end{bmatrix} \quad (\text{B.3b})$$

### Transverse Motion

Let the displacement coordinates for transverse motion be the end displacements and slopes as

$$v(x,t) = \sum_{i=1}^4 \psi_i(x) v_i(t)$$

The shape functions can be derived by considering the equilibrium equation for a beam loaded only at its ends

$$\frac{\partial^2}{\partial x^2} \left( EI \frac{\partial^2 v}{\partial x^2} \right) = 0$$

which satisfy boundary conditions

$$v(0,t) = v_1(t)$$

$$v'(0,t) = v_2(t)$$

$$v(L,t) = v_3(t)$$

$$v'(L,t) = v_4(t)$$

such as:

$$\begin{aligned}
 \psi_1(x) &= 1 - 3 \left(\frac{x}{L}\right)^2 + 2 \left(\frac{x}{L}\right)^3 \\
 \psi_2(x) &= x - 2L \left(\frac{x}{L}\right)^2 + L \left(\frac{x}{L}\right)^3 \\
 \psi_3(x) &= 3 \left(\frac{x}{L}\right)^2 - 2 \left(\frac{x}{L}\right)^3 \\
 \psi_4(x) &= -L \left(\frac{x}{L}\right)^2 + L \left(\frac{x}{L}\right)^3
 \end{aligned} \tag{B.4}$$

Stiffness coefficients  $k_{ij}$  and mass coefficients  $m_{ij}$  are given by [48]

$$k_{ij} = \int_0^L EI \psi_i'' \psi_j'' dx \tag{B.5a}$$

$$m_{ij} = \int_0^L \rho A \psi_i \psi_j dx \tag{B.5b}$$

Substituting equation (13.4) into (B.5a) and (B.5b) gives the following stiffness and mass matrices for a uniform element

$$[K_b^e] = \frac{EI}{L^3} \begin{bmatrix} 12 & 6L & -12 & 6L \\ & 4L^2 & -6L & 2L^2 \\ \text{symm.} & & & 4L^2 \end{bmatrix} \tag{B.6a}$$

$$[M_b^e] = \frac{\rho AL}{420} \begin{bmatrix} 156 & 22L & 156 & -22L \\ & 4L^2 & 156 & 22L \\ \text{symm.} & & & 4L^2 \end{bmatrix} \tag{B.6b}$$

The stiffness and mass matrices of the beam element, which is the superposition of an axial and a Bernoulli-Euler beam, can be expressed as:

$$[K^e] = \begin{bmatrix} \frac{EA}{L} & 0 & 0 & -\frac{EA}{L} & 0 & 0 \\ & \frac{12EI}{L^3} & \frac{6EI}{L^2} & 0 & -\frac{12EI}{L^3} & \frac{6EI}{L^2} \\ & & \frac{4EI}{L} & 0 & -\frac{6EI}{L^2} & \frac{2EI}{L} \\ & & & \frac{EA}{L} & 0 & 0 \\ & & & & \frac{12EI}{L^3} & -\frac{6EI}{L^2} \\ & \text{symm.} & & & & \frac{4EI}{L} \end{bmatrix}$$

$$[M^e] = \frac{\rho AL}{420} \begin{bmatrix} 140 & 156 & 20L & 0 & 54 & -13L \\ & & 4L^2 & 0 & 13L & -3L^2 \\ & & & & 156 & -22L \\ & \text{symm.} & & 140 & 0 & 4L^2 \end{bmatrix}$$

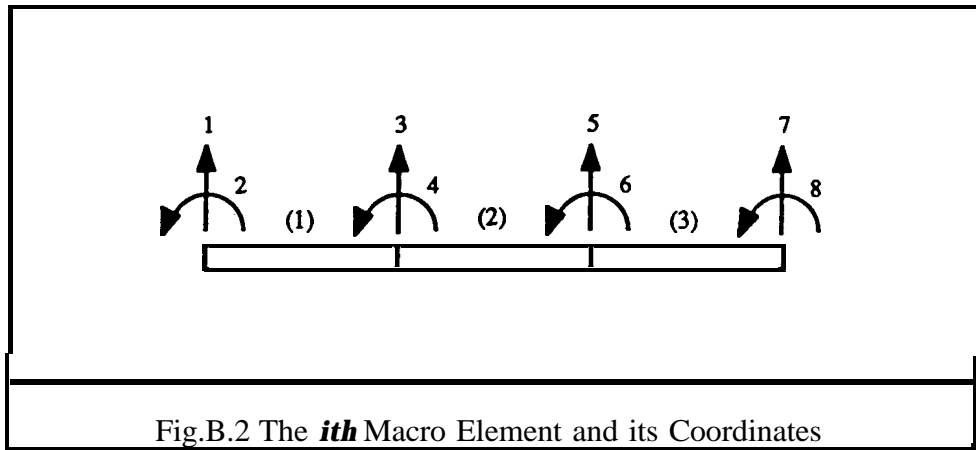
## B.2 CONSTRUCTION OF MACRO ELEMENTS

The mass (or stiffness) matrix of the  $i$ th macro element is formed by a summation of individual mass (or stiffness) matrices

$$[M]_i = \sum_{j=1}^{n_i} [M^e]_j \quad [K]_i = \sum_{j=1}^{n_i} [K^e]_j$$

The construction of the macro element matrices will be illustrated by using a simple structure. If there are three individual elements in the  $i$ th macro element and each node has 2 DoFs, as shown in Fig.B.2, then the mass matrix of the  $i$ th macro element, which is a summation of the three element mass matrices





### B.3 NUMERICAL DATA OF BAY AND GARTEUR STRUCTURES

Elements	Horizontal	Vertical	Diagonal
L	$\frac{5}{7}$ m	$\frac{3}{5}$ m	$\frac{\sqrt{34}}{7}$ m
A	$4.00 \times 10^{-3} \text{ m}^2$	$6.00 \times 10^{-3} \text{ m}^2$	$3.00 \times 10^{-3} \text{ m}^2$
E	$7.50 \times 10^{10} \text{ Pa}$		
I	$7.56 \times 10^{-2} \text{ m}^4$		
$\rho$	$2.80 \times 10^3 \text{ kg/m}^3$		

## APPENDIX C

### THE SINGULAR VALUE DECOMPOSITION

The purpose of this appendix is not to present a detailed explanation of the SVD with a full and **rigorous** mathematical description, but to give a simple introduction with a view to its applications to the determination of the rank of a matrix and to the solution of a set of overdetermined linear systems of equations.

#### C.1 SINGULAR VALUE DECOMPOSITION (SVD)

The SVD is based on the following theorem of linear algebra, whose proof [Ref.49] is beyond our scope:

Any  $\mathbf{M} \times \mathbf{N}$  real matrix  $[\mathbf{A}]$  whose number of rows  $\mathbf{M}$  is greater than or equal to its number of columns  $\mathbf{N}$ , can be written as the product of an  $\mathbf{M} \times \mathbf{M}$  orthonormal matrix  $[\mathbf{U}]$ , an  $\mathbf{M} \times \mathbf{N}$   $[\mathbf{C}]$  with positive or zero elements, and the transpose of an  $\mathbf{N} \times \mathbf{N}$  orthonormal matrix  $[\mathbf{V}]$ . i.e.,

$$[\mathbf{A}]_{\mathbf{M} \times \mathbf{N}} = [\mathbf{U}]_{\mathbf{M} \times \mathbf{M}} [\mathbf{\Sigma}]_{\mathbf{M} \times \mathbf{N}} [\mathbf{V}]_{\mathbf{N} \times \mathbf{N}}^T \quad (\text{C.1})$$

where  $[\Sigma]$  is a real **matrix with** elements  $\sigma_{ij} = \sigma_i$  for  $i = j$  and  $\sigma_{ij} = 0$  for  $i \neq j$ .

Because  $[U]$  and  $[V]$  are **orthonormal** matrices,

$$[U]^T = [U]^{-1} \quad [V]^T = [V]^{-1} \quad (\text{C.2})$$

and

$$[U]^T[U] = [U][U]^T = [V]^T[V] = MM' = [I] \quad (\text{C.3})$$

The values  $\sigma_i$  are called the singular values of the matrix  $[A]$ . Without loss of generality, the singular values can be ordered in descending order

$$\sigma_1 \geq \sigma_2 \geq \sigma_3 \geq \dots \geq \sigma_N \geq 0$$

Thus,

$$[\Sigma] = \begin{bmatrix} \sigma_1 & & & & & \\ & \sigma_2 & & & & \\ & & \cdot & & & \\ & & & \cdot & & \\ & & & & \sigma_N & \\ \hline & & & & & 0 \end{bmatrix}$$

Similarly, the SVD of a complex matrix results in the following:

$$[A]_{M \times N} = [U]_{M \times M} [\Sigma]_{M \times N} [V]_{N \times N}^H$$

where  $[\mathbf{V}]_{N \times N}^H$  is the complex conjugate transpose of  $[\mathbf{V}]$  and  $[\mathbf{U}]$  and  $[\mathbf{V}]$  are unitary matrices, i.e.,

$$[\mathbf{U}]^H[\mathbf{U}] = [\mathbf{U}][\mathbf{U}]^H = [\mathbf{I}]$$

$$[\mathbf{V}]^H[\mathbf{V}] = [\mathbf{V}][\mathbf{V}]^H = [\mathbf{I}]$$

and

$$[\mathbf{U}]^H = [\mathbf{U}]^{-1} \quad [\mathbf{V}]^H = [\mathbf{V}]^{-1}$$

The singular values are the non-negative square roots of the eigenvalues of the matrix  $[\mathbf{A}]^T[\mathbf{A}]$ , if  $[\mathbf{A}]$  is real, and of  $[\mathbf{A}]^H[\mathbf{A}]$ , if  $[\mathbf{A}]$  is complex. Because  $[\mathbf{A}]^T[\mathbf{A}]$  is symmetric and  $[\mathbf{A}]^H[\mathbf{A}]$  is Hermitian, the eigenvalues are always real and non-negative [49] and, therefore, singular values are always real and non-negative.

For simplicity,  $[\mathbf{A}]$  will be assumed to be real from now on. Usually, the SVD computation is performed in two stages: first, a reduction of  $[\mathbf{A}]$  to a tridiagonal form using the Householder transformation [49] and second, a reduction of the superdiagonal elements to a negligible size, using the QR algorithm [49], resulting in a diagonal form.

## C.2 RANK OF A MATRIX

In some applications it is necessary to determine the rank of a matrix, particularly to determine if the matrix is of less than full rank. The rank of  $[A]$  is the largest number of columns (or rows) of  $[A]$  which constitute a linearly independent set. An  $M \times N$  matrix with  $M \geq N$  is said to be of full rank if its rank equals  $N$ , but rank-deficient if its rank is less than  $N$ .

To calculate the rank of a matrix, an algorithm such as Gaussian elimination may be applied and the rank decided from the final reduced form. In practice, the situation is not so simple. In the first place, the elements of a matrix are seldom given exactly and, even if the original matrix is rank-deficient, it is unlikely that its approximation will also be. Thus, instead of asking if the given matrix is rank-deficient, we must ask if it is nearly rank-deficient. In the second place, the transformations of, say, Gaussian elimination may take a matrix which is very nearly deficient in rank and turn it into one which is clearly of full rank. Finally, it is not always easy to **recognise** when even a triangular matrix, which is the end product of Gaussian elimination, is nearly deficient in rank.

The relationship between the SVD and the rank of a matrix is that the value of the rank is equal to the number of non-zero singular values. The advantage of using the SVD to calculate the rank is that if  $r$  rows of an  $N \times N$  matrix are not totally linearly dependent, we shall obtain a small value for  $\sigma_{N-r+1}$ , instead of zero, and we have only to compare this small value with other singular values. If we establish a criterion for the rejection and acceptance of small singular values, we shall have **an answer** concerning **the value** of the rank. This criterion may depend on the accuracy of the expected results and, in practice, may be difficult to establish. A reasonable solution is to calculate the consecutive ratios of the singular values,  $\frac{\sigma_1}{\sigma_2}, \frac{\sigma_2}{\sigma_3}, \dots, \frac{\sigma_{N-1}}{\sigma_N}$ . Representing the ratios graphically, the first peak will indicate the value of the rank. For instance, if the rank of a matrix is  $r$ , then  $\sigma_{r+1}$  will

be very small and the ratio  $\frac{\sigma_r}{\sigma_{r+1}}$  will be very high compared with  $\frac{\sigma_{r-1}}{\sigma_r}$ , which indicates the **rank** of the matrix.

### C.3 THE LEAST-SQUARES PROBLEM

Very often, we have to solve least-squares problems. These happen when we have an , over-specified set of equations with relation to the unknowns, i.e., we have more information than we need to solve the problem. Once it has been established that a coefficient matrix  $[A]$  is of full rank, the least-squares solution **to an** overdetermined set of linear equations

$$[A]_{M \times N} \{x\}_{N \times 1} = \{b\}_{M \times 1}$$

can be obtained from

$$\{x\} = [A]_{N \times M}^+ \{b\}$$

where  $M > N$ , and  $[A]_{N \times M}^+$  is the Moore-Penrose **generalised** inverse,  $([A]^T[A])^{-1}[A]^T$ .

The generalised inverse  $[A]^+$  can easily be computed efficiently by using the **SVD**. From equation (C.1), we obtain

$$[A]_{N \times M}^+ = [V]_{N \times N}^{-T} [\Sigma]_{N \times M}^+ [U]_{M \times M}^{-1} \quad (C.4)$$

Substituting equation (C.3) into equation (C.4) leads to

$$[A]^+ = [V][\Sigma]^+[U]^T$$



# APPENDIX D

## DYNAMIC CHARACTERISTICS OF PUSH ROD

When modal testing is performed using a continuous excitation signal, such as random or sinusoidal, it is necessary to use an exciter connected via a push rod which should have high axial stiffness for transmission of axial force but low lateral or bending stiffness to allow little moment transfer. In order for the push rod not to contaminate test results, the natural frequencies of the push rod should lie well outside the test frequency range. Dimensions and material properties of push rods which were used for the experiment in Chapter 5 are shown in Table D.1.

Table D. 1 Dimensions and Material Properties of Push rods

	d	L	E	$\rho$
Long push rod	1.5 mm	67.0 mm	$2.07 \times 10^{11} \text{ N/m}^2$	$7850 \text{ kg/m}^3$
Short push rod	1.5 mm	13.0 mm	$2.07 \times 10^{11} \text{ N/m}^2$	$7850 \text{ kg/m}^3$

## D.1 FIRST BENDING MODE

The first bending mode of a push rod can be calculated by considering **fixed-fixed** boundary condition as follows [32]:

$$f_b = \frac{1}{2\pi} \sqrt{\frac{k_b}{m}} \quad (\text{D.1})$$

where  $m$  is the mass of the push rod and  $k_b$  is bending stiffness of the push rod which is given by

$$k_b = \frac{192 EI}{L^3} = \frac{192E}{L^3} \frac{\pi d^4}{64} = 9.42 \frac{E d^4}{L^3} \quad (\text{D.2})$$

Substituting equation (D.2) into equation (D.1) leads to

$$f_b = \frac{0.883 d}{L^2} \sqrt{\frac{E}{\rho}} \quad (\text{D.3})$$

### D.1.1 LONG PUSH ROD

$$\begin{aligned} f_b &= \frac{0.883 d}{L^2} \sqrt{\frac{E}{\rho}} \\ &= \frac{(0.883) (1.5 \times 10^{-3})}{(67 \times 10^{-3})^2} \sqrt{\frac{2.07 \times 10^{11}}{7850}} \\ &= 1,515 \text{ (Hz)} \end{aligned}$$

## D.1.2 SHORT PUSH ROD

$$f_b = \frac{(0.883) (1.5 \times 10^{-3})}{(13 \times 10^{-3})^2} \sqrt{\frac{2.07 \times 10^{11}}{7850}}$$

$$= 40,244 \text{ (Hz)}$$

## D.2 AXIAL MODE

In this case, the push rod assembly acts as a spring loaded by the mass of an exciter armature. Thus,

$$f_a = \frac{1}{2\pi} \sqrt{\frac{k_a}{m_m}} \quad (\text{D.4})$$

where  $m_m$  is the mass of the exciter armature and  $k_a$  is the axial stiffness of the push rod which is given by

$$k_a = \frac{A E}{L} \quad (\text{D.5})$$

## D.2.2 LONG PUSH ROD

$$k_a = \frac{(x/4) (1.5 \times 10^{-3})^2 (2.07 \times 10^{11})}{(67 \times 10^{-3})}$$

$$= 5.460 \times 10^6 \text{ (N/m)}$$

$$f_a = \frac{1}{2\pi} \sqrt{\frac{5.460 \times 10^6}{0.02}}$$
$$= 2,630 \text{ (Hz)}$$

### D.2.2 SHORT PUSH ROD

$$k_a = \frac{(X/4) (1.5 \times 10^{-3})^2 (2.07 \times 10^{11})}{(13 \times 10^{-3})}$$
$$= 2.815 \times 10^7 \text{ (N/m)}$$

$$f_a = \frac{1}{2\pi} \sqrt{\frac{2.815 \times 10^7}{0.02}}$$
$$= 5,917 \text{ (Hz)}$$

# APPENDIX E

## GENFRF USER'S GUIDE

### E.1 OVERVIEW

GENFRF is a FORTRAN program designed to run on an IBM PC-AT or PS2. It can generate frequency response functions (**FRFs**) which have various measurement errors such as:

- 1) mass loading effects of force transducer and accelerometer,
- 2) error by shaker/structure interaction;
- 3) input and output random noise;
- 4) signal processing error (leakage)

A flowchart of the program is given in Fig.E.1.

Generated **FRFs** can be directly used as input files of MODENT [37] for modal analysis.

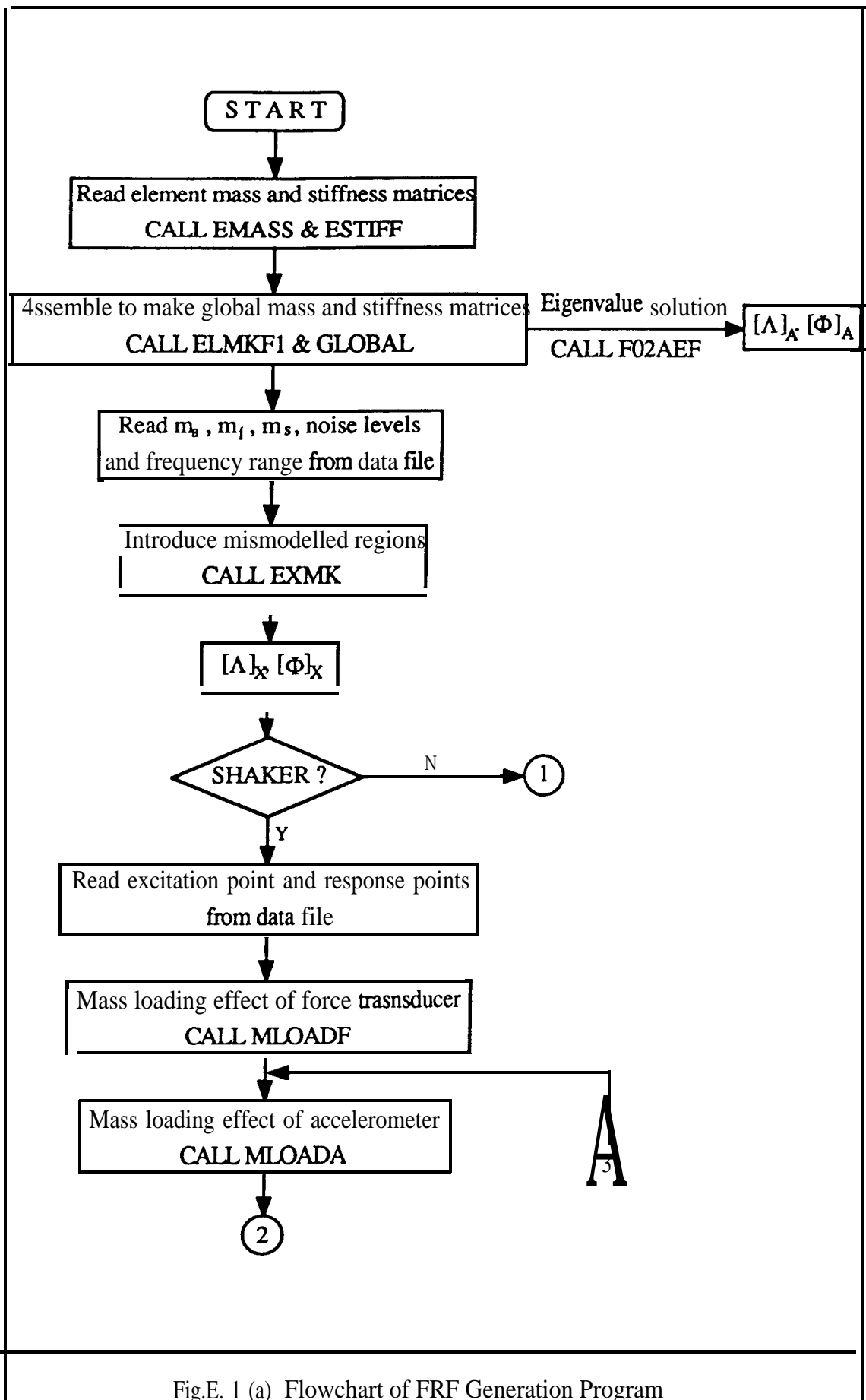


Fig.E. 1 (a) Flowchart of FRF Generation Program

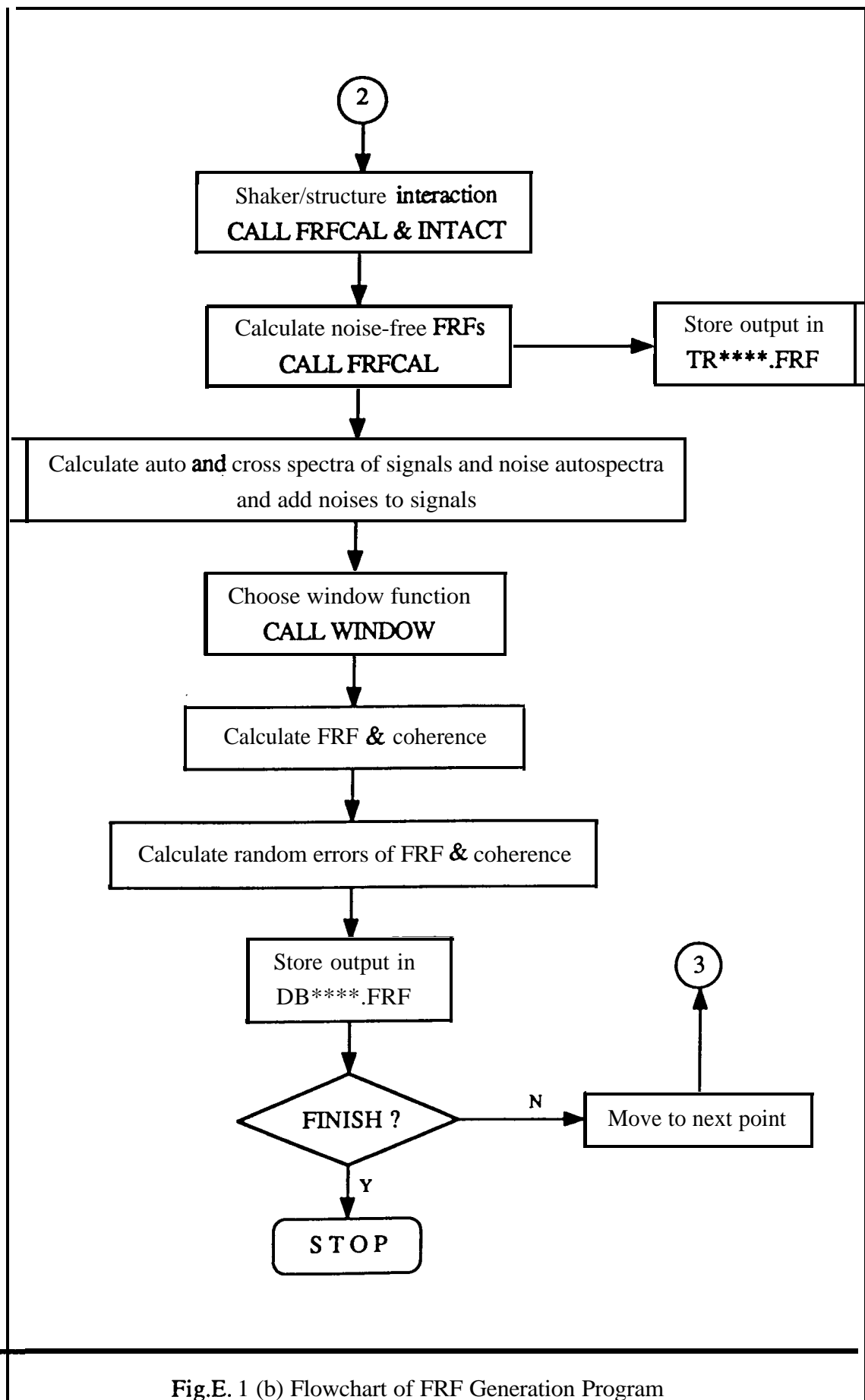


Fig.E. 1 (b) Flowchart of FRF Generation Program

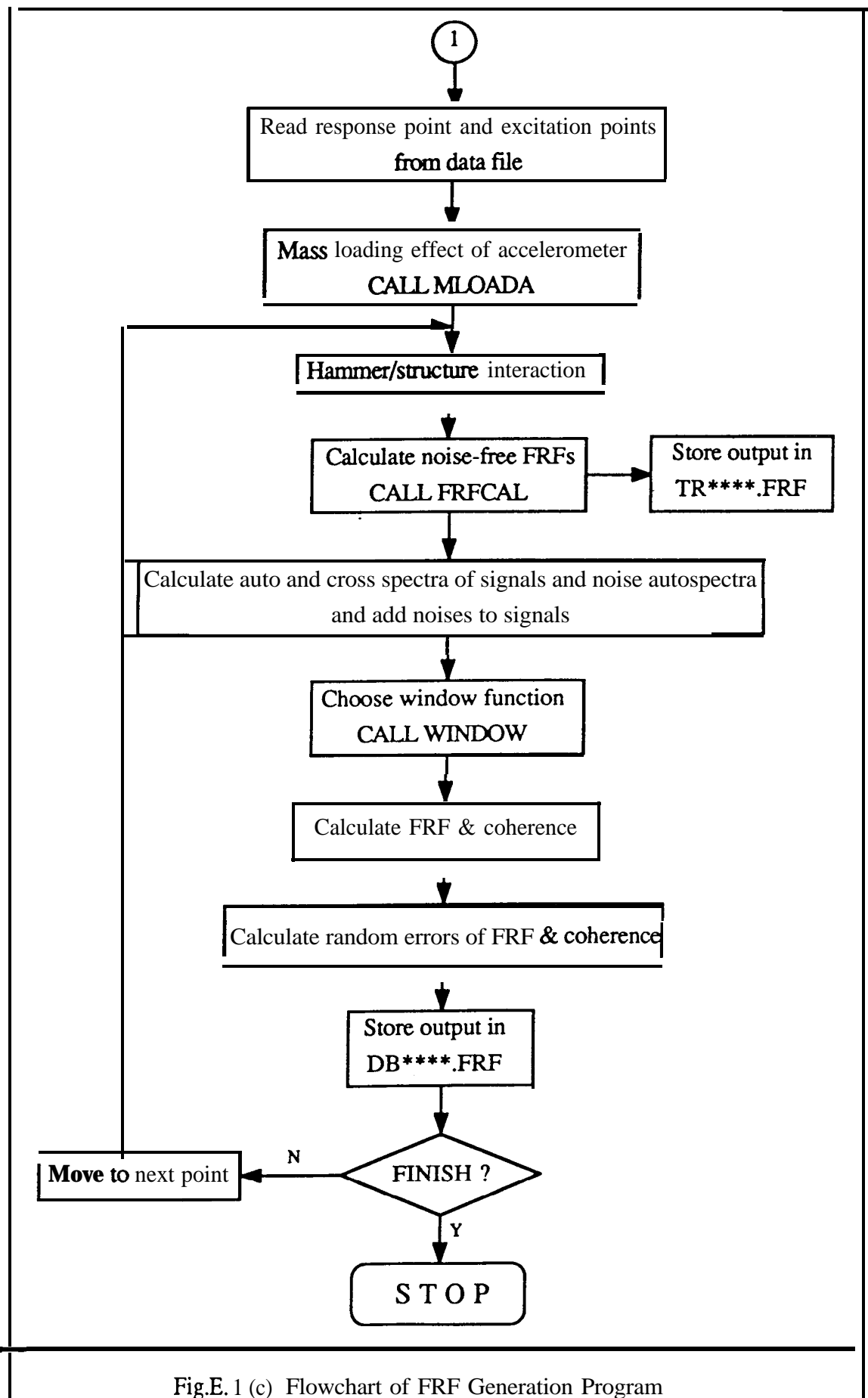


Fig.E. 1 (c) Flowchart of FRF Generation Program

## E.2 INPUT FILE

To run the program, an input file GENFRF.DAT is **necessary**. Its format is **given** in Table E. 1.

Table E. 1 Format of GENFRF.DAT

<u>Record</u>	<u>i a b l e</u>	<u>Name</u>	<u>Type</u>
3	<b>IFTYPE</b>		INT
		FRF Type (1 =Receptance, 2=Mobility, 3=Inertance)	
5	AMS, FTMS, EXMS		REAL
		Masses of accelerometer, force transducer, <b>armature</b> (kg)	
7	GMM, GNN, NAV		<b>REAL,REAL,INT</b>
		Input noise level, Output noise level, No of average	
9	FST, FED		REAL
		<b>Starting freq (Hz), Ending freq (Hz)</b>	
11	ICOH		INT
		0 = No coherence data, <b>1</b> = Coherence data available	
13	IEX		INT
		Global excitation coordinate number	
15	<b>IRS<sub>1</sub>,IRS<sub>2</sub>....IRS<sub>n</sub></b>		INT
		n Global response coordinate numbers	
17	TITLE		CHAR*2
		First two characters of output file names	
19	HEAD		CHAR*80
		Title for <b>FRFs</b>	

**Notes**

- 1) Other records are only used for descriptions of following variables.
- 2) All data to be read in FORTRAN77 free format using the appropriate variable type except TITLE (Record 17).

**E.3 RUNNING GENFRF**

- 1) When you see **C:>**, change to subdirectory **\NAG\** by typing

```
CD NAG
```

- 2) Run GENFRF by typing

```
GENFRF
```

- 3) After several messages, you will be asked:

```
IS SHAKER USED? ( YES = 0 , NO = 1 )
```

Type 0 for shaker excitation (Hammer excitation is not available, if type 1, the program will be terminated.)

- 4) After a while, the computer will give a message

```
** CALCULATING FREQUENCY RESPONSE FUNCTIONS **
```

followed by calculated **FRF** file names.

**E.4 GENFRF OUTPUT FILES**

The output files of GENFRF are as follows:

- 1) Exact modal data ANAL.DAT
- 2) n (no of measurement coordinates) error-free **FRF** data files (**TRN1N2.FRF**) and n noisy **FRF** data files (**DBN1N2.FRF**) where  
N 1; Response coordinate (2 digit)  
N2; Excitation coordinate (2 digit)

- Data format of these files is given in Appendix C of MODENT Reference **Manual**.
- 3) Combined Response Data **file (BEAM.CRD)**. This data file contains the names of individual FRF **files to be analysed globally**. Data format is given in Appendix C of MODENT Reference Manual.

## **E.5 MODIFYING PROGRAM**

GENFRF program uses one of NAG routines, **F02AEF**, for eigenvalue solution which is stored in subdirectory NAG. If you want to modify the program

1) Change to subdirectory **\NAG\**, and modify GENFRF.FOR.

2) After editing, type

```
FL /AH /Opx/FPc genfrf.for /link wlms3+wlms4+wlms5+wlms6+wlms7
```

for compiling and linking because NAG routines were compiled with the options.

3) **Type**

```
GENFRF
```

to run the modified program.

## E.6 COMPUTER PROGRAM

```

C*****C
C*****C
C*****      *****C
C*****    PROGRAM FOR SIMULATING EXPERIMENTAL DATA    *****C
C*****      *****C
C*****C
C*****C
      PROGRAM SIMULATION
C*****C
C*****      *****C
C*****          FREE-FREE BEAM STRUCTURE          *****C
C*****      *****C
C*****C
      PARAMETER(NEL=20,N=42,M=10,NFP=40 1 ,NF2=801)
C*****C
C*****  VARIABLES          *****C
C*****  N ; NO.OF DOF OF SYSTEM          *****C
C*****  M ; NO.OF MEASURED MODES          *****C
C*****  NFP ; NO.OF FREQUENCY POINTS          *****C
c*****  NF2 ; (NFP-1)*2+1          *****C
C*****C
      DOUBLE PRECISION EVAL,EVEC,DUMM,DUMK,DL,E
      DIMENSION DEM(4,4),DEK(4,4)
      DIMENSION DL(N),E(N)
      DIMENSION DUMM(N,N),DUMK(N,N)
      DIMENSION FREQ( 10),COH(NFP)
      DIMENSION GFF(NF2),GXX(NF2)
      CHARACTER TITLE*2,FLNM*10,EX*2,RSP*2
      CHARACTER HEAD*80
      COMPLEX CFRF,GXF(NF2)
      COMMON /CB1/FMF(N,N),FKF(N,N)
      COMMON /CB2/DMM(N,N)
      COMMON /CB3/DM(N,N),DK(N,N)
      COMMON /CB4/EVAL(N),EVEC(N,N)
      COMMON /CB5/CFRF(NF2),FSM(NF2)
C

```

```
C***** ASSEMBLE GLOBAL MASS AND STIFFNESS MATRICES
C
      WRITE(*,*)
      WRITE(*,*)'*** ASSEMBLING MASS AND STIFFNESS MATRICES ***'
      WRITE(*,*)
C
      DO 20 I=1,N
      DO 20 J=1,N
      DM(I,J)=0.
      DK(I,J)=0.
20    CONTINUE
C
      DO 30 K = 1,NEL
      CALL ELMKF1(DEM,DEK,K)
      DO 30 I=1,N
      DO 30 J=1,N
      DK(I,J)=DK(I,J)+FKF(I,J)
      DM(I,J)=DM(I,J)+FMF(I,J)
30    CONTINUE
C
C***** CALCULATE ANALYTICAL NATURAL FREQUENCIES &
C***** MODE SHAPES
C
      DO 40 I=1,N
      DO 40 J=1,N
      DUMM(I,J)=DM(I,J)
      DUMK(I,J)=DK(I,J)
40    CONTINUE
C
      IFAIL=0
C
      CALL F02AEF(DUMK,N,DUMM,N,N,EVAL,EVEC,N,DL,E,IFAIL)
C
C***** INTRODUCE MISMODELLED REGIONS
C
      CALL EXMK
C
C***** READ INPUT FILE (FRF IS INERTANCE)
```

```
C
      OPEN(9,FILE='LEAK2.DAT',STATUS='OLD')
C
      READ(9,*)
      READ(9,*)
      READ(9,*) IFTYPE
      READ(9,*)
      READ(9,*) AMS,FTMS,EXMS
      READ(9,*)
      READ(9,*) GMM,GNN,NAV
      READ(9,*)
      READ(9,*) FST,FED
      READ(9,*)
      READ(9,*) ICOH
      READ(9,*)
      READ(9,*) IEX
      READ(9,*)
      READ(9,*) IRS
      READ(9,*)
      READ(9,9950) TITLE
      READ(9,*)
      READ(9,9960) HEAD
      CLOSE(9)
C
      IF(IEX.LT. 10) THEN
C
      WRITE(EX,9000) IEX
C
      ELSE
C
      WRITE(EX,9100) IEX
C
      ENDIF
C
      FR=(FED-FST)/(NFP-1)
C
C**** CALCULATE EXACT NATURAL FREQUENCIES & MODE SHAPES
C
```

```
        DO 70 I=1,N
        DO 70 J=1,N
        DUMM(I,J)=DM(I,J)
        DUMK(I,J)=DK(I,J)
70 CONTINUE
C
        IFAIL=0
C
        CALL F02AEF(DUMK,N,DUMM,N,N,EVAL,EVEC,N,DL,E,IFAIL)
C
C**** MASS LOADING EFFECTS OF FORCE TRANSDUCER
C
        CALL MLOADF(IEX,FTMS)
C
C
C**** OPEN COMBINED RESPONSE DATA FILE
C
        IDUM=0
C
        WRITE(*,*)
        WRITE(*,*) '*** CALCULATING FRF ***'
        WRITE(*,*)
C
        IF(IRS.LT. 10) THEN
C
        WRITE(RSP,9000) IRS
C
        ELSE
C
        WRITE(RSP,9 100) IRS
C
        ENDIF
C
C MASS LOADING EFFECTS OF ACCELEROMETER
C
        CALL MLOADA(IRS,AMS)
C
C**** CALCULATE NATURAL FREQUENCIES & MODE SHAPES
```

```
C
      DO 110 I=1,N
      DO 110 J=1,N
      DUMM(I,J)=DMM(I,J)
      DUMK(I,J)=DK(I,J)
110   CONTINUE
C
      IFAIL=0
C
      CALL F02AEF(DUMK,N,DUMM,N,N,EVAL,EVEC,N,DL,E,IFAIL)
C
C**** SHAKER/STRUCTURE INTERACTION
C
      CALL FRFCAL(FST,FED,IEX,IEX)
C
      CALL INTACT(EXMS)
C
C   DEFINE EXCITATION NODE(IEN) AND DIRECTION(IED)
C
      IEN=1
      IED=2
C
C   CALCULATE RESPONSE NODE(IRN) AND DIRECTION(IRD)
C
      IRN=5
      IRD=2
C
C**** CALCULATE NOISE-FREE FRF H(IRS,IEX)
C
      CALL FRFCAL(FST,FED,IEX,IRS)
C
      FLNM='TR'//RSP//EX//'.FRF'
C
      OPEN (UNIT=10,FILE=FLNM,STATUS='UNKNOWN')
C
      WRITE(10,9960) HEAD
      WRITE(10,*) IFTYPE
      WRITE(10,9400) NFP,FST,FR
```

```
        WRITE(10,*) '0'
        WRITE(10,*) IEN,IED,IRN,IRD,IDUM
        WRITE(10,*) '    0 0 0 0 0'
        WRITE(10,*) IEX,IRS
        WRITE(10,9500) (CFRF(I*2-1),I=1,NFP)
C
        FIN=FST
C
        DO 111 J=1,(NFP+9)/10
        DO 112 I=1,10
        FREQ(I)=FIN+(I-1)*FR
112 CONTINUE
        WRITE(10,9700) (FREQ(I),I=1,10)
        FIN=FREQ(10)+FR
1 1 1 CONTINUE
C
C**** CALCULATE AU-IO AND CROSS SPECTRA
C
C CALCULATE NOISE-FREE AUTO AND CROSS SPECTRA
C
        GPP=1.0
C
        DO 125 I=1,NF2
        GFF(I)=FSM(I)*GPP
        GXX(I)=(REAL(CFRF(I))**2+AIMAG(CFRF(I))**2)*GFF(I)
        GXF(I)=GXX(I)/CFRF(I)
125 CONTINUE
C
C ADD NOISE TO SPECTRA
C
        DO 130 I=1,NF2
        GFF(I)=GFF(I)+GMM
        GXX(I)=GXX(I)+GNN
1 3 0 CONTINUE
C
C**** LEAKAGE EFFECT
C
        DO 140 I=1,NF2
```

```
CFRF(I)=CMPLX(GFF(I),O.)
140 CONTINUE
c
CALL LEAK(CFRF,FR)
C
DO 150 I=1,NFP
GFF(I*2-1)=REAL(CFRF(I*2-1))
150 CONTINUE
C
DO 160 I=1,NF2
CFRF(I)=CMPLX(GXX(I),0.)
160 CONTINUE
C
CALL LEAK(CFRF,FR)
C
DO 170 I=1,NFP
GXX(I*2-1)=REAL(CFRF(I*2-1))
170 CONTINUE
C
CALL LEAK(GXF,FR)
C
C**** CALCULATE FREQUENCY RESPONSE FUNCTION H2
C
DO 180 I=1,NFP
CFRF(I*2-1)=GXX(I*2-1)/GXF(I*2-1)
180 CONTINUE
C
C**** CALCULATE COHERENCE FUNCTION
C
DO 190 I=1,NFP
COH(I)=CABS(GXF(I*2-1))**2/(GFF(I*2-1)*GXX(I*2-1))
IF(COH(I).GT. 1 .O) COH(I)=1.0
! 190 CONTINUE
C
C**** CALCULATE RANDOM ERROR OF H2
C
DO 200 I=1,NFP
ERH=SQRT((1.-COH(I))/(COH(I)*2. *NAV))
```

```
      IR1=987*I*IRN+1
      IR2=789*I*IRN+1
      RAND1=2.0*(RAN3(IR1)-0.5)
      RAND2=2.0*(RAN3(IR2)-0.5)
      REH =( 1.0+ERH*RAND1)*REAL(CFRF(I*2- 1))
      AIMH=(1.0+ERH*RAND2)*AIMAG(CFRF(I*2- 1))
      CFRF(I*2- 1)=CMPLX(REH,AIMH)
2 0 0  CONTINUE
C
C**** CALCULATE RANDOM ERROR OF COHERENCE
C
      IF(NAV.EQ. 1) THEN
C
      Do 210 I=1,NFP
      COH(I)=1.0
210  CONTINUE
C
      ELSE
C
      Do 220 I=1,NFP
      ERG=(SQRT(2.)*(1.-COH(I)))/SQRT(COH(I)*NAV)
      IRR=897*I*IRN+1
      RAND3=2.0*(RAN3(IRR)-0.5)
      COH(I)=( 1.0+ERG*RAND3)*COH(I)
220  CONTINUE
C
      ENDIF
C
      FLNM=TITLE//RSP//EX//'.FRF'
C
      OPEN (UNIT=10,FILE=FLNM,STATUS='UNKNOWN')
C
      WRITE(10,9960) HEAD
      WRITE(10,*) IFTYPE
      WRITE(10,9400) NFP,FST,FR
      WRITE(10,*) ICOH
      WRITE(10,*) IEN,IED,IRN,IRD,IDUM
      WRITE(10,*) '      0 0 0 0 0
```

```
        WRITE(10,*) IEX,IRS
        WRITE(10,9500) (CFRF(I*2-1),I=1,NFP)
        WRITE(10,9600) (COH(I),I=1,NFP)
C
        FIN=FST
C
        DO 300 J=1,(NFP+9)/10
        DO 310 I=1,10
        FREQ(I)=FIN+(I-1)*FR
310     CONTINUE
        WRITE(10,9700) (FREQ(I),I=1,10)
        FIN=FREQ( 1 0)+FR
300     CONTINUE
C
        CLOSE( 10)
C
9000    FORMAT(1H0,I 1)
9100    FORMAT(I2)
9200    FORMAT(2X,I3,F15.2)
9300    FORMAT(F7.1,7X,2G 10.3)
9400    FORMAT(7X,I5,2F10.3)
9500    FORMAT(8E10.3)
9600    FORMAT(1X,10F7.3)
9700    FORMAT(1X,10F7.1)
9800    FORMAT(2E15.7)
9900    FORMAT( 10I5)
9950    FORMAT(1X,A2)
9960    FORMAT(A70)
C
        STOP
        END
C
```

```

C*****C
C*****      *****C
C*****      SUBROUTINES      *****C
C*****      *****C
C*****C
C
C*****C
C*****      SUBROUTINE EXMK      *****C
C*****C
      SUBROUTINE EXMK
      PARAMETER(N=42)
      DIMENSION DEM(4,4),DEK(4,4)
      COMMON /CB1/FMF(N,N),FKF(N,N)
      COMMON /CB3/DM(N,N),DK(N,N)
C
C**** MASS MODIFICATIONS
C
      CALL ELMKF1(DEM,DEK,1)
C
      DO 10 I=1,N
      DO 10 J=1,N
      DM(I,J)=DM(I,J)+1.0*FMF(I,J)
10  CONTINUE
C
      CALL ELMKF1(DEM,DEK,2)
C
      DO 20 I=1,N
      DO 20 J=1,N
      DM(I,J)=DM(I,J)+1.0*FMF(I,J)
20  CONTINUE
C
C**** STIFFNESS MODIFICATIONS
C
      CALL ELMKF1(DEM,DEK,11)
C
      DO 110 I=1,N
      DO 110 J=1,N
C      DMK(I,J)=DK(I,J)+1.0*FKF(I,J)

```



```

      DK(I,J)=DK(I,J)+1.0*FKF(I,J)
110  CONTINUE
C
      CALL ELMKF1(DEM,DEK,12)
C
      DO 120 I=1,N
      DO 120 J=1,N
C      DMK(I,J)=DMK(I,J)+1.0*FKF(I,J)
      DK(I,J)=DK(I,J)+1.0*FKF(I,J)
120  CONTINUE
C
      RETURN
      END
C
C
C*****C
C*****          SUBROUTINE INTACT          *****C
C*****C
      SUBROUTINE INTACT(EXMS)
      PARAMETER(NF2=801)
      COMPLEX CFRF
      COMMON /CB5/CFRF(NF2),FSM(NF2)
C
C**** SHAKER/STRUCTURE INTERACTION
C
C  FORCE SPECTRUM MODIFICATION FACTOR
C
C   $G_{ff}(I) = G_{pp}(I) / ((1 + EXMS * H(I)) * (1 + EXMS * H(I)))$ 
C
      DO 10 I=1,NF2
      HMS=REAL(CFRF(I))**2+AIMAG(CFRF(I))**2
      FSM(I)=1./(1.+EXMS**2*HMS+2.*EXMS*REAL(CFRF(I)))
10  CONTINUE
C
      RETURN
      END
C
C

```

```
C*****C
C*****          SUBROUTINE MLOADF          *****C
C*****C
      SUBROUTINE MLOADF(IRS,AMS)
      PARAMETER(N=42)
      COMMON /CB3/DM(N,N),DK(N,N)
C
C***** MASS LOADING EFFECTS OF FORCE TRANSDUCER
C
      DM(IRS,IRS) = DM(IRS,IRS)+AMS
C
      RETURN
      END
C
C*****C
C*****          SUBROUTINE MLOADA          *****C
C*****C
      SUBROUTINE MLOADA(IRS,AMS)
      PARAMETER(N=42)
      COMMON /CB2/DMM(N,N)
      COMMON /CB3/DM(N,N),DK(N,N)
      DO 10 I=1,N
      DO 10 J=1,N
      DMM(I,J)=DM(I,J)
10  CONTINUE
C
C***** MASS LOADING EFFECTS OF ACCELEROMETER
C
      DMM(IRS,IRS) = DM(IRS ,IRS)+AMS
C
      RETURN
      END
C
```

```
C*****C
C*****          SUBROUTINE FRFCAL          *****C
C*****C
      SUBROUTINE FRFCAL(FST,FED,IEX,IRS)
      PARAMETER(N=42,NF2=801)
      DOUBLE PRECISION EVAL,EVEC
      COMPLEX CFRF,DNT
      COMMON /CB4/EVAL(N),EVEC(N,N)
      COMMON /CB5/CFRF(NF2),FSM(NF2)

C
C**** FRF(INERTANCE) CALCULATION
C
      FRSL=(FED-FST)/(NF2- 1)

C
      DO 10 IFQ=1,NF2
      FREQ=FST+(IFQ- 1)*FRSL
      SOMGA=(2.*3.1415927*FREQ)**2
      CFRF(IFQ)=(0.,0.)

C
      DO 20 IMD=1,N

C
C      DEFINE LOSS FACTORS (DAMPING IS PROPORTIONAL)
C
      ETA=100./EVAL(IMD)+0.005

C
      DRE=SOMGA-EVAL(IMD)
      DIM=-ETA*EVAL(IMD)
      DNT=CMPLX(DRE,DIM)
      CFRF(IFQ)=CFRF(IFQ)+EVEC(IRS,IMD)*EVEC(IEX,IMD)*SOMGA/DNT

C
20    CONTINUE
C
10    CONTINUE
C
      IF(CABS(CFRF( 1)).EQ.0.) THEN

C
      REC1= (2.*REAL(CFRF(2))- REAL(CFRF(3))) *REAL(CFRF(2))
      AIC1=(2.*AIMAG(CFRF(2))-AIMAG(CFRF(3)))*AIMAG(CFRF(2))
```

```
      CFRF(1)=CMPLX(REC1,AIC1)
C
      ENDIF
C
      RETURN
      END
C
C*****
C**** FUNCTION RAN3                                ****C
C*****
      FUNCTION RAN3(IDUM)
      IMPLICIT REAL*4(M)
      PARAMETER (MBIG=4000000.,MSEED=1618033.,MZ=0.,FAC=2.5E-7)
      DIMENSION MA(55)
C
      DATA IFF /0/
C
      IF(IDUM.LT.0.OR.IFF.EQ.0) THEN
C
      IFF= 1
      MJ=MSEED-IABS(IDUM)
      MJ=MOD(MJ,MBIG)
      MA(55)=MJ
      MK=1
C
      DO 11 I=1,54
      II=MOD(21*I,55)
      MA(II)=MK
      MK=MJ-MK
      IF(MK.LT.MZ) MK=MK+MBIG
      MJ=MA(II)
11  CONTINUE
C
      DO 13 K=1,4
      DO 12 I=1,55
      MA(I)=MA(I)-MA(1+MOD(I+30,55))
      IF(MA(I).LT.MZ)MA(I)=MA(I)+MBIG
12  CONTINUE
```

```
13 CONTINUE
C
    INEXT=0
    INEXTP=3 1
    IDUM=1
C
    ENDIF
C
    INEXT=INEXT+1
    IF(INEXT.EQ.56) INEXT=1
    INEXTP=INEXTP+1
    IF(INEXTP.EQ.56) INEXTP=1
    MJ=MA(INEXT)-MA(INEXTP)
    IF(MJ.LT.MZ) MJ=MJ+MBIG
    MA(INEXT)=MJ
    RAN3=MJ*FAC
C
    RETURN
    END
C
C
C*****C
C*****      SUBROUTINE EMASS      *****C
C*****C
    SUBROUTINE EMASS(DEM,ICLASS)
    DIMENSION DEM(4,4)
C
    DENS=7800.
C
    IF(ICLASS.EQ. 1) THEN
    EL=0.075
    AREA=5.0E-4
    GOT010
C
    ELSEIF(ICLASS .EQ. 2) THEN
    EL=SQRT(1.93)/6.
    AREA=1.25E-4
    GOT0 10
```

```
C
    ELSEIF(ICLASS.EQ. 3) THEN
    EL=0.175
    AREA=1.5E-4
    GO TO 10
C
    ENDIF
C
1 0 CONTINUE
C
    FAC=DENS*AREA*EL/420.
C
C**** UPPER TRIANGULAR ELEMENTS OF ELEMENT MASS MATRIX
C
    DEM(1,1)=156.
    DEM(1,2)=22.*EL
    DEM(1,3)=54.
    DEM(1,4)=-13.*EL
    DEM(2,2)=4.*EL**2
    DEM(2,3)=13.*EL
    DEM(2,4)=-3.*EL**2
    DEM(3,3)=156.
    DEM(3,4)=-22.*EL
    DEM(4,4)=4.*EL**2
C
    DO 15 I=1,4
    DO 15 J=I,4
    DEM(I,J)=FAC*DEM(I,J)
15 CONTINUE
C
C**** WHOLE MASS MATRIX *****C
C
    DO 20 I=2,4
    DO 20 J=I,I-1
    DEM(I,J)=DEM(J,I)
20 CONTINUE
C
    RETURN
```

```
      END
C
C*****
C*****          SUBROUTINE ESTIFF          *****C
C*****C
      SUBROUTINE ESTIFF(DEK,ICLASS)
      DIMENSION DEK(4,4)
      E=209.E9
C
      IF(ICLASS.EQ. 1) THEN
      EL=0.075
      AMI=0.41667E-8
      GO TO 10
C
      ELSEIF(ICLASS.EQ. 2) THEN
      EL=SQRT( 1.93)/6.
      AMI=1.0417E-11
      GO TO 10
C
      ELSEIF(ICLASS.EQ. 3) THEN
      EL=0.175
      AMI=1.25E-11
      GO TO 10
C
      ENDIF
C
      CONTINUE
C
      FAC2=E*AMI/EL**3
C
C**** STIFFNESS MATRIX *****C
C
      DEK(1,1)=FAC2*12.
      DEK(1,2)=FAC2*6.*EL
      DEK(1,3)=-DEK(1,1)
      DEK(1,4)=DEK(1,2)
      DEK(2,2)=FAC2*4.*EL**2
      DEK(2,3)=-DEK(1,2)
```

```
      END
C
C*****
C*****          SUBROUTINE ESTIFF          *****C
C*****
      SUBROUTINE ESTIFF(DEK,ICLASS)
      DIMENSION DEK(4,4)
      E=209.E9
C
      IF(ICLASS.EQ. 1) THEN
      EL=0.075
      AMI=0.41667E-8
      GO TO 10
C
      ELSEIF(ICLASS.EQ. 2) THEN
      EL=SQRT( 1.93)/6.
      AMI=1.0417E-11
      GOT010
C
      ELSEIF(ICLASS.EQ. 3) THEN
      EM. 175
      AMI=1.25E-11
      GOT010
C
      ENDIF
C
      10  CONTINUE
C
      FAC2=E*AMI/EL**3
C
C**** STIFFNESS MATRIX *****C
C
      DEK(1,1)=FAC2*12.
      DEK(1,2)=FAC2*6.*EL
      DEK(1,3)=-DEK(1,1)
      DEK(1,4)=DEK(1,2)
      DEK(2,2)=FAC2*4.*EL**2
      DEK(2,3)=-DEK(1,2)
```

```
      DEK(2,4)=DEK(2,2)/2.
      DEK(3,3)=DEK( 1,1)
      DEK(3,4)=DEK(2,3)
      DEK(4,4)=DEK(2,2)
C
      DO 20 I=2,4
      DO 20 J=1,I-1
      DEK(I,J)=DEK(J,I)
20  CONTINUE
      RETURN
      END

C
C*****C
C*****          SUBROUTINE ELMKF1                      *****C
C*****C
C*****C
      SUBROUTINE ELMKF1(DEM,DEK,K)
      PARAMETER(N=42)
      DIMENSION DEM(4,4),DEK(4,4)
      COMMON /CB 1/FMF(N,N),FKF(N,N)
C
      DO 10 I=1,N
      DO 10 J=1,N
      FMF(I,J)=0.
      FKF(I,J)=0.
10  CONTINUE
C
      IF(K.GE.1 .AND. K.LE.21) THEN
C
          CALL EMASS(DEM,1)
          CALL ESTIFF(DEK, 1)
C
      ELSE
C
          WRIT&*,*) '*** ASSEMBLING ERROR !! ***'
          STOP
C
      ENDIF
C
```

```

      IF(K.GE.1.AND. K.LE.21) THEN
C
      DO 20 I=1,4
      DO 20 J=1,4
      FMF((K-1)*2+I,(K-1)*2+J)=DEM(I,J)
      FKF((K-1)*2+I,(K-1)*2+J)=DEK(I,J)
20    CONTINUE
C
      ELSE
C
      WRITE(*,*)'*** ASSEMBLING ERROR !! ***'
      STOP
C
      ENDIF
C
      RETURN
      END
C
C*****C
C*****          SUBROUTINE GLOBAL          *****C
C*****C
      SUBROUTINE GLOBAL(NI,NJ,DEM,DEK)
      PARAMETER(N=42)
      DIMENSION DEM(4,4),DEK(4,4)
      COMMON /CB1/FMF(N,N),FKF(N,N)
C
      DO 10 I=1,2
      DO 20 J=1,2
      FMF((NI-1)*2+I,(NI-1)*2+J)=DEM(I,J)
      FKF((NI-1)*2+I,(NI-1)*2+J)=DEK(I,J)
20    CONTINUE
      DO 30 J=3,4
      FMF((NI-1)*2+I,(NJ-2)*2+J)=DEM(I,J)
      FKF((NI-1)*2+I,(NJ-2)*2+J)=DEK(I,J)
30    CONTINUE
10    CONTINUE
C
C

```

```

      DO 40 I=3,4
      DO 50 J=1,2
      FMF((NJ-2)*2+I,(NI-1)*2+J)=DEM(I,J)
      FKF((NJ-2)*2+I,(NI-1)*2+J)=DEK(I,J)
50    CONTINUE
      DO 60 J=3,4
      FMF((NJ-2)*2+I,(NJ-2)*2+J)=DEM(I,J)
      FKF((NJ-2)*2+I,(NJ-2)*2+J)=DEK(I,J)
60    CONTINUE
40    CONTINUE
C
      RETURN
      END

C
C*****C
C*****          SUBROUTINE LEAK          *****C
C*****C
      SUBROUTINE LEAK(GXY,FR)
      PARAMETER(NF2=801)
      COMPLEX GXY(NF2),GD(NF2)
C
      Do 10 I=1,NF2,2
C
      IF(I.LE.5 .OR. I.GE.NF2-5) THEN
C
      GD(I)=GXY(I)*3./FR
C
      ELSE
C
      GD(I)=2.*GHAN(FR,2.5*FR)*(GXY(I-5)+GXY(I+5))
1         +2.*GHAN(FR,1.5*FR)*(GXY(I-3)+GXY(I+3))
2         +GHAN(FR,FR)*(GXY(I-2)+GXY(I+2))
3         +2.*GHAN(FR,0.5*FR)*(GXY(I-1)+GXY(I+1))
4         +GHAN(FR,0.)*GXY(I)
C
      ENDIF
C
      GD(I)=GD(I)*FR/3.

```

**10 CONTINUE**

```
C
      Do 20 I=1,NF2
      GXY(I)=GD(I)
2  0  CONTINUE
C
      RETURN
      END

C
C*****C
C*****          FUNCTION GHAN          *****C
C*****C
      FUNCTION GHAN(FR,FX)
C
      IF(FX.EQ.0) THEN
C
      GHAN=2./(3.*FR)
C
      ELSEIF(FX.EQ.FR) THEN
C
      GHAN=1./(6.*FR)
C
      ELSE
C
      CST=FR/3.1415927**2
      T1=2./(3.*FX**2)
      T2=1./6.*(1./(FX+FR)**2+1./(FX-FR)**2)
      T3=1./(FR**2-FX**2)
      X=(3.1415927*FX)/FR
      GHAN=CST*(T1+T2+T3)*SIN(X)**2
C
      ENDIF
C
      RETURN
      END
C
```

## E.7 DATA FILE

FREE-FREE BEAM DATA (PROP. STRUCTURAL DAMPING)  
FRF TYPE (INERTANCE=3)  
3  
MASSES (ACCELEROMETER, FORCE TRANSDUCER& SHAKER)  
0.02 0.01 0.02  
NOISE SPECTRA LEVELS (INPUT & OUTPUT) AND NO. OF AVERAGE  
1.OE-2 1.OE-3 100  
STARTING FREQ. AND END FREQ.  
0. 800.  
COHERENCE FLAG  
1  
EXCITATION COORDINATE  
1  
RESPONSE COORDINATES  
1 5 9 13 17 21 25 29 33 37  
41

# APPENDIX F

## BENDENT METHOD

Even though the Inverse method for SDOF identification of a FRF has some advantages over the Circle-fit method as discussed in Chapter 5, the Inverse method. has some drawbacks such that:

- 1) it is difficult to apply the Line-fit method to complex modes, and
- 2) the extraction of the residual effects of other modes is a **pre-requisite** for an accurate analysis.

A new SDOF method, which is a modified version of the Inverse Method , has been developed by Dobson [51]. This method retains many of the advantages of the Inverse method and can calculate modal parameters of complex modes.

The receptance FRF near resonance can be express as

$$\alpha(\omega) = \frac{A_r}{\omega_r^2 - \omega^2 + i \eta_r \omega_r^2} + R_r \quad (\text{F1})$$

where A, and  $R_r$  are complex. The effect of  $R_r$  can be eliminated by taking the difference between two measured FRF data.

Let

$$\alpha'(\omega) = a(\omega) - \alpha(\Omega) \quad \text{and} \quad \Delta(\omega) = \frac{\omega^2 - \Omega^2}{\alpha'(\omega)} \quad (\text{F2})$$

where  $\Omega$  is a reference frequency. Then,

$$\begin{aligned} \Delta(\omega) &= \frac{(\omega_r^2 - \omega^2 + i \eta_r \omega_r^2)(\omega_r^2 - \Omega^2 + i \eta_r \omega_r^2)}{A_r} \\ &= \text{Re} (A) + \text{Im} (A) \end{aligned} \quad (\text{F3})$$

where  $\text{Re} (A) = m_R \omega^2 + c_R$  and  $\text{Im} (A) = m_I \omega^2 + c_I$

$$\begin{aligned} \text{and } m_R &= \frac{-a_r (\omega_r^2 - \Omega^2) - b_r (\eta_r \omega_r^2)}{|A_r|^2} \\ m_I &= \frac{b_r (\omega_r^2 - \Omega^2) - a_r (\eta_r \omega_r^2)}{|A_r|^2} \\ A_r &= a_r + i b_r \end{aligned}$$

The slopes of the real and imaginary components of A are linear functions of  $\Omega^2$  such that:

$$m_R = n_R \Omega^2 + d_R \quad \text{and} \quad (\text{F4})$$

where the slopes and intercepts are:

$$n_R = \frac{a_r}{|A_r|^2} \quad (\text{F5a})$$

$$d_R = \frac{-a_r \omega_r^2 - b_r \eta_r \omega_r^2}{|A_r|^2} \quad (\text{F5b})$$

$$n_I = \frac{-b_r}{|A_r|^2} \quad (\text{F5c})$$

$$d_I = \frac{-a_r \eta_r \omega_r^2 + b_r \omega_r^2}{|A,|^2} \quad (\text{F5d})$$

This set of equations can be used to extract the modal properties. From equations (F5a) and (F5c)

$$b_r = -\frac{n_I}{n_R} a_r \quad (\text{F6})$$

$$\text{where } p = \frac{n_I}{n_R}$$

From equations (F5b) and (F5d)

$$\eta_r = \frac{q-p}{1+pq} \quad (\text{F7})$$

$$\text{where } q = \frac{d_I}{d_R}$$

From equations (F5a) and (F5b)

$$\omega_r^2 = \frac{-d_R}{n_R(1-p\eta_r)} \quad (\text{F8})$$

and

$$a_r = \frac{\omega_r^2(p\eta_r - 1)}{d_R(1+p^2)} \quad (\text{F9})$$

therefore  $b_r$  can be calculated from equation (F6).

For real modes ( $b_r = 0$ ),  $p = n_I = 0$ , therefore,

$$\eta_r = q = \frac{d_I}{d_R}$$

$$\omega_r^2 = \frac{-d_R}{n_R}$$

$$a_r = A_r = -\frac{\omega_r^2}{d_r}$$

The analysis is in two parts.

1) For the selected FRF data range one point is selected as the reference point  $\Omega$ . All possible values of  $\Delta(\omega)$  are calculated using the remainder of the selected data. The best straight line is then calculated for each of the real and imaginary parts of equation (F3) to determine the values of  $m_r$  and  $m_i$  for that value of  $\Omega$ . The process is repeated using each of the data points in turn as a reference point, and a series of lots made, showing the values for Re (A) and Im (A) against  $\omega^2$ .

2) The slopes of the best fit straight lines for each in part 1 are plotted against the reference frequency  $\Omega$ . The resulting two plots may either be analysed using a straight line fit over the whole range or over the selected range.

# REFERENCES

## REFERENCES

- 1. Ewins, D.J. and Imregun, M.**  
“State-of-the-Art Assessment of Structural Dynamic Response Analysis Methods (DYNAS)”,  
Shock and Vibration Bulletin, Vol. 56, Part 1, August 1986.
- 2. Rodden, W.P.**  
“A Method for Deriving **Influence** Coefficients from Ground Vibration Test”,  
AIAA Journal, Vol. 5, No. 5, 1967, pp. 991-1000.
- 3. Berman, A. and Flannelly, W.G.**  
“**Theory** of Incomplete Models of Dynamic Structures”,  
AIAA Journal, Vol. 9, No. 8, 1971, pp. 1481-1487.
- 4. Baruch, M. and Bar-Itzhack, I.Y.**  
“**Optimal** Weighted **Orthogonalization** of Measured Modes”,  
AIAA Journal, Vol. 16, No. 4, 1978, pp. 346-351.
- 5. Baruch, M.**  
“**Optimization** Procedure to Correct Stiffness and Flexibility **Matrices** Using  
Vibration Data”,  
AIAA Journal, Vol. 16, No. 11, 1978, pp. 1208-1210.

6. **Berman, A.**  
“Comment on Optimal Weighted **Orthogonalization** of Measured Modes”,  
**AIAA Journal**, Vol. 17, No. 8, 1979, pp. 927-928.
7. **Berman, A.**  
“Mass Matrix Correction Using an Incomplete Set of Measured Modes”,  
**AIAA Journal**, **Vol.** 17, No. 10, 1979, pp. 1147-1148.
8. **Berman, A. and Nagy, E.J.**  
“**Improvement** of a Large Analytical Model Using Test Data”,  
**AIAA Journal**, Vol. 21, No. 8, 1983, pp. 1168-1173.
9. **Wei, F.S.**  
“Stiffness Matrix **Correction from** Incomplete Test Data”,  
**AIAA Journal**, Vol.18, No. 10, 1980, pp. 1274-1275.
10. **Caesar, B.**  
“Update and Identification of Dynamic **Mathematical Models**”,  
**Proc. IMAC 4**, 1986, pp. 394-401.
11. **Lin, R.M. and Jung, H.**  
“Possibilities and Limitations of Analytical Model Improvement ---- A Review  
Based on the GARTEUR Exercise”,  
Internal Report **No.90001**, Dynamics Section, Imperial College, Feb. 1990.
12. **To, W.M.**  
“Sensitivity Analysis of Mechanical Structures Using Experimental Data”,  
Ph.D. Thesis, Dept. of **Mech.** Eng., Imperial College, 1990.

13. **Ibrahim, S.R., Stravinidis, C., Fiset, E. and Brunner, O.**  
“A Direct Two Response Approach for Updating Analytical Dynamic Models of Structures with Emphasis on Uniqueness”,  
Proc. IMAC 7, 1989, pp. 340-346.
14. **Collins, J. D., Hart, G. C., Hasselman, T. K. and Kennedy, B.**  
“Statistical Identification of Structures”,  
AIAA Journal, Vol. 12, No. 2, 1974, pp. 185-190.
15. **Chen, J.C. and Garba, J.A.**  
“Analytical Model Improvement Using Modal Test Results”,  
AIAA Journal, Vol. 18, No. 6, 1980, pp. 684-690.
16. **Sidhu, J. and Ewins, D.J.**  
“Correlation of Finite Element and Modal Test Studies of a Practical Structure”,  
Proc. IMAC 2, 1984, pp. 756-762.
17. **He, J.**  
“Identification of Structural Dynamics Characteristics”,  
Ph.D. Thesis, Dept. of Mech. Eng., Imperial College, 1987.
18. **Fiset, E., Stravinidis, C., and Ibrahim, S.R.**  
“Error Location and Updating of Analytical Dynamic Models Using a Force Balance Method”,  
Proc. IMAC 6, 1988, 1063-1070.
19. **Zhang, Q., Lallement, G., Fillard, R., and Piranda, J.**  
“A Complete Procedure for the Adjustment of a Mathematical Model from the Identified Complex Modes”,  
Proc. IMAC 1987, pp. 1183-1190.

20. **Caesar, B.**  
“Updating System Matrices Using Modal Test Data”,  
**Proc. IMAC 5, 1987**, pp. 453-459.
21. **Lin, R.M.**  
“Identification of the Dynamic Characteristics of Nonlinear Structures”,  
Ph.D. Thesis, Dept. of **Mech.** Eng., Imperial College, 1991.
22. **Lieven, N.A.J. and Ewins, D. J.**  
“Expansion of Modal Data for Correlation”,  
**Proc. IMAC 8, 1990**, pp. 605-609.
23. **Gysin, H.**  
“Comparison of Expansion Methods for FE Modeling Error Localization”,  
**Proc. IMAC 8, 1990**, pp. 195-204.
24. **Guyan, R. J.**  
“Reduction of Stiffness and Mass Matrices”,  
AIAA Journal, Vol. 3, No. 2, 1965, p. 380.
25. **Urgueira, A. P. V.**  
“Couple Structure Analysis Using Incomplete Modes”,  
Internal Report No.88012, Dynamics Section, Imperial College, 1988.
26. **Lim, K.B., Junkins, J.L. and Wang, B.P.**  
“Re-examination of Eigenvector Derivatives”,  
J. Guidance, Vol. 10, No. 6, 1987, pp. 581-587.
27. **Allemang, R.J. and Brown, D.L.**  
“A Correlation Coefficient for Modal Vector Analysis”,  
**Proc. IMAC 1, 1982**, pp.110-116.

28. Ewins, **D.J.** and Griffin, J.  
“A State-of-the-Art Assessment of Mobility Measurement Techniques -  
Results for the Mid-Range Structures (30 - 3,000 Hz)“,  
Journal of Sound & Vibration, Vol. 78, Part 2'1981.
29. **Ewins, D.J.**  
“Modal Testing :**Theory** and Practice,,,  
Research Studies Press, London, 1984.
30. **Broch, J.T.**  
“Mechanical Vibration and Shock Measurements”, 2nd ed.,  
**Brüel & Kjær**, 1984.
31. **Mitchell, L.D. and Elliot, K.B.**  
“A Method for Designing Stingers for Use in Mobility Testing”,  
**Proc. IMAC 2**, 1984, pp. 872-876.
32. **Hieber, G.M.**  
“Non-Toxic Stingers”,  
**Proc. IMAC 6**, 1988, pp. 1371-1379.
33. **Rao, D.K.**  
“Blectrodynamic Interaction Between Resonating Structure and an Exciter”,  
**Proc. IMAC 5**, 1987, pp. 1142-1 150.
34. **Bendat, J.S. and Piersol, A.G.**  
“**Engineering** Applications of Correlation and Spectral Analysis”,  
John Wiley & Sons, New York, 1980.
35. **Newland, D.E.**  
“An Introduction to Random Vibrations and **Spectral Analysis**”, 2nd ed.,  
**Longman**, New York, 1984.

- 36. Cawley, P.**  
“**The Reduction of Bias Error in Transfer Function Estimates Using FFT-Based Analyzers**”,  
Journal of Vib., Acoust., Stress and Reliab. in Design, Vol. 106, 1984, pp. 29-35.
- 37. Imregun, M.**  
“**MODENT Reference Manual : Version 3.0**”,  
Modal Testing Unit, Imperial College, 1990.
- 38. Imregun, M.**  
“**MODESH Reference Manual : Version 3.0**”,  
Modal Testing Unit, Imperial College, 1990.
- 39. Ibrahim, S.R.**  
“**Computation of Normal Modes from Identified Complex Modes**”,  
AIAA Journal, Vol. 21, No. 3, 1983, pp. 446-451.
- 40. Zhang, Q., Lallement, G.**  
“**New Method of Determining the Eigensolutions of the Associated Conservative Structure for the Identified Eigensolutions**”,  
**Proc. IMAC 3, 1985, pp. 322-328.**
- 41. Chou, Y.-F. and Chen, J.-S.**  
“**Structural Dynamics Modification via Sensitivity Analysis**”,  
**Proc. IMAC 3, 1985, pp. 483-489.**
- 42. Zhang, Q., Wang, W., Allemang, R. J. and Brown, D. L.**  
“**Prediction of Mass Modification for Desired Natural Frequencies**”,  
**Proc. IMAC 6, 1988, pp. 1026-1032.**

43. **Jonas, S. and Pierce, G.A.**  
“An Efficient Technique for Optimal Design Changes to FEM of Structural Dynamic Systems”,  
**Proc. IMAC 9, 1991, pp. 320-327.**
44. **Eckert, L. and Caesar, B.**  
“Model Updating under Incomplete and Noisy Modal Test Data”,  
**Proc. IMAC 9, 1991, pp. 563-571.**
45. **Piranda, J., Lallement, G. and Cogan, S.**  
“Parametric Correction of Finite Element Models by Minimization of an Output Residual ; Improvement of the Sensitivity Method”,  
**Proc. IMAC 9, 1991, pp. 363-368.**
- 46. Wittrick, W. H.**  
“Rates of Change of Eigenvalues With Reference to Buckling and Vibration Problems”,  
Journal of the Royal Aeronautical Society, Vol. 66, No. 621, Sept. 1962,  
pp. 590-591.
47. **Fox, R. L. and Kapoor, M. P.**  
“Rates of Change of Eigenvalues and Eigenvectors”,  
AIAA Journal, Vol. 6, No. 12, Dec. 1968, pp. 2426-2429.
- 48. Craig Jr., R. R.**  
“**Structural Dynamics - An Introduction to Computer Methods**”,  
John Wiley & Sons, New York, 1981.
19. **Stewart, G.W.**  
“Introduction to Matrix Computations”,  
Academic Press, Orlando, 1973.

**50. Meirovitch, L.**

“Computational Methods in Structural Dynamics”

Sijthoff & Noordhoff International Publishers, Alphen aan den Rijn,

The Netherlands, 1980.

**51. Dobson, B. J.**

“A Straight-Line Technique for Extracting Modal Properties from Frequency  
Response Data”

Mechanical Systems and Signal Processing, Vol. 1, No. 1, 1987.